On the Applicability of the Weak Coupling Expansion for Time-Moments of Heavy Quark Correlators

DISSERTATION

zur Erlangung des akademischen Grades
doctor rerum naturalium
(Dr. rer. nat.)
im Fach: Physik
Spezialisierung: Theoretische Physik

eingereicht an der
Mathematisch-Naturwissenschaftlichen Fakultät
der Humboldt-Universität zu Berlin

von

Leonardo Chimirri

Präsidentin der Humboldt-Universität zu Berlin:
Prof. Dr. Julia von Blumenthal

Dekanin der Mathematisch-Naturwissenschaftlichen Fakultät:
Prof. Dr. Caren Tischendorf

Gutachter/innen:
1. Prof. Dr. Rainer Sommer
2. Prof. Dr. Marcus Petschlies
3. Dr. Valentina Forini

Tag der mündlichen Prüfung: 17. August 2023

Acknowledgments

First and foremost I would like to express my gratitude to my supervisor Rainer Sommer, for his continuous support and guidance throughout the years. His expertise and rigor not only taught me how to carry out high quality research, but also how to critically think and approach problems. I learned how to always question my understanding in order to deepen my comprehension of physical systems and grow as a researcher.

Next, let me thank Nikolai Husung and Tomasz Korzec for sharing invaluable code resources and time to explain them to me. I would also like to extend my heartfelt thanks to the other researchers whose experience and knowledge I had the pleasure to learn from, namely Agostino Patella at Humboldt, Stefan Schaefer at DESY and Stefan Sint through the EuroPLEx network.

Indeed, I am also deeply indebted to the EuroPLEx network, which was the source of my funding, but also much more. Throughout the years, schools, workshops, and conferences kept me engaged and interested, while at the same time giving me the sense of an extended European research community. Many memorable moments were shared with the fellows and the other members of the network, both in person and through video calls when the pandemic forced everybody at home. I also offer my sincere appreciation to the scientific coordinator Francesco di Renzo for always trying to help out the fellows throughout all stages of the project.

Then, I want to thank my particle physics office colleagues, Alessandro and Jens at Humboldt, Ben and, again, Nikolai at DESY Zeuthen. They were always there to help out when something simply would not work, but also to discuss any sort of problems, be at the black board, in front of a terminal, or on a couch over some coffee.

In these years in Berlin I have been given the possibility to grow so much academically, but also as a person. Next to me in this journey were my family and many friends, both here in Germany and faraway. You have made these years of my life wonderful and in dark times you kept supporting and believing in me, no matter what. From the bottom of my heart, thank you.

Abstract

WITHIN particle physics the development of a multitude of computational techniques has been necessary in order to tackle the highly complex problems posed by interacting quantum field theories. Weak coupling, perturbative expansions – with their well-known graphical representation via *Feynman diagrams* – were incredibly successful and brought us to our current understanding of high energy physics. They remain of central importance today, however, also methods applicable to strongly coupled, *non-perturbative* systems are needed to complement our knowledge. The arguably most important such field theory where both methodologies are needed is *quantum chromodynamics* (QCD), which has a coupling decreasing with energy due to *renormalization* effects, and, for asymptotically high energies, the theory becomes non-interacting. On the other hand, low energy characteristics such as mesonic and baryonic bound states – which include properties such as masses of protons and neutrons – need be studied through non-perturbative computations.

Discretizing spacetime into a regular lattice and simulating QCD on supercomputers has become a highly successful tool to carry out these non-perturbative computations from first principles. In this thesis we study in detail time-moments of heavy quark correlators to high precision. These moments are used in literature to extract the QCD coupling α_S (as well as charm and bottom quark masses) by comparing lattice and perturbative computations, a procedure which requires these observables to be dominated by energies where both methods may be applied. Scales reachable with lattice calculations are in practice limited from above by a momentum cutoff of the order of the inverse lattice spacing a^{-1}. These *cutoff effects* increase when trying to compute observables at higher energies. At the same time, perturbation theory contains a truncation error due to the higher order unknown terms. If the first n terms of the series are known, an error of order $\mathcal{O}(\alpha_S^{n+1})$ is unavoidable, and such error increases with decreasing energy. Thus, one is left with a window of energies where the moments method may work, and a precise assessment of its systematic uncertainties is necessary, since these directly propagate in numerous particle physics computations, such as Higgs decays to b-quarks or gluons, Z-boson partial widths as well as having implications in topics such as the electroweak vacuum stability.

Herein, we carry out a *quenched* study of time moments, where the effect of dynamical quarks is neglected, and we argue this to give good quantitative (or approximate quantitative) information about the fully dynamical case. This is of great algorithmic advantage and allows us to reach down to lattice spacings of $a \sim 0.01$ fm, a precision currently not reachable in our setup for full QCD in large volume; we simulate $L^3 \times T \sim (2\,\mathrm{fm})^3 \times 6\,\mathrm{fm}$ volumes and impose open boundary conditions in time to avoid the issue of topological freezing present at fine lattice spacing. We compute moments for

several energies μ of $0.8\,m_{\text{charm}} \lesssim \mu \lesssim 3.5\,m_{\text{charm}}$, which allows us to study the variation with energy of the coupling and of the truncation error of these observables. To tackle the large cutoff effects, we use a non-perturbatively improved Wilson-clover fermion doublet with a twisted mass term, tuned to maximal twist. Operators appearing in the two-point function are chosen to be pseudoscalar densities, to avoid the presence of explicit renormalization factors and to have small statistical noise stemming from the numerical Markov chain Monte Carlo integration. Beyond the coupling itself, we also study its running to infinite energy, encoded in the Λ-parameter, and the truncation errors therein.

Moments in the time-momentum representation are defined as time integrals of the correlator weighted with t^n. Lower moments are more perturbative than higher ones, yet for $n = 4$ large cutoff effects are present and it was necessary to set up a special procedure to reliably extrapolate to the continuum, currently under further development. From ratios of higher moments, with $n = 6, 8, 10$, we could obtain acceptable continuum limit estimates.

Our results, based on ratios of moments R_6/R_8 and R_8/R_{10}, show that the Λ-parameter extracted has sizeable deviations of order 5% to 10% – depending on the observable – at energy scales of $\mu \sim 2m_{\text{charm}} \simeq 2.5$ GeV (in the $\overline{\text{MS}}$-scheme) with respect to the latest step-scaling result. An extrapolation to $\alpha_S \to 0$ is possible, but with a considerable slope. These extrapolations include neither higher orders in α_S nor power corrections. Moreover, variations of the perturbative renormalization scale to estimate the truncation error, quite widespread in the literature and considered to be a rather "safe" and conservative estimate, definitely seem to undershoot the real size of the errors in the case of moments. Finally, we note that as expected the above mentioned deviation – encoded in the slope as one extrapolates $\alpha_S \to 0$ – is larger for R_8/R_{10}.

The emerging picture is rather bleak: the less perturbative observable R_8/R_{10} (which has a slower convergence) is closer to known values, while the more perturbative R_6/R_8 (with a better behaved convergence) seems to be farther away from them. As a matter of fact, this study unfortunately does not help much in settling the recently emerged tension between earlier quenched results and the aforementioned latest step-scaling result. Caution should be used when using high order perturbation theory at flavor physics scales for moments of heavy quarks correlators and truncation errors should not be underestimated.

Zusammenfassung

Im Rahmen der Teilchenphysik war die Entwicklung einer Vielzahl von Rechentechniken notwendig, um die hochkomplexen Probleme zu lösen, die durch wechselwirkende Quantenfeldtheorien entstehen. Störungstheoretische Entwicklungen in einer schwachen Kopplung – mit ihrer bekannten grafischen Darstellung durch *Feynman-Diagramme* – waren extrem erfolgreich und brachten uns zu unserem heutigen Verständnis der Hochenergiephysik. Sie sind auch heute noch von zentraler Bedeutung. Allerdings werden zusätzlich Methoden benötigt, die auf stark gekoppelte, nicht-störungsbehaftete Systeme anwendbar sind, um unser Wissen zu ergänzen. Die wohl wichtigste Feldtheorie, in der beide Methoden benötigt werden, ist die *Quantenchromodynamik* (QCD), deren Kopplung aufgrund von *Renormierungseffekten* mit der Energie abnimmt und die bei asymptotisch hohen Energien nicht mehr wechselwirkt. Andererseits müssen die Eigenschaften mesonischer und baryonischer gebundener Zustände bei niedriger Energie – zu denen Eigenschaften wie die Massen von Protonen und Neutronen gehören – mit Hilfe von nicht-perturbative Berechnungen untersucht werden.

Die Diskretisierung der Raumzeit auf einem regelmäßigen Gitter und die Simulation der QCD auf Supercomputern hat sich zu einem sehr erfolgreichen Verfahren entwickelt, um diese nicht-perturbativen Berechnungen ausgehend von Grundprinzipien durchzuführen. In dieser Arbeit untersuchen wir im Detail die Zeit-Momente schwerer Quark-Korrelatoren mit hoher Präzision. Diese Momente werden in der Literatur verwendet, um die QCD-Kopplung α_S (sowie die Massen der charm- und bottom-Quarks) durch den Vergleich von Gitter- und Störungsberechnungen zu extrahieren. Dieses Verfahren erfordert, dass diese Observablen von Energien dominiert werden, bei denen beide Methoden angewendet werden können. Die mit Gitterrechnungen erreichbaren Skalen werden in der Praxis durch einen Impuls-Cutoff in der Größenordnung des inversen Gitterabstandes a^{-1} nach oben hin begrenzt. Diese *Diskretisierungseffekte* nehmen zu, wenn man die Observablen bei höheren Energien berechnet. Gleichzeitig enthält die Störungstheorie aufgrund der unbekannten Terme höherer Ordnung einen Trunkierungsfehler. Wenn die ersten n Terme der Reihe bekannt sind, ist ein Fehler der Ordnung $\mathcal{O}(\alpha_S^{n+1})$ unvermeidlich, und dieser Fehler nimmt mit abnehmender Energie zu. Somit bleibt ein Fenster von Energien übrig, in dem die Momente-Methode funktionieren kann. Eine genaue Abschätzung ihrer systematischen Unsicherheiten ist notwendig, da diese sich direkt in zahlreichen Berechnungen der Teilchenphysik auswirken, wie z.B. Higgs-Zerfälle zu b-Quarks oder Gluonen, Z-Bosonen-Partialbreiten, und auch Auswirkungen auf Themen wie die elektroschwache Vakuumstabilität haben.

Wir führen eine sog. *quenched* Untersuchung der Zeitmomente durch, bei der der Effekt der

dynamischen Quarks vernachlässigt wird, und wir argumentieren, dass dies gute quantitative (oder annährende quantitative) Informationen über den vollständig dynamischen Fall liefert. Dies ist von großem algorithmischen Vorteil und erlaubt es uns, Gitterabständen von bis zu $a \sim 0.01$ fm zu erreichen. Diese Präzision ist derzeit in unserem Setup für die vollständige QCD in großen Volumen nicht erreichbar. Wir simulieren $L^3 \times T \sim (2\,\mathrm{fm})^3 \times 6\,\mathrm{fm}$ Volumen und setzen offene Randbedingungen in der Zeit ein, um das Problem des topologischen Einfrierens zu vermeiden, das bei feinen Gitterabständen auftritt. Wir berechnen Momente für verschiedene Energien μ von $0.8\,m_{\mathrm{charm}} \lesssim \mu \lesssim 3.5\,m_{\mathrm{charm}}$, was uns erlaubt, die Veränderung der Kopplung und des Trunkierungsfehler dieser Observablen bei wechselnder Energie zu untersuchen. Um die großen Diskretisierungseffekte zu kontrollieren, verwenden wir ein nicht-perturbativ verbessertes Wilson-Clover-Fermionen-Dublett mit einem twisted mass Term, der auf maximalen twist eingestellt ist. Die in der Zweipunktfunktion auftretenden Operatoren werden als pseudoskalare Dichten gewählt, um das Auftreten expliziter Renormierungsfaktoren zu vermeiden und um ein geringes statistisches Rauschen zu erhalten, das aus der numerischen Markov-Ketten-Monte-Carlo-Integration stammt. Neben der Kopplung untersuchen wir auch ihren Verlauf bis zur unendlichen Energie, kodiert im Λ-Parameter, und die darin enthaltenen Trunkierungsfehler.

Momente in der Zeit-Impuls-Darstellung sind als Zeitintegrale des mit t^n gewichteten Korrelators definiert. Niedrigere Momente sind perturbativer als höhere, jedoch für $n = 4$ gibt es große Diskretisierungseffekte, die es erforderlich machten ein spezielles Verfahren zu entwickeln. Dieses ist derzeit noch in der Weiterentwicklung und es wird ermöglichen, zuverlässig in das Kontinuum zu extrapolieren. Aus den Quotienten höherer Momente, mit $n = 6, 8, 10$, konnten wir akzeptable Kontinuumsgrenzwertschätzungen erhalten.

Unsere Ergebnisse, die auf den Quotienten der Momente R_6/R_8 und R_8/R_{10} beruhen, zeigen, dass der extrahierte Λ-Parameter bei Energieskalen von $\mu \sim 2m_{\mathrm{charm}} \simeq 2.5$ GeV (im $\overline{\mathrm{MS}}$-Schema) in Bezug auf das neueste step-scaling Ergebnis beträchtliche Abweichungen in der Größenordnung von 5% bis 10% – abhängig von der Observable – aufweist. Eine Extrapolation bis $\alpha_S \to 0$ ist möglich, allerdings mit einer beträchtlichen Steigung. Diese Extrapolationen beinhalten weder höhere Ordnungen in α_S noch Potenzkorrekturen. Darüber hinaus scheinen Variationen der perturbativen Renormierungsskala zur Abschätzung des Trunkierungsfehlers, die in der Literatur weit verbreitet sind und als "sichere" und konservative Schätzung gelten, im Fall der Momente definitiv die tatsächliche Größe der Fehler zu unterschätzen. Schließlich stellen wir fest, dass die oben erwähnte Abweichung – die in der Steigung bei der $\alpha_S \to 0$ Extrapolation kodiert ist – für R_8/R_{10} erwartungsgemäß größer ist.

Es ergibt sich ein recht düsteres Bild: Die weniger störungsbehaftete Observable R_8/R_{10} (die eine langsamere Konvergenz aufweist) liegt näher an den bekannten Werten, während die stärker störungsbehaftete Observable R_6/R_8 (die eine bessere Konvergenz aufweist) weiter von ihnen entfernt zu sein scheint. In der Tat ist diese Studie leider nicht in der Lage die kürzlich aufgetretenen Spannungen zwischen früheren gequenchten Ergebnissen und dem oben erwähnten neuesten step-scaling Ergebnis zu lösen. Bei der Verwendung der Störungstheorie hoher Ordnung auf den Skalen der Flavor-Physik für die Momente der Korrelatoren schwerer Quarks ist Vorsicht geboten, da große Trunkierungsfehler auftreten können.

Contents

1 | Introduction

MUCH time has passed since Einstein's famous "annus mirabilis" 1905, during which he laid the interpretative ground stone of what would later become two of the main disciplines of contemporary theoretical physics: quantum mechanics and special relativity. Over the past century the key ideas underlying these two theories have been of central importance in building up what is now our understanding of particle physics. The theoretical effort and workforce necessary to understand how to explain microscopic phenomena starting off from these two foundational theories was enormous. A historical perspective is by no means within the scope of the current thesis, here we will only mention briefly the conclusion of said effort, namely the development of quantum field theory and especially of gauge theories. In modern language the fundamental entities governing the microscopic world are relativistic fields which obey the principles of quantum mechanics. It becomes necessary to consider fields with infinite degrees of freedom to account for phenomena such as particle creation and annihilation. These fields permeate spacetime and their localized excitations are what one calls particles. In trying to understand several microscopic phenomena related to light, nuclei, and radioactivity it was slowly understood what the appropriate theories at the scale of the particle world were, which today are summarized by the *standard model of particle physics* (SM). In terms of this theory, a dazzling amount of properties can be computed to unprecedented accuracy within science.

The standard model of particle physics will be very briefly described in the next section, for now let us mention much of its conceptual basis has been known for several decades, oftentimes by gaining insight through the use of perturbative techniques. Nowadays, particle physics, both in its theoretical and experimental incarnation, has become a mature field which longs for high precision results in the search for deviations from the SM. Much of the progress during the last decades has been possible not only thanks to the stunning theoretical, experimental, and mathematical advances, but also because of the advent of ever-growing computational resources.

It is within this context that the core of this thesis lies. Large scale simulations on supercomputers have been carried out to study numerically physics of non-perturbative nature, namely the strong coupling regime of *quantum chromodynamics* (QCD), one of the fundamental gauge theories within the SM. One specific method for computing quantum chromodynamics' coupling α_S (also called the *strong coupling*), which we will refer to as the *moments method*, has been thoroughly studied to high accuracy in order to understand its precision and limitations.

1.1. THE STANDARD MODEL OF PARTICLE PHYSICS

1.1.1. Content of the Theory

The key ideas underlying the SM are the usage of quantized field theory and of gauge symmetry. Here we will only sketch some features of the latter, necessary for following discussions. The relevant symmetries are expressed in terms of Lie groups of local transformations[I]. Each of these *gauge* symmetry transformations is associated to an interaction, i.e. to a gauge field following Bose-Einstein statistics. They act on the scalar Higgs boson [85] and on matter fields, which follow Fermi-Dirac statistics. Three symmetries are at play, collectively denoted

$$\mathscr{G}_{\mathrm{SM}} = SU(3) \otimes SU(2) \otimes U(1)\,, \tag{1.1}$$

which are associated, respectively, to the strong, the weak and the electromagnetic force[II]. The Lie algebra valued vector potentials generating the groups are the bosonic gauge fields. A very large part of particle physics consists in studying observables which are gauge invariant, since these symmetries entail a redundancy in the description, but where one needs to *fix the gauge* at intermediate steps of the computation in order to apply the most widespread technique: perturbation theory. We will see later that it is not necessary to go through gauge fixing or even to use the Lie Algebra valued gauge potential $A_\mu(x)$, since the lattice formulation of QCD will be explicitly gauge invariant and written in terms of Lie *group* variables. The matter fields encompassed by the SM come in three *generations*, as is necessary for the anomaly cancellation of theories where both gauge invariance and coupling of gauge bosons to chiral currents are required [73]. Each generation contains *leptons*, consisting of electron (e), muon (μ), and tau (τ), each with a neutrino (ν) associated to them, and quark doublets, given by

$$Q = \begin{pmatrix} u \\ d \end{pmatrix}, \begin{pmatrix} c \\ s \end{pmatrix}, \begin{pmatrix} t \\ b \end{pmatrix}. \tag{1.2}$$

Here we will not go into the details of the handedness and the related multiplet structure in which these fields appear within the SM.

All the matter fields interact weakly, all but the neutrino have electrical charge, and the quark fields are distinguished due to their strong interaction. Moreover, due to the non-Abelian nature of the gauge group, also interaction between different bosons is possible, as we will see in detail in the case of QCD. In fig. 1.1 all SM interactions are represented by blue lines connecting the different fields/particles, represented by darker blobs. Finally, let us mention for completeness the last piece of the puzzle, namely the Higgs boson, the only scalar present in the SM. Beyond its self-interaction, it interacts with non-neutrino leptons, with quarks, and with weak bosons, thereby making them massive through the

[I] We refer to standard literature, such as [70].

[II] This distinction is somewhat superficial and sloppy, for the sake of exposition. Note that in order to distinguish weak and electromagnetic forces, one first needs to spontaneously break – in a gauge fixed language – $SU(2) \otimes U(1) \to U(1)_{em}$ through a non-zero Higgs field vacuum expectation value, a phenomenon associated to the mass generation and for which we refer to standard QFT literature such as [136].

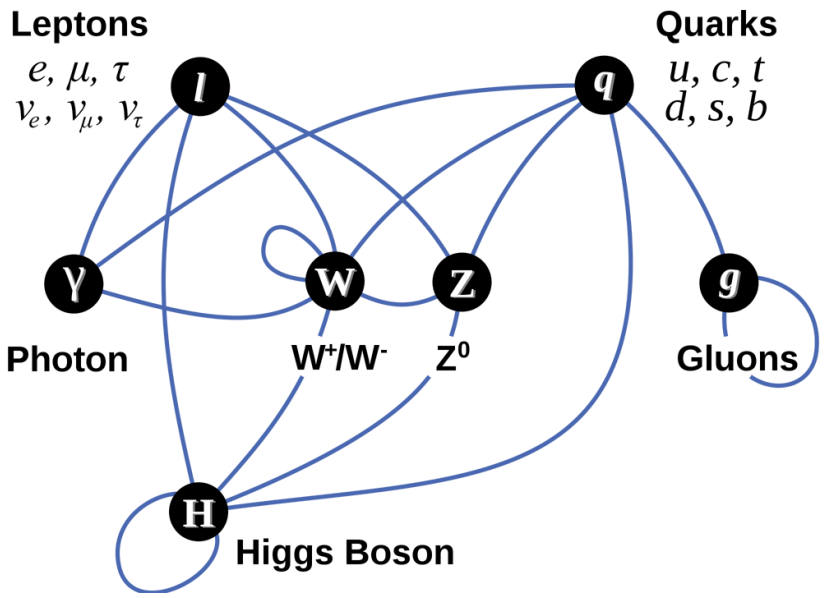

Figure 1.1: *Different fields are represented by black blobs, while the blue line connecting two of them represents the possibility of interacting at lowest order within the Standard Model. Image taken from [161].*

celebrated Higgs mechanism, unfolding during electroweak symmetry breaking [158, 85].

1.1.2. The Necessity for Renormalization

Observables in quantum field theory are expressed as expectation values of operators, with a given set of quantum numbers, acting on an infinite dimensional Hilbert space $\mathscr{H}$ of states. In these expectation values one sums over all possible field configurations leading, in Fourier space, to integrals which are oftentimes divergent. For instance, in *quantum electrodynamics* (QED)[III], the 1 loop perturbative correction to the photon propagator with momentum p – chosen here for its similarity to the central observable we analyze in this thesis, namely the (scalar) vacuum polarization defined in eq. (2.1) – is

$$\widetilde{\Pi}^{(1\mathrm{L})}_{\mu\nu}(p,m) = \int \langle 0|\, \mathscr{T}\left\{A^{\mathrm{int}}_{\mu}(x)A^{\mathrm{int}}_{\nu}(y)\right\}|0\rangle\, e^{i(x-y)\cdot p}\, \mathrm{d}^4(x-y)\Big|_{1L} =$$

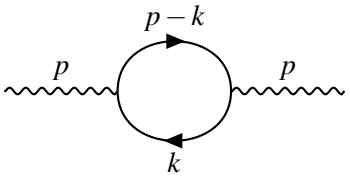

where the photon fields are in the interacting theory and we are here considering contributions at leading order. The details are unimportant at this stage, what we want to stress here is the following: this diagram has a diverging behavior for large k, or, more precisely, for $k/m, k/p \gg 1$ one has

$$\widetilde{\Pi}^{(1\mathrm{L})}_{\mu\nu}(p,m) \propto \int_{-\infty}^{\infty} \mathrm{tr}\left\{\frac{\gamma_\rho k_\rho + m}{k^2+m^2}\gamma^\nu \frac{\gamma_\rho (p-k)_\rho + m}{(p-k)^2}\gamma^\mu\right\} \mathrm{d}^4k \underset{k\gg 1}{\sim} \int_0^\infty k\cdot f(m,p)\,\mathrm{d}k\,, \qquad (1.3)$$

[III] As is usual also for perturbative computations, we use here Euclidean signature.

which contains an *ultraviolet* divergence for large momentum k. To obtain eq. (1.3) we simply naively counted the powers of k appearing, i.e. k^2 in the numerator, k^4 in the denominator, and a k^3 factor from the integration measure when switching to spherical coordinates. In order to make sense of this, one *needs to regularize* the integral, i.e. introduce some extra small parameter making the integral finite. The lattice discretization cuts the propagation of momenta above $\sim a^{-1}$ off, but also an arbitrary (complex) number of dimensions $d = 4 - \varepsilon$, typical of dimensional regularization [88], acts as a regulator. Integrating only up to said cutoff $\Lambda = \pi/a$, one obtains

$$\int_0^\Lambda k \cdot f(m,p)\,\mathrm{d}k \sim \Lambda^2 F(p,m)\,, \tag{1.4}$$

which clearly diverges in the limit $a \to 0$, $\Lambda \to \infty$. The key idea is to then reparametrize the Lagrangian so that couplings in it (masses included) are tied to some physical, finite quantity accessible experimentally, a procedure known as *renormalization* of the theory. One obtains finite integrals upon removal of the regulator at constant renormalized couplings; these can be both physical, taken from experimental input, or un-physical, which are still finite at zero regulator, but are not observables. For instance, in perturbative expansions renormalization requires the introduction of a further unphysical *renormalization scale* μ, on which observables cannot depend, so that (renormalized) Lagrangian parameters that do *are not physical, measurable quantities*, as in the case of the popular $\overline{\text{MS}}$-schemes [88].

Divergences as the ones presented are unavoidable in a quantum mechanical setting, where integrals over all momenta are present, both perturbatively and not. We discuss further details and implications of renormalization directly in the lattice setup in Chapter 3.

1.1.3. Perturbative vs Non-Perturbative

Several successful computations in QFT which have shed light into previously not understood phenomena have been carried out in perturbation theory (PT), i.e. as expansions in the small coupling. An expectation value computed via a path integral [59], where interactions are proportional to some coupling α of the action $\mathscr{S}$, has the form

$$\langle \mathscr{O}[\Phi] \rangle = \mathscr{Z}^{-1} \int_\Phi \mathrm{D}[\Phi]\mathscr{O}[\Phi] \exp\left\{ i\mathscr{S}_{\text{free}}[\Phi] + i\mathscr{S}_{\text{int}}[\Phi;\alpha] \right\}, \tag{1.5}$$

where Φ collectively denotes all possible fields in the theory and $\mathscr{Z}$ its partition function. The measure $\mathrm{D}[\Phi]$ remains unspecified at this point, but let us mention analogously to the standard quantum mechanics path integral, where one is summing over all possible trajectories, in QFT one is summing over all possible field configurations – or quantum fluctuations – with a weight given by the action in the exponential: the minimum of $\mathscr{S}$ corresponds to dominating contribution, the classical configuration. In PT one expands the action in the path integral around the trivial, non-interacting theory, treating interactions as small perturbations. This is realized by "taking down" fields present in the interacting Lagrangian from the exponential and, order by order, inserting them into the operator product $\mathscr{O}[\Phi]$. Today weak coupling expansions remain a crucial aspect of almost all QFT studies, while it has become

possible to explore the strong coupling regime, too, where perturbative computations are not feasible.

A key characteristic of renormalization is, indeed, the dependence of the renormalized coupling on a scale μ, leading to the name of a "running coupling" $\alpha(\mu)$. Whether a given theory possesses a weak coupling regime and for what values of μ is thus a question of central importance. QED processes of interest in particle physics are dominated by scales at which the coupling is weak. How it changes with energy is encoded in the $\beta_{\text{QED}}(\alpha_{\text{QED}})$-function, defined by

$$\beta_{\text{QED}}(\alpha_{\text{QED}}) = \mu \frac{\mathrm{d}}{\mathrm{d}\mu} \alpha_{\text{QED}}(\mu)\Big|_{\alpha_{\text{bare}}} \overset{\alpha_{\text{QED}}\to 0}{\sim} \beta_0\, \alpha^2_{\text{QED}}(\mu) + \beta_1\, \alpha^3_{\text{QED}}(\mu) + \mathscr{O}(\alpha^4_{\text{QED}}(\mu))\,, \tag{1.6}$$

where the coefficients $\{\beta_i\}$ can be calculated in PT. The first two turn out to be positive [68], hence $\alpha_{\text{QED}}(\mu)$ grows with energy. This phenomenon was historically called *screening*, since it appears the (for instance, electron) charge becomes less and less screened through a sort of *vacuum polarization* when going to larger distances, a purely quantum relativistic effect. We stress here this picture is heuristic and mostly used for illustration and historical purposes, since the charge is not a measurable, physical observable. Eventually the QED coupling diverges[IV], if no other mechanism is considered, a phenomenon labeled *Landau pole* [101, 100, 99].

On the other hand, QCD has an exactly opposite behavior, known as asymptotic freedom [74, 140] (or, in analogy with QED, at times referred to as *anti-screening*), where the high energy regime is weakly coupled and the coupling grows with *decreasing* energy, due to the negative coefficients in the β-function $\beta_0 < 0, \beta_1 < 0$. A Landau pole alike problem is avoided completely through the (widely accepted, yet formally unproven) assumption of *color confinement*, which claims only "colorless" or $SU(3)$ neutral states are allowed.

1.2. QUANTUM CHROMODYNAMICS

Quantum chromodynamics is the quantum field theory describing interactions between fields charged under $SU(3)$, the three charges appearing named colors. As usual, the starting point for defining a field theory is its Lagrangian density (or, equivalently, its integral over spacetime, the action) given by

$$\mathscr{L}_{\text{QCD}}(x) = \frac{1}{4g^2} F^a_{\mu\nu}(x) F^a_{\mu\nu}(x) + \sum_{i=1}^{N_f} \overline{\psi}_i(x) \left(\not{D}(x) + m_i\right) \psi_i(x), \tag{1.7}$$

with Euclidean signature and where we define the *field strength tensor* $F^a_{\mu\nu}(x)$[V] and the *covariant derivative* $D_\mu(x)$ by

$$\begin{cases} F^a_{\mu\nu}(x) = \partial_\mu A^a_\nu(x) - \partial_\nu A^a_\mu(x) + f^{abc} A^b_\mu(x) A^c_\nu(x) \\ \not{D}(x) = \gamma^\mu D_\mu(x) = \gamma^\mu \left(\partial_\mu + i A_\mu(x)\right) \end{cases}, \tag{1.8}$$

[IV] Note this effect is of great theoretical, but little practical relevance, since the problematic energies are out of reach by many orders of magnitude.

[V] We choose a widespread convention in the lattice field theory literature where $D_\mu(x)$ contains no coupling constant whereas the pure gauge term has an explicit $1/g^2$; a trivial rescaling of the fields $A_\mu \to gA_\mu$ yields the more known standard QFT textbook convention.

f^{abc} being the structure constants[VI] of $\mathfrak{su}(3)$, the Lie algebra of the Lie group $SU(3)$. If they do not vanish, as in the case of non-Abelian (i.e. non-commutative) groups, the presence of two $F_{\mu\nu}(x)$ factors in eq. (1.7) yields terms with three and four vector potentials. In a perturbatively expanded QCD path integral, this leads to 3-gluon and 4-gluon vertices, unlike in the case of Abelian field theories such as QED, where the only interaction is between fermions and gauge bosons. In order for the Lagrangian density to be invariant for a local (i.e. spacetime dependent) transformation $\Omega(x) \in SU(3)$ of the fermion fields, the following need be true

$$\psi(x) \longrightarrow \psi'(x) = \Omega(x)\psi(x)\,, \tag{1.12}$$

$$\overline{\psi}(x) \longrightarrow \overline{\psi}'(x) = \overline{\psi}(x)\Omega^{\dagger}(x)\,, \tag{1.13}$$

$$A_\mu(x) \longrightarrow A'_\mu(x) = \Omega(x)A_\mu(x)\,\Omega^{\dagger}(x) + \big(\partial_\mu\Omega(x)\big)\,\Omega^{\dagger}(x)\,. \tag{1.14}$$

In eq. (1.2) we saw the number of quarks present in nature to be $N_f = 6$. Yet, their widely different masses – although remaining an open problem referred to as (quark) *mass hierarchy problem* – conveniently allows for different simplifications and approximations, depending on the physics of interest. Thanks to the decoupling of heavy fields [7] with mass m_h, at some energy $E \ll m_h$ corrections in massive renormalization schemes are suppressed by powers of E/m_h. For any study at hadronic energies the top quark, with its mass of $m_t \simeq 173$ GeV, is clearly irrelevant, as is the case also for the bottom quark (beyond its possible presence in the valence). This is obtainable in (unphysical) mass-independent schemes, too, where decoupling is equivalent to the matching of theories with different numbers of quarks at their mass thresholds. This introduces some caveats, since across thresholds the β-function changes [159, 19]. We will describe more the QCD β-function in Section 2.5, for now let us only mention it is known in the $\overline{\text{MS}}$ scheme to 5 loops [11, 106, 83, 105] and the mentioned matching conditions between the $N_f - 1$ and N_f theory are known to 4 loops [146, 41]. Recent numerical studies convincingly show that the perturbative matching of charm quarks [8] has a very small effect despite their rather low mass, and is thus under control at the current target precision. In this way, one can conveniently study a, say, $N_f = 3$ setup and run to infinite energy while perturbatively matching at each threshold.

Thus, QCD with its two key mechanisms of asymptotic freedom and confinement can be regarded as a fundamental theory, consistent and valid at all scales. For energies of $\mathcal{O}(10)$ GeV to $\mathcal{O}(200)$ GeV and above (explored for instance at LHC), many QCD computations can be carried out in PT, with remaining issues being, for instance, the appearance of multiple logs if multiple scales are present

[VI] Our convention for $SU(N)$ is that of antihermitean group generators. Given

$$A_\mu(x) = \sum_{a=1}^{N^2-1} T^a A^a_\mu(x)\,, \quad \text{one has} \tag{1.9}$$

$$[T_a\,,T_b] = -\,i\,f_{abc}T_c\,, \quad \text{tr}\{T_a\,T_b\} = -\frac{1}{2}\delta_{ab}\,. \tag{1.10}$$

Also, let us mention from Minkowskian to Euclidean spacetime anti-commutation relations of the γ-matrices change

$$\{\gamma_\mu\,,\gamma_\nu\} = 2g_{\mu\nu}\mathbb{1}_{\text{spin}} \longrightarrow \{\gamma_\mu\,,\gamma_\nu\} = 2\delta_{\mu\nu}\mathbb{1}_{\text{spin}}\,, \tag{1.11}$$

where we used the mostly minus convention for the metric tensor components.

in the problem, and hadronization [141, 66] effects which need to be taken account via modeling when comparing to experiment. Moreover, PT is unfit for a thorough treatment of the crucially important lower energies, which are the natural scale of QCD bound states. The hadronic regime of, say, $\mathcal{O}(0.2)\,\text{GeV}$ to $\mathcal{O}(2)\,\text{GeV}$ is characterized by a large coupling, the exact size of which depends on the renormalization scheme. To cite an example, in [31] at $\mu \approx 0.5\,\text{GeV}$ a value of $\alpha \approx 1.3$ was found, so that the necessity of non-perturbative techniques becomes evident. The tools employed herein are those of lattice QCD, with which ab-initio calculations in the low energy regime are possible and which delivered in the past abundant numerical evidence of QCD being valid at all scales. To conclude, let us mention that small coupling does not automatically imply PT is safe to use, as we explain thoroughly in Section 2.2.

1.3. MOTIVATION: α_S IS A FUNDAMENTAL PARAMETER

The SM contains several fundamental parameters that can only be extracted from comparison with experimental data. These are inputs to theoretical computations, so that they can be determined from a set of relations of the form

$$\mathcal{O}_i^{\text{exp}} = \mathcal{O}_i^{\text{th}}\left(\vec{b}\right), \quad \text{where} \quad \vec{b} = (b_1, b_2, \ldots, b_N), \quad i = 1, 2, \ldots, N, \tag{1.15}$$

where $\vec{b}$ are N generic input parameters. Let us suppose we have some way of computing the N functions $\mathcal{O}_i^{\text{th}}(\vec{b})$ to a desired level of accuracy for some input $\vec{b}$, as well as a measurement of all N experimental quantities $\mathcal{O}_i^{\text{exp}}$. Once this set of equations is solved for $\vec{b}$, the fundamental parameters have been computed; but as simple as this may seem, actually being able to both compute and measure such observables *with controlled errors* can be highly challenging.

In the case of pure QCD, the Lagrangian parameters are the renormalized coupling α_S and quark masses m_i, $i = 1, 2, \ldots, N_f = 6$, for a total of $N_f + 1 = 7$. In principle, one way to determine them is choosing some renormalization scheme X and giving perturbative estimates of $\mathcal{O}_i^{\text{th}}(\vec{b}_X)$, to then obtain $\vec{b}_X$ via eq. (1.15). Let us stress in this way any component of $\vec{b}_X$ is only known to the order of the perturbative expansion used to determine it, which we may call L, so that an intrinsic *truncation error* of order $\mathcal{O}(\alpha^{L+1})$ is present.

What is done on the lattice, instead, is employing some hadronic quantities – typical choices being hadron masses and decay constants, one for the overall scale and N_f sensitive to a specific quark's mass – which possess the key property of being computable with moderate numerical effort and reasonable statistical uncertainty. The bare parameters of the lattice theory are tuned in order to reproduce these $N_f + 1$ observable quantities[VII]. Then, after tuning $N_f + 1$ parameters, *all further dimensionless ratios are a prediction of the theory*. Once the lattice setup is appropriately tuned, one can compute any other observable and turn eq. (1.15) around: $\mathcal{O}_i^{\text{exp}}$ may be replaced with lattice results and, by comparing to the perturbative expression of $\mathcal{O}_i^{\text{th}}$, used to extract $\vec{b}_X$. The only experimental input is then the one

[VII] To be more precise, once an overall scale of mass dimension one is defined, what one tunes is the ratio of the remaining N_f mass parameters with it. The scale we actually employ, t_0, is introduced in Subsection 3.3.1, whereas how we tune the mass of the heavy quark is explained in detail in Chapter 5.

utilized for the lattice parameters' precise tuning, which has the advantage of being obtained from independent dedicated studies.

Herein, we will be mostly concerned with determinations of the coupling. Note that the comparison of lattice and PT results also bypasses issues such as the complicated hadronization corrections [141, 66].

Schemes and Impact In the case of a well defined, finite, dimensionless observable depending on one scale q only, it is possible to define a non-perturbative coupling as follows. Indicating some physical – thus automatically gauge invariant, too – observable with $\mathscr{B}$, in PT in an unspecified mass-less scheme X one has

$$\mathscr{B}(q) \overset{\mu\to\infty}{\sim} \sum_{k=0}^{L} p^{(k)}(s)\,\alpha_X^k(\mu) + \mathscr{O}(\alpha_X^{L+1}) + \mathscr{O}\left(\frac{1}{q^\delta}\right), \quad q = s\mu\,, \quad \delta > 0\,, \tag{1.16}$$

where $p^{(1)}$ can be shown to be a pure constant (see footnote I in Subsection 6.1.5) and we allow for a scale factor s (more about s is explained in Section 2.2). The above suggests the conventionally used normalization

$$\alpha_{\mathscr{B}}(q) \overset{\text{def.}}{=} \frac{\mathscr{B}(q) - p^{(0)}}{p^{(1)}} \overset{\mu\to\infty}{\sim} \alpha_X(\mu)\left\{1 + \frac{p^{(2)}(s)}{p^{(1)}}\alpha_X(\mu) + \mathscr{O}(\alpha^2)\right\} + \mathscr{O}(q^{-\delta})\,, \tag{1.17}$$

where the subscript $\mathscr{B}$ labels this non-perturbative renormalization scheme. Note the above coupling definition is non-perturbative and thus valid also at low energies, whereas the relation to the X-scheme is valid only for high enough energies $\mu \to \infty$ and if $\mathscr{B}$ is a pure short distance object. The hard-to-estimate [122] terms $q^{-\delta}$ are so called *power corrections*, which decrease faster than any polynomial in α for decreasing coupling. Still, avoiding too low energies where PT error estimates are unreliable, as well as avoiding fits (or removal) of non-perturbative power corrections with complicated data-driven analyses can help in limiting the introduction of uncontrolled errors.

Since high precision is required in several particle physics computations, it is of great importance to obtain these fundamental parameters with multiple, independent methods, possibly with distinct systematic uncertainties and at different scales. In these kind of endeavors it is customary to express the QCD parameters in terms of the $\overline{\text{MS}}$-scheme ones, since these are of widespread use in perturbation theory, and to quote the coupling at the Z-boson pole-mass (fig. 1.2) [165].

Several particle physics problems, even beyond pure QCD ones, depend considerably on the precise value for the strong coupling. For any cross section or even decay rate depending on some power of the coupling, the parametric uncertainty on it may play a relevant role at the current levels of precision; note the majority of processes measured at LHC enter in this category. Among the most important ones we cite (see also [60]) the partial widths $H \to b\bar{b}$ [12], $H \to gg$ [1, 81], the gg-fusion and the related cross section for the generation of $t\bar{t}$ [4, 45], the hadronic Z-boson widths [81, 20]. It also plays a non-negligible role in top width, mass, and Yukawa-coupling computations [86], as well as having implications in studies about the electroweak vacuum stability [42].

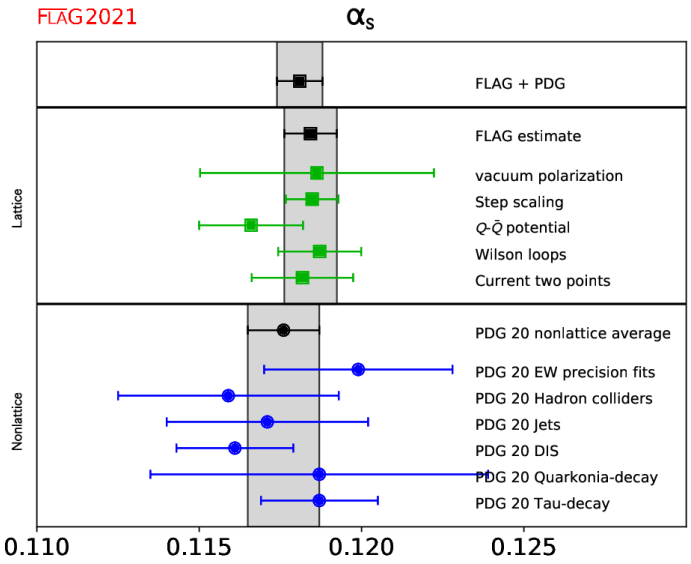

Figure 1.2: *Comparison of α_S values from lattice and non-lattice results, figure taken from [6]. The reported lattice computations are the ones that passed all the criteria stated from the FLAG working group.*

Objective of the Thesis: The precise knowledge of the strong coupling with controlled errors is of major importance for several aspects of particle physics. Lattice QCD computations nowadays play a central role in this endeavor. Multiple methods to extract the coupling, both on and off the lattice, act as non-trivial crosschecks, and here we will focus on the *moments method* ("current two points" in fig. 1.2). The main focus will be to analyze the main systematic errors within this method, namely the discretization effects originating from the discrete spacetime lattice and the truncation errors intrinsically present in perturbation theory. As we will explain in detail, the two are strongly tied to one another. Our goal herein is to precisely quantify these systematics and to gain a deeper understanding of the limitations and of the potential present in the moments method. In order to do so, we will study a simplified setting without any dynamical quarks – a great algorithmic advantage – and we will argue no fundamental difference is expected in scenarios containing dynamical quarks. Several high-precision lattice computations have been carried out as part of this project; these, together with high order perturbative computations present in literature, are used to compute the coupling at different scales. Our final goal and result is the coupling's scaling over a range of energies, which allows us to quantify the truncation error (and thus the asymptotic scaling with $\alpha_{\overline{\text{MS}}}(\mu)$ of the Λ_{RGI}-parameter extracted from moments).

The structure of the thesis is as follows:

Chapter 2 - We introduce moments and some of their properties in the continuum, focusing on how to extract fundamental parameters from them and on general aspects of perturbation theory.

Chapter 3 - Here we introduce the lattice discretization along with its main characteristics such as doubling, scale setting and unavoidable systematic errors. Finally, we speak about our own setup: twisted mass QCD at maximal twist.

Chapter 4 - First we explain how to simulate lattice gauge theories, what algorithms we used and how to carry out the statistical error analysis. Critical slowing down is also addressed. Then, we show two trivial, but nonetheless important, example computations of typical lattice observables: effective masses and decay constants.

Chapter 5 - We go into depth about our own simulations, starting from our ensembles, describing how input parameters are tuned and measurements carried out. We give an assessment of the errors committed during this procedure and show some results related to the tuning, such as quark current masses and renormalization factors.

Chapter 6 - In the key chapter of the thesis, we present our fundamental physical results: continuum extrapolations of moments, how to extract the coupling from them and finally the Λ-parameter and its scaling towards the asymptotic $\alpha \to 0$ region.

Chapter 7 - In the final chapter, we sum up our findings and comment what lessons can be learned from this project.

2 | Moments of Heavy Quark Correlators

THE main observables of interest in this thesis are moments of heavy quark correlators, which have been computed up to $\mathcal{O}(\alpha^3)$ in perturbation theory [39, 40, 38, 120, 153, 121]. These observables can then be computed on the lattice as well and from a comparison of the two computations, the strong coupling and the heavy quark mass can be extracted. "Heavy" quarks refers to masses from the order of the charm to that of the bottom quark mass, and possibly even beyond. This procedure, however, contains systematic errors both on the lattice and on the perturbative side, the most important ones being, respectively, finite lattice spacing effects and truncation errors. These need both to be studied and understood with care. For now, we start by defining these observables in continuum QCD and by explaining some of their key properties.

2.1. Definition

Let us define the polarization function of a two-quark operator $J(x)$ in Minkowski spacetime as

$$\widetilde{\Pi}(q^2, m_h) = i \int \mathrm{d}^4x \, e^{iq\cdot x} \langle 0| \mathscr{T} \left\{ J^\dagger(x) J(0) \right\} |0\rangle \,, \tag{2.1}$$

where we denote by $\mathscr{T}$ the time ordering symbol, by q^2 the (Minkowskian) norm squared of the external four-momentum q and by m_h the "heavy" mass of the fields appearing in $J(x)$. If the two-quark operator is $J_\mu(x) = \overline{\psi}(x)\gamma_\mu\psi(x)$, this is the standard textbook vacuum polarization of some vector field. The observable defined in eq. (2.1) contains two relevant energy scales only, namely m_h and q^2, since $m_h \gg \Lambda_{\mathrm{RGI}}$ and $m_h \gg m_l$, where Λ_{RGI} is an intrinsic QCD scale discussed later (Section 2.5), and where m_l is the light quark mass, set to zero in perturbation theory[I]. There are three different kinematical regimes [97] in which perturbative computations can be carried out: (1) the low energy region $q^2/4m_h^2 \ll 1$, (2) the (Euclidean) high energy region $-q^2/4m_h^2 \gg 1$, and (3) the quark pair production threshold $q^2 \simeq 4m_h^2$, which can be understood as an expansion in small velocity of the heavy quark. Throughout this thesis we will study moments of eq. (2.1) related to the low energy region (1), in the case of the pseudoscalar density

$$J(x; m_h) = i m_h \overline{\psi}_h(x) \gamma_5 \psi_{h'}(x) \,, \tag{2.2}$$

[I] Other even heavier fields, such as top quarks, have masses far above m_h and are effectively decoupled, see Section 1.2.

so that we will directly restrict the discussion to this observable. The extra m_h factor makes the operator J renormalization group invariant in chirally symmetric regularizations (or when a sufficient subset of chiral symmetry is present, see Subsection 3.5.2). Quark fields have a subscript h and h' in order to avoid contractions (in the sense of Wick's theorem [160]) of the field at the same spacetime point in eq. (2.1), in lattice jargon to avoid quark disconnected diagrams, which are unfit to be reliably computed in PT at large distances. A further motivation as to why we are interested in the pseudoscalar density is of computational nature and will be given in Chapter 4.

The small q^2 expansion of eq. (2.1) can be written like

$$\widetilde{\Pi}(q^2,m_h) = q^2\Pi(q^2,m_h) = q^2\frac{3m_h^2}{16\pi^2}\sum_{k>0} C_{2k+2}\, z^k\,, \quad z=\frac{q^2}{4m_h^2}\,, \tag{2.3}$$

with some coefficients C_{2k+2}. The moments $\mathscr{M}_{2k}$ are defined as

$$\mathscr{M}_{2k}(m_h) = \left[\frac{1}{k!}\left(\frac{\partial}{\partial q^2}\right)^k \widetilde{\Pi}(q^2,m_h)\right]_{q^2=0}\,, \tag{2.4}$$

namely derivatives of the polarization function w.r.t. the center of mass energy q^2, taken in the $q^2/4m_h^2 \to 0$ limit. There is only one leftover energy scale, the heavy quark mass, on which they can depend. They are related to the coefficients C_{2k} via

$$\mathscr{M}_{2k}(m_h) = \frac{3}{4\pi^2}\frac{m_h^{4-2k}}{2^{2k}} C_{2k}\,. \tag{2.5}$$

2.2. PERTURBATIVE EXPANSION AND TRUNCATION

The adimensional coefficients C_{2k} can expanded in powers of α_S in the (mass-independent) $\overline{\text{MS}}$-scheme

$$C_{2k} \overset{\alpha\to 0}{\sim} C_{2k}^{(0)} + \sum_{i=1}^{L} \alpha_{\overline{\text{MS}}}^i(\mu) \times \left\{ C_{2k}^{(i0)} + \sum_{j=1}^{i-1} C_{2k}^{(ij)} \log^j\left(\mu^2/\overline{m}^2_{\overline{\text{MS}}}(\mu)\right)\right\} + \mathscr{O}(\alpha^{L+1})\,, \tag{2.6}$$

where μ is the perturbation theory renormalization scale and $C_{2k}^{(i,j)}$ are numerical coefficients known for $1 \le i \le L = 3$ [121].

For later convenience let us define a scale factor s via

$$\mu_s \overset{\text{def.}}{=} s \times \overline{m}_{\overline{\text{MS}}}(\mu_s)\,, \tag{2.7}$$

so that (2.6) becomes

$$C_{2k} \overset{\alpha\to 0}{\sim} C_{2k}^{(0)} + \sum_{i=1}^{3} \alpha_{\overline{\text{MS}}}^i(\mu_s) \times \left\{ C_{2k}^{(i0)} + \sum_{j=1}^{i-1} C_{2k}^{(ij)} \log^j(s^2)\right\} + \mathscr{O}(\alpha^4)\,, \tag{2.8}$$

where a chosen value of s corresponds in a univocal way to a renormalization scale μ_s. For the choice $s=1$, one has $C_{2k}^{(ij)}\log^j(s^2) \equiv 0$ for $0 < j < i-1$, whereas the importance of the log-part changes

when $s \gg 1$ or $s \ll 1$. The special case $s = 1$ is labeled m_*

$$m_* \overset{\text{def.}}{=} \overline{m}_{\overline{\text{MS}}}(m_*)\,, \tag{2.9}$$

since it is used several times throughout this thesis. Note that no μ-dependence is written in C_{2k}, since in the r.h.s. of eq. (2.6) – at a given order – it cancels out, *up to higher terms in* $\alpha(\mu)$. Thus, in practice, quite an important, spurious μ-dependence is de facto introduced when the series is truncated.

Before commenting more on this, let us discuss the nature of the series in eq. (2.6). As most series in quantum field theory, it is an asymptotic series for the coupling $\alpha \to 0$ with zero radius of convergence. Divergent, asymptotic series can approximate functions with very good accuracy. In some instances, even few terms yield a very good approximation, especially if compared to convergent Taylor series with the same number of terms. However, being divergent, their nature is slightly different from a convergent series. The definition of an asymptotic series [15] for an observable $\mathscr{M}(\alpha)$, taken to be adimensional for convenience, is given by

$$\mathscr{M}(\alpha) \overset{\alpha\to 0}{\sim} \sum_{n=0}^{\infty} c_n(s)\,\alpha(\mu_s)^n \iff \lim_{\alpha\to 0}\left|\mathscr{M}(\alpha) - \sum_{n=0}^{N} c_n(s)\,\alpha(\mu_s)^n\right| = \mathscr{O}(\alpha^{N+1})\,, \quad \forall N < \infty\,, \tag{2.10}$$

i.e. for any finite, *fixed* N, the series will approximate $\mathscr{M}$ *in the limit* $\alpha \to 0$ with a given error $\mathscr{O}(\alpha^{N+1})$ due to the truncation. For any given N, there is a domain in α where the asymptotic series "behaves well", but it is not clear a priori what the applicability domain of these asymptotic expansions is. Conversely, at some fixed value of α where one notices the first few terms of the expansion to decrease and give thus an accurate result, one knows eventually adding more terms to the sum will make it diverge – the coefficients will increase in an uncontrolled manner.

If we now take eq. (2.8) for $s \ll 1$ or $s \gg 1$ it becomes clear the overall coefficient of α^i

$$C_{2k}^{(i)}(s) = C_{2k}^{(i,0)} + \sum_{j=1}^{i-1} C_{2k}^{(i,j)} \log^j\left(s^2\right)\,, \tag{2.11}$$

increases uncontrollably in size because of the $\log(s)$-term. This then spoils the above explained "good behavior" of the series, so that μ_s really needs to stay close to $\overline{m}_{\overline{\text{MS}}}(\mu_s)$, which sets the natural energy scale of the moment.

One way oftentimes used to assess the size of the truncated term is the following. Physical observables cannot depend on the unphysical renormalization scale μ, so there is a relation between how coefficients and α depend on μ. However, when truncating the series, we mentioned one is inevitably introducing a spurious μ dependence in the perturbative estimate of the observable. In an effort to evaluate this systematic error, one can compute the same observable at different values of s, and then take the spread of results as a further theoretical uncertainty. This procedure may be a good estimate in some situations, but it is not complete, since knowing $C_{2k}^{(L)}$ *does not mean having any knowledge about the non-log term* $C_{2k}^{(L+1,0)}$.

In table 2.1 we report the perturbation theory values of moments $\mathscr{R}_n^{PT}(z,\mu_s)$, evaluated at $s = 1$, for varying heavy quark mass (see Subsection 3.5.2 for unexplained notation, here it suffices to know:

they are properly normalized, adimensional observables built out of moments evaluated at some mass scale value $z = \sqrt{8t_0} M_{\rm RGI}$, where $M_{\rm RGI}$ is a heavy quark mass defined in eq. (2.33), and $\sqrt{t_0}$ is a scale in fermi used in lattice computations defined in eq. (3.24)). To give an idea of how different error assessments may vary considerably, for each value 3 different truncation error estimates are reported, (1) the difference between the last and the second-to-last known term for $s = 1$, (2) the scale variation $|\mathscr{R}_n^{PT}(z, 2m_*) - \mathscr{R}_n^{PT}(z, m_*)|$, and (3) the scale variation $|\mathscr{R}_n^{PT}(z, m_*) - \mathscr{R}_n^{PT}(z, m_*/2)|$. The general picture that emerges is the expected one, i.e. perturbative uncertainties increase at lower energies. The error estimate (1) always decreases with increasing n or decreasing z, whereas the scale variation is a bit more complicated. For $\mathscr{R}_4^{PT}$ and $\mathscr{R}_8^{PT}$ the variation below m_* is much more inaccurate than the one above it, whereas for $\mathscr{R}_6^{PT}$ the two are comparable. However, let us also mention that (as emphasized in the recent review [53] for the case of $N_f = 2+1$ moments), anomalously small coefficients may appear and may lead procedure (1) to estimate significantly smaller errors compared to the scale variation, procedure (2) and (3).

$m_*/\overline{m}_{\rm charm}$	z	$\mathscr{R}_4^{PT}(z, m_*)$	$\mathscr{R}_6^{PT}(z, m_*)$	$\mathscr{R}_8^{PT}(z, m_*)$
3.5	13.5	1.12053 (299)(150)(568)	1.04995 (208)(37)(19)	1.02292 (190)(5)(75)
2.5	9	1.13700 (437)(238)(1037)	1.05674 (297)(58)(35)	1.02619 (270)(8)(128)
1.6	6	1.15895 (677)(401)(2118)	1.06569 (444)(96)(72)	1.03056 (401)(13)(235)
1.2	4.5	1.17962 (966)(609)(3864)	1.07399 (612)(143)(130)	1.03464 (550)(19)(387)
0.8	3	1.22085 (1736)(1201)(1103)	1.09006 (1031)(273)(351)	1.04262 (915)(36)(873)

Table 2.1: *Comparison of perturbative error Ansätze. The moments themselves $\mathscr{R}_n^{PT}$ (defined in eqs. (3.63) and (3.64)) are computed at $\mu = m_*$ for each $z = \sqrt{8t_0} M_{RGI}$ or, equivalently, for each $m_*/\overline{m}_{charm}$ (z is exact, whereas for the latter a reference approximate value with no error is reported; note that this ratio is independent of the scheme). The three errors reported for each z in the second line are, respectively: (1) the difference between the 3 loop and 4 loop evaluated observable, for $s = 1$, (2) the scale variation $|\mathscr{R}_n(z, 2m_*) - \mathscr{R}_n(z, m_*)|$, and (3) the scale variation $|\mathscr{R}_n(z, m_*) - \mathscr{R}_n(z, m_*/2)|$.*

2.3. MOMENTS IN POSITION SPACE

The definition given in Section 2.1 is the starting point for all high order perturbative calculations. However, an equivalent, more convenient expression partially in position space is employed when we

compute the moments on the lattice. First, let us note that eq. (2.4) is completely equivalent to[II]

$$\mathscr{M}_n(m_h) = \left[\frac{1}{(n)!}\left(\frac{\partial}{\partial q}\right)^n \widetilde{\Pi}(q^2, m_h)\right]_{q=0}, \tag{2.12}$$

where $q = \sqrt{q_0^2 - \vec{q}^2}$. To explicitly see this, it suffices to apply the derivatives in the above definition to eq. (2.3). In (2.1) we now explicitly Wick-rotate to Euclidean spacetime, setting, without loss of generality, $q_\mu = q^\mu = (q_0, \vec{0})$ and obtaining

$$q_0^2\,\Pi(q_0^2, m_h) = \int_{-\infty}^{\infty} \mathrm{d}t\, \mathrm{e}^{itq_0} \int \mathrm{d}^3\vec{x}\, \left\langle J^\dagger(x; m_h) J(0; m_h)\right\rangle \overset{\text{def.}}{=} \int_{-\infty}^{\infty} \mathrm{d}t\, \mathrm{e}^{itq_0} G(t; m_h)\,, \tag{2.13}$$

with $J(x;m_h)$ as in eq. (2.2), where we indicate by $\langle\cdot\rangle$ the path integral representation of the two point function and we define $G(t; m_h)$ the resulting time-slice correlator. Since $\vec{q} = \vec{0}$, the spatial Fourier transform acts as a projection to zero spatial momentum. The q_0-derivatives will thus act on the exponential only and one gets

$$\begin{aligned}\mathscr{M}_n(m_h) &= \frac{1}{n!}\left(\frac{\partial}{\partial(iq_0)}\right)^n (iq_0)^2\, \widetilde{\Pi}\left((iq_0)^2; m_h\right)\Big|_{q_0=0} \\ &= \frac{1}{n!}\left\{\left(\frac{\partial}{\partial(iq_0)}\right)^n \int_{-\infty}^{\infty} \mathrm{d}t\, \mathrm{e}^{itq_0} G(t; m_h)\right\}\Big|_{q_0=0} = \frac{1}{n!}\int_{-\infty}^{\infty} \mathrm{d}t\, t^n G(t; m_h)\,,\end{aligned} \tag{2.14}$$

which we will use, in its discretized version, for lattice computations.

In eq. (2.14) one can perform an *operator product expansion* (OPE) of the currents' product, where the leading term's divergence is given from simple power counting. Evaluating this at tree-level PT one gets

$$J^\dagger(x; m_h) J(0; m_h) \overset{|x|\to 0}{\sim} \frac{\mathbb{1}}{|x|^6}\left(c_0 + \sum_{d>0} c_d\, |x|^d\, \mathscr{O}^{[d]}\right), \quad |x| = \sqrt{t^2 + \vec{x}^2}\,, \tag{2.15}$$

where the leading term c_0 is a simple constant, since the product of two pseudoscalars has the same quantum numbers of the identity operator, thus mixing with it. In the above, summing over $\mathscr{O}^{[d]}$ indicates all other higher dimensional operators with the same quantum numbers, which will yield subleading contributions for small distances. Fourier transforming one obtains

$$G(t; m_h) = \int \mathrm{d}^3x \left\langle J^\dagger(x; m_h) J(0; m_h)\right\rangle \overset{t\to 0}{\sim} \frac{1}{|t|^3}\left(1 + \mathscr{O}\left(|t|^2\right)\right). \tag{2.16}$$

Noticing the integral in eq. (2.14) is over all t, in order for the integrand to be finite for $t \to 0$, one requires $n \geq 4$. Note that the integral over $\vec{x}$ does not really invalidate the assumption $|x| \to 0$, since correlations between the operators at large distances are exponentially suppressed, i.e.

$$J^\dagger(x; m_h) J(0; m_h) \overset{|x|\to\infty}{\sim} \mathrm{e}^{-2m_h|x|}\,. \tag{2.17}$$

[II] Note that the subscript n present here is not the k of previous sections: the finite moment $n = 4$ here, corresponds to *two* $\partial/(\partial q^2)$ derivatives acting on eq. (2.3), i.e. what is $k = 2$ there.

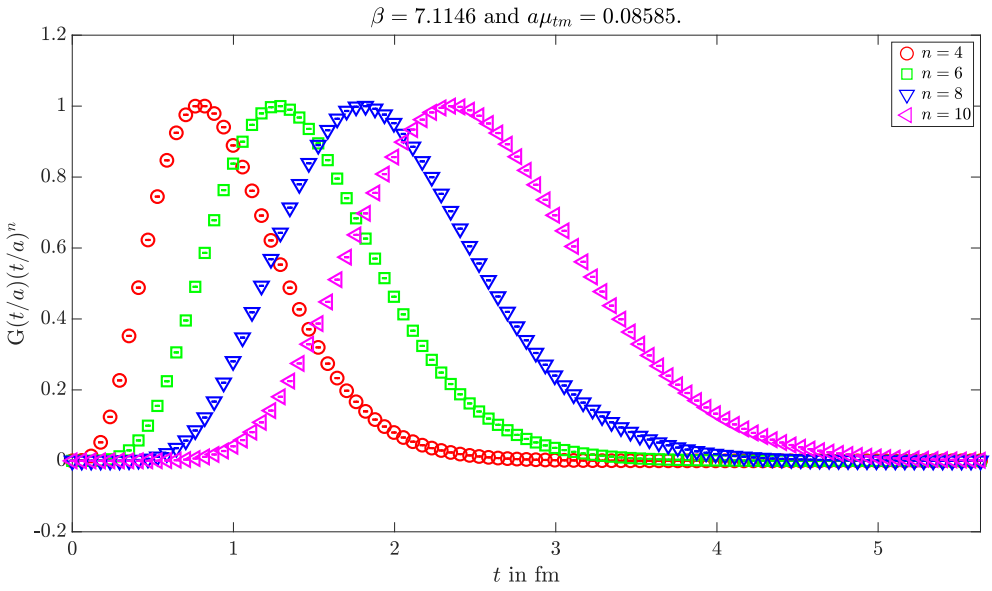

Figure 2.1: *Dependence of $t^n G(t,a,\mu_{\rm tm})$ on t in fm, which integrated (or, on the lattice, summed) over defines the moment. This observable is dominated by longer distances as n increases. Different n are normalized so that all peaks have unit height.*

Any connected diagram in PT (see discussion about diagrams after eq. (2.2)) can easily be shown to have this $\exp\{-2m_h|x|\}$-factor at leading order. Disconnected diagrams, on the other hand, cannot be reliably computed in PT since these contributions contain massless gluons propagating at large distances.

Here it is convenient to show *lattice data* for the integrand of eq. (2.14), which will be precisely define later (so that it is actually a summand, see eq. (3.57)), where two important observations are in order: (1) the region in energy/distances dominating the integral is quite low/high, so that sizable deviations w.r.t. PT may be expected and (2) the observable is dominated by longer distances as n increases, see figs. 2.1 and 2.2.

2.4. COUPLING AND MASS FROM MOMENTS

Since the perturbative estimate of $\mathscr{M}_n$ in eq. (2.5) is a function of m_h and α, one can *extract* these if some other way of computing $\mathscr{M}_n$ is available, up to some truncation error of $\mathscr{O}(\alpha^4)$, by inverting the perturbative expansion formula. One way to do this is, of course, by computing the moment on the lattice, on which we will elaborate much in the rest of the thesis. However, let us mention also another possibility, namely choosing $J_\mu(x) = \overline{\psi}(x)\gamma_\mu\psi(x)$ instead of the pseudoscalar (we skip the details of the additional Lorentz indices present in eq. (2.1)) and noting in this case

$$\mathscr{M}_{2k}^{\rm exp}(m_h) = \int \frac{{\rm d}s}{s^{2k}} R(s,m_h)\,, \quad R(s,m_h) = \frac{\sigma_{e^+e^-\to h\bar{h}}(s)}{\sigma_{e^+e^-\to\mu^+\mu^-}(s)}\,, \tag{2.18}$$

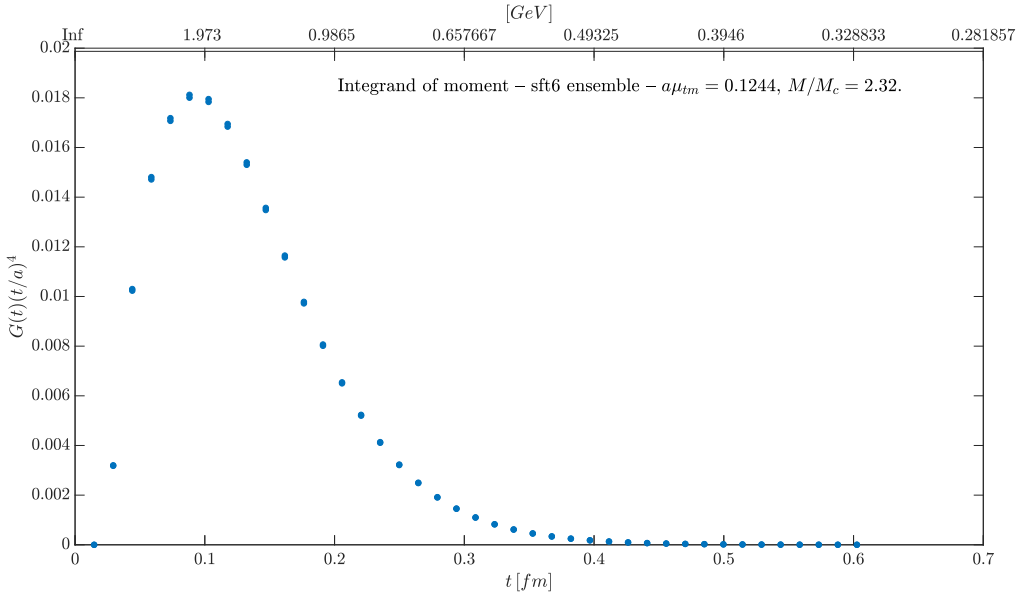

Figure 2.2: *Energy and distance scale for lattice moment $n = 4$, the most perturbative. What is shown is the integrand as a function of Euclidean time. Contributions to the integral at small energies seem sizable.*

where $s = q^2$ is the center of mass energy of the system. Obtaining eq. (2.18) is not trivial, and requires a dispersion relation to express the vacuum polarization as an integral transform of its imaginary part (cfr. Kramers-Kronig relations and Sokhotski-Plemelj theorem) and the optical theorem to relate said imaginary part to a ratio of forward scattering amplitudes [22]. One can thus compute the moment at $m_h = m_{\text{charm}}$ or $m_h = m_{\text{bottom}}$ from experimental R-ratio data and extract m_h and α, but only at the scale m_h itself (or scales close m_h, since s cannot be too far from $s = 1$), whereas on the lattice one can really freely vary m_h – tuning it also to non-physical values – and compute coupling and mass at different energy scales. This means being able to see the variation of the truncated term in eq. (2.8) as a function of energy and probe the truncation error and the applicability domain of PT.

To be more specific, in the case of $\mathscr{M}_4$, eq. (2.5) is adimensional and only depends on the heavy quark mass logarithmically, through the coupling. Thus, it can be used to extract the coupling, whereas for higher moments one can rewrite eq. (2.5) as

$$m_h = \left\{ \frac{4\pi^2}{3} \frac{2^{2k}}{C_{2k}} \mathscr{M}_{2k}^{\text{exp}} \right\}^{\frac{1}{4-2k}}, \quad n = 2k = 6, 8, \dots, \tag{2.19}$$

and use it to extract the heavy quark mass. Also adimensional ratios of higher moments can be defined, where the strong mass dependence cancels as follows

$$\widetilde{\mathscr{M}_{2k}} \overset{\text{def.}}{=} [\mathscr{M}_{2k}]^{\frac{1}{4-2k}} \implies \frac{\widetilde{\mathscr{M}_{2k}}}{\widetilde{\mathscr{M}_{2k+2}}} = 2 \frac{[C_{2k}]^{\frac{1}{4-2k}}}{[C_{2k+2}]^{\frac{1}{2-2k}}}, \quad n = 2k = 6, 8, \dots, \tag{2.20}$$

so that $[\widetilde{\mathscr{M}_{2k}}] = -1$, $\forall n = 2k \geq 6$, and explicit mass factors cancel in the ratio. Given the perturbative expansion for two such moments, their ratio can be re-expanded and, again, only logarithmic

dependence on the mass will appear. These ratios can thus be used to extract the coupling, too.

2.5. RENORMALIZATION GROUP INVARIANT PARAMETERS

The fundamental parameters of QCD discussed so far, the coupling $\alpha(\mu)$ (or $\overline{g}^2(\mu)$, with $\overline{g}^2(\mu) = 4\pi\alpha(\mu)$) and the masses[III] $\overline{m}_i(\mu)$, are both renormalization scale and scheme dependent. Here we introduce alternative, convenient parameters called *renormalization group invariant parameters*, which beyond being scale independent are either scheme-independent, as in the case of the masses, or exactly relatable between schemes, as in the case of the Λ-parameter, associated to the coupling. They can be thought of as integration constants of the renormalization group equations (RGEs), or Callan-Symanzik equations [154, 34]. These express the independence of a renormalized, physical quantity $\mathscr{G}_R(p,\mu,\overline{g}(\mu),\overline{m}(\mu))$, where p is some momentum, on the renormalization scale μ one needs to introduce in the renormalization procedure. In the case of $\mathscr{G}_R$, for a *mass-independent renormalization scheme*, they are

$$\mu\frac{\mathrm{d}}{\mathrm{d}\mu}\mathscr{G}_R(p,\mu,\overline{g}(\mu),\overline{m}(\mu)) = 0 \implies \left(\partial_{\ln\mu} + \beta(\overline{g})\partial_{\overline{g}} + \tau(\overline{g})\partial_{\ln\overline{m}}\right)\mathscr{G}_R = 0\,, \tag{2.21}$$

where the anomalous dimensions $\beta(\overline{g})$ and $\tau(\overline{g})$ contain the relevant information, namely the running of the renormalized parameters. They are given by

$$\begin{cases} \beta\left(\overline{g}\left(\mu\right)\right) \overset{\text{def.}}{=} \mu\dfrac{\mathrm{d}\overline{g}\left(\mu\right)}{\mathrm{d}\mu}\,, & (2.22)\\[2ex] \tau\left(\overline{g}\left(\mu\right)\right) \overset{\text{def.}}{=} \dfrac{\mu}{\overline{m}(\mu)}\dfrac{\mathrm{d}\overline{m}\left(\mu\right)}{\mathrm{d}\mu}\,, & (2.23) \end{cases}$$

and they dictate how these parameters depend on the unphysical renormalization scale μ. Now, let us reparametrize the general solution $\mathscr{G}_R$ in terms of two special solutions, both of mass dimension 1. The first, is a generic function $\Lambda(\mu,\overline{g}(\mu))$ with no dependence on momenta and mass, whereas the second is a generic function $M(\overline{m}(\mu),\overline{g}(\mu))$, independent of p and (explicitly, at least) of μ. Thus, because of dimensional reasons, both need to be given by

$$\Lambda(\mu,\overline{g}(\mu)) = \mu\phi_g(\overline{g})\,, \tag{2.24}$$

$$M(\overline{m}(\mu),\overline{g}(\mu)) = \overline{m}(\mu)\phi_m(\overline{g}(\mu))\,, \tag{2.25}$$

where the ϕ_i functions are dimensionless. One obtains

$$\frac{\mathrm{d}}{\mathrm{d}\mu}\mathscr{G}_{\mathrm{RGI}}(\Lambda,M) = 0 \implies \begin{cases} \left(\partial_{\ln\mu} + \beta(\overline{g})\partial_{\overline{g}}\right)\Lambda = 0 \implies \left(1+\beta(\overline{g})\partial_{\overline{g}}\right)\phi_g(\overline{g}) = 0\,, & (2.26)\\ \left(\tau(\overline{g})\partial_{\ln\overline{m}} + \beta(\overline{g})\partial_{\overline{g}}\right)M = 0 \implies \left(\tau(\overline{g}) + \beta(\overline{g})\partial_{\overline{g}}\right)\phi_m(\overline{g}) = 0\,, & (2.27) \end{cases}$$

[III] We will restrict our discussion from the $N_f = 6$ masses of full QCD to our setup of two mass-degenerate flavors, i.e. only one mass parameter.

which can be integrated to obtain the $\phi_i(\overline{g})$ functions. To do so, one can expand β and τ in PT[IV] as

$$\beta(\overline{g}) \underset{\overline{g}\to 0}{\sim} -b_0\overline{g}^3 - b_1\overline{g}^5 - b_2\overline{g}^7 + \mathscr{O}(\overline{g}^9)\,, \tag{2.28}$$

$$\tau(\overline{g}) \underset{\overline{g}\to 0}{\sim} -d_0\overline{g}^2 - d_1\overline{g}^4 + \mathscr{O}(\overline{g}^6)\,, \tag{2.29}$$

where (in a mass-independent scheme) the first two β-coefficients and the first τ-coefficient are universal, i.e. scheme independent. Integrating for the coupling one gets

$$\begin{aligned}\int \frac{\partial\phi_g}{\phi_g} = -\int \frac{\partial\overline{g}}{\overline{g}} \implies \frac{\Lambda}{\mu} &= \phi_g(\overline{g}) \\ &= \left(b_0\overline{g}^2\right)^{-b_1/(2b_0^2)} \mathrm{e}^{-1/(2b_0\overline{g}^2)} \exp\left\{-\int_0^{\overline{g}} \mathrm{d}x \left[\frac{1}{\beta(x)} + \frac{1}{b_0x^3} - \frac{b_1}{b_0^2x}\right]\right\}, \end{aligned} \tag{2.30}$$

and, for the mass

$$\begin{aligned}\int \frac{\partial\phi_m}{\phi_m} = -\int \partial\overline{g}\frac{\tau(\overline{g})}{\beta(\overline{g})} \implies \frac{M}{\overline{m}(\mu)} &= \phi_m(\overline{g}) \\ &= \left[2b_0\overline{g}^2(\mu)\right]^{-\frac{d_0}{2b_0}} \exp\left\{-\int_0^{\overline{g}(\mu)} \mathrm{d}x \left[\frac{\tau(x)}{\beta(x)} - \frac{d_0}{b_0x}\right]\right\}, \end{aligned} \tag{2.31}$$

where two things should be noted: (1) the overall factors are a convention and (2) the integral has been re-written in order to avoid any divergences for $x \to 0$, since said divergences have been explicitly integrated and written as prefactors. We can finally define

$$\Lambda_{\mathrm{RGI}} \overset{\mathrm{def.}}{=} \mu(b_0\overline{g}(\mu)^2)^{-b_1/(2b_0^2)} \exp\left\{-\frac{1}{2b_0\overline{g}(\mu)^2} - \int_0^{\overline{g}(\mu)} \mathrm{d}x \left[\frac{1}{\beta(x)} + \frac{1}{b_0x^3} - \frac{b_1}{b_0^2x}\right]\right\}, \tag{2.32}$$

$$M_{\mathrm{RGI}} \overset{\mathrm{def.}}{=} \overline{m}(\mu)\left[2b_0\overline{g}^2(\mu)\right]^{-\frac{d_0}{2b_0}} \exp\left\{-\int_0^{\overline{g}(\mu)} \mathrm{d}x \left[\frac{\tau(x)}{\beta(x)} - \frac{d_0}{b_0g}\right]\right\}, \tag{2.33}$$

where the RGI-subscript indicates that the two parameters, being constants arising from the integration of the differential equation, are actually independent of the chosen μ at which they are evaluated. Since any μ yields the same RGI-parameters, also

$$\Lambda_{\mathrm{RGI}} = \lim_{\mu\to\infty} \mu\left(b_0\overline{g}^2(\mu)\right)^{-b_1/(2b_0^2)} \exp\left\{-\frac{1}{2b_0\overline{g}(\mu)^2}\right\}, \tag{2.34}$$

$$M_{\mathrm{RGI}} = \lim_{\mu\to\infty} \overline{m}(\mu)\left\{2b_0\overline{g}^2(\mu)\right\}^{-\frac{d_0}{2b_0}}, \tag{2.35}$$

is oftentimes useful, where only the universal perturbative behavior is necessary. From eq. (2.34) and eq. (2.35) a quick computation shows a scheme change leaves M_{RGI} unchanged, whereas Λ_{RGI} changes by a factor calculable *exactly* through a 1 loop computation. Many lattice computations, among which the present one, evaluate $\overline{g}(\mu)$ (and $\overline{m}(\mu)$) at a hadronic scale, and then run it with the

[IV] Note, we expand in PT only for convenience, the final result will depend on universal coefficients only and does not rely explicitly on this expansion.

5-loop $\beta_{\overline{\rm MS}}$ [83, 105] (and the 4-loop $\tau_{\overline{\rm MS}}$ [157, 37]) to infinite energy. From the truncation of the perturbative series used to determine $\alpha_{\overline{\rm MS}}(\mu)$, one obtains an approximated $\Lambda_{\rm RGI}$ (or $M_{\rm RGI}$), with a leading unknown $\alpha^n_{\overline{\rm MS}}(\mu)$ term for some n. An extrapolation to $\mu \to \infty$, or equivalently to $\alpha_S \to 0$, of the approximated $\Lambda_{\rm RGI}$ ($M_{\rm RGI}$) then gets rid of leftover $\alpha_{\overline{\rm MS}}$-dependence. Let us stress that given some value of $\Lambda_{\rm RGI}$ (or of $M_{\rm RGI}$) there is a one-to-one correspondence with $\overline{g}$ (or with $\overline{m}$) in some scheme, *once the renormalization scale μ is fixed*.

To conclude, *one can trade the scheme-dependent running parameters for renormalization group invariant ones, in terms of which any physical QCD observable may be written*. Indeed, in this thesis we *fix the bare mass in our simulations through M_{RGI}*, as explained in Subsection 5.4.2. Beyond the coupling, we compute $\Lambda_{\rm RGI}$ at several values of the mass scale, in order to see how its truncation errors vary and whether an extrapolation to infinite energy with controlled errors is feasible. Finally, we stress that being able to switch to RGI-parameters does not mean perturbative schemes, such as the $\overline{\rm MS}$, become unimportant. Converting to the $\overline{\rm MS}$ is oftentimes necessary in order to make contact to PT results in high energy regimes, where its reliability is out of question.

3 | Lattice Quantum Chromodynamics

HERE we discuss how to discretize quantum chromodynamics, with the goal to obtain a lattice definition of moments that we can use. We also introduce a few general topics of lattice computations which will be necessary to explain and justify our setup and choices and to better understand its possibilities and key mechanisms. Note that in lattice QCD one is simulating a fictitious world where only the strong interaction and fields interacting through it are present. In the last decade or so attempts to expand this and to simulate electrically charged hadrons have been carried out with several methods [135]. Throughout this thesis we will restrict ourselves to the standard setup, where, taking full QCD as an example, pions in the $SU(2)_f-$triplet are mass degenerate, i.e. neither isospin breaking nor QED effects are taken into account.

3.1. Basics of Discretizing Field Theory

We start by substituting continuous spacetime by a 4-dimensional hyper-cubic lattice with a spacing between vertices, or *sites*, denoted by a. A very general property of waves propagating in a lattice with finite a (in physical units), is the absence of wavelengths below a certain cutoff. As far as QFT's ultraviolet divergences, which make regularization and renormalization necessary, emerge from short wavelength physics, the presence of a cutoff is a natural candidate for a regulator of the theory. It becomes necessary to understand how to transcribe one-to-one the fundamental degrees of freedom of QCD, namely the gauge and fermion fields, onto this discrete spacetime. When doing so, one needs to be careful about preserving some of the key properties of the theory, though. For instance, the lattice formulation is almost always chosen to preserve gauge invariance, whereas symmetries such as chiral and rotational symmetry will be broken and then only be restored in the continuum.

The starting point is to note that lattice field theory is formulated in *Euclidean* spacetime. What properties and physical information of Minkowskian field theory can be recovered from the Euclidean one is a non-trivial topic, see for instance [102, 119]. In Euclidean spacetime the path integral – in contrast to the Minkowskian highly oscillating factor $\exp[i\mathscr{S}_M]$ – contains a term $\exp[-\mathscr{S}_E]$, which can be interpreted as a probability weight once properly normalized. One can then attempt to solve the highly dimensional path integrals with a stochastic approach, namely with Markov Chain Monte Carlo methods (see Subsection 3.3.2). To start, we define gauge parallel transporters from x to y in the continuum as

$$U(y \leftarrow x) = \mathscr{P} \exp\left\{ i \int_x^y A_\mu(z) \mathrm{d}z^\mu \right\}, \tag{3.1}$$

where $\mathscr{P}$ denotes the path-ordered product. From this definition, the common approach introduced in [162] consists of assigning fermion fields to sites of the lattice, while the gauge field can be defined as a parallel transporter along *a straight path between two neighboring* sites, i.e.

$$U(x,\mu) \overset{\text{def.}}{=} U(x+a\hat{\mu} \leftarrow x) = \exp\left\{ i \int_x^{x+a\hat{\mu}} A_\mu(z)\mathrm{d}z \right\}, \tag{3.2}$$

where $\hat{\mu}$ is a unit vector in direction μ. Note that $A_\mu(x) \in \mathfrak{su}(3)$, whereas $U(x,\mu) \in SU(3)$, i.e. gauge fields on the lattice take values in the *group* rather than in the *algebra*. One can imagine the gauge field $U(x,\mu)$ to reside on a directed link of the lattice connecting the point x with its neighboring point $x+a\hat{\mu}$. These are the fundamental fields in the lattice description and in path integrals they are *integrated over*.

3.1.1. Wilson's Action

Next, we introduce the lattice gauge action, which must reproduce the standard Yang-Mills [166] action in the continuum limit. Wilson [162] introduced first such an action, namely

$$\mathscr{S}_W \overset{\text{def.}}{=} \frac{1}{g_0^2} \sum_{x,\mu<\nu} \mathrm{Re}\left\{ \mathrm{tr}\left[\mathbb{1} - U(x)_{\mu,\nu} \right] \right\}, \tag{3.3}$$

$$U(x)_{\mu,\nu} \overset{\text{def.}}{=} U(x,\mu)\, U(x+a\hat{\mu},\nu)\, U^{-1}(x+a\hat{\nu},\mu)\, U^{-1}(x,\nu), \tag{3.4}$$

where periodic boundary conditions in all directions are imposed. The color-trace of a directed closed loop built out of gauge links, known as a *Wilson loop*, is gauge invariant by construction. The simplest possible Wilson loop is indeed $U(x)_{\mu,\nu}$, called *plaquette*, so that the Wilson action is built of gauge invariant objects. Actually, the whole lattice approach is manifestly gauge invariant and *there is no need for gauge fixing*, unless some perturbative, saddle point expansion of the path integral is carried out. In this case zero-modes coming from the quadratic part of the action must still be avoided. Thus, all actions throughout this work are gauge invariant, just like any path integral measure $\mathrm{D}[\Phi]$, where the *Haar measure* (also known as Hurwitz measure) is always intended; note also that the discrete lattice yields a finite number of integrals, namely it is a method to rigorously *define the path integral*.

It is a trivial exercise to expand $\mathscr{S}_W$ in eq. (3.3) for $a \to 0$ and to see it reproduces $\mathscr{S}_{\mathrm{YM}}$, with corrections in powers of a starting from $\mathscr{O}(a^2)$.

3.1.2. Recovering Continuum Physics

Lattice simulations are necessarily done at finite a, where the cutoff acts as a regulator. This can be compared to dimensional regularization, where a continuous small number ε changes the dimensions from $d = 4$ to $d = 4-\varepsilon$. The renormalized physics is recovered in the limit $a \to 0$, where the number of degrees of freedom becomes infinite – a situation that can clearly not be simulated on a computer. However, multiple ensembles with decreasing a can be generated, from which the continuum physics is obtained as an *extrapolation*.

Naively sending $a \to 0$ is not enough to obtain meaningful continuum physics, though, which is immediate to realize in pure gauge where a is the only dimensionful quantity. Due to dimensional reasons some generic observable M with mass dimensions has to be given by

$$M = \frac{f(g_0)}{a}\,, \tag{3.5}$$

for some $f(g_0)$. For this to be finite in the limit $a \to 0$, one needs to *tune the bare coupling* g_0 while varying a, i.e. $g_0 = g_0(a)$. From M's independence on a, one can formally write, up to scaling violations $\mathcal{O}(a^2)$

$$\left.\frac{dM}{d\log a}\right|_{\overline{g}} = \mathcal{O}(a^2) = \left\{\frac{1}{a}\frac{\partial f}{\partial g_0}\frac{\partial g_0}{\partial \log a} - \frac{f(g_0)}{a}\right\}\Bigg|_{\overline{g}} \implies \begin{cases} \beta_{\text{lat}}(g_0) \overset{\text{def.}}{=} -\frac{\partial g_0}{\partial \log a}\big|_{\overline{g}}\,, \\ f(g_0) = -\frac{\partial f}{\partial g_0}\beta_{\text{lat}}(g_0)\,, \end{cases} \tag{3.6}$$

where we introduced the lattice beta-function $\beta_{\text{lat}}(g_0)$. It contains the dependence of the bare coupling on the cutoff and can be shown perturbatively to be related to the β-function of eq. (2.28) [51, 78], establishing universality of the first two coefficients. This implies the continuum limit to be reached for $g_0 \to 0$. A definition of Λ_{lat} [78] analogous to eq. (2.34) can then be given

$$\Lambda_{\text{lat}} \overset{\text{def.}}{=} \lim_{g_0 \to 0}\left\{\frac{1}{a}\exp\left(\frac{1}{-2b_0 g_0^2}\right)\left(b_0 g_0^2\right)^{-b1/(2b_0^2)}\right\}, \tag{3.7}$$

which is a dimensionful parameter surviving the continuum limit, a phenomenon known as dimensional transmutation [44]. Any dimensionful quantity M_i of, say, mass dimension $[M_i] = 1$, can be written as

$$M_i = \Lambda_{\text{lat}}\, C_i\,, \tag{3.8}$$

in the continuum limit for some numerical, adimensional constant C_i. Differently stated, there is some part of parameter space sufficiently close to the continuum where a scaling region is present, in which all M_i have the same dependence on g_0, yielding

$$\frac{M_i}{M_j} = \frac{C_i}{C_j}\left(1 + \mathcal{O}(a^2 M^2)\right). \tag{3.9}$$

For $SU(N_c)$, with $N_f < 11 \cdot N_c/2$, one has that $g_0 = 0$ is a zero of the beta function and corresponds to the $a \to 0$ limit. This implies that $g_{cr.} = 0$ is a critical surface of the lattice theory where correlation lengths diverge. One can hope to take a meaningful continuum limit only due to this key property of criticality. Tuning g_0 as described is equivalent to the renormalization of the theory.

If one now adds quarks, the same kind of reasoning applies: whilst sending the cutoff to zero all bare parameters will have to be tuned in order to keep both the renormalized coupling and a set of renormalized masses fixed, one for each quark flavor. Given some scale – from a theoretical perspective one has the dimensionful Λ_{RGI} of eq. (2.32) – the masses can be tuned in such a way as to keep, for instance, their RGI-mass (eq. (2.33)) in units of Λ_{RGI} fixed, although in practical situations mostly hadronic masses or decay constants that are sensitive to a specific quark are used, as explained in

Section 1.3.

3.2. LATTICE FERMIONS

How to appropriately discretize fermions on the lattice is not obvious and hereafter we will mention a few salient points, mostly related to Wilson fermions. The most naive fermion lattice action one may think of is a gauge-link transcription of the action in eq. (1.7), where quark fields are now located at single lattice points. Possible gauge invariant observables are now not only closed loops of gauge links multiplied by one another, but also gauge-link strings with quark-antiquark fields at their endpoints. Starting from discretizing the *free* fermion action in a straightforward manner (with implicit fermion species indices, $\Psi^T = (\psi_1, ..., \psi_{N_f})$ and $\mathbb{M}$ a diagonal fermion mass matrix)

$$\mathscr{S}_F = a^4 \sum_x \overline{\Psi}(x) \left(D\Psi\right)(x), \quad D = \sum_{\nu=0}^{3} \gamma_\nu \frac{\partial_\nu + \partial_\nu^*}{2} + \mathbb{M}, \quad \text{where} \tag{3.10}$$

$$\begin{cases} \left(\partial_\nu \Psi\right)(x) = \frac{\Psi(x+a\hat{\nu}) - \Psi(x)}{a} \\ \left(\partial_\nu^* \Psi\right)(x) = \frac{\Psi(x) - \Psi(x-a\hat{\nu})}{a} \end{cases}, \tag{3.11}$$

one can introduce the gauge field by substituting the simple derivative with a *gauge covariant derivative* ∇_ν , depending on the group-valued gauge fields $U(x,\nu)$ of eq. (3.2)

$$\begin{cases} \left(\nabla_\nu \Psi\right)(x) = \frac{U(x,\mu)\Psi(x+a\hat{\nu}) - \Psi(x)}{a} \\ \left(\nabla_\nu^* \Psi\right)(x) = \frac{\Psi(x) - U^\dagger(x-a\hat{\nu},\nu)\Psi(x-a\hat{\nu})}{a} \end{cases}, \tag{3.12}$$

and again compactly write

$$\mathscr{S}_F = a^4 \sum_x \overline{\Psi}(x) D \Psi(x), \tag{3.13}$$

where D will be referred to as *Dirac operator* or *Dirac matrix*; we will indicate the aforementioned matrix generically with D, specifying its content, where necessary, from case to case.

3.2.1. Doubler Modes

The fermion action eq. (3.10), however, suffers from a non-trivial problem. Each pole of the propagator, i.e. poles of the inverse of D in Fourier space, represents a particle contained within the theory. Extra fermion species, so called *doublers*, are even present in the free theory, where a computation in Fourier space leads to the following (single) fermion propagator (functions in Fourier space are indicated by tildes)

$$\widetilde{S}(p,a,m) = \mathscr{F}[D^{-1}] = \frac{m - ia^{-1}\sum_{\mu=0}^{3} \gamma_\mu \sin\left(ap_\mu\right)}{m^2 + a^{-2}\sum_{\mu=0}^{3} \sin^2(ap_\mu)}, \tag{3.14}$$

where $\mathscr{F}[f]$ is the Fourier transform of f. In the relevant region[I] of $p_\mu \in (-\pi/a, \pi/a]$ the propagator correctly shows the physical pole at $p = 0$, but also further unphysical ones whenever at least one of its components is π/a. This adds up to 15, or $2^d - 1$, extra poles, d being the number of spacetime dimensions. Taking a continuum limit of such a theory would thus lead to unphysical results, since the doubler modes present in the propagator will, for instance, show up in loops and alter the computations. This result is of general nature and can be avoided only by sacrificing some other key property, a statement first exposed in [129, 130] and which goes by the name of *Nielsen-Ninomiya no-go theorem*. Therein under rather general assumptions it is shown that an equal number of left and right handed Weyl fermion species has to appear in a lattice discretized theory. This can be proven in several ways, such as via topological arguments [129, 130] or via differential geometry [65]. We here report the following version: no massless lattice action (in its first Brillouin zone) can satisfy all of the below conditions simultaneously:

1. Locality of interactions present in the Dirac operator, which is equivalent to analyticity in the complex p-plane of the momentum space propagator $\widetilde{S}(p,a,0)$.
2. Reproduce appropriately a full Dirac fermion, with its left and right components, in the continuum limit, i.e.
$$\lim_{a\to 0} \widetilde{S}(p,a,0) = \widetilde{S}(p,0,0) = \frac{-i\not{p}}{p^2}\,. \tag{3.15}$$
3. Invariance under *continuum* chiral symmetry: $\{\gamma_5, \widetilde{S}(p,a,0)\} = 0$.
4. Doubler modes are absent in the first Brillouin zone.
5. *Reflection positivity* is satisfied, i.e.
$$\widetilde{S}(p,a,0) = \gamma_0 \widetilde{S}\big((-p_0,\vec{p}),a,0\big)\gamma_0\,, \tag{3.16}$$
which is necessary in the Euclidean to have unitarity in Minkowskian spacetime, and thus hermiticity of the Hamiltonian operator (a thorough explanation of this can be found in [131, 132, 133, 134]).
6. Cubic symmetry in the action:
$$\widetilde{S}(p,a,0) = \gamma_i \widetilde{S}^\dagger\left(R_i(p),a,0\right)\gamma_i\,, \quad [R_i(p)]_j = p_j(1-2\delta_{ij})\,. \tag{3.17}$$

To give an admittedly too simple, yet very intuitive idea of the theorem, one can think in one dimension: here the key concept greatly simplifies to the trivial notion that a periodic, continuous function must have an even number of zeros within one period.

Unitarity of the theory, its locality, encoded in the analyticity of the propagator in p, and the correct continuum limit – i.e. reproducing a continuum Dirac fermion upon removal of the cutoff – cannot really be renounced. Still, multiple approaches have been developed to utilize lattice discretized

[I] Also known as the first *Brillouin zone*, a primitive cell which contains the relevant information, since periodic functions within it represent the functional space of interest in the $a \to 0$ limit.

fermions, either by accepting (a reduced number of $2^{d/2}-1$) doubler modes – as in the case of *staggered fermions* [98] – or by eliminating them and thereby having continuum chiral symmetry breaking.

3.2.2. Wilson Fermions

What Wilson proposed [163] was to introduce an extra term in the action with mass quantum numbers which would thus explicitly break chiral symmetry (even with massless fermions), but eliminate the doubler modes[II]. The explicit form of the *Wilson term* is

$$\mathscr{S}_F = a^4 \sum_x \overline{\Psi}(x) \left\{ \sum_{\nu=0}^{3} \left(\gamma_\nu \frac{\nabla_\nu + \nabla_\nu^*}{2} - \underbrace{\frac{a}{2} \nabla_\nu^* \nabla_\nu}_{\text{Wilson term}} \right) + \mathbb{M} \right\} \Psi(x) \,, \tag{3.18}$$

which evidently converges to the same continuum action. From the Dirac operator's Fourier transform one can obtain the propagator, explicitly computed at TL for twisted mass Wilson fermions in Appendix C. The *inverse* propagator, which is more convenient to write, is obtained by setting $\mu_{\text{tm}} = 0$ in eq. (C.38), giving

$$\widetilde{S}^{-1}(p,a,m) = m + a^{-1} \sum_{\mu=0}^{3} \left[1 - \cos\left(a p_\mu\right) + i \gamma_\mu \sin\left(a p_\mu\right) \right] , \tag{3.19}$$

which now *only contains the physical pole* in the first Brillouin Zone. It is immediate to see that continuum chiral symmetry $\{\gamma_5, \widetilde{S}(p,a,0)\} = 0$ is lost, but γ_5*-hermiticity*

$$\left[\gamma_5 \widetilde{S}(p,a,m) \right]^\dagger = \gamma_5 \widetilde{S}(p,a,m) \,, \tag{3.20}$$

is still a symmetry of the theory.

3.3. PROPERTIES OF THE LATTICE THEORY

3.3.1. Scale Setting

As mentioned in the previous section, to extract meaningful physical results, parameters need to be tuned in order for the ratio of some observables to equate their physical value. Equivalently, one can think of the lattice as computing dimensionful observables in units of a as a function of the bare parameters. In order to then extract dimensionful quantities, one needs to *fix the scale*, namely set a in physical units. The most natural QCD scale that comes to mind is the mass of some hadron, such

[II] A twisted mass term can be added to the Wilson proposal, too, which we will discuss at length in later sections, for we employed it in this study. Let us mention for completeness that more options exist, most importantly the example of fermions obeying the *Ginsparg-Wilson equation* [71], such as *overlap fermions* [127, 128] or the approximate solution of *domain wall fermions* [95]. All of these modify the lattice theory so that it respects some form of exact *lattice* chiral symmetry [110], thereby rendering, however, chirality a gauge-field-dependent and non-strictly-local concept.

as the proton's mass m_p. However, the scale needs to be computable with controlled errors, since its uncertainties will propagate into any other dimensionful observable [152]. Multiple hadronic quantities with small statistical and systematic errors exist. One also does not want the scale's numerical computation to be costly and, moreover, a weak quark mass dependence is highly preferable in order to have an independent tuning of the scale and of quark masses. Altogether, in full QCD, $N_f + 1$ parameters need to be tuned, after which any other ratio of dimensionful observables must be equal to the corresponding physical value. In our case the number of parameters reduces to *two*:

1. The scale, which we tune via t_0, coming from the so called "gradient flow" scale [111], as explained in the following.
2. The heavy valence quark mass, the tuning of which is described in Chapter 5.

The scale t_0 is defined through observables in a smoothed theory. We start in the continuum by introducing a field $B_\mu(t,x)$, which depends on the spacetime position x and on an additional t, via

$$B_\mu(t,x)\big|_{t=0} = A_\mu(x)\,, \tag{3.21}$$

$$\frac{\partial B_\mu(t,x)}{\partial t} = -\frac{\delta S_{\mathrm{YM}}}{\delta B_\mu(t,x)} = [D_\nu\,, G_{\nu\mu}(t,x)]\,, \tag{3.22}$$

where one can see the *flow time* t needs to have mass dimension $[t] = -2$ and where $G_{\mu\nu}(t,x)$ is the field strength tensor of B_μ. In leading order perturbation theory it can be seen that eq. (3.22) acts as a smoothing of gauge fields over a radius of roughly $\sqrt{8t}$ [111]. From here one can define the flowed action density

$$E(t,x) = -\frac{1}{2}\mathrm{tr}\left\{G_{\mu\nu}(t,x)\,G_{\mu\nu}(t,x)\right\}, \tag{3.23}$$

which remarkably is finite in the flowed theory. As shown in [114] through a perturbative analysis of the 5-dimensional theory, gradient-flow-smoothed observables at $t > 0$ need no renormalization beyond the one for the Lagrangian parameters. The continuum limit of the appropriately discretized version of eq. (3.22) is well defined for an arbitrary gauge invariant quantity based on smoothed gauge fields[III]. We are now ready to define t_0 through the implicit equation [111]

$$t^2\,\langle E(t,x)\rangle\,\big|_{t=t_0} \overset{\text{def.}}{=} 0.3\,, \tag{3.24}$$

which can be computed from an integration of eq. (3.22). Note the scale is set through purely gauge fields and no costly quark propagators are needed, although the scale will have a dependence on N_f.

Once $\sqrt{8t_0}/a$ has been computed, the overall scale of the lattice, or a in fermi, is set once a physical value for t_0 is known. Unlike scales such as hadron masses, for which an experimental value is available, it is meaningless to think of an experimental measurement of t_0 (or of any other gradient flow scale, such as w_0 [26]). Some physically accessible scale is necessary, popular choices being, for instance, decay constants f_π and f_K [29] or the Ω mass m_Ω [25]. Simultaneous, precise computations

[III] For instance, the plaquette does not have the additional additive renormalization term for the a^{-4} divergence originating from mixing with the identity.

of scale ratios within dedicated studies permits the extraction of physical values in fermi for "theory" scales such as t_0.

3.3.2. A Statistical Approach

Lattice simulations are based on Markov chain Monte Carlo [124, 80], a stochastic method to sample distributions. The appropriately normalized exponential of the Euclidean action $\exp[-\mathscr{S}_E]$ is treated as a Boltzmann weight which yields a well defined probability distribution. To evaluate the expectation value of some gauge invariant operator $\mathscr{O}$, we sample the path integral (in pure gauge for simplicity) according to

$$\langle \mathscr{O}[U] \rangle = \mathscr{Z}^{-1} \int \mathrm{D}[U]\, \mathrm{e}^{-\mathscr{S}_W[U]} \mathscr{O}[U] = \lim_{N\to\infty} \frac{1}{N} \sum_{U_n \in P[U]}^{N} \mathscr{O}[U_n] \tag{3.25}$$

$$\approx \frac{1}{N} \sum_{U_n \in P[U]}^{N} \mathscr{O}[U_n], \quad P[U] = \mathrm{D}[U] \mathrm{e}^{-\mathscr{S}_W[U]} \mathscr{Z}^{-1}, \tag{3.26}$$

where $\mathscr{Z}$ is the partition function of the theory. This means results are intrinsically of statistical nature with a statistical error associated to them (for more on this, see Section 4.1).

Here, we can comment on one of the reasons for which we have chosen the pseudoscalar density as a central observable in this work, as anticipated in eq. (2.2), namely that the pseudoscalar has statistical fluctuations which are almost independent of Euclidean time. This is in contrast with operators with other Γ-structures and below we will only briefly sketch the reasoning to understand this claim. Indicating here the pseudoscalar density (PS) with $P(x) = \overline{h}(x)\gamma_5 h'(x)$ and considering $\mathscr{O}_{PP}(x,y) = P^\dagger(x)P(y)$ one can estimate [109]

$$\left\langle \sum_{\vec{x}} \mathscr{O}_{PP}(x,y) \right\rangle \overset{|x_0-y_0|\to\infty}{\propto} \mathrm{e}^{-m_{\mathrm{PS}}|x_0-y_0|} + \dots, \tag{3.27}$$

whereas its variance $\sigma^2(\mathscr{O}_{PP})$ can be written as

$$\sigma^2(\mathscr{O}_{PP}) = \left\langle \left[\sum_{\vec{x}} \mathscr{O}_{PP}(x,y)\right] \left[\sum_{\vec{x}'} \mathscr{O}_{PP}(x',y)\right] \right\rangle - \left\langle \sum_{\vec{x}} \mathscr{O}_{PP}(x,y) \right\rangle^2. \tag{3.28}$$

The second term is simply the square of the pseudoscalar propagator, while the first one's influence on the variance can be guessed by recognizing it also contributes to a π (pion) 4-point function, present in a $\pi\pi$ propagator. From this one can conclude that the large t asymptotic variance decays like

$$\sigma^2(\mathscr{O}_{PP}) \overset{|x_0-y_0|\to\infty}{\propto} \mathrm{e}^{-2m_{\mathrm{PS}}|x_0-y_0|} + \dots, \tag{3.29}$$

so that for asymptotically large t the signal-to-noise ratio is t-independent up to subleading corrections (see [109] for a simple, introductory explanation). This drastically changes with other Γ-structures which suffer from problematic signal to noise ratios.

3.3.3. Systematic Effects of Lattice Computations

Beyond the statistical fluctuations, multiple sources of systematic errors are unavoidably present in lattice computations, the estimation of which plays a central role in the research field. We list them here and give a brief overview for clarity.

1. Typical of numerical physics is the *tuning of parameters* in order to reproduce the physics of interest, an aspect complicated by renormalization which introduces a *non-trivial relationship between bare, simulation parameters and renormalized quantities* related to physical observables. A detailed description of how this systematic effect was assessed in this work is given in Section 5.5.

2. As explained in Section 1.2, decoupling permits to simulate QCD without heavier quarks. However, the effect of quenching light (u, d, and even s) quarks on hadronic observables may be considerable and might, to some extent, be regarded as a topic no longer of great interest today. Including light quarks is nowadays feasible with multiple setups, but it has to be kept in mind *simulations carried out in this thesis are fully quenched*. What this means precisely as well as what its consequences might be for the conclusions presented herein are commented upon in the introduction of Chapter 4.

3. A computer can only consider a finite number of degrees of freedom, implying the necessity of a *finite volume* (FV); in most applications one wants it much larger than the other scales of the problem – rendering it effectively infinite[IV] – as is the case in this study. A check of this for moments in our setup is shown in the discussion of fig. 5.1. In general, FV-effects can be shown to be exponentially suppressed in mL (a specific computation of FV effects at TL for the moments can be found in Appendix C.2), where m is the smallest mass that can propagate in the theory. For the case of full QCD this is given by the light pions, $m_\pi \simeq 140\,\text{MeV}$, whereas in the pure gauge case by much heavier glueballs $m_{0^{++}} \simeq 1730\,\text{MeV}$, which greatly ameliorates the issue of FV-effects.

4. In dynamical simulations a universe with heavier-than-physical pions is thus more convenient, after which *extrapolations to the physical point*, i.e. $m_\pi \to m_\pi^{\text{phys}}$, can be performed. The interested reader may consult lattice literature or reviews, for instance [57, 76, 87], regarding this topic of great interest to the lattice community, but not for the specific work at hand.

5. Finally, an extrapolation in the lattice spacing a at which simulations are carried out is necessary. To reduce the range in which a must be varied (or simply to lessen the extrapolation error), one oftentimes relies on *Symanzik improvement* (see [155, 156, 107] or [108, 67] for a pedagogical introduction): action and operators are modified by irrelevant terms in order to change the leading discretization effects from $\mathcal{O}(a)$ to $\mathcal{O}(a^2)$, thereby speeding up the approach to the continuum. A brief description of it and especially of the *automatic-$\mathcal{O}(a)$* improvement relevant for twisted mass fermions used in this work, can be found in Appendix A.

[IV] Important exceptions exist, such as finite temperature computations or FV renormalization schemes.

3.4. TWISTED MASS QCD IN THE CONTINUUM

3.4.1. Chiral Symmetry

Before introducing QCD with a chirally twisted mass term, we will briefly summarize some aspects of the chiral-flavor symmetries of QCD. Let us start with the bare fermionic action of continuum Euclidean QCD with N_f fermions of degenerate mass M

$$\mathcal{S}_F = \int \mathrm{d}^4x \overline{\Psi}(x) \left[\left(\not{D} + M \right) \mathbb{1}_{N_f} \right] \Psi(x) \,. \tag{3.30}$$

When $M \neq 0$ some of the theory's global flavor symmetries $\mathcal{G}$ are explicitly broken

$$\mathcal{G} = SU(N_f)_L \otimes SU(N_f)_R \otimes U(1)_V \longrightarrow SU(N_f)_V \otimes U(1)_V \,, \tag{3.31}$$

where the $SU(N_f)_V$ transformations (subscript V indicating vector generators) can be written as

$$\begin{cases} \Psi'(x) = \exp\left\{ i\omega^a T^a \mathbb{1}_{\text{spin}} \right\} \Psi(x) \\ \overline{\Psi}'(x) = \overline{\Psi}(x) \exp\left\{ -i\omega^a T^a \mathbb{1}_{\text{spin}} \right\} \end{cases} , \quad a = 1, \ldots, \dim\left[SU(N_f)\right] = N_f^2 - 1 \,, \tag{3.32}$$

where T^a are the generators of $SU(N_f)$ and ω^a parametrize its elements. We explicitly wrote $\mathbb{1}_{\text{spin}}$ to emphasize the vector transformations eq. (3.32) indiscriminately act on L and R (left and right) components of spinors. The part of the symmetry which mixes L with R at non-zero mass is denoted by $SU(N_f)_A$ (for axial vector generators). Its action on spinors is given by

$$\begin{cases} \Psi'(x) = \exp\left\{ i\gamma_5 \omega^a T^a \right\} \Psi(x) \\ \overline{\Psi}'(x) = \overline{\Psi}(x) \exp\left\{ i\gamma_5 \omega^a T^a \right\} \end{cases} , \quad a = 1, \ldots, N_f^2 - 1 \,. \tag{3.33}$$

Besides the explicit breaking, there is also a spontaneous symmetry breaking at play, i.e. the ground state is not invariant for the whole symmetry $\mathcal{G}$, even at $M = 0$. This can be seen, e.g., considering $N_f = 2$ and the (large) non-degeneracy of the nucleon mass with its negative parity partner, $N^\star$, as well as from the large mass gap between the lightest mesons (pions) and the rest of the spectrum. The pions are the (would be) Goldstone bosons of the broken symmetry, their relatively tiny mass given by the aforementioned explicit breaking due to the non-zero light quark masses.

3.4.2. Chiral Twist in the Continuum

Let us now simplify the exposition by setting $N_f = 2$ for the rest of this thesis (unless explicitly stated otherwise), since this is the numerical setup we employed[V]. One can perform the following global

[V] With $N_f = 2$ here we mean we consider a doublet of mass-degenerate *valence* quarks, since, as explained in Chapter 4, our ensembles will be generated in the quenched approximation, usually referred to as $N_f = 0$.

field transformation which is non-anomalous in the $N_f = 2$ case

$$\begin{cases} \chi(x) = R_\omega \Psi(x) \\ \overline{\chi}(x) = \overline{\Psi}(x) R_\omega \end{cases} , \quad R_\omega = \exp\left\{ -i\omega \frac{\tau^3}{2} \gamma_5 \right\} \subset SU(2)_A \tag{3.34}$$

where χ denote the new, *chirally rotated* fields. This is trivially equivalent, at a path integral level, to a change of integration variables. The continuum action for the χ fields will change form, and after a few lines of algebra one obtains

$$\mathscr{S}_F = \int \mathrm{d}^4x\, \overline{\chi}(x) \left[\left(\not{D} + m_q \right) \mathbb{1}_{N_f} + i\mu_{\mathrm{tm}} \gamma_5 \tau^3 \right] \chi(x) , \quad \begin{cases} m_q = M \cos\omega \\ \mu_{\mathrm{tm}} = M \sin\omega \end{cases} , \tag{3.35}$$

so that $\tan(\omega) = \mu_{\mathrm{tm}}/m_q$ and $M = \sqrt{m_q^2 + \mu_{\mathrm{tm}}^2}$. This is the continuum form of the twisted mass QCD (tmQCD) action, introduced in [64], equivalent, of course, to the standard QCD action; we just performed a change of variables. Advantages of twisted mass are related to the finite cutoff theory and are discussed later.

Let us explore a few key points of the action in eq. (3.35). It clearly has an additional parameter, the *twist angle* ω, with respect to the action in eq. (3.30) (equivalently, there is a second bare mass parameter, μ_{tm}, beyond the standard one). Observables are expectation values of operators, which, using eq. (3.34), can be related in the two theories through

$$\begin{aligned} \left\langle \mathscr{O}[\Psi, \overline{\Psi}] \right\rangle_{(M,0)} &= \mathscr{Z}_{(M,0)}^{-1} \int \mathrm{D}[\Psi, \overline{\Psi}, U] \mathscr{O}[\Psi, \overline{\Psi}] \mathrm{e}^{-\mathscr{S}_F(M,0)} \\ = \left\langle \mathscr{O}[R_\omega^{-1}\chi, \overline{\chi} R_\omega^{-1}] \right\rangle_{(M,\omega)} &= \mathscr{Z}_{(M,\omega)}^{-1} \int \mathrm{D}[\chi, \overline{\chi}, U] \mathscr{O}[R_\omega^{-1}\chi, \overline{\chi} R_\omega^{-1}] \mathrm{e}^{-\mathscr{S}_F(M,\omega)} . \end{aligned} \tag{3.36}$$

With the somewhat redundant notation we want to stress what is in the twisted basis and what is at $\omega = 0$, to emphasize that at $\omega \neq 0$ operators, in general, can *change form*. Fields within a chiral multiplet have the same transformation rules w.r.t. R_ω, implying some correlation function in tmQCD is given by a linear combination of correlation functions in standard QCD, and vice-versa, yielding what can be seen as a formal dictionary between the two theories. Hereafter, we are interested in

$$\mathscr{A}_\mu^\pm = \overline{\Psi} \gamma_\mu \gamma_5 \frac{\tau^1 \pm i\tau^2}{2} \Psi , \qquad A_\mu^\pm = \overline{\chi} \gamma_\mu \gamma_5 \frac{\tau^1 \pm i\tau^2}{2} \chi , \tag{3.37}$$

$$\mathscr{V}_\mu^\pm = \overline{\Psi} \gamma_\mu \frac{\tau^1 \pm i\tau^2}{2} \Psi , \qquad V_\mu^\pm = \overline{\chi} \gamma_\mu \frac{\tau^1 \pm i\tau^2}{2} \chi , \tag{3.38}$$

$$\mathscr{P}^\pm = \overline{\Psi} \gamma_5 \frac{\tau^1 \pm i\tau^2}{2} \Psi , \qquad P^\pm = \overline{\chi} \gamma_5 \frac{\tau^1 \pm i\tau^2}{2} \chi , \tag{3.39}$$

where curly letters indicate operators at $\omega = 0$, whereas non-curly uppercase letters are written in terms of fields χ. When taken at $\omega = \pi/2$, referred to as *maximal twist*, we have

$$\chi(x)|_{\omega \equiv \pi/2} = \begin{pmatrix} h(x) \\ h'(x) \end{pmatrix} . \tag{3.40}$$

This point in parameter space is of central importance, as can be seen by obtaining relations between the the two theories, namely

$$\mathscr{P}^{\pm} = P^{\pm}, \tag{3.41}$$
$$\mathscr{A}_{\mu}^{\pm} = \cos\omega A_{\mu}^{\pm} \mp i \sin\omega V_{\mu}^{\pm}, \tag{3.42}$$
$$\mathscr{V}_{\mu}^{\pm} = \cos\omega V_{\mu}^{\pm} \mp i \sin\omega A_{\mu}^{\pm}. \tag{3.43}$$

For instance, chiral Ward identities [69, 21, 104] (always to be understood as operator insertions) with the above fixed flavor assignment become

$$\begin{cases} \partial_{\mu}\mathscr{A}_{\mu}^{\pm} = 2M\mathscr{P}^{\pm} \\ \partial_{\mu}\mathscr{V}_{\mu}^{\pm} = 0 \end{cases} \longrightarrow \begin{cases} \partial_{\mu}V_{\mu}^{\pm} = \pm 2i\mu_{\mathrm{tm}}P^{\pm} \\ \partial_{\mu}A_{\mu}^{\pm} = 2m_q P^{\pm} \end{cases}, \tag{3.44}$$

so that PCAC-mass measurements in the twisted theory, where $m_q = 0$, may be employed as a numerical check on deviations w.r.t. the $\omega = \pi/2$ condition; measurements on our ensembles are reported in Subsection 5.5.2.

One consequence which should be kept in mind when rotating the fields is the non-standard form of symmetries (see [149, 150]), such as parity and time reversal; the operator defining the moments is still symmetric w.r.t. physical time-reversal, although in general time reversal and parity are not symmetries of the full quantum theory at $a > 0$.

Furthermore, we have shown the relation between physical observables and a given Γ-structure changes between standard QCD and tmQCD. Take for instance the pion decay constant, tied to the overlap of the pseudoscalar groundstate with the four-divergence of the axial vector current: in tmQCD it will be given by the overlap of a pion state with the four-divergence of the *vector current*. This may be of great advantage, depending on the renormalization properties of the specific lattice discretization.

3.5. TWISTED MASS AND THE LATTICE

The full fermionic action chosen for this work in terms of bare, chirally rotated field doublets χ is given by

$$\mathscr{S}_F = a^4 \sum_x \overline{\chi}(x) \left\{ \sum_{\nu=0}^{3} \left(\gamma_\nu \frac{\nabla_\nu + \nabla_\nu^*}{2} - \frac{a}{2}\nabla_\nu^*\nabla_\nu + c_{sw}\, a \sum_{\mu=0}^{3} \frac{i}{4}\sigma_{\mu\nu}\hat{F}_{\mu\nu} \right) \mathbb{1}_{N_f} + m_0 \mathbb{1}_{N_f} + i\mu_{\mathrm{tm}}\gamma_5\tau_3 \right\} \chi(x). \tag{3.45}$$

The factor proportional to c_{SW} is the Sheikholeslami-Wohlert (SW) term [147] necessary for $\mathscr{O}(a)$-improvement of standard Wilson fermions and which contains: $\hat{F}_{\mu\nu}$, an appropriate discretization of the field strength tensor, and $\sigma_{\mu\nu}$, a commutator of γ-matrices (we defer the explicit form as well as some introductory explanation of these details to Appendix A.1). Here it is only crucial to note its explicit form, as that of Wilson's term, are the ones conventionally written with standard Wilson fermions, although we are in the twisted theory. This is a widespread convention, although a priori one

may also take the standard Wilson action in the physical basis and rotate it, obtaining a non-standard form for SW and Wilson terms. Furthermore, we stress the SW improvement term is not necessary for $\mathcal{O}(a)$-improvement, yet it is kept since there is evidence it ameliorates $\mathcal{O}(a^2)$-effects [13, 54].

Let us mention the original motivations for introducing the chirally twisted mass terms are several, among which the absence of zero modes, equivalent to a strictly positive Dirac operator. Writing here eq. (3.45) as

$$\mathcal{S}_F = a^4 \sum_x \overline{\chi}(x) \left\{ D_W + i\mu_{\rm tm}\gamma_5\tau_3 \right\} \chi(x)\,, \tag{3.46}$$

D_W's determinant is readily seen[VI] to be

$$\det\left\{D_W + i\mu_{\rm tm}\gamma_5\tau_3\right\} = \det\left\{\gamma_5 D_W + i\mu_{\rm tm}\tau_3\right\} \tag{3.47}$$

$$= \det\begin{pmatrix} \gamma_5 D_W + i\mu_{\rm tm} & 0 \\ 0 & \gamma_5 D_W - i\mu_{\rm tm} \end{pmatrix} = \det\left\{(\gamma_5 D_W)^2 + \mu_{\rm tm}^2\right\} > 0\,. \tag{3.48}$$

3.5.1. Renormalization

To show that the dictionary between correlation functions mentioned after eq. (3.36) is not spoiled by renormalization, it suffices for members of a chiral multiplet to renormalize in the same way and for renormalization factors to be independent of the angle ω. These properties can be obtained through the Ginsparg-Wilson regularization and in a mass-independent renormalization scheme. Invoking then the well established property of universality, one obtains the equivalence of the two theories, though we remind a rigorous proof of non-perturbative universality remains unknown.

For continuum, renormalized quantities in the Euclidean the following operator identity can be derived from chiral Ward identities

$$\partial_\mu \mathcal{A}^{\pm}_{\mu,R}(x) = 2M_R \mathcal{P}^{\pm}_R(x)\,. \tag{3.49}$$

In terms of the twisted fields we have

$$\mathcal{A}^a_{\mu,R}(x) = \lim_{a\to 0} \left\{ Z_A(g_0) A^a_\mu(x) \cos\omega + \varepsilon^{3ab} \widetilde{V}^b_\mu(x) \sin\omega \right\}, \tag{3.50}$$

where $\widetilde{V}_\mu$ is the point-split vector current

$$\widetilde{V}^b_\mu(x) = \frac{1}{2}\overline{\chi}(x)\left(\gamma_\mu - 1\right)\frac{\tau^b}{2} U_\mu(x)\chi(x+a\hat{\mu}) + \frac{1}{2}\overline{\chi}(x+a\hat{\mu})U^\dagger_\mu(x)\left(\gamma_\mu + 1\right)\frac{\tau^b}{2}\chi(x)\,, \tag{3.51}$$

which is exactly conserved in standard Wilson theory, i.e. $Z_{\widetilde{V}} = 1$. Since one is free to choose a mass-independent renormalization scheme and determine Z-factors in the chiral limit, where all masses are set to zero, $Z_{\widetilde{V}} = 1$ still holds. Now, from the vector lattice chiral ward identity with twisted fields

[VI] We remind here that D_W is γ_5-hermitean, i.e. $(\gamma_5 D_W)^\dagger = \gamma_5 D_W$, or equivalently $D_W^\dagger = \gamma_5 D_W \gamma_5$.

one can, as long as $y \neq x_1, ..., x_n$, obtain the *exact lattice identity*

$$\frac{\partial}{\partial y^\mu} \left\langle \widetilde{V}^b_\mu(y) \mathscr{O}(x_1, ..., x_n) \right\rangle = 2\,\mu_{\rm tm}\,\varepsilon^{dc3} \left\langle P^d(y) \mathscr{O}(x_1, ..., x_n) \right\rangle . \tag{3.52}$$

From eqs. (3.49) and (3.50) one may obtain

$$Z_A\,\nabla^*_\mu A^\pm_\mu(x)\,\cos\omega \mp i\,\nabla^*_\mu \widetilde{V}^\pm_\mu(x)\,\sin\omega = 2\,Z_P\,P^\pm(x) \sqrt{Z^2_{\mu_{\rm tm}}\,\mu^2_{\rm tm} + Z^2_m\,m^2_q}\,, \tag{3.53}$$

where now $m_q = m_0 - m_{\rm cr}$, which at maximal twist becomes

$$\mp i\,\nabla^*_\mu \widetilde{V}^\pm_\mu(x) = 2\,(Z_{\mu_{\rm tm}}\,\mu_{\rm tm})\,(Z_P\,P^\pm(x))\,, \tag{3.54}$$

where confronting eq. (3.54) with eq. (3.52) implies the crucial identity

$$Z_{\mu_{\rm tm}}\,Z_P = 1\,. \tag{3.55}$$

Any explicit renormalization-related Z prefactor of the maximally twisted moments cancels out, elucidating one of the key reasons for our choice of discretization. All put together, one obtains

$$\left\langle \partial_\mu \mathscr{A}^\pm_{\mu,R}(x)\,\mathscr{P}^\mp(y) \right\rangle = \lim_{a\to 0} 2\mu_{\rm tm} \left\langle P^\pm(x)\,P^\mp(y) \right\rangle \big|_{\omega=\pi/2}\,, \tag{3.56}$$

where this identity is of particular importance since it avoids the presence of the Z_A factor in the evaluation of decay constants, and we will employ it in Subsection 4.4.2.

3.5.2. Twisted Mass Moments

We are now ready to give our twisted mass, lattice definition[VII] of moments, namely

$$\mathscr{M}_n(a,z) \overset{\rm def.}{=} 2 \lim_{T,L\to\infty} \left(\frac{a}{L}\right)^3 \sum_{t=0}^{T} a\,t^n \sum_{\vec{x},\vec{y}=0}^{L-a} a^3 \left\langle J^\dagger(t,\vec{x},\mu_{\rm tm})\,J(0,\vec{y},\mu_{\rm tm}) \right\rangle \quad \text{where} \tag{3.57}$$

$$J(t,\vec{x},\mu_{\rm tm}) = i\,\mu_{\rm tm}\,\overline{h}(t,\vec{x})\,\gamma_5\,h'(t,\vec{x}) \tag{3.58}$$

where we exploited the property of our observable to be invariant for $t \to -t$ at maximal twist, like in the continuum. Note, due to eq. (3.55), no further renormalization constants are present and eq. (3.57) is finite for $n > 3$, i.e. once short-time divergences explicitly seen in eq. (2.16) are removed.

All computations present in literature employing the pseudo-scalar density operator make use of discretizations where explicit renormalization constants are absent, be it staggered fermions [138, 36] or domain wall fermions [126] (let us mention here also the only twisted mass result by ETMC [93], which remains unpublished).

Up to now, all collaborations working with moments [3, 36, 126, 138] normalized them by their

[VII] Of course, in simulations $J(0,\vec{y})$ has to be far enough from boundaries (if present, as in our case, see Subsection 4.2.2) and the sum over time-slices will be truncated, both to reduce noise and, again, to avoid coming close to boundaries. These further lattice details will be presented in Section 5.3.

finite a tree-level, computed numerically on a lattice alike the one of the non-perturbative computation, but with all gauge links set to $U_\mu(x) = \mathbb{1}$. We opted for an analytical computation, done both in finite and infinite volume, detailed in Appendix C. This so called "tree-level improvement" is naively expected to reduce scaling violations and ameliorate the continuum limit due to the following. Given a lattice observable $\mathscr{B}(a,m)$ – m indicating any energy scale the observable may depend on – its bare lattice perturbation theory expansion is formally

$$\mathscr{B}(a,m) = \mathscr{B}^{(0)}(a,m) + \alpha_{\text{bare}}\mathscr{B}^{(1)}(a,m) + \mathscr{O}(\alpha_{\text{bare}}^2)\,, \tag{3.59}$$

which one can divide by $\mathscr{B}^{(0)}(a,m)$ obtaining

$$\frac{\mathscr{B}(a,m)}{\mathscr{B}^{(0)}(a,m)} = 1 + \alpha_{\text{bare}}\frac{\mathscr{B}^{(1)}(a,m)}{\mathscr{B}^{(0)}(a,m)} + \mathscr{O}(\alpha_{\text{bare}}^2)\,. \tag{3.60}$$

Supposing now lattice artefacts to start at order l

$$\mathscr{B}^{(i)}(a,m) = \mathscr{B}^{(i)}(0,m) + p_1^{(i)}a^l + \mathscr{O}(a^{l+1})\,, \quad \forall i \geq 0\,, \tag{3.61}$$

in eq. (3.60) the leading $\mathscr{O}(a^l)$ effects are naively suppressed by an α_{bare} factor, with leftover $\mathscr{O}(\alpha_{\text{bare}}a^l)$ cutoff effects; for improved observables $l = 2$.

Let us be specific to moments: their tree-level is

$$\mathscr{M}_n^{\text{TL}}(a\mu_{\text{tm}}, L/a) \overset{\text{def.}}{=} \mathscr{M}_n^{(\text{lat})}\big|_{g_0=0}\,, \tag{3.62}$$

which we analytically computed in order to define the following tree-level normalized version of moments

$$R_n(a,z) \overset{\text{def.}}{=} \begin{cases} \frac{\mathscr{M}_n(aM_{\text{RGI}},z)}{\mathscr{M}_n^{\text{TL}}(a\mu_{\text{tm}}^{\text{TL}},L/a)}\,, & n = 4, \\ \left(\frac{\mathscr{M}_n(a,z)}{\mathscr{M}_n^{\text{TL}}(a\mu_{\text{tm}}^{\text{TL}},L/a)}\right)^{\frac{1}{n-4}}\,, & n = 6, 8, 10 \end{cases}\,. \tag{3.63}$$

This division greatly improves the continuum approach of moments, as can be seen in figs. 3.1a and 3.1b. However, we glossed over some important details, namely:

1. In eq. (3.61) we supposed the leading cutoff effects to come in powers of a, as is oftentimes done, but which is known to be an incomplete picture due to the presence of logarithmic dependence on a [90].
2. Although the correlator indeed has $l = 2$, this does not suffice to conclude the same for *the moment*, an observable integrated over all time distances, including $t \to 0$ [43].
3. Although the cutoff effects are indeed observed to decrease in absolute size not only for the correlator, but for moments as well (see section 3.5.2), the tree-level division may enhance the curvature complicating the functional form of the a-extrapolation, as observed for the $n = 4$ case [43] described in Subsection 6.1.2.

Let us conclude the chapter by writing the full, tree-level normalized version of eq. (2.20), which we

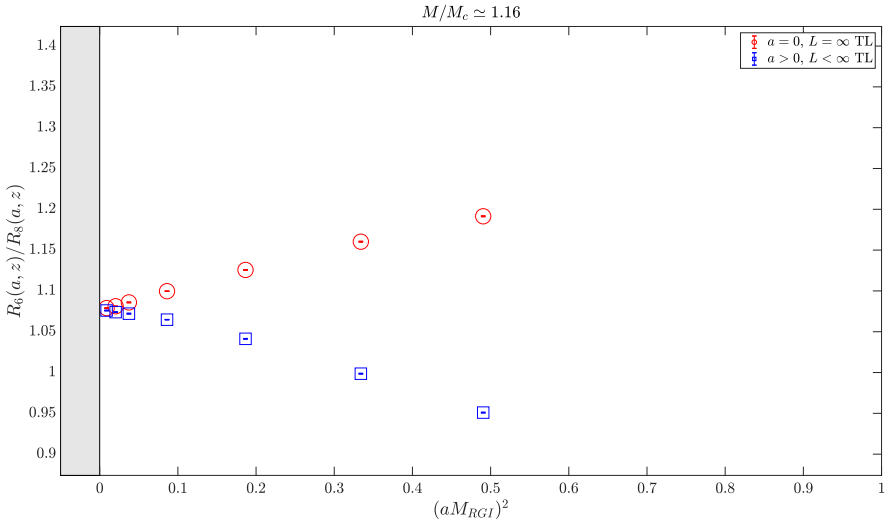

(a) *Close to the continuum, a mild improvement can be seen for the ratio R_6/R_8 at $z = 4.5$, one of the lower mass values.*

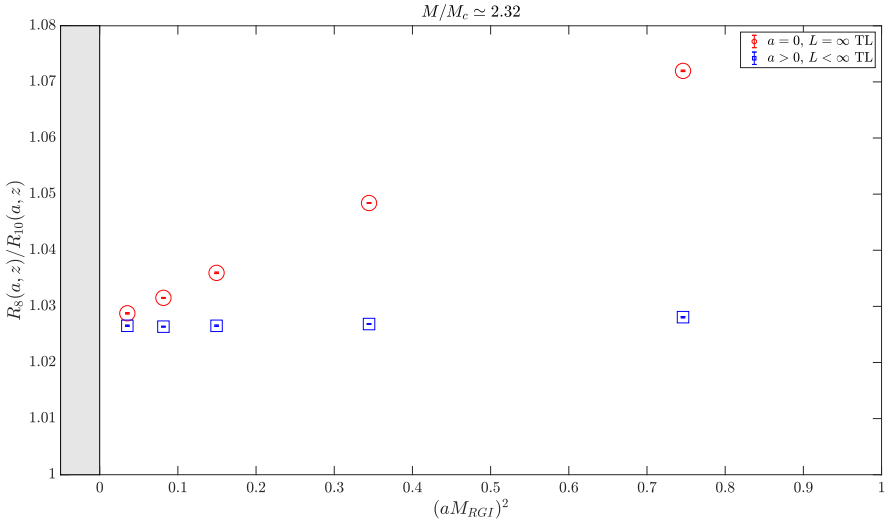

(b) *Ratio R_8/R_{10} for $z = 9$, one of the higher masses: here, a very strong improvement is immediately noticeable.*

Figure 3.1: *Comparison of continuum approach for two different tree-level normalizations. In red the moment divided by the continuum tree-level calculated in infinite volume, whereas blue points have been obtained with a computation at finite volume and lattice spacing, with the sum over spatial momentum in eq. (C.68) performed numerically.*

will study in depth in the next chapters in order to extract the coupling, namely

$$\mathscr{R}_n(z, aM_{\mathrm{RGI}}) \overset{\text{def.}}{=} \begin{cases} R_4(z, aM_{\mathrm{RGI}}) & n = 4\,, \\ \frac{R_n(z,a)}{R_{n+2}(z,a)} & n = 6,\, 8 \end{cases} \quad , \tag{3.64}$$

which we again stress is dimensionless and thus only depends on z and aM_{RGI}. Obtaining the perturbative coefficients of $\mathscr{R}_n$ with $n > 4$, which we refer to as $\{\tilde{r}_n^{(i)}\}$, from $\{r_n^{(i)}, r_{n+2}^{(i)}\}$ poses no problem and just requires some algebra and a perturbative re-expansion.

4 | Lattice Computations

LATTICE QCD's success in multiple applications owes much to its key feature, the possibility of performing computer simulations for several observables of interest. In these computations regions of parameter space difficult to access with other methods, for instance when the physical coupling is large and perturbative expansions become meaningless, can be studied with a systematically improvable methodology.

Lattice QCD computations are labeled by the number N_f of dynamical quark flavors present in the action, which defines the probability distribution of the generated ensemble of field configurations. This work has $N_f = 0$, also called *quenched theory*, meaning the underlying gauge fields are distributed according to a pure Yang-Mills weight and the costly inversion of the Dirac matrix D is necessary only for computing quark-related observables, unlike the $N_f > 0$ case where already the ensemble generation itself requires it. To make this more precise, consider the path integral needed to compute some observable $\mathcal{O}[\overline{\psi}, \psi, U]$

$$\langle \mathcal{O}[\psi,\overline{\psi},U]\rangle = \mathcal{Z}_{N_f}^{-1} \int \mathrm{D}[\overline{\psi},\psi,U]\, \mathcal{O}[\psi,\overline{\psi},U] e^{-\mathcal{S}_W[U]-\mathcal{S}_F[U,\psi,\overline{\psi}]} \tag{4.1}$$

$$= \mathcal{Z}_{N_f}^{-1} \int \mathrm{D}[U] \det\{D[U]\}\, e^{-\mathcal{S}_W[U]} \widetilde{\mathcal{O}}_{N_f}[U] \tag{4.2}$$

$$\overset{N_f\to 0}{\simeq} \mathcal{Z}_0^{-1} \int \mathrm{D}[U] \underbrace{\det\{\cancel{D[U]}\}}_{\text{set to 1}} e^{-\mathcal{S}_W[U]} \widetilde{\mathcal{O}}_0[U], \quad \text{where} \tag{4.3}$$

$$\mathcal{Z}_{N_f} = \int \mathrm{D}[\psi,\overline{\psi},U] e^{-\mathcal{S}_W[U]-\mathcal{S}_F[U,\psi,\overline{\psi}]} = \int \mathrm{D}[U] \det\{D[U]\}\, e^{-\mathcal{S}_W[U]} \tag{4.4}$$

$$\overset{N_f\to 0}{\Longrightarrow} \mathcal{Z}_0 \overset{\text{def.}}{=} \int \mathrm{D}[U] \underbrace{\det\{\cancel{D[U]}\}}_{\text{set to 1}} e^{-\mathcal{S}_W[U]}, \quad \text{and} \tag{4.5}$$

$$\widetilde{\mathcal{O}}_0[U] = \underbrace{\frac{1}{\det\{\cancel{D[U]}\}}}_{\text{set to 1}} \int \mathrm{D}[\psi,\overline{\psi}] \mathcal{O}[\psi,\overline{\psi},U] e^{-\mathcal{S}_F[U,\psi,\overline{\psi}]}, \tag{4.6}$$

so that quark fields present are the ones contained in the observable only, i.e. *valence quarks*. In perturbation theory this would amount to setting all internal quark loops to zero. The name "quenching limit" indeed comes from the equivalence with the infinite quark-mass limit, which means they are "frozen in place" and cannot propagate. The quenched model is thus expected to better approximate the full theory the heavier the quenched quark flavor is.

Note that D is a very large, yet sparse, matrix. Each spinor field carries $n_{\text{dof}} = N_c \times \dim[R_D]$ indices, where N_c is the number of colors and $R_D = (1/2,0) \oplus (0,1/2)$ (yielding $\dim[R_D] = 4$) is the reducible

Dirac spinor representation. Thus, an action quadratic in these fields has a Dirac matrix of size $\dim[D] = (n_{\text{dof}} \cdot V_4) \times (n_{\text{dof}} \cdot V_4)$, where V_4 is the 4 dimensional volume of the lattice. This implies a very large number of degrees of freedom, for instance with $V_4 = 32^4$ one has a matrix D with more than 10 million columns and rows. In most theories, however, since the action is local, D will be a sparse matrix which is a key advantage for its inversion.

The choice of carrying out this study in the quenched model is due to the algorithmic advantage, differently stated it becomes cheaper and thus feasible to reach smaller lattice spacings. The main objective of this work is not computing a value of the coupling competitive w.r.t. other computations, rather it is to study the two main systematic errors of the moments method for a varying energy range: the cutoff effects and the truncation error. Regarding the former, the largest source is expected to come from heavy quarks (up to logarithmic corrections, see [43]), while the latter is determined by two factors: the unknown coefficient $C_{2n}^{(4,0)}$ of eq. (2.8) (plus higher order corrections) and by the coupling's value and running at a given scale. How the size of the truncated part *changes with the scale* is, in turn, encoded in the $\beta_{\overline{\text{MS}}}(\alpha_{\overline{\text{MS}}})$-function; quantitatively put, in the asymptotic region

$$\beta_{\overline{\text{MS}}}(\alpha_{\overline{\text{MS}}}) \overset{\alpha \to 0}{\sim} -\beta_0 \alpha_{\overline{\text{MS}}}^2(\mu) - \beta_1 \alpha_{\overline{\text{MS}}}^3(\mu) + \mathcal{O}(\alpha^4), \quad \text{with} \tag{4.7}$$

$$[\beta_0, \beta_1] = \left[\frac{1}{(4\pi)} \left(11 - \frac{2}{3} N_f \right), \frac{1}{(4\pi)^2} \left(102 - \frac{38}{3} N_f \right) \right] \simeq \begin{cases} [0.88, 0.65], & N_f = 0 \\ [0.66, 0.33], & N_f = 4 \end{cases}, \tag{4.8}$$

so that there is strong perturbative indication to expect a very similar behavior, qualitatively but also quantitatively, between the quenched and the fully dynamical (lattice accessible) case, namely $N_f = 4$. To conclude, a quenched computation is a well motivated first step into studying the size of the asymptotic scaling region of moments.

4.1. THE GAMMA-METHOD

Using an approach statistical in nature, as introduced in Subsection 3.3.2, poses the question of how to practically generate configurations which are statistically (close to) independent. One needs an algorithm that generates the next configuration in the Markov chain by updating the link variables of the lattice, but it is in practice unavoidable to have some leftover correlation between subsequent elements, called *auto-correlation*. Common approaches to evaluate this effect are the statistical bootstrap and the jackknife method, combined with some binning procedure. Within the ALPHA collaboration the so called Γ-*metohd* is used [164], in which one explicitly tries to compute the *auto-correlation function*, to be introduced below. What is explained in [164], with some further improvements discussed in [145], is implemented in the MATLAB package `dobs`. Below we give a short description of the Γ-method, mostly following the above mentioned references.

Given a sample of random values $(a^1, a^2, ..., a^N)$, such as measurements of some primary quantity[I] on Monte Carlo generated configurations which are here supposed to be thermalized and in equilibrium,

[I] In this context primary quantity refers to the average of a directly measured observable, whereas secondary or derived quantity refers to a function of several such averages.

the standard estimators (in this section always indicated by hats) for their expectation value $\langle a^i \rangle$ and variance $\sigma^2_{a^i} = \left\langle (a^i - \langle a^i \rangle)^2 \right\rangle$ are

$$\hat{a} = \frac{1}{N}\sum_{i=1}^{N} a^i, \quad \hat{\sigma}^2_a = \frac{1}{N-1}\sum_{i=1}^{N} \left(a^i - \hat{a}\right)^2 . \tag{4.9}$$

Now, the estimator $\hat{a}$ on a sample of the ensemble is a random variable as well, because its value on different samples will fluctuate around the "true" value $\langle a \rangle$ with variance

$$\sigma^2_{\hat{a}} = \left\langle \left(\hat{a} - \langle a \rangle\right)^2 \right\rangle = \frac{1}{N^2} \left\langle \sum_{i,j=1}^{N} \left(a^i - \langle a^i \rangle\right)\left(a^j - \langle a^j \rangle\right) \right\rangle \stackrel{\text{def}}{=} \frac{1}{N^2} \sum_{i,j=1}^{N} \Gamma_a(i-j), \tag{4.10}$$

where $\langle a^i \rangle = \langle a^j \rangle = \langle a \rangle$ and $\Gamma_a(t)$ is the auto-correlation function (with $t = i - j$). For uncorrelated data this reduces to the well-known result $\sigma^2_{\hat{a}} = \sigma^2_a / N$, expressing the $N^{-1/2}$ decrease in the error of the estimator. Note that we have assumed $\hat{a}$ fluctuates around the "true value" $\langle a \rangle$ in a Gaussian fashion, which is guaranteed by the central limit theorem[II]. Let us now introduce the auto-correlation function for multiple primary quantities, indexed by α and β, again with $t = i - j$

$$\Gamma_{\alpha\beta}(t) = \left\langle \left(a^i_\alpha - \langle a^i_\alpha \rangle\right)\left(a^j_\beta - \langle a^j_\beta \rangle\right) \right\rangle . \tag{4.11}$$

Introducing for later notational convenience the deviations $\Delta_\alpha = a_\alpha - \langle a_\alpha \rangle$, we can calculate for correlated data

$$\langle \Delta_\alpha \Delta_\beta \rangle = \frac{1}{N^2} \sum_{i,j=1}^{N} \Gamma_{\alpha\beta}(i-j) \stackrel{\text{III}}{=} \frac{1}{N^2} \sum_{t=-(N-1)}^{t=-N-1} \sum_{k=1}^{N-|t|} \Gamma_{\alpha\beta}(t) = \sum_{t=-N}^{N} \frac{N-|t|}{N^2} \Gamma_{\alpha\beta}(t) \tag{4.12}$$

$$= \frac{1}{N}\Gamma_{\alpha\beta}(0) + \frac{1}{N} \sum_{t=-N}^{N} \Gamma_{\alpha\beta}(t) \left(1 - \frac{|t|}{N}\right) , \tag{4.13}$$

which we can further elaborate as follows: $\Gamma_{\alpha\beta}(t)$ typically has an asymptotic (associated to its slowest mode) exponential decay with $|t|$ characterized by some scale τ_{exp}, the factor $1 - t/N$ can be dropped for N large enough, i.e. for $\tau_{\text{exp}} < |t| < N$, whereas for $0 < |t| < \tau_{\text{exp}}$ the term is extremely close to unity. Thus, we obtain

$$\langle \Delta_\alpha \Delta_\beta \rangle = \frac{1}{N} \sum_{t=-N}^{N} \Gamma_{\alpha\beta}(t) \times \left(1 + O\left(\frac{\tau_{\text{exp}}}{N}\right)\right) . \tag{4.14}$$

Now consider a secondary quantity defined as a function of primary quantities, i.e. $F = f(\langle a_\alpha \rangle)$ estimated via $\hat{F} = f(\hat{a}_\alpha)$. *Assuming* N large enough to have accurate estimates and justifying Taylor

[II] The key idea being that for $N \to \infty$ the properly normalized sum of N independent random variables with finite expectation value and variance is distributed according to a normal distribution, which acts therefore as an *attractor distribution*, even though the individual a^i need not be normally distributed.

[III] In this equality we have changed variables with a mapping of the square $[1,N] \times [1,N]$ into $[-(N-1),(N-1)] \times [1, N-|t|]$ for convenience.

expanding around the "true value" $\langle F \rangle$ we write

$$\hat{F} = f(\hat{a}_\alpha) + \sum_\alpha \frac{\partial f}{\partial a_\alpha}\bigg|_{a_\delta} \hat{\Delta}_\alpha + \frac{1}{2}\sum_{\alpha\beta} \frac{\partial^2 f}{\partial a_\alpha \partial a_\beta}\bigg|_{a_\delta} \hat{\Delta}_\alpha \hat{\Delta}_\beta + \dots , \tag{4.15}$$

with $\hat{\Delta}_\alpha = a_\alpha - \hat{a}_\alpha$ and from which follows that the estimator for F is biased unless one is dealing with a linear $f(a_\alpha)$. The bias is usually small compared to statistical errors [164]. The error on the derived quantity F can then be obtained by

$$\sigma_F^2 = \langle (F - \langle F \rangle)^2 \rangle \simeq \frac{1}{N} \sum_{\alpha\beta} \frac{\partial f}{\partial a_\alpha}\bigg|_{a_\delta} \frac{\partial f}{\partial a_\beta}\bigg|_{a_\delta} \sum_{t=-\infty}^{\infty} \Gamma_{\alpha\beta}(t) , \tag{4.16}$$

which, once we define

$$v_F \overset{\text{def.}}{=} \sum_{\alpha\beta} \frac{\partial f}{\partial a_\alpha}\bigg|_{a_\delta} \frac{\partial f}{\partial a_\beta}\bigg|_{a_\delta} \Gamma_{\alpha\beta}(0) , \tag{4.17}$$

can be rewritten as

$$\tau_{\text{int},F} \overset{\text{def.}}{=} \frac{1}{2v_F} \sum_{\alpha\beta} \frac{\partial f}{\partial a_\alpha}\bigg|_{a_\delta} \frac{\partial f}{\partial a_\beta}\bigg|_{a_\delta} \sum_{t=-\infty}^{\infty} \Gamma_{\alpha\beta}(t) \tag{4.18}$$

$$\sigma_F^2 = 2\frac{\tau_{\text{int},F}}{N} v_F \quad , \tag{4.19}$$

where v_F is F's variance in the absence of auto-correlations. This factor is multiplied by the *integrated auto-correlation time* $2\tau_{\text{int},F}$, which almost always[IV] increases the error due to auto-correlation. It can be thought of as the Monte Carlo time needed to actually produce two configurations which are independent, meaning $N/2\tau_{\text{int},F}$ represents an "effective" number of measurements, thereby assessing the efficiency of the algorithm.

As an estimator for $\Gamma(t)_{\alpha\beta}$ we use

$$\hat{\Gamma}(t)_{\alpha\beta} \overset{\text{def.}}{=} \frac{1}{N-t} \sum_{i=1}^{N-t} (a_\alpha^i - \hat{a}_\alpha)(a_\alpha^{i+t} - \hat{a}_\alpha) , \tag{4.20}$$

from which we define

$$\hat{\Gamma}_F(t) \overset{\text{def.}}{=} \sum_{\alpha\beta} \frac{\partial f}{\partial a_\alpha}\bigg|_{a_\delta} \frac{\partial f}{\partial a_\beta}\bigg|_{a_\delta} \hat{\Gamma}_{\alpha\beta}(t) , \tag{4.21}$$

for the derived quantity F. It is now trivial do define

$$\hat{v}_F \overset{\text{def.}}{=} \hat{\Gamma}_F(0) , \tag{4.22}$$

whereas some care must be taken for the integrated auto-correlation time. The sum over t will be

[IV] It can happen that $\rho(t) = \Gamma(t)/\Gamma(0) < 0$ for some t, a phenomenon called anti-correlation.

truncated after W steps, giving

$$\hat{\tau}_{\text{int},F} \overset{\text{def.}}{=} \frac{1}{2\hat{v}_F}\left[\hat{\Gamma}_F(0) + 2\sum_{t=1}^{W}\hat{\Gamma}_F(t)\right], \tag{4.23}$$

where W has to be large enough w.r.t. the decay time τ_{exp} introduced above, in order to suppress the systematic error coming from the truncation itself. This error decays roughly exponentially with W/τ_{exp}. At the same time W needs to be small enough as to not include the t region where the signal is exponentially suppressed while the noise becomes prominent. The selection of W is carried out in order to minimize the sum of the absolute value of the two mentioned errors, using approximations based on [118]. A similar balancing of errors for both simple and jackknife binning, where the bin size B plays an analogous role to $2W$, leads to a an error estimator which has a slightly larger error [164], whereas with the Γ-method a slightly quicker decay with N is achieved. The root of the disadvantage of binning methods lies in the systematic error decaying only as an inverse power of B.

4.2. CRITICAL SLOWING DOWN

As described in Section 3.1, lattice QCD's continuum limit $a \to 0$ corresponds to $g_0 \to g_{\text{critical}} = 0$, i.e. the lattice theory has a critical surface which is approached for $a \to 0$. At the critical surface the correlation lengths in lattice units ξ/a diverge, meaning one can extract finite physical quantities in the $a \to 0$ limit. From an algorithmic perspective, though, this means the correlation between configurations in the Markov chain grows and it becomes computationally more costly to efficiently update the gauge links so that two subsequent configurations are effectively independent. The auto-correlation times are non-universal: they depend on the algorithm, on the observable, and on the chosen discretization. The topological charge Q, which we define below, is known to have large auto-correlation times [52, 145]. This property is an effect of the strong coupling of Q to slow modes of the Markov process' transition matrix and by no means an intrinsic property of the topological charge itself. How strong a slow mode couples to some observable cannot be known a-priori. Moreover, an observable's weak coupling to a slow mode does not necessarily imply no significant contribution to its statistical error is present.

4.2.1. Topological Charge

Simulating theories on a necessarily finite lattice requires some care in the choice of boundary conditions; a specific choice may be particularly fruitful depending on the situation. The most common choice is that of periodic and anti-periodic boundary conditions for, respectively, gauge and fermion fields. Thus, translation invariance is preserved, which has both theoretical and practical advantages.

One of the main drawbacks of periodic boundary conditions is the emergence of multiple so called topological sectors, which are disconnected in the continuum limit. These are sets of classical gauge configurations in different non-trivial homotopy classes, which can be labeled by a winding number,

commonly called *topological charge* [14, 79, 142]

$$Q = \int \mathrm{d}^4x \frac{1}{32\pi^2} \varepsilon_{\mu\nu\rho\sigma} \operatorname{tr}\left\{F_{\mu\nu}(x) F_{\rho\sigma}(x)\right\}, \tag{4.24}$$

which can be shown to be integer valued and where $F_{\mu\nu}$ is defined in eq. (1.8). Upon quantization also discontinuous configurations are present, stemming from the strongly fluctuating gauge fields in the path integral, so that disconnected field space has to be understood in the classical sense. Integer valued Q is related to the fact that, given periodic boundary conditions, the relevant quantity to determine connectedness of classical configurations is the third homotopy group π_3 of $SU(3)$, which is $\pi_3(SU(N)) = \pi_3(SU(2)) = \mathbb{Z}, \forall N \geq 2$. Integer valued winding numbers also emerge in very simple cases such as a free quantum mechanical particle on a circle or $U(1)$ gauge theory in $d = 2$, which are used to study alternative approaches to avoid the issue of *topological freezing* [145, 52]. This problem can be understood as follows: at finite lattice spacing any value for Q is possible, but moving towards the $a \to 0$ limit the relative weight of configurations with non-integer valued Q decreases with a high power of a, rendering the link update – which achieves transitions between sectors – more and more difficult. Thus, one has the *emergence* of disconnected sectors in the continuum limit as a dynamical property of fully quantized, lattice fields, rather than having them stemming from a classical continuity assumption.

The Atiyah-Singer index theorem [9], which we here only mention for the continuum case (for a lattice discussion, see [79]), somewhat unexpectedly states a connection between the topological charge, a quantity defined fully in terms of gauge degrees of freedom, and the number zero modes of fermion fields. Thus, various lattice definitions are possible and one might be advantageous over another, depending on the situation. In this study we employ a standard, symmetric gluonic field tensor definition in terms of a gradient-flow-smoothed plaquette operator (see eq. (3.21) and eq. (3.4)), namely

$$Q(t) = a \sum_{x_0>0}^{T-1} \sum_{\vec{x}} a^3 \frac{-1}{32\pi^2 2^4} \sum_{\alpha\beta\rho\sigma=\pm1}^{\pm4} \varepsilon_{\alpha\beta\rho\sigma} \operatorname{tr}\left\{U(t,x)_{\alpha,\beta} U(t,x)_{\rho\sigma}\right\}, \tag{4.25}$$

where $\varepsilon_{\alpha\beta\rho\sigma} = -\varepsilon_{(-\alpha)\beta\rho\sigma}$ and where the x_0-sum extrema are due to open boundary conditions, explained in the following.

4.2.2. Open Boundary Conditions

The effect of using open boundary conditions to ameliorate topological freezing in the case of HMC and SMD algorithms was studied in [113]. The continuum boundary conditions for the gauge potential $A_\mu(x)$ are periodic in space and

$$F_{0k}(x)|_{x_0=0} = F_{0k}(x)|_{x_0=T} = 0, \quad k = 1,2,3, \tag{4.26}$$

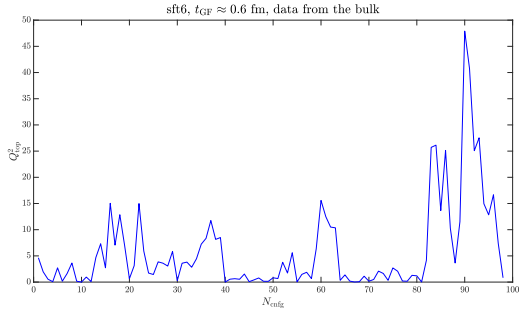

(a) *Evolution in simulation time of topological charge squared* $Q^2(t_{GF})$.

(b) *Distribution of the topological charge squared* $Q^2(t_{GF})$.

Figure 4.1: *Topological charge Q for ensemble sft6.*

in time, so that gauge invariance is preserved. Quark fields satisfy

$$P_+ \psi(x)|_{x_0=0} = P_- \psi(x)|_{x_0=T} = 0\,, \quad P_\pm = (\mathbb{1}_4 \pm \gamma_0)/2\,, \tag{4.27}$$

$$\overline{\psi} P_-|_{x_0=0} = \overline{\psi} P_+|_{x_0=T} = 0\,, \tag{4.28}$$

which implies $\overline{\psi}\psi$ vanishes at the boundaries and no boundary counterterms will be necessary. With this setup it has been shown [113] that classical field space is not disconnected into topological sectors and the topological charge can vary smoothly by "flowing through" the time boundary. In order to check that we are not affected by topological freezing, we monitor Q^2 as a function of simulation time. We use *Q squared*, since Q is parity odd and its ensemble average vanishes [145]. In figs. 4.1a and 4.2a it can be seen for our second and third finest ensembles, where the critical slowing down can be severe (more plots in Appendix D, figs. D.1 and D.2). Clearly, Q^2 varies among a large and non-integer set of values, although the aforementioned flowing in/out through the (physical) time boundary takes a non negligible (simulation) time, so that subsequent configurations tend to have somewhat similar values of Q^2. Still, given the small number of configurations the overall distribution of Q^2 in figs. 4.1b and 4.2b is satisfactory enough to claim no significant topological freezing is observed.

Finally, let us mention o.b.c. require an additional factor at the boundary in eq. (3.3), namely

$$\mathcal{S}_W \overset{\text{def.}}{=} \frac{1}{g_0^2} \sum_{x,\mu<\nu} w(x,\mu)\,\mathrm{Re}\left\{\mathrm{tr}\left[\mathbb{1} - U(x)_{\mu,\nu}\right]\right\}\,, \tag{4.29}$$

where $w(x,\mu) = 1$ for all plaquettes of the lattice, except for the ones lying entirely on the boundary time slice, where $w(x,\mu) = 1/2$.

4.3. COMPUTING CORRELATORS

The computation of a meson correlator on the lattice amounts to:

1. The computation of the quark propagator $S(x,y,\mu_{tm})$.
2. The contraction of the propagators in order to form the desired correlator.

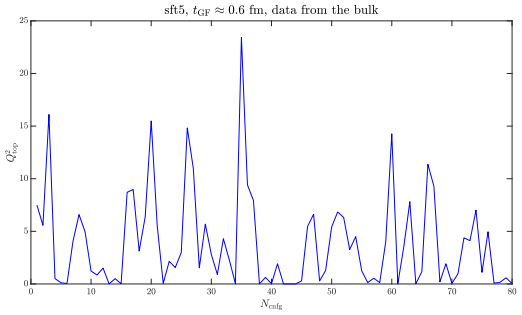

(a) *Evolution in simulation time of topological charge squared* $Q^2(t_{\mathrm{GF}})$.

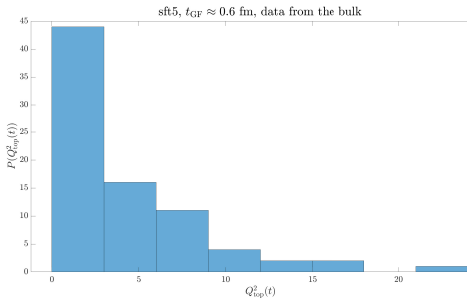

(b) *Distribution of the topological charge squared* $Q^2(t_{\mathrm{GF}})$.

Figure 4.2: *Topological charge Q for ensemble sft5.*

3. The average over configurations within the ensemble, eq. (3.26).

An efficient way of doing this is by using stochastic noise sources, which we call η, placed at the time slice of the quark source.

4.3.1. Stochastic Estimation of the Trace

The noise sources are random fields following some distribution, typical choices being $U(1)$ (our choice), Gaussian, $\mathbb{Z}_2$, and which obey

$$\langle \eta_i(\vec{x}) \rangle_{\mathrm{src}} = 0\,, \quad i = 1,2,\ldots N_s\,, \tag{4.30}$$

$$\left\langle \eta_i^\dagger(\vec{x})\eta_j(\vec{y}) \right\rangle_{\mathrm{src}} = \delta_{i,j}\delta_{\vec{x},\vec{y}}\,, \quad i = 1,2,\ldots N_s\,. \tag{4.31}$$

They are placed on the source time-slice x_0, whereas the sink is located at y_0 and we label their distance in time by $t = x_0 - y_0$. The inserted noise sources have to be equivalent to a stochastic representation of $\mathbb{1}$, i.e. they have to be decoupled from the dynamical fields and cannot affect the physics, while at the same time computing

$$G(t,a) = L^{-3}\sum_{\vec{x},\vec{y}} C(x,y) = L^{-3}\sum_{\vec{x},\vec{y}} \left\langle \overline{h}'(x)\Gamma_A h(x)\,\overline{h}(y)\overline{\Gamma}_B h'(y) \right\rangle \tag{4.32}$$

in a more efficient way. Here we indicate by Γ a generic Dirac matrix structure[V]. The above, after the fermionic path integral, can be rewritten in the case of mass degenerate twisted mass Wilson fermions as

$$G(t,a) = -L^{-3}\sum_{\vec{x},\vec{y}} \mathrm{tr}\left\langle \Gamma_A S(x,y,-\mu_{\mathrm{tm}})\overline{\Gamma}_B S(y,x,\mu_{\mathrm{tm}}) \right\rangle^{\mathrm{gauge}}\,, \tag{4.33}$$

where the propagator S is defined by

$$\sum_y D(x,y)\,S(y,z,\mu_{\mathrm{tm}}) = \sum_y \left[D_W(x,y) + i\mu_{\mathrm{tm}}\gamma_5\right] S(y,z,\mu_{\mathrm{tm}}) = \mathbb{1}\,\delta_{x,z}\,. \tag{4.34}$$

[V] We refer the reader to the very clear proceedings [109] for more details.

In eq. (4.33) we have performed the path integral over fermion fields exactly, which corresponds to the possible Wick contractions [160], usually schematically written as

$$C(x,y) = \mathscr{Z}^{-1} \int \mathrm{D}\,[\overline{\psi},\psi,U]\, \overline{h}'(x)\Gamma_A\, h(x)\, \overline{h}(y)\overline{\Gamma}_B\, h'(y) \mathrm{e}^{-\mathscr{S}_W[U]-\mathscr{S}_F[U,\psi,\overline{\psi}]} \tag{4.35}$$

$$= \mathscr{Z}^{-1} \int \mathrm{D}[U] \det\{D[U]\} \operatorname{tr}\left\{\Gamma_A S(x,y,-\mu_{\mathrm{tm}})\overline{\Gamma}_B S(y,x,\mu_{\mathrm{tm}})\right\} \mathrm{e}^{-\mathscr{S}_W}\,, \tag{4.36}$$

where, of course, the propagator still depends on gauge fields. Here, also one of the motivations to choose two different flavors (h, h') mentioned at the beginning (see eq. (2.2)) becomes clear, namely to avoid contractions at the same spacetime point which are (1) costly to evaluate and (2) hard to quantify reliably in perturbation theory.

Since $C(x,y)$ at fixed x_0 and y_0 contains any possible point on the time slices (point-to-point correlator), its computation is quite expensive. The noise sources compute efficiently the correlator *between time-slices* $G(t,a)$, with *sums over space and trace included*. This is achieved by defining the two following stochastic observables

$$\begin{cases} \zeta_{x_0}(u) &= \sum_v [D_W + i\gamma_5\mu_{\mathrm{tm}}]^{-1}(u,v)\,\eta_{x_0}(v) \\ \xi_{x_0}(u) &= \sum_v [D_W + i\gamma_5\mu_{\mathrm{tm}}]^{-1}(u,v)\gamma_5\Gamma_A^\dagger\,\eta_{x_0}(v) \end{cases}, \tag{4.37}$$

and computing the time-slice correlator as

$$G(t,a) = -L^{-3}\sum_{\vec{y}} \left\langle \xi^\dagger_{x_0}(y)\gamma_5\overline{\Gamma}_B\zeta_{x_0}(y)\right\rangle^{\text{noise, gauge}}. \tag{4.38}$$

One can show the equivalence of $G(t,a)$'s definition with eq. (4.38) by expanding the latter

$$G(t,a) = -L^{-3}\sum_{\vec{y}} \Big\langle \sum_k \eta^\dagger_{x_0}(k)\Gamma_A\gamma_5(\gamma_5 D_W\,\gamma_5 - i\mu_{\mathrm{tm}}\gamma_5)^{-1}(k,y)\gamma_5\overline{\Gamma}_B \times \tag{4.39}$$

$$\sum_l (D_W + i\gamma_5\mu_{\mathrm{tm}})^{-1}(y,l)\,\eta_{x_0}(l)\Big\rangle^{\text{noise, gauge}}$$

$$= -L^{-3}\sum_{\vec{y}} \Big\langle \sum_k \eta^\dagger_{x_0}(k)\Gamma_A(D_W - i\mu_{\mathrm{tm}}\gamma_5)^{-1}(k,y)\overline{\Gamma}_B \times \tag{4.40}$$

$$\sum_l (D_W + i\gamma_5\mu_{\mathrm{tm}})^{-1}(y,l)\eta_{x_0}(l)\Big\rangle^{\text{noise, gauge}}$$

$$= -L^{-3}\sum_{\vec{y},k,l} \Big\langle \delta_{k_0,x_0}\delta_{l_0,x_0}\delta_{\vec{k},\vec{l}}\,\delta_{\text{color, spin}}\Gamma_A(D_W - i\mu_{\mathrm{tm}}\gamma_5)^{-1}(k,y)\overline{\Gamma}_B \times \tag{4.41}$$

$$(D_W + i\gamma_5\mu_{\mathrm{tm}})^{-1}(y,l)\Big\rangle^{\text{gauge}},$$

so that we have obtained $G(t,a)$ as we wrote it in eqs. (4.33) and (4.34).

4.3.2. Solvers

In order to solve the Dirac equation a variety of algorithms exist [109, 144]. We use the conjugate gradient [84] on normal equations (CGNE) for most of the computations (a very clear review can be found in [148]), in which from a γ_5-symmetric D the Hermitean operator $Q = \gamma_5 D$ is defined (not to be confused with the topological charge), so that $Q^2 = D^\dagger D$ is positive definite. From a Dirac equation $D\psi = \eta$ the corresponding system for Q^2 can be solved through the conjugate gradient. Now, the γ_5-symmetry defined as

$$D^\dagger = \gamma_5 D \gamma_5 \,, \tag{4.42}$$

is valid for most lattice Dirac operators, such as D_W, but not for the ($N_f = 2$ mass degenerate) twisted Wilson case. However, normal equations on which to apply the CG can still be obtained as above, with purely positive eigenvalues, since

$$D^\dagger(\mu_{\rm tm}) = (D_W + i\mu_{\rm tm}\gamma_5\tau_3)^\dagger = \gamma_5 D_W \gamma_5 - i\mu_{\rm tm}\gamma_5\tau_3 \equiv \gamma_5 D(-\mu_{\rm tm})\gamma_5 \,, \tag{4.43}$$

already discussed in eq. (3.47). We stress that in theory the zero eigenvalue limit is well defined, however on a practical level small masses may still be troublesome. For standard CGNE, the iterations I are expected to scale as $I \sim \kappa^{-1/2} = \lambda_{\rm max}/\lambda_{\rm min} \sim (a\mu_{\rm tm})^{-1}$, where κ is the condition number of the matrix Q and λ are its eigenvalues.

However, on larger lattices the computational time scales quite badly, as detailed in table 4.1. The number of iterations times $a\mu_{\rm tm}$ is indeed constant (see fig. 4.3), but the time per iteration increases unexpectedly. The slowdown occurs during the inversion of the Dirac operator, an effect not observed with the SAP [103, 112] preconditioned GCR solver [10, 58], which instead scales much closer to the expected behavior. Measurements on the largest lattices (see Chapter 5 for details about configurations and measurements) were thus carried out with this solver.

Machine	Ens.	$L/a \cdot T/a$	$a\mu_{\rm tm}$	$c \cdot h$	$\frac{c\cdot h\cdot a\mu_{\rm tm}}{V_4}\cdot 10^6$	$\frac{c\cdot h\cdot}{\text{it.}\cdot V_4}\cdot 10^8$	$T/a \cdot \vec{L}/a\vert_{\rm loc.}$
Super	sft7	$192 \cdot 480$	0.0887	88.8 K	2.316	2.483	$20 \cdot 24^3$
MUC	sft6	$128 \cdot 320$	0.1244	8.72 K	1.615	1.702	$20 \cdot 16^2 \cdot 32$
Pax11	sft5	$96 \cdot 320$	0.1717	2.05 K	1.242	1.289	$40 \cdot 24^3$
	sft4	$64 \cdot 192$	0.2604	208	1.074	1.094	$24 \cdot 16^3$
Pax10	qb649	$48 \cdot 144$	0.3846	46.4	1.120	1.120	$18 \cdot 12^2 \cdot 24$
Pax9	qb628	$36 \cdot 108$	0.3446	8.28	1.133	1.129	$6 \cdot 18^3$

Table 4.1: *Comparison of computing time needed for measurement on 1 configuration for most of our ensembles, with* $z = \sqrt{8t_0}M_{RGI} = 9$, $N_S = 16$ *(for ens. qb628* $N_S = 8$ *was used, so the number of* $c \cdot h$ *is multiplied by 2), and* $c =$ core, $h =$ hour. *The last column reports the size of the local lattices utilized.*

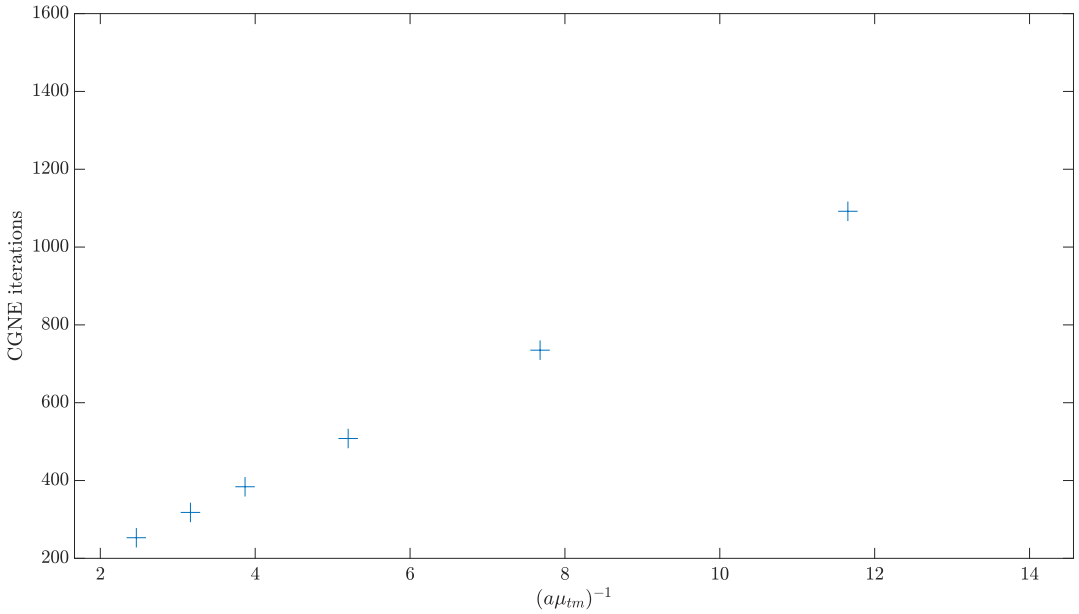

Figure 4.3: *The CGNE iterations necessary to reach a target relative precision of* $\varepsilon = 10^{-12}$ *scale linearly with the inverse input mass in lattice units, as expected.*

4.4. A SIMPLE LATTICE COMPUTATION

Let us start here by presenting two of the most simple lattice observables that can be studied through a two-point function: the effective mass and the decay constant of a meson. The results here can be used in order to cross-check the parameter tuning by comparing with known results, which we show later, in Subsection 5.5.3.

4.4.1. Effective Mass

Since we are interested in vacuum expectation values, we consider the pseudoscalar densities' correlator in a finite spatial volume, but with $T \to \infty$. This condition is a good enough approximation if no boundary effect can be resolved (as discussed in the next chapter, see fig. 5.2). Understanding sums over space $\sum_{\vec{x}}$ as over $x, y, z = 0, 1a, 2a, ..., L-a$, we start from

$$G(x_0 - y_0, a) = \frac{1}{L^3} \sum_{\vec{x},\vec{y}} \langle 0 | \hat{P}_{h,h'}(x) \hat{P}^{\dagger}_{h,h'}(y) | 0 \rangle = \frac{1}{L^3} \sum_{\vec{x},\vec{y}} \langle 0 | e^{\hat{H}x_0} \hat{P}_{h,h'}(\vec{x}) e^{-\hat{H}x_0} e^{\hat{H}y_0} \hat{P}_{h',h}(\vec{y}) e^{-\hat{H}y_0} | 0 \rangle \,, \tag{4.44}$$

which by defining $t = x_0 - y_0$ and by denoting E_0 the energy of the vacuum becomes

$$G(t, a) = \frac{1}{L^3} \sum_{\vec{x},\vec{y}} \langle 0 | \hat{P}_{h,h'}(\vec{x}) \, e^{-\hat{H}t} \hat{P}^{\dagger}_{h,h'}(\vec{y}) | 0 \rangle \, e^{E_0 t} \,. \tag{4.45}$$

Inserting the finite-volume completeness relation written in terms of eigenstates of the Hamiltonian (n labeling all relevant quantum numbers, except for the definite spatial momentum $\vec{p}$)

$$\mathbb{1} = \sum_{(n,\vec{p})} \frac{1}{2E(n,\vec{p})L^3} |n,\vec{p}\rangle \langle n,\vec{p}| \,, \tag{4.46}$$

we obtain, relabeling with $E(n,\vec{p})$ the energy *difference* w.r.t. E_0

$$\begin{aligned} G(t,a) &= \sum_{\vec{x},\vec{y}} \sum_{n,\vec{p}} \frac{1}{2E(n,\vec{p})L^6} \langle 0|\hat{P}_{h,h'}(\vec{x})|n,\vec{p}\rangle \langle n,\vec{p}|\hat{P}^{\dagger}_{h,h'}(\vec{y})|0\rangle \, \mathrm{e}^{-tE(n,\vec{p})} \\ &= \sum_{n,\vec{p}} \frac{1}{2E(n,\vec{p})L^6} \sum_{\vec{x}} \mathrm{e}^{i\vec{p}\cdot\vec{x}} \langle 0|\hat{P}_{h,h'}(\vec{0})|n,\vec{p}\rangle \sum_{\vec{y}} \mathrm{e}^{-i\vec{p}\cdot\vec{y}} \langle n,\vec{p}|\hat{P}^{\dagger}_{h,h'}(\vec{0})|0\rangle \, \mathrm{e}^{-tE(n,\vec{p})} \\ &= \sum_{n} \frac{\mathrm{e}^{-E(n,\vec{0})}}{2E(n,\vec{0})} \left| \langle 0|\hat{P}_{h,h'}(\vec{0})|n,\vec{0}\rangle \right|^2 , \end{aligned} \tag{4.47}$$

where the sum over $\vec{x}$ acts as a projection to zero three-momentum. For charm quarks the first excitable state with the quantum numbers of the pseudoscalar density is the $|\eta_c\rangle$, thus by analogy with this case we write $|\eta_h\rangle$, obtaining for large time separation

$$G(t,a) \underset{t\to\infty}{\simeq} \frac{\mathrm{e}^{-tm_{\eta_h}}}{2m_{\eta_h}} \left| \langle 0|\hat{P}_{h,h'}(\vec{0})|\eta_h\rangle \right|^2 + \mathscr{O}(\mathrm{e}^{-t(m_{\eta_h}+E(1,\vec{0}))}) \,. \tag{4.48}$$

We kept all multiplicative factors, since they will be necessary for the decay constant, but in the case of the effective mass they drop out (which is why we defer the exact details of the lattice, 1-particle state normalization to the next section) if one takes the following ratio

$$\frac{G(t+a,a)}{G(t,a)} \overset{t\to\infty}{\sim} \mathrm{e}^{-am_{\eta_h}} \longrightarrow m_{\eta_h} \overset{t\to\infty}{\sim} -\frac{1}{a}\log\left(\frac{G(t+a,a)}{G(t,a)}\right) , \tag{4.49}$$

which is expected to plateau after all higher order corrections in eq. (4.48) have decayed. This behavior is confirmed by our own data, reported in figs. 4.4a and 4.4b. Given the good and clean signal the plateaus' extrema were safely selected by eye inspection, leading to a solid result with a controlled error.

4.4.2. Decay Constant

When dealing with hadron decays, it is natural for the hadronic and the weak scale to appear. These are quite disparate, with about two orders of magnitude between them. An effective interaction which couples weak with hadronic currents can then be written down, leading to matrix elements of local currents between hadronic states: these can be computed non-perturbatively on the lattice. An important such matrix element defines what is referred to as decay constant of some meson, namely, in the charmonium case for Minkowskian signature

$$\langle 0|\hat{A}^{\pm}_{\mu}(x)|\eta_c(q)\rangle \overset{\text{def.}}{=} if_{\eta_c} q_\mu \mathrm{e}^{-iq\cdot x} \,, \tag{4.50}$$

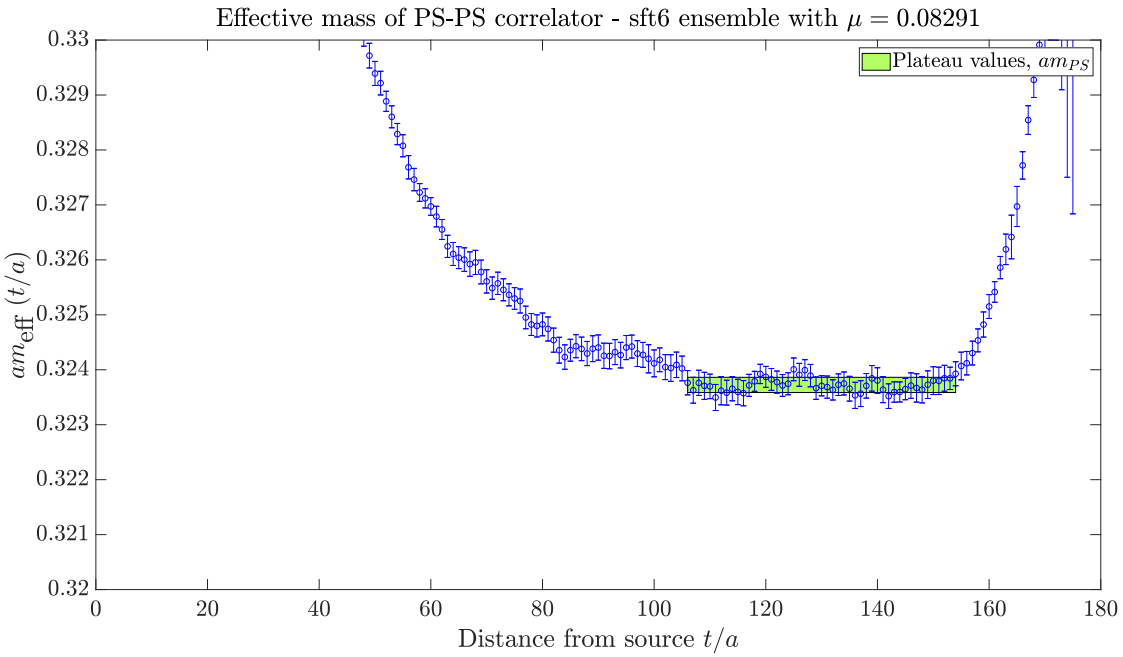

(a) *Second finest lattice, $a \simeq 0.015$ fm and $\overline{m}/\overline{m}_{charm} \simeq 1.6$. A large enough plateau before signal deterioration is present and can be used to extract the mass.*

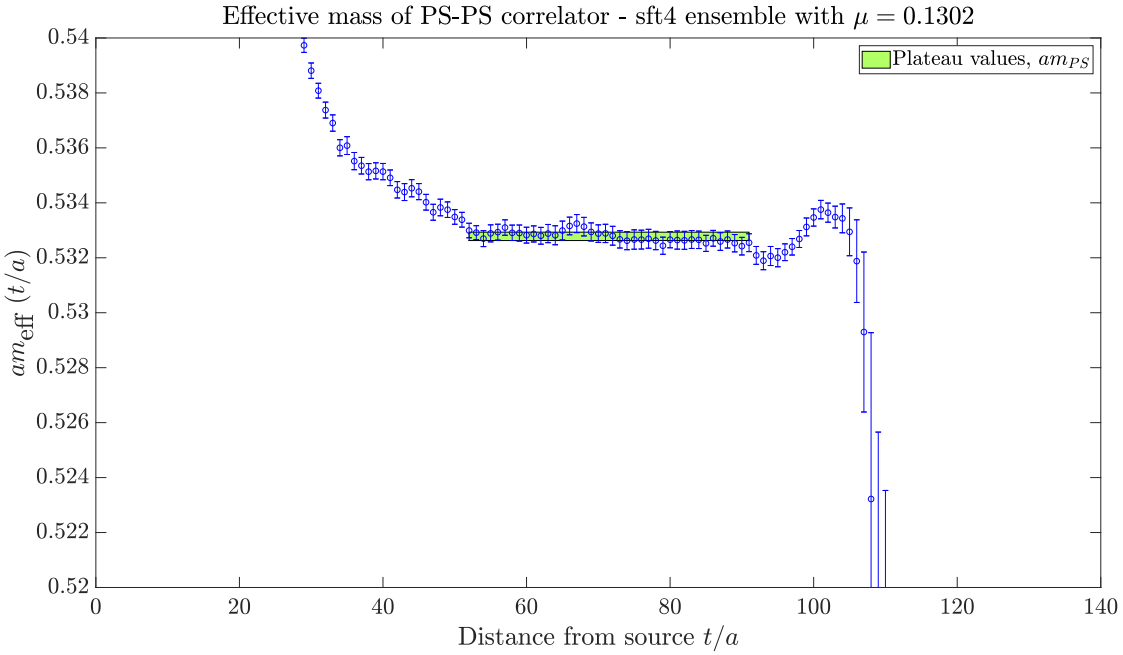

(b) *Lattice spacing $a \simeq 0.030$ fm and $\overline{m}/\overline{m}_{charm} \simeq 1.2$, also here there is a large and stable plateau, with no visible oscillations beyond the expected Gaussian fluctuations.*

Figure 4.4: *Behavior of effective pseudoscalar mass, which plateaus for high enough source-sink distance t. As explained in the text, the signal is good enough for a safe and solid estimate of the plateau region without the introduction of a complicated estimator for the systematic error.*

where the $\pm$ notation is the same of eq. (3.37). Note that the q_μ-factor is present as far as it is the only available quantity with the correct Lorentz vector structure. Taking the four-divergence of eq. (4.50) one obtains

$$\partial_\mu \langle 0|\hat{A}^{\pm}_{\mu}(x)\,|\eta_c(q)\rangle = f_{\eta_c}\, q^2 \mathrm{e}^{-iq\cdot x}\,, \quad q^2 = m^2_{\eta_c}\,. \tag{4.51}$$

Translating the axial vector correlator to the origin we obtain

$$\partial_\mu \langle 0|\,\mathrm{e}^{i\hat{P}\cdot x}\hat{A}^{\pm}_{\mu}(0)\mathrm{e}^{-i\hat{P}\cdot x}\,|\eta_c(q)\rangle = \partial_\mu \langle 0|\hat{A}^{\pm}_{\mu}(0)\,|\eta_c(q)\rangle\,\mathrm{e}^{-iq\cdot x} = f_{\eta_c} m^2_{\eta_c}\mathrm{e}^{-iq\cdot x}\,, \tag{4.52}$$

where translation invariance of the interacting vacuum was used.

In eq. (3.49) we mentioned the following operator identity

$$\partial_\mu \hat{A}^{\pm}_{\mu}(x) = 2m\hat{P}^{\pm}(x)\,, \tag{4.53}$$

where m is the current quark mass, can be obtained from chiral Ward identities. This was written in the continuum, where[VI]

$$f_{\eta_c} = \frac{2m}{m^2_{\eta_c}} \langle 0|\,\hat{P}^{\pm}(0)\,|\eta_c(q)\rangle\,, \tag{4.55}$$

is equivalent to eq. (4.50). Now, as previously mentioned, with twisted mass fermions at maximal twist, the axial current will rotate to the vector current so that an exact lattice identity can be established (see (3.54)), whereas $\hat{P}^{\pm}$ does not rotate. Putting the pieces together, eq. (4.55) remains valid for the maximally twisted lattice theory with $m \to \mu_{tm}$ and without any further renormalization factor such as Z_A (a great advantage w.r.t. standard Wilson fermions). In Euclidean space with correlators projected to zero three-momentum $\vec{q} \equiv \vec{0}$, so that $q^2 = q_0^2 = m^2_{\eta_c}$, the decay constant at large source-sink separation becomes

$$f_{\eta_h} = \frac{2\mu_{\mathrm{tm}}}{m^2_{\eta_h}} \langle 0|\,\hat{P}_{h,h'}(\vec{0})\,|\eta_h\rangle \underset{t\to\infty}{\simeq} \frac{2\mu_{\mathrm{tm}}\,\mathrm{e}^{m_{\eta_h}t/2}}{m^2_{\eta_h}} \sqrt{2m_{\eta_h}G(t,a)}\,, \tag{4.56}$$

for which we show results in figs. 4.5a, 4.5b and D.3. Again, the plateaus' extrema were selected arbitrarily without limiting the solidity of our result and obtaining a controlled error.

[VI] This definition entails a specific one particle state normalization, namely

$$\langle \vec{p}, n \mid \vec{q}, m\rangle = \begin{cases} 2E(n,\vec{p})(2\pi)^3\delta_{n,m}\delta^3(p-q)\,, & L=\infty \\ 2E(n,\vec{p})L^3\delta_{n,m}\delta_{\vec{p},\vec{q}}\,, & L<\infty \end{cases}, \tag{4.54}$$

where the 2π or L factors are placed according to the typical physicists' asymmetric normalization convention of Fourier transform and antitransform. This means Fourier transforms are normalized by 1, whereas antitransforms by L^{-3} or $(2\pi)^{-3}$. Moreover, the combination $2E_{\vec{p}}\,\delta^3(p-q)$, just like $\mathrm{d}^3p/2E_{\vec{p}}$, is relativistically invariant. This is also reflected in the field normalization when expanded in creation and annihilation operators, where a $1/\sqrt{2E_{\vec{p}}}$ normalization is common (this also explains the $\sqrt{2}$ factor, appearing naturally when "rotating" from the fundamental/canonical conjugate field pair to creation/annihilation operators).

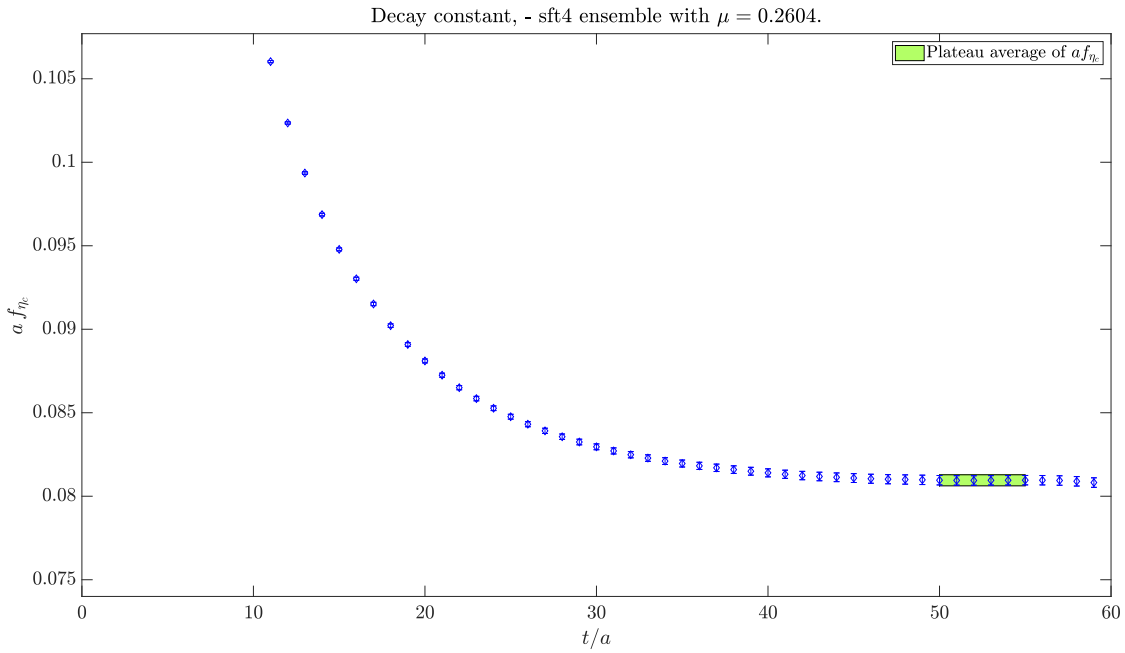

(a) *Lattice spacing of* $a \simeq 0.030$ *fm and* $\overline{m}/\overline{m}_{charm} \simeq 2.3$*; a short plateau can be seen, but which is good enough to reliably extract decay constant also the large mass value and with the coarser lattice.*

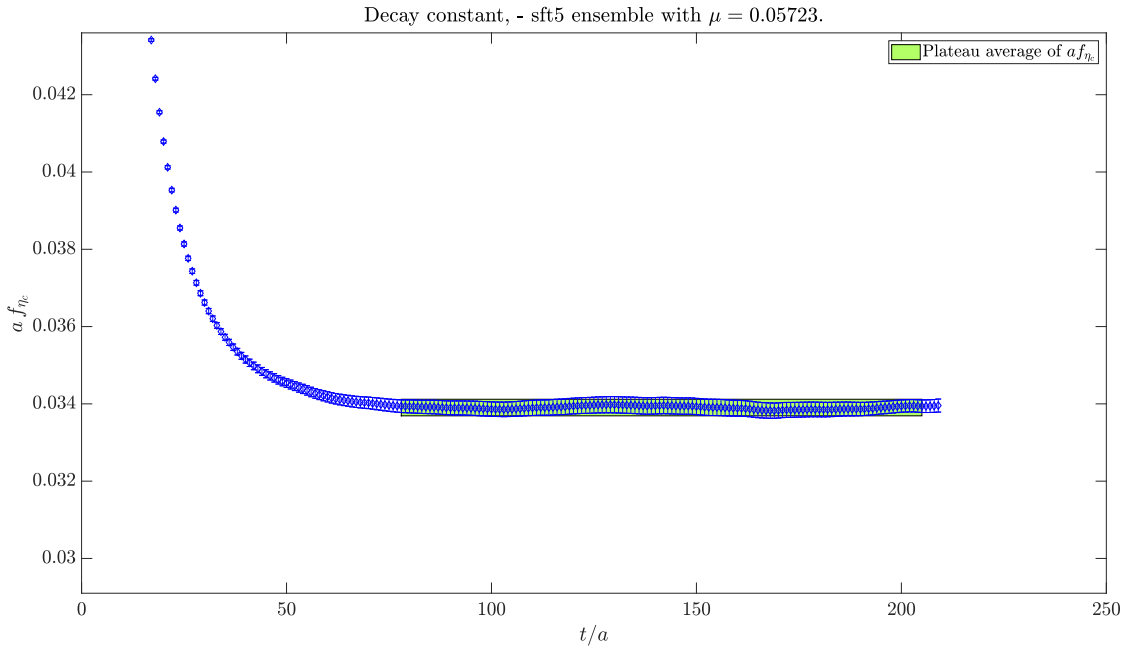

(b) *Lattice spacing* $a \simeq 0.020$ *fm and* $\overline{m}/\overline{m}_{charm} \simeq 0.8$*, the plateau region is very stable and large.*

Figure 4.5: *Behavior of pseudoscalar decay constant as a function source-sink distance* t/a*, with a plateau for large time difference. The Gaussian fluctuations are very small and the plateau is very stable.*

5 | Input Parameters and Measurements

LONG times and large effort is dedicated in lattice QCD to preparing the numerical setup, studying how to best tune input parameters as well as to assess of what size the errors committed during this procedure are. This chapter describes how the input parameters for both the generation of gauge configurations and the measurements carried out were selected, together with an error assessment related to said choices.

5.1. Gauge Configurations

Pure gauge theory with the plaquette action is simulated (see table 5.1) with `openQCD-1.6` using HMC [56] for the range $\beta \leq 6.4956$; the exact lattice coupling values are chosen equal to the ones in [35], in order to use their determination of κ_c in the $N_f = 0$ theory, found in [82], Table C.1. For $\beta > 6.5$ we use the gauge fields generated by [91] with local updates, which comprised a first pseudo heat-bath sweep [32] succeeded by several over-relaxation sweeps acting on SU(2) subgroups [46, 28, 2].

The lattice size is $L \simeq 2\,\text{fm}$, with at least $T/L \gtrsim 2$ (cfr. table 5.1) to keep sources and sinks far from the open boundaries. In pure gauge the exponentially suppressed volume effects have a scale given by the glueball mass $m_{0++} = 1730(50)(80)\,\text{MeV}$ [125] and, with $L \simeq 2\,\text{fm}$, they are clearly suppressed since $m_{0++}L \simeq 17.5 \gg 1$. This is a quite favorable situation compared to $N_f > 0$, where the effect of the (much lighter, $m_\pi \simeq 135\,\text{MeV}$) pion has to be carefully monitored. It may be propagating around the torus which arises due to the periodic boundary conditions.

In the quenched theory one might be worried about the analog of the pion, i.e. a pseudoscalar meson composed of heavy valence quarks. This is not the problematic since our RGI-masses are in the range 1 GeV to 6 GeV, see table 5.4, leading to a meson mass $m_{h,h'} > m_{0++}$.

The gradient flow scale t_0/a^2 is computed employing the standard plaquette definition for the action, both for the gradient flow in eqs. (3.21) and (3.22) and in the definition of the Lagrangian density $E(t)$. Other, more symmetric definitions, are known to have smaller discretization effects, but the scale's dependence is suppressed since the mass only enters logarithmically into the coupling. Nevertheless, we compare results with the two definitions of $E(t)$ on our coarsest lattice for R_4 – the most short distance dominated observable – finding a relative difference of $\lesssim 2\%$. We are thus confident changing definition of $E(t)$ does not affect in a significant manner our overall cutoff effects. The first order gradient flow equations are then solved with a third order Runge-Kutta algorithm, where errors in the

Run Name	β	$l^3 \times t$	N_{cnfg}	t_0/a^2	$a[fm]$	$\tau_{\text{int}}(t_0)$[cfg]	$\frac{\text{GB}}{\text{cnfg}}$
q_beta616	6.1628	$32^3 \times 96$	128	5.1604(98)	0.071	0.78	1.7
q_beta628	6.2885	$36^3 \times 108$	137	7.578(22)	0.059	1.37	2.7
q_beta649	6.4956	$48^3 \times 144$	109	13.571(50)	0.044	1.55	8.5
sft4	6.7859	$64^3 \times 192$	200	29.390(98)	0.030	1.00	27
sft5	7.1146	$96^3 \times 320$	80	67.74(23)	0.020	0.55	152
sft6	7.3600	$128^3 \times 320$	98	124.21(91)	0.015	1.03	360
sft7	7.700	$192^3 \times 480$	31	286.3(4.7)	0.010	–	1,823

Table 5.1: *Gauge run details, $l = L/a$, $t = T/a$, with plaquette definition for E(t).*

step-size are subleading [111].

On our finest lattice, `sft7`, we do not measure the scale explicitly to save computational resources, since we are able to precisely reconstruct it as follows. From available Wilson loop measurements on our ensembles [91], taken similarly to what is described in [55], we (unexplained notation can be found in the mentioned papers) compute $\alpha_{qq}(x, a/r)$ with $x = r/\sqrt{8t_0} = 0.25$ on ensembles `sft1-6`. Extrapolating to the continuum, we then obtain $\alpha_{qq}^{\text{cont.}}(0.25) = \alpha_{qq}(0.25, 0)$. Through Wilson loop measurements on `sft7`, we can compute the qq-coupling on this ensemble for varying r/a, in order to interpolate and find a/r_* defined as $\alpha_{qq}^{\text{sft7}}(x, a/r_*) \equiv \alpha_{qq}^{\text{cont.}}(0.25)$. Thanks to the negligible cutoff effects in α_{qq} already for `sft6`, from this a we are able to obtain a precise determination of the scale, through

$$\left.\frac{\sqrt{8t_0}}{a}\right|_{\text{sft7}} = \frac{\sqrt{8t_0}}{r} \cdot \frac{r_*}{a} = \frac{1}{x}\frac{r_*}{a} = \frac{1}{0.25} \cdot \frac{r_*}{a} = 47.85(39)\,, \tag{5.1}$$

also reported in the last row of table 5.1.

5.2. MEASUREMENTS

The meson two-point functions are measured using the `openQCD-1.6`-compatible version of `mesons`, which implements twisted-mass, Wilson fermions[I], that we set to maximal twist by tuning κ to its critical value κ_c as described in Subsection 5.4.1. The non-perturbative, quenched Sheikholeslami-Wohlert coefficient is taken from (5.15) of [117] (valid $\forall \beta \geq 6$) in order to alleviate $\mathcal{O}(a^2)$ effects [63, 13, 54]. The zero three-momentum Fourier transform of the fermionic two-point function is evaluated

[I] We thank Tomasz Korzec for allowing us to use an updated version of the publicly available code `https://github.com/to-ko/mesons`.

through stochastic noise sources, see eq. (4.38). The explicit two point function we build is

$$G(t,a,\mu_{\rm tm}) = \mu_{\rm tm}^2 \sum_{\vec{x}} a^3 \left\langle \overline{h}(x)\gamma_5 h'(x)\overline{h}'(0)\gamma_5 h(0) \right\rangle \tag{5.2}$$

$$= -\mu_{\rm tm}^2 \sum_{\vec{x}} a^3 \,\mathrm{tr}\left\langle S_h(x,0;\mu_{\rm tm})\gamma_5 S_{h'}(0,x;-\mu_{\rm tm})\gamma_5 \right\rangle = -\mu_{\rm tm}^2 \sum_{\vec{x}} a^3 \,\mathrm{tr}\left\langle S_h(x,0;\mu_{\rm tm}) S_{h'}^{\dagger}(x,0;\mu_{\rm tm}) \right\rangle , \tag{5.3}$$

where $S_h(x,0;\mu_{\rm tm})$ is the propagator from 0 to x for an h-quark, $x_i = 0,1,\ldots,L-a$, $i = 1,2,3$, and we use $N_{\rm src}$ noise sources (typically around 16, table 5.5) with a $U(1)$ distribution, through which good statistical precision is reached.

5.3. SOURCE POSITION AND SUM CUTOFF

On the lattice, remembering $G(t,a,\mu_{\rm tm}) = G(-t,a,\mu_{\rm tm})$, moments of the correlator $G(t,a,\mu_{\rm tm})$ can be computed via

$$\mathscr{M}_n(z,a) = \lim_{L,T\to\infty} \sum_{t=-T/2}^{T/2} a t^n G(t,a,\mu_{\rm tm}) = 2 \lim_{L,T\to\infty} \sum_{t=0}^{T/2} a t^n G(t,a,\mu_{\rm tm}) \tag{5.4}$$

$$\simeq 2 \lim_{L,T\to\infty} \sum_{t=0}^{\delta} a t^n G(t,a,\mu_{\rm tm}) , \tag{5.5}$$

where $t = 0$ corresponds to the source's time-slice and the sum is cut off at δ, as far as the exponential decay of $G(t,a,\mu_{\rm tm})$ makes the long distance part of the correlator unimportant for $\mathscr{M}_n$. No significant variation of the moment or of its statistical error is found when varying the cutoff δ, if one stays in the region where the sum has saturated (this is true for all runs and masses). As will be explained in Subsection 5.5.2, through the monitoring of the PCAC-mass it becomes clear the stopping criteria of our algorithms are inadequate for the depth of the bulk, where the obtained correlator values are evidently unreliable, as a result of their exponential decay. Thus we select a value δ which ensures our correlators are not computed in a region were numerical errors may invalidate the result. The criterion is to select δ smaller than the time-slice at which the PCAC-mass starts showing deviations from its plateau value. This is well within the region where the sum defining the moments has saturated.

Explicit checks are carried out regarding the size of finite volume effects and the absence of boundary effects. To study the first, we generate additional ensembles at $\beta = 6.2885$, $L/a = 36$ (and $\mu_{\rm tm} = 0.258459$), on which we compute the moments for $n = 4, 6, 8, 10,$ giving the results in fig. 5.1. Within statistical fluctuations, no significant finite volume effect can be seen. The results in the $L \simeq 2.4\,$fm volume agree perfectly with the ones at $L \simeq 2.1\,$fm.

To understand whether the source is far enough from the boundary, we place it around $x_0 \simeq 1.00$ fm on a coarse lattice, specifically at $x_0/a = 16$ on the q_beta616 ensemble (32×96 lattice, see table 5.5). We evaluate the correlator $G(t,a,\mu_{\rm tm})$ around the source-slice (see fig. 5.2 and table 5.2) and find no difference can be resolved up to very close to the boundary, i.e. boundary effects are of the size of the

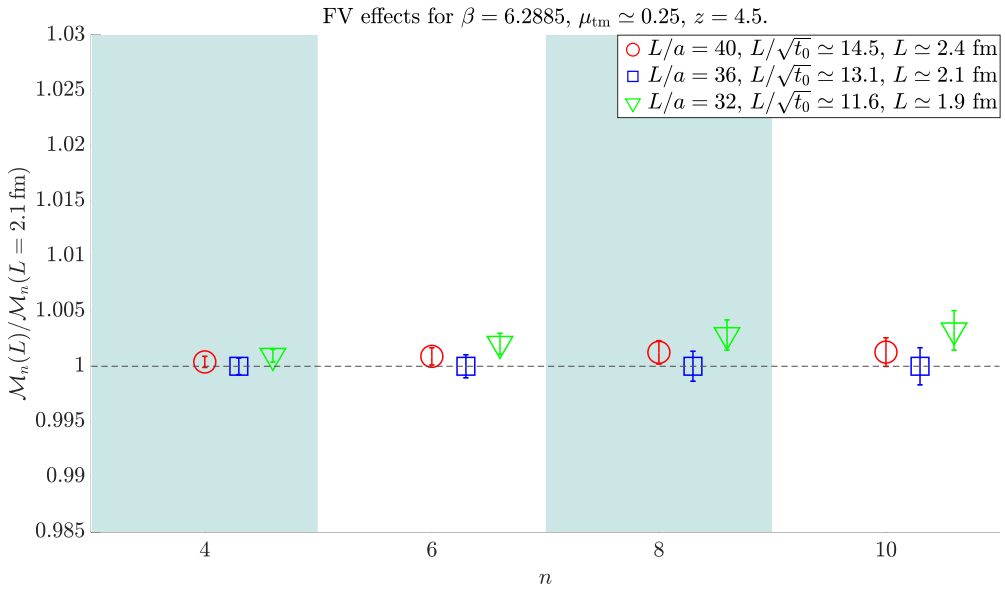

Figure 5.1: *Moments computed for different number of points L/a, while all other parameters are kept constant. Normalized by the result at $L \simeq 2.1$ fm, the volume used throughout the thesis.*

statistical error or smaller in the region $x_0 \gtrsim 0.3$ fm. Thus to current precision no boundary effects are seen for our choice of the source position.

t/a	1	2	3	4	5	6	7	8
ε_d	0.692	1.115	2.056	2.514	1.136	1.028	1.046	0.960
t	9	10	11	12	13	14	15	16
ε_d	0.953	0.843	0.755	0.721	0.848	0.989	1.160	1.637
t	17	18	19	20	21	22	23	24
ε_d	2.149	4.072	22.80	3.921	1.873	1.094	0.753	0.494
t	25	26	27	28	29	30	31	32
ε_d	0.316	0.192	0.112	0.063	0.036	0.021	0.018	0

Table 5.2: *Ensemble sft4, $z = 3$. With $d = 2|G(t,a,\mu_{\rm tm}) - G(-t,a,\mu_{\rm tm})|/[G(t,a,\mu_{\rm tm}) + G(-t,a,\mu_{\rm tm})]$ and Δd indicating the statistical error, we show $\varepsilon_d = \Delta d/d$ as a function of the distance to the source, placed at $x_0 = 32$, i.e. $t = 32$ corresponds to the boundary. Some asymmetry becomes relevant w.r.t. the statistical error for $t \geq 24$, i.e. at 8 time-slices from the boundary.*

5.4. MASS TUNING

As introduced in Subsection 3.5.1, maximal twist is achieved by tuning κ to its critical value, so that then $\mu_{\rm tm}$ fixes the mass of the computation. How κ is tuned and $\mu_{\rm tm}$ chosen in order to correspond to a desired physical mass will be explained in this section.

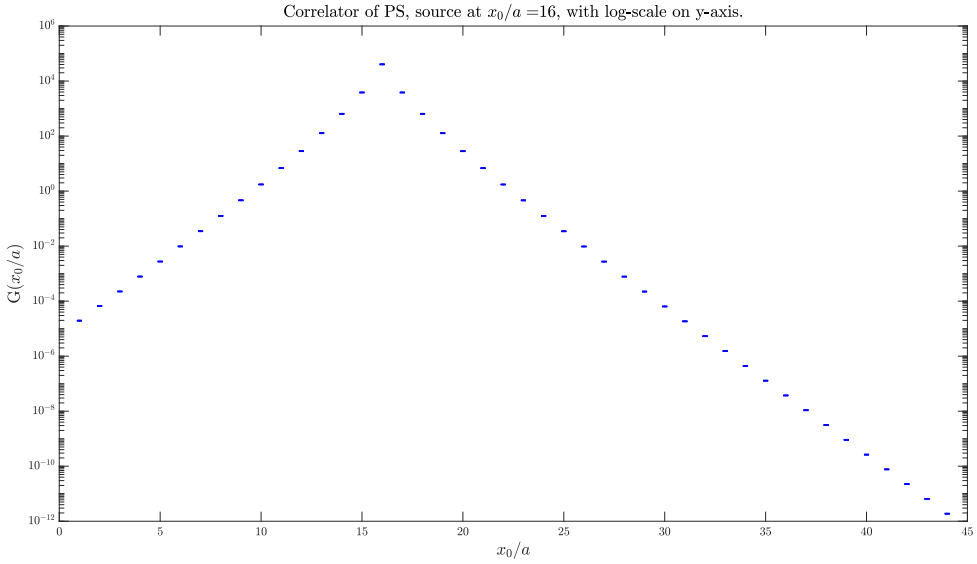

Figure 5.2: *Visualization of symmetry of correlator around source. Errorbars cannot be seen. Numerically no difference can be resolved as illustrated in table 5.2.*

5.4.1. κ_c

The Hopping parameters we use can be found in table 5.5. For ensembles with $\beta \leq 6.4956$ they are directly taken from Table C.1 of [82], where it was tuned by setting the bare mass m_{PCAC}

$$m_{PCAC} = \frac{\left\langle \sum_{\vec{x}\in V_3} \partial_\mu A^I_\mu(x)\, P(0)\right\rangle}{2\left\langle \sum_{\vec{x}\in V_3} P(x)\, P(0)\right\rangle} = \frac{\left\langle \sum_{\vec{x}\in V_3} \partial_0 A^I_0(x)\, P(0)\right\rangle}{2\left\langle \sum_{\vec{x}\in V_3} P(x)\, P(0)\right\rangle}, \quad A^I_\mu(x) = A_\mu(x) + c_A(g_0)\,\partial^*_\mu P(x), \quad (5.6)$$

to zero. Other definitions, which converge to the same continuum value, are possible. For instance, from the GMOR relation [69] (valid at linear order in the mass) m_π^2 is known to be proportional to the physical, light quark mass. Thus, the difference between $m_{PCAC} = 0$ and $m_\pi = 0$ at finite lattice spacing is of $\mathcal{O}(a)$ (in the improved theory $\mathcal{O}(a^2)$), i.e. κ_c has an $\mathcal{O}(a^2)$ (with improvement $\mathcal{O}(a^3)$) ambiguity. In [82] κ_c for the above mentioned β-values was computed in the SF-scheme with quenched, $\mathcal{O}(a)$-improved Wilson fermions in a volume of $2L_{max} = 1.436 r_0$, with non-perturbative improvement of c_{SW}, c_A and the 2-loop value of the pure gauge boundary counterterm c_t. For `sft4` ($\beta = 6.7859$) we take over the value found in figure 5.2 of [94] and we employ a similar strategy for $\beta > 6.7859$, i.e. interpolating the data[II] in table 1 of [117]. We try several fit Ansätze, namely interpolations with polynomials in g_0^2 and β, subtracting 1-loop perturbation theory, taken from the same paper. We vary the smallest power of g_0 labeled $n_{min} = 0, 1, 2$, where $g_0^{2n_{min}}$, as well as the range of used points. Given the four values of κ_c at $\beta = 6.8, 7.4, 8.0, 9.6$, we fit the first 3 points, the last 3 points, and all points, for each Ansatz. We find good consistency among fits with acceptable χ^2 and use their mean value, reported in table 5.3.

[II] Therein, κ_c is again defined as the value where the unrenormalized PCAC-mass vanishes and with: $T = 2L$, the non-perturbative c_{SW} and c_A, zero boundary gauge fields and angles $\theta_k = 0$.

β	κ_c
7.1146	0.134545(24)
7.360	0.1341360(26)
7.700	0.133605(7)

Table 5.3: *κ_c values for high β, taken as mean of several, consistent fit Ansätze. The error reported is half of the spread of the values, which is slightly larger than the standard deviation of the single result. What error one chooses is unimportant, as will be described in more detail below, since κ tuning errors are strongly subleading w.r.t. other error sources.*

5.4.2. Twisted Mass Value

Once the hopping parameter is tuned to its critical value, the physical mass depends only on the twisted mass, up to $\mathcal{O}(a^2)$. We fix $a\mu_{\rm tm}$ in order to keep

$$z \overset{\text{def.}}{=} \sqrt{8t_0}\, M_{\rm RGI} = \frac{\sqrt{8t_0}}{a} a M_{\rm RGI} = \frac{\sqrt{8t_0}}{a} \frac{M_{\rm RGI}}{\overline{m}_{SF}(\mu)\, Z_P^{SF}(a\mu,\beta)} a\mu_{\rm tm}\,, \tag{5.7}$$

constant (see table 5.4), where $\sqrt{t_0} = 0.1638(10)\,\text{fm}$ is taken from [111, 152] for the quenched case. This defines our line of constant physics. Note that the renormalization constant $Z_A(\beta)$ is absent at maximal twist, unlike with standard Wilson fermions. The non-negligible uncertainty of the quenched, continuum mass ratio $M_{\rm RGI}/\overline{m}_{SF}(\mu)$, of order $\varepsilon(M/\bar{m}) \sim 1\%$, is a continuum factor (see [35]) affecting indiscriminately the tuning at each β. This systematic effect should thus be accounted for directly in the continuum-extrapolated value of $\mathscr{R}_n$. A precise discussion of this error is deferred to the next chapter where continuum limits are discussed in detail; for now, notice one can think about this as being along a constant physics trajectory at fixed $\bar{z}$ given by

$$\bar{z} = z \frac{\overline{m}_{SF}(\mu)}{M_{RGI}} = \frac{\sqrt{8t_0}}{a} \frac{a\mu_{\rm tm}}{Z_P^{SF}(\mu)}\,, \tag{5.8}$$

which does not affect at all the discussion herein. Used z values can be found in table 5.5, where the charm RGI quark mass is $M_{\rm RGI}^{\rm charm} = 1.654(45)\,\text{GeV}$ [143] in the quenched approximation (as a reference, $M_{\rm RGI}^{\rm charm} = 1.526(17)\,\text{GeV}$ is the FLAG world average for $N_F = 2+1$ [123, 167, 126, 137]).

z	$M_{\rm RGI}$ [GeV]	$M_{\rm RGI}/M_{\rm RGI}^{\rm charm}$
13.5	5.76	3.48
9	3.84	2.32
6	2.56	1.55
4.5	1.92	1.16
3	1.28	0.77

Table 5.4: *Renormalization group invariant mass values used in the measurements, from $M_{RGI} = (\hbar c) z/\sqrt{8t_0}$ [GeV]. The first column is exact, whereas the other two are to be understood as approximate size statements to get an idea of the energies at play, their exact value and error being unimportant here.*

β	κ_c	c_{SW}	Source Position	z	$a\mu_{\mathrm{tm}}$	N_{src}	N_{meas}
6.1628	0.13565(1)	1.63567	16	6	0.421422	16	128
				4.5	0.316066	8	128
				3	0.210711	16	128
6.2885	0.13575(1)	1.569579	18	6	0.344612	8	137
				4.5	0.258459	8	137
				3	0.172306	16	137
6.4956	0.135590(8)	1.495162	24	13.5	0.576848	16	109
				9	0.384566	16	109
				6	0.256377	16	109
				4.5	0.192283	16	109
				3	0.128189	16	109
6.7859	0.135120(5)	1.427724	32	13.5	0.390666	16	100
				9	0.260444	16	100
				6	0.173629	16	100
				4.5	0.130222	16	100
				3	0.086815	16	50
7.1146	0.134545(48)	1.376876	54	13.5	0.257536	16	60
				9	0.171690	16	80
				6	0.114460	16	80
				4.5	0.085845	16	80
				3	0.057230	16	80
7.3600	0.1341360(52)	1.348577	72	13.5	0.186492	16	49
				9	0.124360	16	49
				6	0.082907	16	49
				4.5	0.062180	16	49
				3	0.041453	16	49
7.7000	0.133605(13)	1.317630	108	13.5	0.121474	32	31
				9	0.080983	32	31
				6	0.053989	32	31
				4.5	0.040491	32	31
				3	0.026994	32	31

Table 5.5: *Input parameters of the measurement runs of meson correlators.*

5.4.3. Renormalization and Running Factors

The renormalization factor $Z_P(a\mu,\beta)$ and the running of the mass $M_{\mathrm{RGI}}/\overline{m}_{SF}(\mu)$ in [94], which includes and extends the range of the previous results of [35], are computed at $\mu = (2L_{max})^{-1} \simeq (1.436r_0)^{-1}$, where $2L_{\mathrm{max}}$ is the largest available volume of this step scaling study (for the methodology of step scaling, see [115]). In [94] the fit for Z_P is valid for $6.0 \leq \beta \leq 7.0$, whereas we reach a higher value $\beta = 7.70$. In order to extend the result and obtain more precise results for Z_P and $M_{\mathrm{RGI}}/\overline{m}$, we reanalyze the data in [35] at a higher energy scale – twice the one used in the study (or at half the

lattice extent L) – as explained in the following.

We use as a reference scale $\mu_{\rm ref} = (2L_{\rm ref})^{-1}$, with $L_{\rm ref}$ implicitly defined from $u_{\rm ref} = \overline{g}^2_{\rm SF}(L_{\rm ref}/a, g_0) = 2.4484$, which has a unique solution if one of its arguments is kept fixed and which amounts to half the spatial extent of [94]. The physical trajectory is identified by choosing some L/a value and then tuning g_0 in order to obtain the desired $u_{\rm ref}$. Let us start by defining

$$s_P(u_{\rm ref}) \stackrel{\rm def.}{=} \frac{M_{\rm RGI}}{\overline{m}(2L_{\rm ref})} = \frac{M_{\rm RGI}}{\overline{m}(2^{-n}L_{\rm ref})} \frac{\overline{m}(2^{-n}L_{\rm ref})}{\overline{m}(2L_{\rm ref})}\,, \tag{5.9}$$

where in the last expression the first factor is computed in perturbation theory, with the 2-loop mass anomalous dimension and 3-loop beta function[III], whereas the second term is obtained from

$$\frac{\overline{m}(2^{-n}L_{\rm ref})}{\overline{m}(2L_{\rm ref})} = \sigma_P^{-1}(u_{\rm ref}) \prod_{i=1}^{n} \sigma_P^{-1}(u_i)\,, \quad u_i = \sigma(u_{i+1})\,, \quad i = 1, \ldots, n\,. \tag{5.10}$$

The two step scaling functions $\sigma(u)$ and $\sigma_P(u)$ are obtained from a fit of the continuum step scaling function data as described in Section 5 of [35]. The coupling $u_{\rm ref}$ at which the step scaling evolution starts from is explicitly written in eq. (5.9) since it is an *input*, whereas u_i for $i \geq 1$ are computed by inverting the fit for $\sigma(u)$.

We can now give several Z_P definitions[IV]

$$Z_{P,1}(g_0) \stackrel{\rm def.}{=} \frac{s_P(2.4484)}{s_P(3.48)} \cdot Z_P^{\rm SF}(g_0, 2L/a)\big|_{2L/a = 1.436\, r_0/a}\,, \tag{5.11}$$

$$Z_{P,2}(g_0) \stackrel{\rm def.}{=} \frac{s_P(2.4484)}{s_P(3.48)} \cdot Z_P^{\rm SF}(g_0, 2L/a)\big|_{\overline{g}^2(L/a, g_0) = 3.48}\,, \tag{5.12}$$

$$\begin{aligned} Z_{P,3}(g_0) &\stackrel{\rm def.}{=} \frac{s_P(2.4484)}{s_P(3.48)} \cdot \sigma_P(3.48)\, Z_P^{\rm SF}(g_0, 2L/a)\big|_{\overline{g}^2(L/a, g_0) = 2.4484}\,, \\ \sigma_P(3.48) &= \lim_{a \to 0} \Sigma_P(u = 3.48, a/L)\,, \end{aligned} \tag{5.13}$$

$$Z_{P,4}(g_0) \stackrel{\rm def.}{=} Z_P^{\rm SF}(g_0, 2L/a)\big|_{\overline{g}^2(L/a, g_0) = 2.4484}\,. \tag{5.14}$$

Let us mention $Z_{P,3}$ is reported here because it was used before the $s_P(u)$ functions had been computed. The Z_P factors used in our tuning are

$$Z_{P,1} \quad \text{for} \quad 6.0 < \beta < 6.5\,, \tag{5.15}$$

$$Z_{P,2} \quad \text{for} \quad \beta = 6.7859\ (\texttt{sft4})\,, \tag{5.16}$$

$$Z_{P,3} \quad \text{for} \quad \beta = 7.1146\ (\texttt{sft5})\,, \tag{5.17}$$

$$Z_{P,4} \quad \text{for} \quad \beta = 7.36, 7.70\ (\texttt{sft6}, \texttt{sft7})\,. \tag{5.18}$$

[III] To check that PT can safely be applied for this factor at $\mu = 2^{-n}L_{\rm ref}$, it was also computed with the 1-loop mass anomalous dimension and 2-loop beta function, finding a relative difference of less than 4 per-mille in all cases we discuss.

[IV] The reason for this is that at coarser lattice spacings, at the beginning of the project, we used the reference scale of [94]. For those cases we need an extra ratio of s_P to set their scale to the desired one, i.e. $\mu = (2L_{\rm ref})^{-1}$.

Now, for any of the above definitions, z can be written as

$$z = \frac{\sqrt{8t_0}}{a} a\mu_{\text{tm}} \left[Z^{\text{SF}}_{P,i}(g_0,u)\right]^{-1} s_P(u)\Big|_{u=2.4484}\,, \tag{5.19}$$

and in the continuum only the newly obtained

$$\frac{M_{\text{RGI}}}{\overline{m}_{SF}(2L_{\text{ref}})} = 1.379(11)\,, \tag{5.20}$$

will be used. In fig. 5.3 we show both some Z_P values of [35] and the $Z_{P,i}$ at our β values. These have been obtained by linear fits interpolating the raw values in [35] at $\mu = \mu_{\text{ref}}$. The errors originating from the tuning of previously discussed parameters as well as the ones shown in the just mentioned plot are the topic of the next section.

5.5. TUNING ERRORS

A physical trajectory is identified by some fixed value of M_{RGI}, but as described after eq. (5.8), we extrapolate to the continuum for fixed $\overline{m}_{\text{SF}}(L_{\text{ref}})$ and correct with the continuum factor $M_{\text{RGI}}/\overline{m}_{\text{SF}}(L_{\text{ref}})$ only afterwards. In order to evaluate the variation of $\mathscr{R}_n(aM_{\text{RGI}},z)$ upon slight mistunings, we Taylor-expand it around the true value (th = theoretical value) of its parameters, or rather, their logarithm. This is of advantage, since at maximal twist the factors defining z are all multiplicative, meaning there is no difference in using z or $\bar{z}$. Here, we explain the general approach for computing any of the tuning errors, but we defer the inclusion of the aforementioned continuum factor and its possible correlation to other error sources to Subsection 6.1.4. One can write

$$\begin{cases} \mathscr{R}_n\left(\vec{b}\right) = \mathscr{R}_n^{\text{th}} + \sum_i \frac{\partial \mathscr{R}_n}{\partial \ln b_i}\Big|_{\text{th}} \Delta(\ln b_i) + \mathscr{O}\left((\Delta\vec{b})^2\right) \\ \frac{\partial \mathscr{R}_n}{\partial \ln b_i}\Big|_{\text{th}} = \frac{\partial \mathscr{R}_n}{\partial \ln z}\frac{\partial \ln z}{\partial \ln b_i}\Big|_{\text{th}} \end{cases} \quad , \quad \text{for } \vec{b} = \left(Z_P,\, \frac{t_0}{a^2},\, M_{\text{RGI}}/\overline{m}_{\text{SF}}(\mu),\, \kappa\right) \tag{5.21}$$

where the tuning error squared amounts to

$$\Delta^2\left(\mathscr{R}_n\right) = \left(\mathscr{R}_n - \mathscr{R}_n^{\text{th}}\right)^2\,, \tag{5.22}$$

where correlations beyond those of the Markov chains are taken into account and where we neglect explicit lattice artefacts[V] of $\mathscr{R}_n(aM_{\text{RGI}},z)$, considering those of z only. The derivatives are evaluated at the used input values instead of the theoretical one, the difference being subleading in a. The error related to κ's tuning needs some special care and will be described in Subsection 5.5.1, for now let us

[V] Which amounts to dropping terms like

$$\mathrm{d}_{\ln a}\mathscr{R}_n^{(1)}(z,aM_{\text{RGI}}) = \partial_{\ln z}\mathscr{R}_n^{(1)}\,\partial_{\ln a}\ln z + \cancel{\partial_{\ln a}\mathscr{R}_n^{(1)}(z,aM_{\text{RGI}})} + \ldots\,, \quad \text{where} \tag{5.23}$$

$$\mathscr{R}_n(z,aM_{\text{RGI}}) = \mathscr{R}_n^{(0)}(z,0) + a^2M_{\text{RGI}}^2\mathscr{R}_n^{(1)}(z,aM_{\text{RGI}}) + \mathscr{O}(a^4)\,, \tag{5.24}$$

where the dropped part is small w.r.t. the leading term in eq. (5.23). This is explicitly checked by quadratically interpolating $\mathscr{R}_n(z,aM_{\text{RGI}})$ for 3 different masses and at fixed $a > 0$, finding minimal, unimportant deviations with the above approximation.

note it turns out being orders of magnitude smaller w.r.t. other tuning errors and it is thus neglected. The log-derivative of the moment is a common, continuum factor which we evaluate numerically at the scale m_* (remembering its definition eq. (2.9) and that $\{\tilde{r}_n^{(i)}\}$ are the perturbative coefficients of the adimensional $\mathscr{R}_n$ defined in eq. (3.64))

$$\begin{aligned}\rho \overset{\text{def.}}{=} \frac{\partial \mathscr{R}_n}{\partial \ln z} &= \frac{\partial}{\partial \ln z}\left\{1+\tilde{r}_n^{(1)}\,\alpha_{\overline{\text{MS}}}(m_*)+\tilde{r}_n^{(2)}\,\alpha^2_{\overline{\text{MS}}}(m_*)+\tilde{r}_n^{(3)}\,\alpha^3_{\overline{\text{MS}}}(m_*)+\mathscr{O}(\alpha^4)\right\}\\ &= \left\{\beta_{\overline{\text{MS}}}(\alpha_{\overline{\text{MS}}})\left(\tilde{r}_n^{(1)}+\tilde{r}_n^{(2)}2\alpha_{\overline{\text{MS}}}(m_*)+\tilde{r}_n^{(3)}3\alpha^2_{\overline{\text{MS}}}(m_*)+\mathscr{O}(\alpha^3)\right)\right\}+\mathscr{O}(a^2)\,, \quad (5.25)\end{aligned}$$

yielding, all put together

$$\Delta^2(\mathscr{R}_n) = \sum_i \left\{\frac{\partial \mathscr{R}_n}{\partial \ln z}\frac{\partial \ln z}{\partial \ln b_i}\bigg|_{\text{th}}\Delta(\ln b_i)\right\}^2 \simeq \rho^2 \sum_i \left\{\frac{\partial \ln z}{\partial \ln b_i}\bigg|_{\text{th}}\Delta(\ln b_i)\right\}^2, \quad \vec{b} = \left(t_0/a^2, Z_P\right). \quad (5.26)$$

Three pieces are present in eq. (5.26): (1) ρ, with values tabulated in table 5.6, (2) $\partial_{\ln t_0/a^2}\ln z$, for which, since t_0/a^2 and the correlator are measured on the same gauge configurations, non-trivial correlations need to be taken into account (however, only mild relative effects of order $\sim 10\%$ are observed, since the scale only enters through the mass tuning), and (3) $\partial_{\ln Z_P}\ln z$, for which some care is necessary, as we explain in the following. In fig. 5.3 all $Z_{P,i}$ are shown, where the $\beta = 6.7859$ points

$M_{\text{RGI}}/M_{\text{RGI}}^{\text{charm}}$	3.48	2.32	1.55	1.16	0.77
z	13.5	9	6	4.5	3
$n=4$	-0.0402	-0.0533	-0.0745	-0.0986	-0.1603
$n=6$	-0.0922	-0.1264	-0.1832	-0.2498	-0.4253
$n=8$	-0.1080	-0.1504	-0.2227	-0.3093	-0.5445
$n=10$	-0.1009	-0.1415	-0.2112	-0.2956	-0.5275

Table 5.6: *Values of $\rho = \partial\mathscr{R}_n/\partial\log m_*$ for different n and z.*

(`sft4`) obtained at different scales perfectly agree with one another. However, for $\beta = 7.1146$ (`sft5`) there is quite some discrepancy between $Z_{P,3}$ (used value, green) and $Z_{P,4}$ (from the fit of higher β values, red, considered superior). To compensate for this error, we take the distance between the central values coming from the two determinations and add its effect on $\mathscr{R}_n$ in quadrature as an extra error. Again, the shift's coefficient has been obtained through analytical, leading order perturbation theory,

Finally, one more subtlety is present for $Z_{P,1}$. Once some L/a is chosen the bare coupling g_0 is tuned in order to give $L/a = r_0/a \times 0.718(16)$. The number $L/r_0 = 0.718$ comes from a continuum limit of $L/a \times a/r_0$, where the scale setting is done in large volume. This procedure entails an extra error in L/r_0 that we sum in quadrature to the others. To estimate it we start from

$$Z_P(g_0, L/a) = 1+\gamma_P^{(1)} g_0^2 \log\left(\frac{L}{a}\right)+\mathscr{O}(g_0^4) = 1+\gamma_P^{(1)}\bar{g}^2(L/a, g_0)\log\left(\frac{L}{a}\right)+\mathscr{O}(\bar{g}^4)\,, \quad (5.27)$$

where $\gamma_P^{(1)} = -d_0 = -8/(4\pi^2)$ is the leading order coefficient of the pseudoscalar (up to a sign it

corresponds in our case to the leading order mass anomalous dimension, since $Z_P Z_{\mu_{\rm tm}} = 1$ holds). Differentiating we obtain

$$\frac{\partial Z_P(L/a,g_0)}{\partial \log L} = \gamma_P^{(1)} \left\{ \underbrace{\frac{\partial \bar{g}^2(L/a,g_0)}{\partial \log L}}_{\approx \bar{g}^4} \log(L/a) + \bar{g}^2(L/a,g_0) \right\} + \mathcal{O}(g^4)$$
$$= \gamma_P^{(1)} \bar{g}^2(L) + \mathcal{O}(g^4)\,, \quad (5.28)$$

which amounts to

$$\Delta(Z_P)\big|_{L_{\rm max}/r_0} = \frac{\partial Z_P(L/a,g_0)}{\partial \log L} \Delta(\log L) \simeq \gamma_P^{(1)} \bar{g}^2(L) \Delta \log L + \mathcal{O}(g^4) = -\frac{8}{4\pi^2} 3.48 \frac{16}{718} + \mathcal{O}(u^2)\,. \quad (5.29)$$

Upon inclusion of this error, the uncertainty in $Z_{P,1}$ changes as reported in table 5.7 and it is clear one must include this factor.

β	$Z_{P,1}$	$\Delta(Z_{P,1})$	$\Delta(Z_{P,1}\vert_{\rm full})$
6.0219	0.6254	0.0046	0.0066
6.1628	0.6208	0.0046	0.0066
6.2885	0.6203	0.0048	0.0067
6.4956	0.6147	0.0046	0.0065

Table 5.7: *Comparison of $\Delta(Z_{P,1})$ – the error before adding in quadrature the error related to L/r_0 – with the full error $\Delta(Z_{P,1}\vert_{\rm full})$.*

5.5.1. Mistuning of κ

For the full case, out of maximal twist (now the relation between the different parameters is not linear anymore and we prefer using $\bar{z}$ for this part), definition eq. (5.8) of $\bar{z}$ becomes

$$\bar{z}\left(am_q, a\mu_{\rm tm}, \sqrt{8t_0}/a; Z_{P,SF}, Z_A, Z_{\Delta m}\right) = \frac{\sqrt{8t_0}}{a} Z_{P,SF}^{-1} \sqrt{(a\mu_{\rm tm})^2 + (Z_A Z_{\Delta m}\, am_q)^2} \quad (5.30)$$
$$= \frac{\sqrt{8t_0}}{a} Z_{P,SF}^{-1} \sqrt{(a\mu_{\rm tm})^2 + (Z_A\, am_{PCAC})^2}\,, \quad (5.31)$$

where all possible dependencies of $\bar{z}$ have been written explicitly. In the quenched case the renormalization factors Z_A and $Z_{\Delta m}$ can be taken from [116] and from [75], respectively. Let us remind that the tuning of κ we are following stems from an improved Wilson theory (see Section 5.4.1) in a Schrödinger functional setup, with no twisted mass. In this section we compute the error committed when tuning to κ_c, whereas the residual $\mathcal{O}(a\mu_R)$-effects in κ_c originating from the discretization of the twisted mass term will be described in the next section.

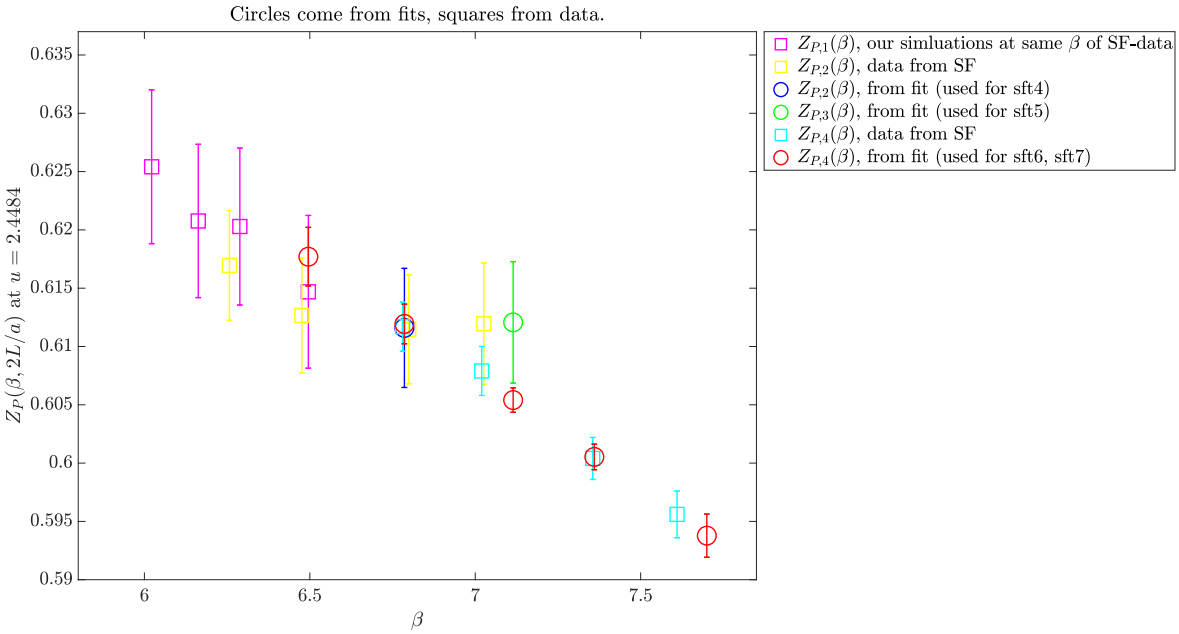

Figure 5.3: *Results for different definitions $Z_{P,i}$ used, description in the text. Note how thanks to the re-analysis of the data in [35], we not only slightly gain in precision for the running factor, but also for Z_P at finest lattice spacings (red points), which are the most important ones for the continuum limit.*

In this case we need $\mathscr{R}_n$ expanded to second order, since

$$\frac{\partial \ln \bar{z}}{\partial m_q} = \frac{Z_A^2 Z_{\Delta m}^2 m_q}{\mu_{\text{tm}}^2 + (Z_A Z_{\Delta m} m_q)^2} \overset{m_q \to 0}{\longrightarrow} 0\,. \tag{5.32}$$

The second order expansion is given by

$$\mathscr{R}_n\left(\vec{b}\right) = \mathscr{R}_n^{\text{th}} + \sum_{b_i} \frac{\partial \mathscr{R}_n}{\partial b_i}\bigg|_{\text{th}} \Delta(b_i) + \frac{1}{2}\frac{\partial^2 \mathscr{R}_n}{\partial b_i^2}\bigg|_{\text{th}} \Delta^2(b_i) + \ldots\,, \tag{5.33}$$

where it is immediate to see that for $m_q \to 0$ one term only survives, since

$$\frac{\partial^2 \mathscr{R}_n}{\partial m_q^2}\bigg|_{\text{th}} = \frac{\partial \mathscr{R}_n}{\partial \ln \bar{z}} \frac{\partial^2 \ln \bar{z}}{\partial m_q^2}\bigg|_{\text{th}} + \cancel{\frac{\partial^2 \mathscr{R}_n}{\partial \ln \bar{z}^2}\left(\frac{\partial \ln \bar{z}}{\partial m_q}\right)^2}\bigg|_{\text{th}}\,. \tag{5.34}$$

The derivative w.r.t. κ is given by

$$\frac{1}{2}\frac{\partial^2 \mathscr{R}_n}{\partial \kappa^2}\bigg|_{\text{th}} = \frac{1}{2}\frac{\partial \mathscr{R}_n}{\partial \ln \bar{z}} \frac{\partial^2 \ln \bar{z}}{\partial m_q^2}\left(\frac{\partial m_q}{\partial \kappa}\right)^2\bigg|_{\text{th}} = \frac{\partial \mathscr{R}_n}{\partial \ln \bar{z}} \frac{Z_A^2(\beta) Z_{\Delta m}^2(\beta)}{\mu_{\text{tm}}^2} \frac{1}{8\kappa^4}\,, \tag{5.35}$$

so that as a final estimate for the deviation of $\mathscr{R}_n$, caused by a mistuning of κ, we get

$$\Delta^2(\mathscr{R}_n)\big|_\kappa = \rho^2 \frac{Z_A^4 Z_{\Delta m}^4}{64\,\mu_{\text{tm}}^4 \kappa^8} (\Delta\kappa)^4\,. \tag{5.36}$$

For numerically evaluating the above we have, as mentioned before, taken the used input values of

β, κ, and μ_{tm}, since the difference with the "true" value is of subleading order in the lattice spacing. Computing the moments' relative error w.r.t. κ via eq. (5.36), it turns out being (at least) about 3-4 orders of magnitude suppressed if compared to the largest error source. It is thus safe to completely neglect it.

Finally, there is also a systematic error committed by taking the results of [117], since therein κ_c was determined at fixed $L/a = 16$. This means there is a leftover ambiguity in κ_c, as emphasized in Section I.2.4.1 of [151] for the analogous case of improvement coefficients. Due to the suppression of errors in κ, eq. (5.32), this effect will be unimportant. We will nevertheless briefly describe it, since it will affect the PCAC mass error, used to assess deviations from maximal twist. In perturbation theory cutoff effects in κ in the improved SF setup are $\mathcal{O}\left((a/L)^3\right)$. Beyond it, however, the appearance of non-perturbative length scales may complicate this behavior since a^3 effects are equivalent to $\mathcal{O}\left((a/L)^3 f(L/r)\right)$ deviations, for some unspecified scale r and where f is an unknown function. The authors of [117] find, when varying $L/a = 8 \to L/a = 16$, that the values for κ_c agree within 2×10^{-5}. We take this as a safe estimate which yields a variation in the PCAC mass[VI] of

$$\Delta(am_{PCAC})\big|_{\Delta\kappa_c^{\text{syst}}} = \frac{\Delta\kappa_c}{2\kappa_c^2} \simeq 5.5 \times 10^{-4}\,, \tag{5.37}$$

to be summed in quadrature to other errors when determining the a-dependence of the PCAC mass, see next section.

5.5.2. Deviations from Maximal Twist

Beyond the error in tuning κ to its critical value at $\mu_{\text{tm}} = 0$, there is an $\mathcal{O}(a\mu_{\text{tm}})$ effect in m_{PCAC}. This does not spoil $\mathcal{O}(a)$-improvement, since the operators needed to define the PCAC-mass have opposite $\gamma_5\tau^1$-parity, implying m_{PCAC} is $\gamma_5\tau^1$-odd and thus *it is an $\mathcal{O}(a)$-effect* (see Appendix A.2 for more details). Here it suffices to point out that for $a \to 0$ one expects m_{PCAC} to have a linear behavior in a, which we observe and for which we show results in the following.

To quantify deviations from maximal twist we monitored the bare, improved PCAC-mass as defined in eq. (5.6), with fixed flavor assignments (i.e. combinations as described in eq. (4.35)). For each mass some *fixed* physical (Euclidean) time value $x_0^*/\sqrt{8t_0}$ can simply be chosen by eye inspection, as long as it is well within the approximate plateau region for all β values. In some instances at $\beta_{\text{sft4}} = 6.4956$ a definitely clean plateau cannot be identified, but this problem is not seen for $\beta > \beta_{\text{sft4}}$ and is thus not important to us, having several smaller lattice spacings at our disposal. We define[VII] the PCAC mass of eq. (5.6) at these values $m_{PCAC}(x_0^*)$, represented by vertical lines in figs. 5.4, 5.5 and D.5 to D.7. In

[VI] Exactly which of our values of κ_c is taken for the numerical evaluation below does not matter; we choose a typical value, namely $\kappa \simeq 0.135$.

[VII] The PCAC relation is an exact identity broken only by lattice artefacts. If some physical scale is varied, such as $L/\sqrt{t_0}$ or $x_0/\sqrt{t_0}$, the coefficients of the leading order discretization effect will change, a difference which however disappears in the continuum limit. Measuring m_{PCAC} in the time region where excited state contamination of the correlation function is absent leads to better behaved cutoff effects, but measuring in their presence would not be theoretically wrong (as would be for the effective mass of Subsection 4.4.1). The big advantage here over some m_{eff}, as the one defined in eq. (4.49), is that no careful estimate of the plateau range and averages therein are necessary.

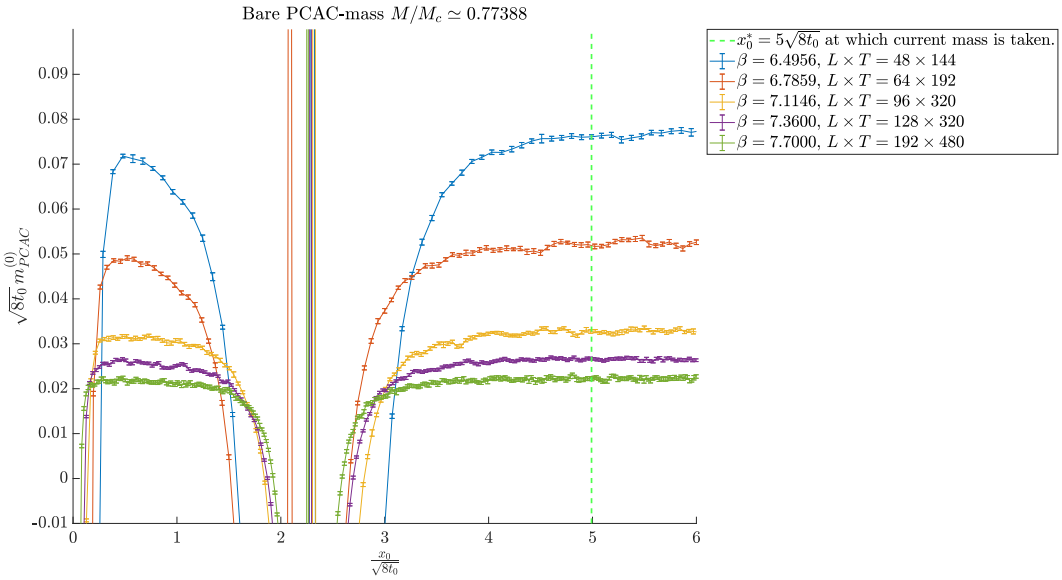

Figure 5.4: *Bare PCAC mass as a function of Euclidean time (in physical units), for several β values, all at fixed physical mass $M/M_c \simeq 0.77$. Close to $x_0/\sqrt{8t_0} = 0$ the effect of the boundary can be seen, whereas the results we use are in the depth of the bulk, on the opposite side of the source time-slice.*

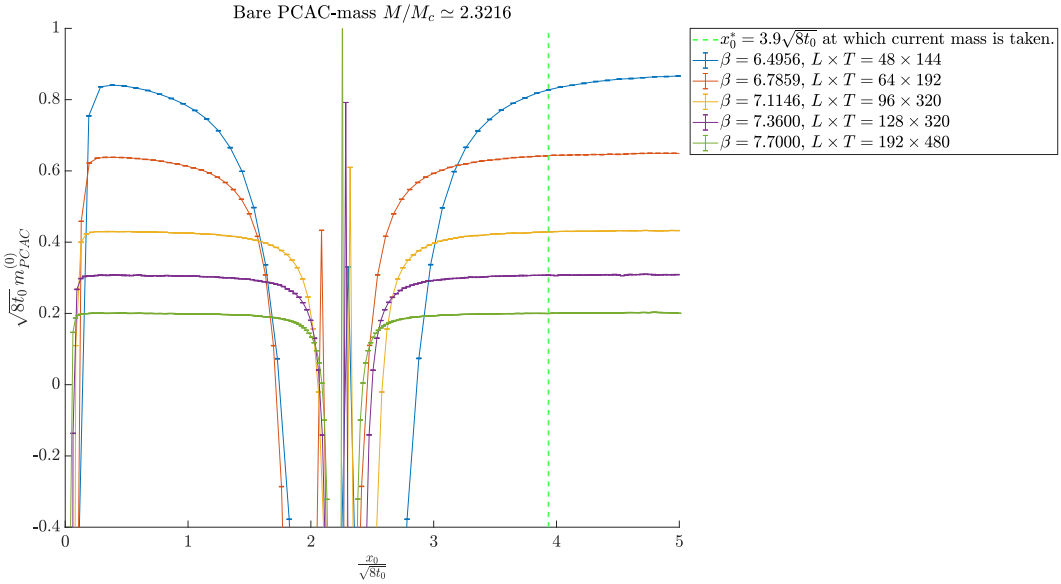

Figure 5.5: *Bare PCAC mass as a function of Euclidean time (in physical units), for several β values, all at fixed physical mass $M/M_c \simeq 2.32$. Close to $x_0/\sqrt{8t_0} = 0$ the effect of the boundary can be seen, whereas the results we use are in the depth of the bulk, on the opposite side of the source time-slice.*

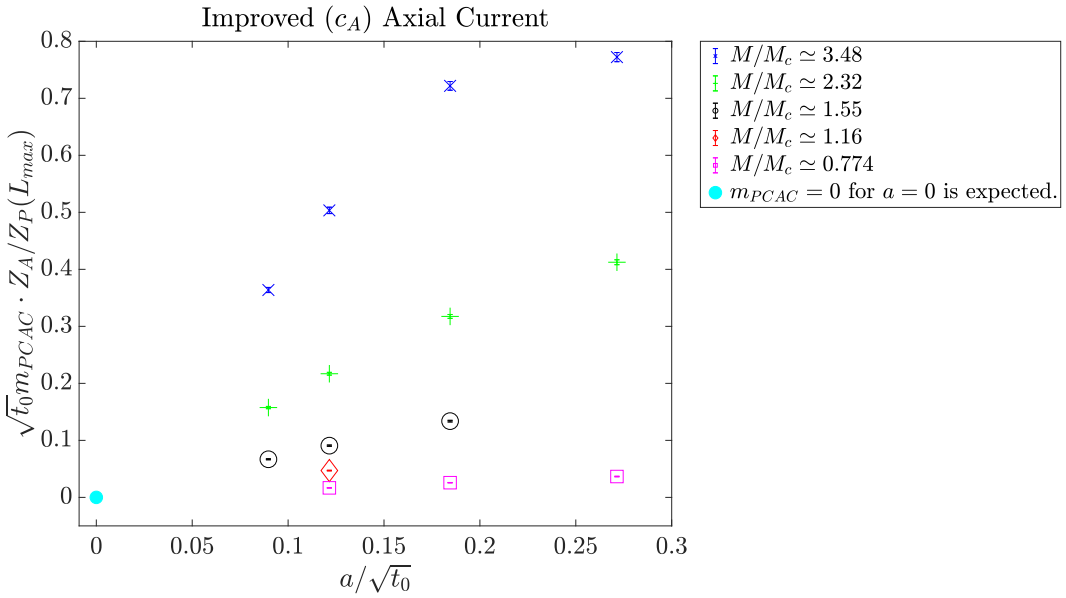

Figure 5.6: *Improved PCAC-mass as a function of $a/\sqrt{t_0}$, multiple heavy quark mass values; leftover discretization effects at small a scale approximately linearly, as expected.*

fig. 5.6 one can roughly see the dependence of the PCAC-masses on a is linear, as expected for an odd operator under $\gamma_5\tau^1$-parity and if a is small enough that higher order effects are suppressed.

In figs. 5.7 and 5.8 the improved PCAC-mass as a function of $a/\sqrt{t_0}$ is shown, where LiP indicates a linear fit of i points. Green fits have one degree of freedom less than the blue ones, since they are constrained to pass through the origin. They are compatible with the 3rd point whereas the unconstrained, blue curves extrapolated to zero are compatible with passing through the origin. Therefore linear discretization effects in the PCAC mass are observed as expected, with visible deviations starting above the $a \simeq 0.07$ fm region for the highest masses.

Having obtained values of the PCAC mass, we can now test whether we can reduce cutoff effects in the moments. If we change the PCAC mass by an $\mathcal{O}(a\mu_{\text{tm}})$ effect, we might obtain a reduction of $\mathcal{O}(a^2)$ corrections. To quantify how big the effect of non-zero PCAC mass is on our observables, we again Taylor-expand around the true theoretical value, in this case $m_{PCAC} = 0$. The idea is then to derive a shift in the moments just like has been done in Subsection 5.5.1, by approximating the derivative of the moment w.r.t. the log of the mass with a continuum β-function and by then computing the rest of the derivative explicitly, taken at the input value of the simulation. We did so for R_4, expanding to second order and getting, for the equivalent of eq. (5.35)

$$\frac{1}{2}\frac{\partial^2 R_4}{\partial m_{PCAC}^2}\bigg|_{\text{th}} = \frac{1}{2}\frac{\partial R_4}{\partial \ln \bar{z}}\frac{\partial^2 \ln \bar{z}}{\partial m_{PCAC}^2}\bigg|_{\text{th}} = \frac{1}{2}\frac{\partial R_4}{\partial \ln \bar{z}}\frac{Z_A^2(\beta)}{\mu_{\text{tm}}^2}. \tag{5.38}$$

This leads to $R_4 \to R_4^{shift} = R_4 + \Delta R_4$, with

$$\Delta R_4 = \rho \frac{Z_A^2}{(a\mu_{\text{tm}})^2}\Delta^2 (am_{PCAC}), \tag{5.39}$$

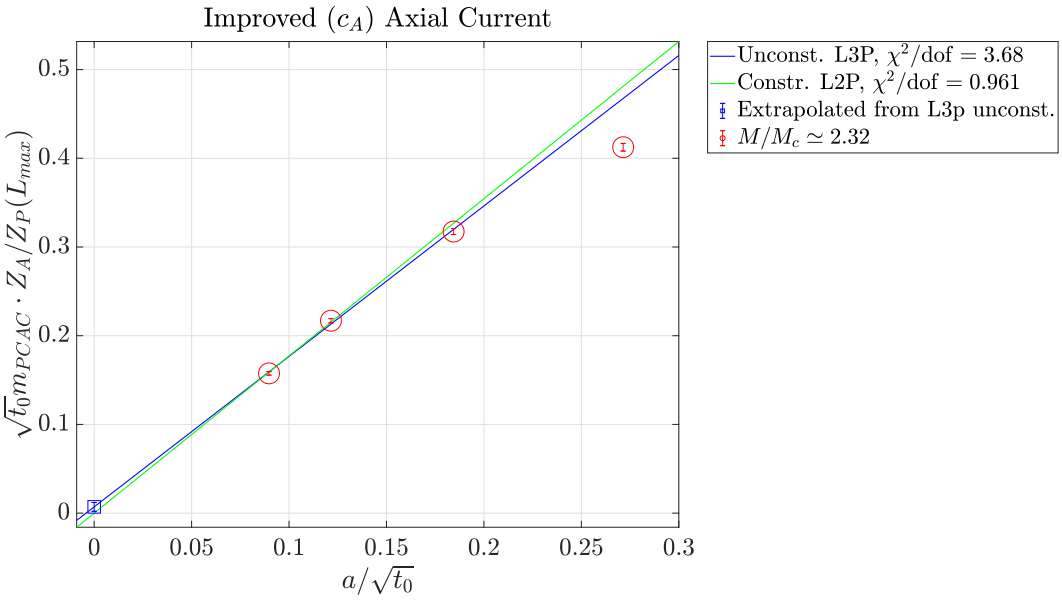

Figure 5.7: *Linear fits for the improved PCAC-mass as a function of $a/\sqrt{t_0}$, expected to be an $\mathcal{O}(a)$-effect at maximal twist, for a quark mass of $z = 9$ or $m/m_{charm} \simeq 2.3$.*

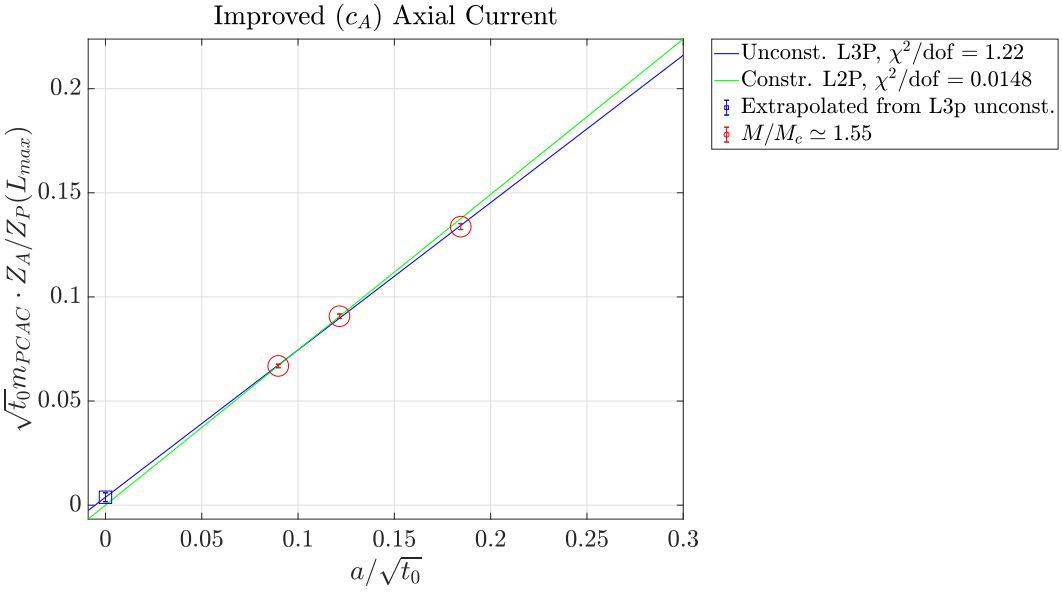

Figure 5.8: *Linear fits for the improved PCAC-mass as a function of $a/\sqrt{t_0}$, expected to be an $\mathcal{O}(a)$-effect at maximal twist, for a quark mass of $z = 6$ or $m/m_{charm} \simeq 1.6$.*

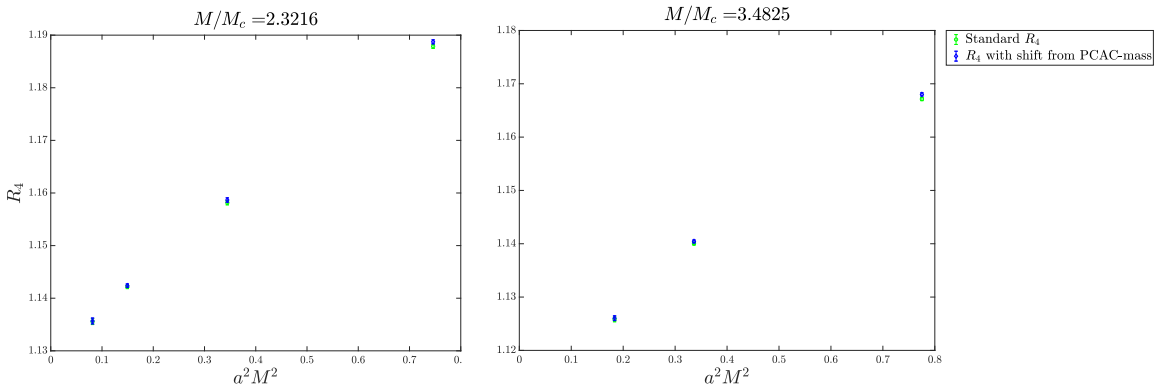

Figure 5.9: *Shifted R_4 obtained from correcting for non-zero PCAC mass at finite lattice spacing via eq. (5.39).*

where $\Delta(am_{PCAC})$ is nothing but the measured PCAC-mass. In fig. 5.9 the effect of this shift on the two highest masses is shown, where it is expected to have the biggest impact, as we observed. However, it can barely be seen on the coarsest lattices – remember the fourth moment is the one with the largest discretization effects – and thus does not help in a significant way to tame discretization effects.

5.5.3. Checks on Parameter Tuning

In Section 4.4 we computed the effective mass and the decay constant of a meson, showing some results for the plateaus of eq. (4.49) and eq. (4.56). These measurements serve as a cross-check of our input parameters in two ways: firstly, we ensure their continuum limits in figs. 5.10 and D.4 to be smooth, as expected if the parameters have been tuned consistently along a line of constant physics and, secondly, we verify the dependence of the decay constant on the mass, once extrapolated to the continuum (fit parameters given in table 5.8). This dependence, reported in fig. 5.11, has a universal behavior and can be quantitatively compared to other studies. A quadratic fit of our points is also shown in the figure, together with the point by [33], showing numerical consistency of the two studies.

		$z = 13.5$	$z = 9$	$z = 6$	$z = 4.5$	$z = 3$
$\sqrt{t_0}\,m_{PS}$	c_2	-6.2(1.1)	-4.21(1.2)	-6.3(1.3)	2.59(40)	1.38(41)
	c_1	-5.82(11)	-2.30(11)	-0.590(12)	-1.023((68))	-0.477(73)
	c_0	6.9894(24)	4.9954(18)	3.6131(23)	2.9201(25)	2.1700(28)
$\sqrt{t_0}\,f_{\eta_c}$	c_2	21.3(1.8)	7.1(2.1)	-1.5(2.2)	0.16(66)	0.03(46)
	c_1	1.90(17)	0.51(18)	0.58(19)	0.24(11)	0.102(75)
	c_0	0.5031(35)	0.4132(25)	0.3440(33)	0.3134(33)	0.2749(24)

Table 5.8: *Fit parameters for $\sqrt{t_0}m_{PS} = c_0 + c_1\,a^2/t_0 + c_2\,a_4/t_0^2$ and for $\sqrt{t_0}m_{\eta_c}$, with analogous notation for c_i.*

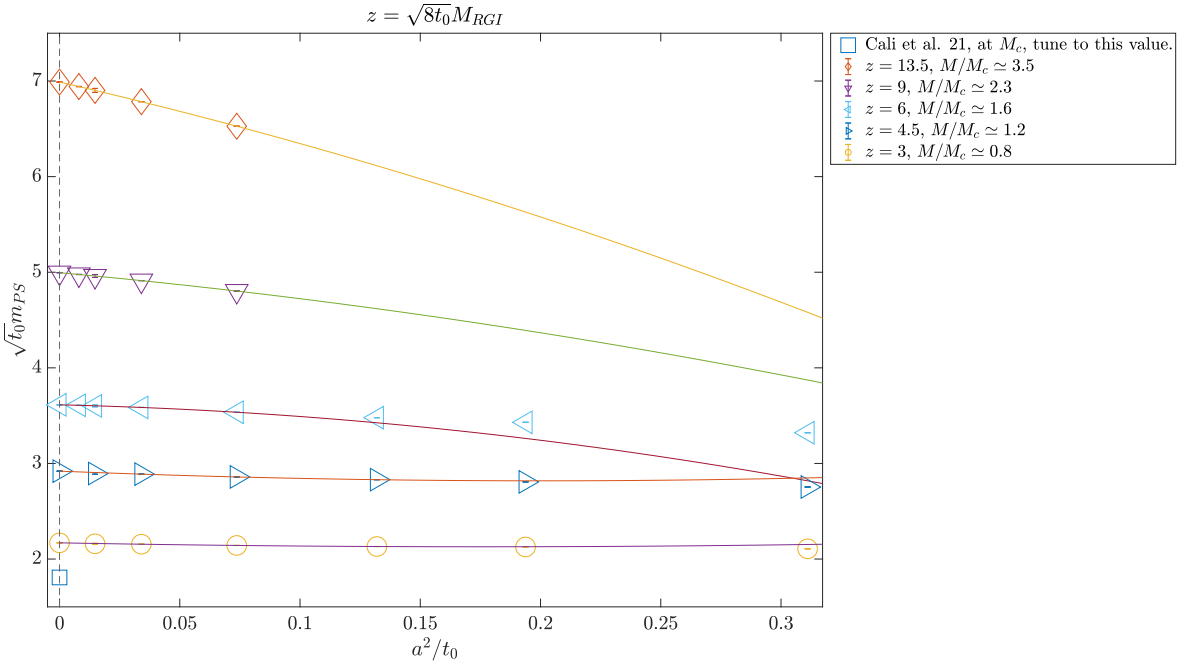

Figure 5.10: *Continuum limits of m_{PS} for all z values show a smooth behavior and validate our tuning was carried out well. Note, of the point by Calì et al. [33] at $a = 0$ only the magnitude matters, since their M_c differs from ours. Whatever value they were to choose, the behavior of (m_{PS}, f_{η_c}) in fig. 5.11 would still be universal.*

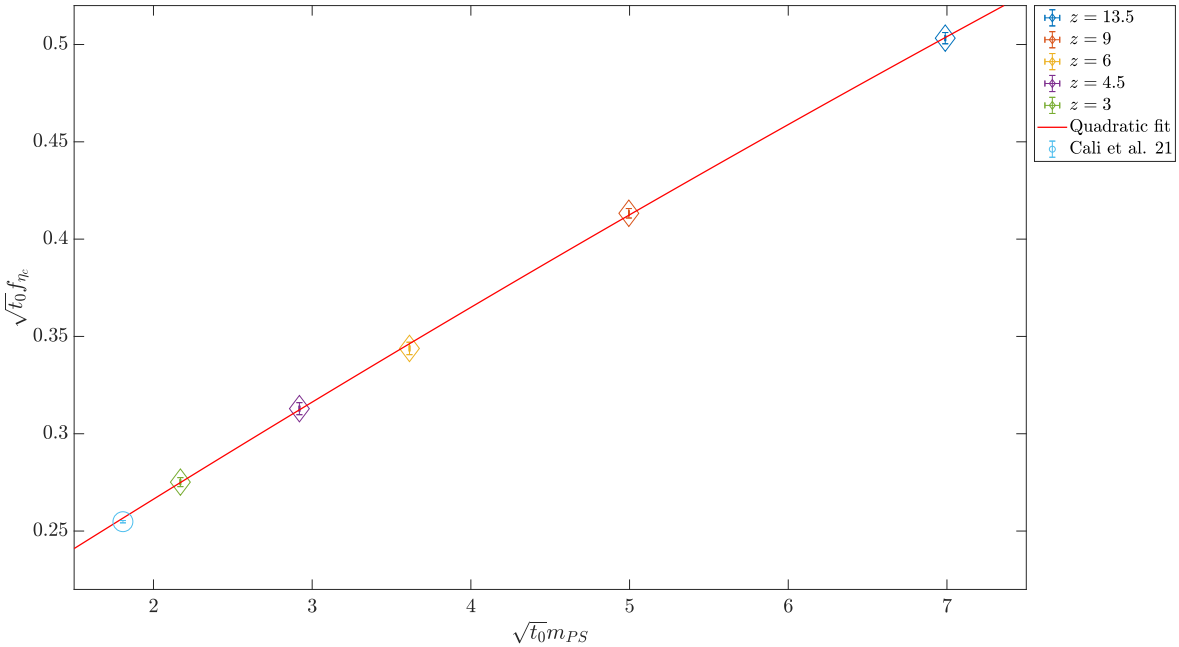

Figure 5.11: *Continuum extrapolated decay constant f_{η_c}, as throughout the rest of the thesis only considering (fermion)-connected contributions, as a function of the continuum extrapolated pseudoscalar mass m_{PS}, all in $\sqrt{t_0}$ units. A quadratic fit of all available masses is compatible with the point by [33], in light blue. A possibly (very slight) deviation is of no concern, since extrapolating towards the low mass region a bending is expected (which we are likely not sensitive to at our heavy mass values).*

6 | Results

AFTER a careful and lengthy discussion of several error sources within our lattice simulations, necessary to obtain controlled and reliable results, we are now ready to finally describe what physical result we can extract. Starting from the continuum extrapolation of moments, we are then able to compute the strong coupling by inverting the moments' perturbative expansion, *up to a given order*. This result can then be run (perturbatively) to infinite energy yielding the Λ_{RGI}-parameter, again, *to a given order*. In conclusion we here quantitatively answer the following questions: how does this leftover uncertainty, stemming from the truncation of the perturbative series, change with the scale? What is the size of deviations at scales of interest to flavor physics? Differently stated, we report here what we can learn about the applicability domain of asymptotic expansions for the case of integrated heavy-quark two-point functions, finding this to be quite a difficult topic within the context of precision physics.

6.1. Continuum Limits

As explained in Section 3.1, renormalized continuum physics is obtained as an extrapolation of computations necessarily restricted to $a > 0$. The size of cutoff effects in a given observable is related to how close the relevant energy scales present in the problem are close to the cutoff π/a, although the precise size is a priori not known. Cutoff effects in moments become larger for increasing mass values and decreasing n, where particular care needs to be given to the case $n = 4$. In this section we start by discussing the effect of the tree-level normalization, giving the full calculation in an appendix for readability, then show our continuum extrapolations for ratios of moments with $n > 4$.

6.1.1. The Fourth Moment

Here we only want to briefly sketch – for completeness – what we have realized throughout this research project for the case $n = 4$, leaving any further details of this underway effort to future publications (the interested reader may find a first account of this in [43]).

Symanzik improvement [155, 156] (discussed in Appendix A) describes how correlation functions at finite, small a depend on the lattice spacing. This is achieved through methods of effective field theory (EFT) [159] by treating lattice artefacts as if a^{-1} were a new physics scale of which ordinary continuum QCD is the low energy theory. We look at the case of $\mathcal{O}(a)$-improved time-slice correlator $G^{\mathrm{I}}(t,a)$, the relevant one for this work, and set $a/t \ll 1$, $[G] = 3$. We focus on the region $tM_{\mathrm{RGI}} \ll 1$,

in which t is thus the only available scale, except for the lattice spacing. This enables powerful dimensional counting arguments to be employed. The prediction of the aforementioned EFT at *leading order* (and thus in absence of any renormalization related logs of the kind studied in [90, 89], which appear at higher order in the coupling) is

$$G^{\mathrm{I}}(t,a) = G(t,0) + \frac{a^2}{t^5}k_L + \mathscr{O}(a^4) + \mathscr{O}(t^2M^2)\,, \tag{6.1}$$

for some constant k_L and where higher odd powers of a are absent in our maximal twist case. We are here interested in small t behavior, i.e. in short distance properties which may give rise to divergences once integrated. The larger t region of the integral or sum does not have such issues and differences due to these terms, as ones related to trapezoidal-rule-approximation of the integral, will here be dropped. For the integrated quantity defining *the moment* $n = 4$, with integration extrema $a \ll t_1 < t_2 \ll M_{\mathrm{RGI}}^{-1}$, one thus obtains

$$\Delta_{\mathscr{M}_4}(t_1,t_2) \overset{\text{def.}}{=} a\sum_{t_1}^{t_2} t^4 G(t,a) - \int_{t_1}^{t_2} t^4 G(t,0)\mathrm{d}t \overset{a\ll t_1}{\sim} a^2 \int_{t_1}^{t_2} \frac{k_L}{t^5} t^4 \mathrm{d}t = k_L a^2 [\log(t_2/a) - \log(t_1/a)]\,, \tag{6.2}$$

where we have inserted a factors in the logs. Sum and integral in the above definition being linear operators, one can trivially split $\Delta_{\mathscr{M}_4}(0,t_2) = \Delta_{\mathscr{M}_4}(0,t_1) + \Delta_{\mathscr{M}_4}(t_1,t_2)$ only using the above equality (valid for any a), where $\Delta_{\mathscr{M}_4}(0,t_2)$ clearly cannot depend on t_1. Thus, such pieces must combine to form an a^2 term with some different constant k'

$$\Delta_{\mathscr{M}_4}(0,t_2) \sim \underbrace{\left[\Delta_{\mathscr{M}_4}(0,t_1) - k_L a^2 \log(t_1/a)\right]}_{\equiv k' a^2} + k_L a^2 \log(t_2/a)\,. \tag{6.3}$$

Let us stress terms in the above equation have mass dimension -2 and a is the only scale present in the first part, there simply is no other choice. This shows the presence in the *summed* observable of a log-dependence *solely due to the sum over small separations, already at leading order*; the dimensional analysis exposed here can be done beyond tree-level [43], but the size of discretization effects is then determined by an unknown function. The leading order analysis carried out gives quite some insight into the structure of cutoff effects in integrated correlation functions. This sort of behavior has been noted before in [77] for lattice studies of the hadronic vacuum polarization [18], which contains an integral with an analogous short time behavior.

Finally, let us mention that by simple power counting analogous to what is seen in eq. (6.2), higher moments also have logarithmic a-dependence, but only appearing at higher order terms in the Symanzik expansion. For instance, when $n = 6$, two more powers of a are required for dimensional consistency, meaning a $\log(a)$ term does not appear multiplied by a^2, as for $n = 4$, but by a^4. The higher the moment the more log-terms at tree-level of perturbation theory are pushed to higher orders in the Symanzik expansion.

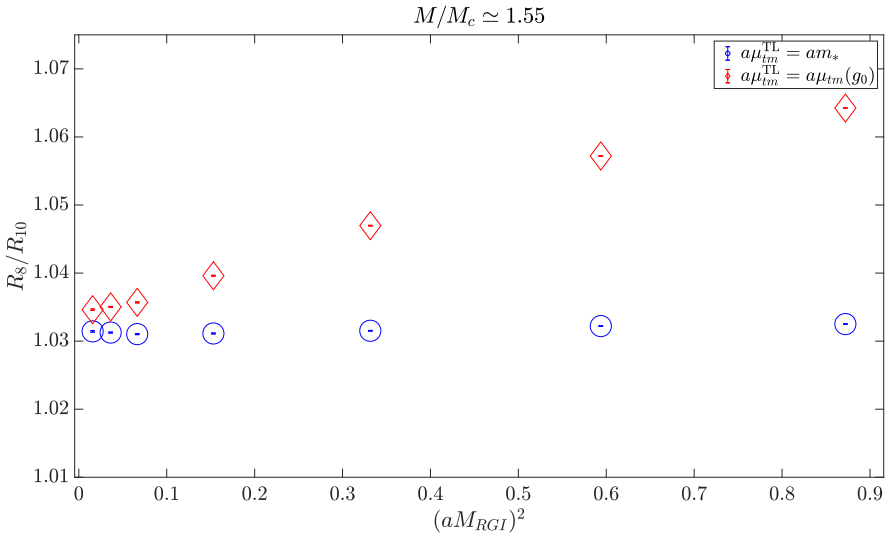

Figure 6.1: *Comparison of scaling towards the continuum with different scales in the finite L, finite a tree-level normalization. The choice $a\mu_{\rm tm}^{TL} = am_*$ diminishes the size of cutoff effects in almost all cases.*

6.1.2. Effect of Tree-Level Normalization

In Subsection 3.5.2 we argued heuristically why one expects the division of moments by their tree-level to alleviate cutoff effects, hinting at a possible breakdown of those arguments. Here we explore these ideas in more detail, looking at the relative freedom in the choice of TL input parameters.

The TL has by definition $g_0 = 0$ and thus, at finite volume, two input parameters are necessary: $a\mu_{\rm tm}^{\rm TL}$ and L/a. For the TL's computation L/a is set to the values of the non-perturbative simulation, whereas our choice for the mass requires further comment. One needs $a\mu_{\rm tm}^{\rm TL} = am + \mathcal{O}(g^2)$ with m any definition of the mass. Instead of the usual choice found in literature $a\mu_{\rm tm}^{\rm TL} = a\mu_{\rm tm}(g_0)$, where $a\mu_{\rm tm}(g_0)$ is the bare twisted mass of the simulation at coupling g_0, we notice $a\mu_{\rm tm}^{\rm TL} = am_*$ to be a much better choice, where m_* is a renormalized mass, our choice being $m_* = \overline{m}_{\overline{\rm MS}}(m_*)$. In fig. 6.1 the $a\mu_{\rm tm}(g_0)$ normalization is represented by red diamonds while the am_* normalization by blue circles; clearly the latter shows a much flatter scaling towards the continuum.

6.1.3. Dimensionless Ratios of Moments

The ratios introduced in eq. (2.20) are dimensionless by construction, with only a weak logarithmic dependence on the mass originating in the coupling. To parametrize cutoff effects and then reliably extrapolate we try out several fit-function Ansätze, as well as varying the range in a of points used for these fits. Whenever $a^2M_{\rm RGI}^2 > 0.35$, we drop those data points. We try continuum limits linear and quadratic in $a^2M_{\rm RGI}^2$, stressing these are to be understood as functional forms which *try to* capture the cutoff effects well, of course with some theoretically motivated structure in them, such as the absence of odd powers in a (thanks to the $\gamma_5\tau_1$ symmetry of twisted mass, see Appendix A.2).

We also compute the goodness-of-fit, or *p-value*, in order to apply a cut of $p > 0.05$ to our fit functions [30]. Fits that do not obey this inequality, are discarded; 2-point linear fits and 3-point

quadratic fits (which have zero degrees of freedom and are exact extrapolations) are only used when no other fit passes the above criteria. We compute the p-value through an upper incomplete Gamma, function of n_{dof} and χ^2_{fit}, as

$$p(n_{\text{dof}}/2, \chi^2_{\text{fit}}/2) \overset{\text{def.}}{=} \frac{1}{\Gamma(n_{\text{dof}})} \int_{\chi^2_{\text{fit}}}^{\infty} t^{n_{\text{dof}}-1} \mathrm{e}^{-t} \, \mathrm{d}t \,, \tag{6.4}$$

since to a reasonable approximation our data are uncorrelated. An exception to the above criteria is $\mathscr{R}_8$ at $M/M_c \simeq 2.3$, fig. 6.3b, where we make use of a 5-point quadratic fit with $p = 0.035$ and a 4-point one with $p = 0.024$, since no other fit beyond 2-point linear and 3-point quadratic are usable. Due to a large relative fluctuation of the 3 points closest to the continuum, fits with zero degrees of freedom are inappropriate to extrapolate, which prompted the usage of fits with lower p-values. What eq. (6.4) represents is the probability of having a $\chi^2 \geq \chi^2_{\text{fit}}$, where we remind the fit parameters are obtained by minimization of the χ^2. The cut can be thought of as follows: too low p-value, say $p \leq 0.05$, indicates it is desirable to reject the null hypothesis and discard the fit, with a probability of falsely rejecting said hypothesis of less than or equal to 5%.

Selecting an Extrapolation: The final result is obtained through the following, quite conservative, strategy: we quote the extrapolation with the largest statistical uncertainty, to which we add in quadrature a systematic error obtained from the set of all the fits employed. It consists of half the spread between largest and smallest accepted extrapolated (a.e.) values, i.e.

$$\Delta(z)|_{\text{c.l. syst.}} = \frac{1}{2} \left(\max_{\text{a.e.}} \{\mathscr{R}_n(z,0)\} - \min_{\text{a.e.}} \{\mathscr{R}_n(z,0)\} \right) \tag{6.5}$$

thus somehow parametrizing the error committed when choosing a fit Ansatz over another one while at the same time utilizing the information about cutoff effects contained in all accepted fits.

In figs. 6.2a, 6.3a and D.10 to D.12 our continuum extrapolations for R_6/R_8 for several fit Ansätze are given, showing considerable $\mathscr{O}(a^2)$ lattice artefacts, especially remembering the sensitivity to the coupling is given by $\mathscr{R}_n - 1$, i.e. the distance from 1. As the mass grows, quite an extrapolation may be needed from the smallest lattice spacing $a \simeq 0.01$ fm, which we remind readers to be only reachable today in the quenched theory.

Continuum extrapolations of R_8/R_{10} can be found in figs. 6.2b, 6.3b and D.13 to D.15, where cutoff effects are milder, as expected (the higher n, the more the observable is dominated by long distances, cfr. fig. 2.1). However, we cannot help but notice quite some curvature is noticeable even at very small lattice spacings; this seems to be a property of this observable present both in this discretization and in others, such as with staggered quarks [138, 3].

Results for the continuum extrapolated values will be given in Subsection 6.1.5, since a few more details need to be discussed first. In table 6.1 we report only the coefficients c_i, with $i = 1, 2$, corresponding to the powers a^{2i}, for two different possible parametrizations of the cutoff effects: as polynomials in $x = (aM_{\text{RGI}})^2$ and in $x = a^2/t_0$. It becomes clear, simply by comparing their size, that the relevant scale to consider is the heavy quark mass, especially as z increases as far as there the

differences become larger.

		$z = 13.5$	$z = 9$	$z = 6$	$z = 4.5$	$z = 3$
R_6/R_8	c_2	–	-0.171(67)	-0.280(12)	-0.18(0.40)	1.38(41)
	c_1	–	-0.094(13)	-0.1072(40)	-0.127(41)	-0.477(73)
	$\bar{c}_2$	–	-17.5(6.9)	-5.67(24)	-1.2(2.6)	1.75(52)
	$\bar{c}_1$	–	-0.952(13)	-0.482(18)	-0.32(10)	-0.537(82)
R_8/R_{10}	c_2	0.0229(42)	0.0098(62)	0.033(46)	0.23(19)	0.53(1.52)
	c_1	-0.0068(18)	-0.0023(26)	-0.0076(84)	-0.027(20)	-0.049(70)
	$\bar{c}_2$	11.9(2.2)	1.00(64)	0.67(93)	1.5(1.2)	0.67(1.92)
	$\bar{c}_1$	-0.155(41)	-0.023(26)	-0.034(38)	-0.068(51)	-0.055(79)

Table 6.1: *Fit parameters encoding the speed of the continuum approach, i.e. the cutoff effects. Fit functions are* $f_{t_0} = \bar{c}_0 + \bar{c}_1 a^2/t_0 + \bar{c}_2 a^4/t_0^2$ *and* $f_{M_{RGI}} = c_0 + c_1 a^2 M_{RGI}^2 + c_2 a^4 M_{RGI}^4$. *Note how the latter is a visibly better parametrization since the heavy quark mass is the intrinsic scale present in this observable.*

6.1.4. Running Error

An approach analogous to the inclusion of tuning errors at finite a, namely that of Taylor expanding and estimating derivatives analytically, is used for the error component induced by the uncertainty on $M_{\mathrm{RGI}}/\overline{m}_{\mathrm{SF}}(L_{\mathrm{ref}})$. However, as previously pointed out, this is a continuum factor which does not contain any information useful for the continuum extrapolation and its effect on $\Delta\mathscr{R}_n$ can be summed in quadrature to other error sources. Taking the log-derivative of the (perturbatively) re-expanded ratio eq. (3.64), i.e.

$$\frac{\partial}{\partial \log z}\mathscr{R}_n(z) = \frac{\partial}{\partial \log z}\left[1 + \tilde{r}_n^{(1)}\alpha_{\overline{\mathrm{MS}}} + \tilde{r}_n^{(2)}\alpha_{\overline{\mathrm{MS}}}^2 + \tilde{r}_n^{(3)}\alpha_{\overline{\mathrm{MS}}}^3 + \mathscr{O}(\alpha_{\overline{\mathrm{MS}}}^4)\right], \tag{6.6}$$

where denote by $\tilde{r}_n^{(i)}$ the i-th perturbative coefficient of $\mathscr{R}_n$ [121], i.e. for $n = 4$ trivially $\tilde{r}_n^{(i)} \equiv r_n^{(i)}$, whereas for $n > 4$ a re-expansion in $\alpha_{\overline{\mathrm{MS}}}(\mu)$ of the ratio R_n/R_{n+2} needs to be carried out, so that in this case $\tilde{r}_n^{(i)} = f(r_n, r_{n+2})$. This can be carried out with any symbolic computation software, such as `Maple` or `Mathematica`. We also remind the reader that once the perturbative scale is fixed $\partial_{\log z} = \partial_{\log m_*}$, thanks to the multiplicative relationship between M_{RGI} and $\overline{m}(m_*)$. Comments on the correlations between $M_{\mathrm{RGI}}/\overline{m}$ and Z_P can be found in Appendix B.

6.1.5. Results

We are now in the position to give the first physical results of the present work, namely the continuum extrapolations of adimensional ratios of moments, with all possible error sources included. Note that these are purely non-perturbative quantities and do not suffer from any perturbative uncertainty, unlike the coupling we want to extract from them which we therefore discuss in the next section. The continuum limits are given in table 6.2, together with the corresponding values for $\alpha_{\mathscr{R}_n}$. This is nothing but the non-perturbative, scale-independent coupling in eq. (1.17), defining what we there

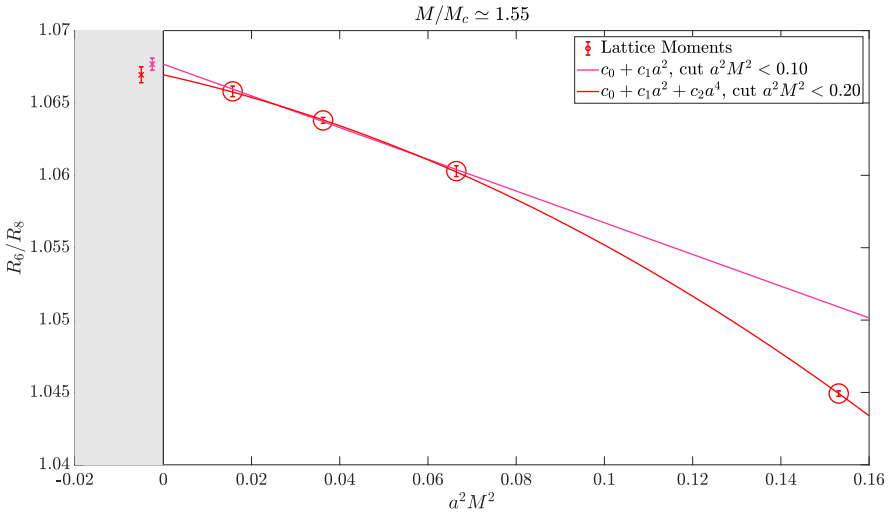

(a) *For R_6/R_8 at intermediate mass, sizable cutoff effects are present, but one can extrapolate well anyway.*

(b) *All extrapolation Ansätze agree very well for R_8/R_{10}.*

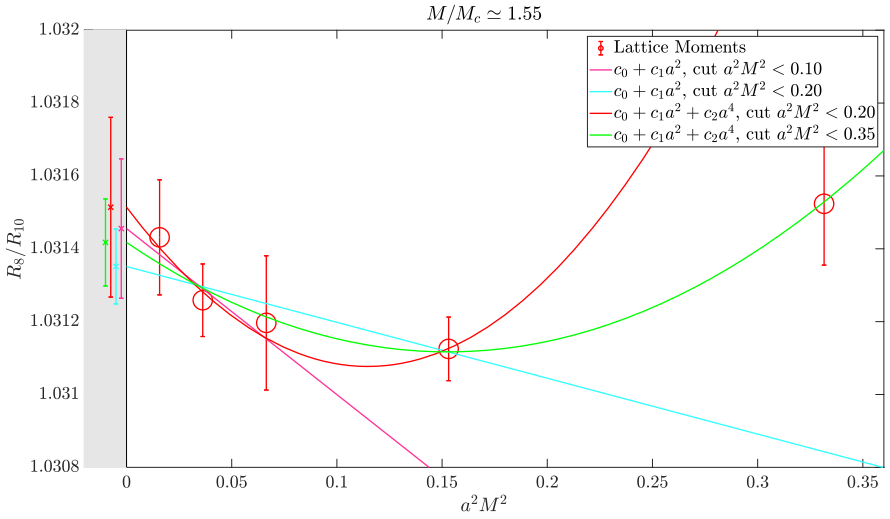

Figure 6.2: *Continuum limits for mass $M/M_c \simeq 1.55$, $z = 6$. Several fit Ansätze are shown. In the gray band on the left hand side the value and error of the extrapolation for each Ansatz are plotted next to one another for better visibility.*

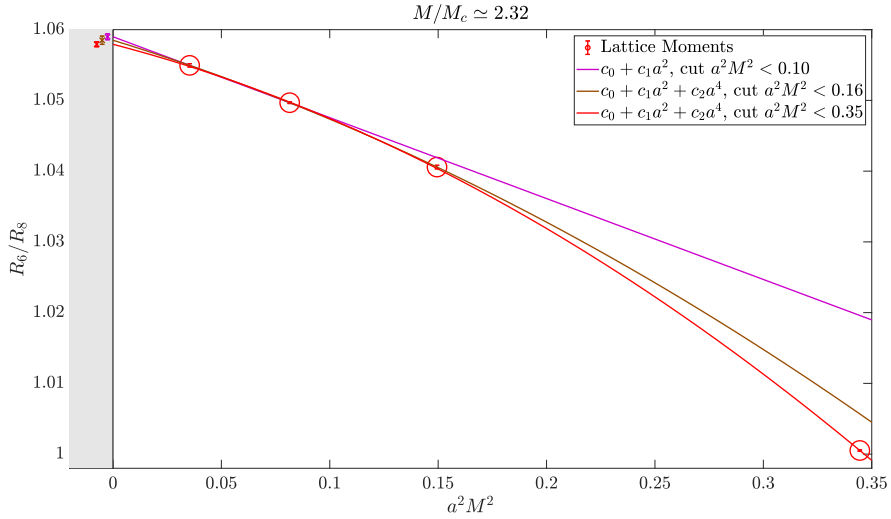

(a) *At this higher mass quite an extrapolation is necessary for R_6/R_8.*

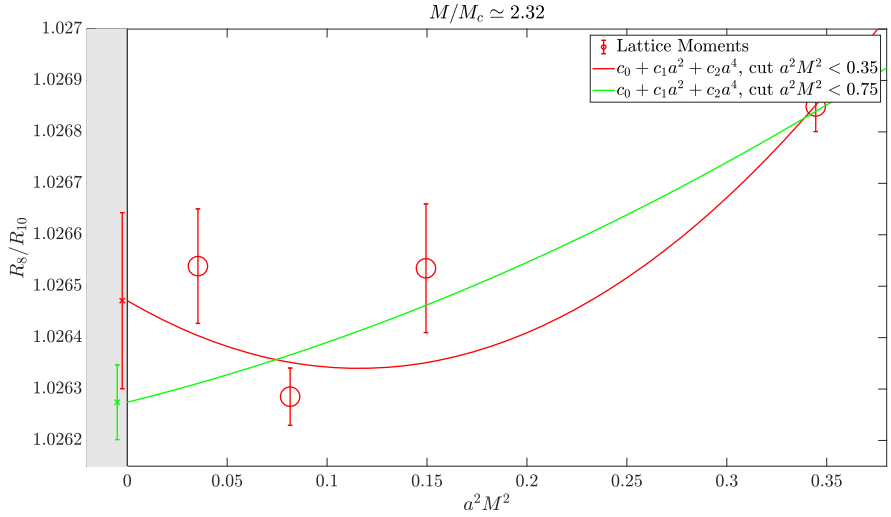

(b) *The extrapolation for R_8/R_{10} , given the fine scale on the y-axis, is under better control, still here fits with a p-value lower than 0.05 needed to be used.*

Figure 6.3: *Continuum limits for mass $M/M_c \simeq 2.32$, $z = 9$. Several fit Ansätze are shown. In the gray band on the left hand side the value and error of the extrapolation for each Ansatz can be seen.*

call $\mathscr{B}$-scheme and which will now be labeled $\mathscr{R}_n$-scheme, with $n = 6, 8$. For moments with our normalization we can thus write

$$\alpha_{\mathscr{R}_n}(M_{\mathrm{RGI}}) = \frac{\mathscr{R}_n - 1}{\tilde{r}_n^{(1)}} \overset{\alpha\to 0}{\sim} \alpha_{\overline{\mathrm{MS}}}(\mu_s) + \frac{\tilde{r}_n^{(2)}(s)}{\tilde{r}_n^{(1)}}\alpha^2_{\overline{\mathrm{MS}}}(\mu_s) + \frac{\tilde{r}_n^{(3)}(s)}{\tilde{r}_n^{(1)}}\alpha^3_{\overline{\mathrm{MS}}}(\mu_s) + \mathscr{O}(\alpha^4_{\overline{\mathrm{MS}}}), \tag{6.7}$$

where we allow for a scale factor s (just like in eq. (1.16)) and with $\mu_s = s\overline{m}_{\overline{\mathrm{MS}}}(\mu_s)$, as defined in eq. (2.7). Note two things: (1) once s is fixed, μ_s and M_{RGI} are in one-to-one correspondence through eq. (2.33) and (2) no scale factor s enters in the left hand side of eq. (6.7), since for dimensionless observables such as $\mathscr{R}_n$ the first coefficient $\tilde{r}_n^{(1)}$ is s-independent[I]. Thus, eq. (6.7) represents an effective

	$z = 3$	$z = 4.5$	$z = 6$	$z = 9$	$z = 13.5$
$\mathscr{R}_6 = R_6/R_8$	1.0965(12)	1.07708(82)	1.06695(70)	1.05850(81)	1.0526(11)
$\alpha_{\mathscr{R}_6}$	0.3221(40)	0.2573(27)	0.2235(23)	0.1953(27)	0.1757(38)
$\mathscr{R}_8 = R_8/R_{10}$	1.04758(57)	1.03647(40)	1.03151(28)	1.02647(21)	1.02323(26)
$\alpha_{\mathscr{R}_8}$	0.3652(44)	0.2799(30)	0.2419(22)	0.2032(16)	0.1788(20)

Table 6.2: *Final results for continuum limits – together with corresponding α_{eff} values – with all error sources taken into account, i.e.: (1) the statistical error, (2) tuning errors related to fixing the mass and stemming from Z_P, t_0/a^2, the full twist condition (see chapter 5), (3) the extra systematic continuum limit error estimated via the spread of different fit Ansätze eq. (6.5) as well as (4) the continuum running error factor discussed in Subsection 6.1.4.*

coupling, the magnitude of which indicates whether the renormalization scale is sufficiently high for the perturbative series to be in its asymptotic regime. This value is one of the crucial parameters that the authors of the FLAG initiative responsible for the coupling [5, 6] use to judge the quality of studies, and which they call α_{eff}. The report states, referring to its quality criteria: "To each such source of error for which systematic improvement is possible we assign one of three coloured symbols: green star, unfilled green circle [...] or red square". The strong coupling chapter sets as quantitative criteria $\alpha_{\mathrm{eff}} < 0.2$ for green star, $\alpha_{\mathrm{eff}} < 0.4$ and at least one point $\alpha_{\mathrm{eff}} \leq 0.25$ for green circle, and red square otherwise. Note that a red square in *any* error source disqualifies a result from being part of the averages carried out in the report.

Indeed, too large α_{eff} may lead to power-law like, "non-perturbative" effects [122] of the type in eq. (1.17) and which have an uncontrolled size, as in the case of τ decays [139] (for which $\alpha_{\mathrm{eff}} \approx 0.3$, but see also the more recent [17, 16]).

[I] To see this, simply suppose it to have such dependence and apply a derivative w.r.t. μ, i.e.

$$\mathscr{R}_n = 1 + \tilde{r}_n^{(1)}(s)\alpha_{\overline{\mathrm{MS}}}(\mu) + \tilde{r}_n^{(2)}(s)\alpha^2_{\overline{\mathrm{MS}}}(\mu) + \mathscr{O}(\alpha^3_{\overline{\mathrm{MS}}}) \overset{\partial_{\log\mu}}{\Longrightarrow} \tag{6.8}$$

$$\overset{\partial_{\log\mu}}{\Longrightarrow} 0 = \beta_{\overline{\mathrm{MS}}}(\alpha_{\overline{\mathrm{MS}}})\tilde{r}_n^{(1)}(s) + \alpha_{\overline{\mathrm{MS}}}(\mu)\partial_{\log\mu}\tilde{r}_n^{(1)}(s) + \alpha^2_{\overline{\mathrm{MS}}}(\mu)\partial_{\log\mu}\tilde{r}_n^{(2)}(s) + \mathscr{O}(\alpha^3_{\overline{\mathrm{MS}}}) \tag{6.9}$$

$$\overset{\partial_{\log\mu}}{\Longrightarrow} 0 = \alpha_{\overline{\mathrm{MS}}}(\mu)\partial_{\log\mu}\tilde{r}_n^{(1)}(s) + \alpha^2_{\overline{\mathrm{MS}}}(\mu)\left(\partial_{\log\mu}\tilde{r}_n^{(2)}(s) - \beta_0\tilde{r}_n^{(1)}(s)\right) + \mathscr{O}(\alpha^3_{\overline{\mathrm{MS}}}), \tag{6.10}$$

where eq. (6.10) has to be valid order by order in $\alpha_{\overline{\mathrm{MS}}}$, yielding $\partial_{\log\mu}\tilde{r}_n^{(1)}(s) = 0$.

6.2. EXTRACTING THE QCD COUPLING

After having obtained renormalized, continuum extrapolated results for the moments in infinite volume, the coupling is extracted by comparing these with the perturbative expression for the moments, as introduced in Section 2.4. One needs to first choose a perturbative renormalization scale, i.e. fix some value of s, after which a quick inversion gives $\alpha_{\overline{\text{MS}}}(\mu_s)$.

The scale factor serves as an extra handle one can turn to study the system. Especially, let us remind the reader a scale variation is oftentimes used in order to estimate the size of the truncation error. How much such a procedure is under control in the realm of high precision physics is unclear, though, since, as stressed in the introduction, there is no real knowledge about the s-independent part of the $(L+1)$-th coefficient, with L the number of known loops.

6.2.1. Methodology

The key formula for extracting the coupling from any of the measured observables

$$\mathscr{R}_n(z, aM_{\text{RGI}}) = \begin{cases} R_n(z, aM_{\text{RGI}}), & n = 4, \\ \frac{R_n(z,a)}{R_{n+2}(z,a)}, & n = 6, 8, \dots, \end{cases} \tag{6.11}$$

is simply their perturbative expansion in the $\overline{\text{MS}}$-scheme. The general perturbative expansion thus reads

$$\lim_{a\to 0}\{\mathscr{R}_n(z, aM_{\text{RGI}})\} = 1 + \tilde{r}_n^{(1)}\alpha_{\overline{\text{MS}}}(\mu_s) + \tilde{r}_n^{(2)}(s)\alpha^2_{\overline{\text{MS}}}(\mu_s) + \tilde{r}_n^{(3)}(s)\alpha^3_{\overline{\text{MS}}}(\mu_s) + \mathscr{O}(\alpha^4_{\overline{\text{MS}}}), \tag{6.12}$$

which can be inverted once a fixed value of s is chosen, either numerically or iteratively order by order. The extracted coupling is a function of the mass, which fixes the scale of the observable, and of s, which fixes the perturbative renormalization scale w.r.t. the above mentioned mass. Once s is fixed, z (or M_{RGI}) is in one-to-one correspondence with $\overline{m}_{\overline{\text{MS}}}(\mu_s)$ through eq. (2.33). Inverting this, at a given z, i.e. once the heavy quark mass is fixed, a choice of s is equivalent to fixing some value for μ_s. Here we stress again that any results for the coupling intrinsically have a truncation error, namely

$$\alpha^{\text{extracted}}_{\overline{\text{MS}}}(\mu_s) = \alpha_{\overline{\text{MS}}}(\mu_s) + \mathscr{O}\left(\alpha^4_{\overline{\text{MS}}}(\mu_s)\right). \tag{6.13}$$

For clarity, we here remind the reader the full expansion to be

$$\begin{aligned}\mathscr{R}_n(z,0) = 1 + \tilde{r}_n^{(1)}\alpha_{\overline{\text{MS}}}(\mu_s) + \left(\tilde{r}_n^{(2,0)} + \tilde{r}_n^{(2,1)}\log s^2\right)\alpha^2_{\overline{\text{MS}}}(\mu_s) + \\ + \left(\tilde{r}_n^{(3,0)} + \tilde{r}_n^{(3,1)}\log s^2 + \tilde{r}_n^{(3,2)}\log^2 s^2\right)\alpha^3_{\overline{\text{MS}}}(\mu_s) + \mathscr{O}(\alpha^4_{\overline{\text{MS}}}),\end{aligned} \tag{6.14}$$

where all coefficients are known [121]. The iterative procedure simply solves for $\alpha_{\overline{\text{MS}}}$ at leading order, with uncertainty $\mathscr{O}(\alpha^2_{\overline{\text{MS}}})$, then substitutes it into the quadratic equation, obtaining $\alpha_{\overline{\text{MS}}}$, this time with uncertainty $\mathscr{O}(\alpha^3_{\overline{\text{MS}}})$. This can be iterated order by order in the coupling, and since both methods

give close-to-indistinguishable results, we here report the numerical ones only, found in table 6.3 for different choices of s (for s_{opt} see next sect section). We can see the approach to the asymptotic

	z	s_{opt}	$s=1$	$s=1.5$	$s=2$
R_6/R_8	13.5	0.1784(40)	0.1749(38)	0.1553(30)	0.1443(26)
	9	0.1989(29)	0.1945(27)	0.1705(21)	0.1575(18)
	6	0.2287(25)	0.2228(24)	0.1918(17)	0.1756(15)
	4.5	0.2650(32)	0.2569(30)	0.2164(21)	0.1963(17)
	3	0.3368(49)	0.3234(45)	0.2613(29)	0.2331(23)
R_8/R_{10}	13.5	0.1820(21)	0.1680(18)	0.1501(14)	0.1401(12)
	9	0.2078(18)	0.1896(15)	0.1671(11)	0.1550(10)
	6	0.2498(25)	0.2234(20)	0.1929(15)	0.1772(12)
	4.5	0.2925(37)	0.2561(28)	0.2170(20)	0.1976(17)
	3	0.3957(63)	0.3280(41)	0.2667(27)	0.2390(22)

Table 6.3: *Values of the coupling $\alpha_{\overline{\text{MS}}}(\mu_s)$ extracted from R_6/R_8 (upper half) and R_8/R_{10} (lower half) at different heavy quark masses z and values of the the scale parameter s. For s_{opt} see fig. 6.4 and eq. (6.15), numerical values are $s_{opt}=0.94$ for R_6/R_8 and $s_{opt}=0.78$ for R_8/R_{10}. The error contains all possible error sources except, of course, the truncation error, which is what we want to study here, see next section. Also reported the coupling from R_6/R_8 at $z=13.5$, for completeness, although in that case we were not able to reliably extrapolate to the continuum.*

scaling region as z grows, thanks to QCD's asymptotic freedom. Also, there seems to be an increase in precision (also the relative one) as s grows, but note this only reflects a rearrange of terms in different orders, so that the truncated part will actually turn out (see fig. 6.5) to be larger.

6.2.2. Fastest Convergence

The "Fastest Apparent Convergence" (FAC) or "optimal" scale is defined as the value s_{opt} at which the first μ-dependent coefficient is zero. Naming the coefficients appearing in eq. (6.7) $c_i(s) = \tilde{r}_n^{(i+1)}(s)/\tilde{r}_n^{(1)}$, with $i=1,2$, the implicit definition is

$$c_1(s_{\text{opt}}) \overset{\text{def.}}{=} 0 \iff \mu = \mu_{\text{opt}}\,, \tag{6.15}$$

so that in

$$\alpha_{\mathscr{R}_n}(M_{\text{RGI}}) = \alpha_{\overline{\text{MS}}}(\mu_s)\cdot\left(1+c_1(s)\alpha_{\overline{\text{MS}}}(\mu_s)+c_2(s)\alpha^2_{\overline{\text{MS}}}(\mu_s)\right)+\mathscr{O}(\alpha^4)\,, \tag{6.16}$$

α^2 terms disappear, yielding

$$\alpha_{\mathscr{R}_n}(M_{\text{RGI}}) \overset{\alpha\to 0}{\sim} \alpha_{\overline{\text{MS}}}(\mu_{\text{opt}})\cdot\left(1+c_2(s_{\text{opt}})\alpha^2_{\overline{\text{MS}}}(\mu_{\text{opt}})\right)+\mathscr{O}(\alpha^4)\,. \tag{6.17}$$

For this scale, there is expectation for the spurious μ-dependence introduced in the l.h.s. when estimating it with the perturbative expansion on the r.h.s. to be weaker, since a considerable part of the observable is reabsorbed into the leading term, whereas the higher order terms – suppressed by powers of α – decrease in importance.

(a) *As expected* s_{opt} *is not too far from* $s = 1$ *and higher for* $\mathscr{R}_6$ *than for* $\mathscr{R}_8$.

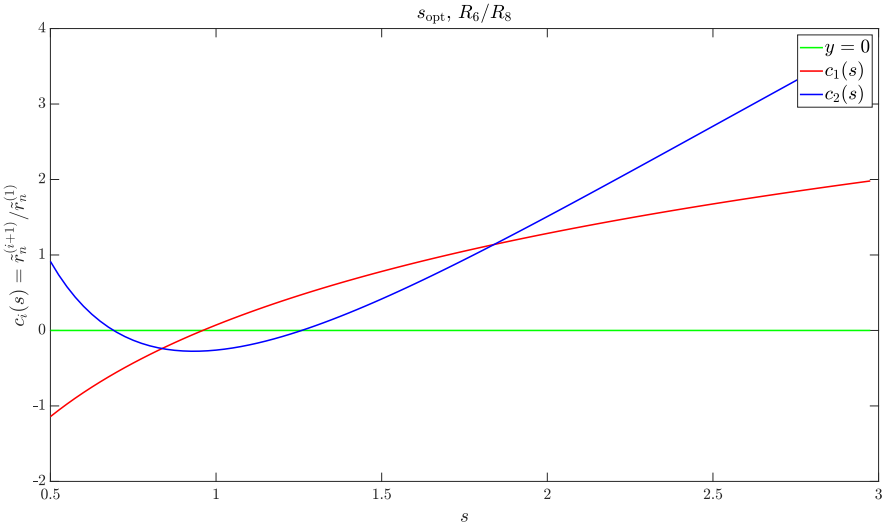

(b) *Here* s_{opt} *is smaller, but still not too far from* $s = 1$*; the overall pattern is very similar, but results more squeezed.*

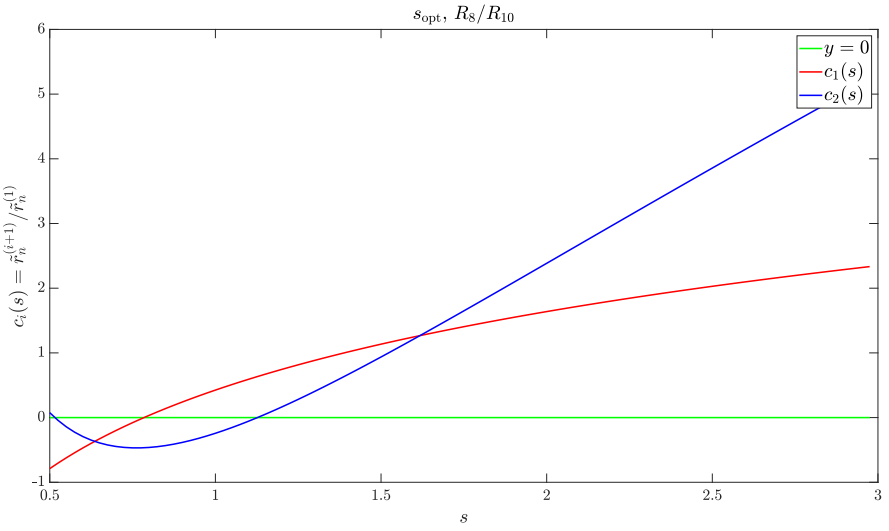

Figure 6.4: *Evolution of coefficients* $c_i(s)$ *in eq. (6.16) with scale factor s. Where the red line crosses 0, in green for visibility,* $s \equiv s_{\text{opt}}$*, at which the second coefficient (blule line) has a global minimum.*

From the above one can easily obtain s_{opt} numerically, as one can see in figs. 6.4a and 6.4b showing $c_1(s)$ and $c_2(s)$ for the two different moments' ratios. We obtain $c_1(s_{\text{opt}}) = 0$ at $s_{\text{opt}} \simeq 1.16$ for $n = 4$, whereas $s_{\text{opt}} \simeq 0.94$ for $\mathscr{R}_6$ and finally $s_{\text{opt}} \simeq 0.78$ for $\mathscr{R}_8$. Also, in all three cases we note this corresponds to a global minimum of $c_2(s_{\text{opt}}) = \min_s[c_2(s)]$.

6.3. EXTRACTING THE Λ-PARAMETER

We start this section by motivating why our results are presented in terms of the Λ_{RGI} parameter. It has become customary to quote the coupling's value at the Z-boson's mass in the $\overline{\text{MS}}$ scheme [165]. As mentioned towards the end of Section 2.5, the Λ_{RGI}-parameter can be *exactly* converted between schemes through a 1-loop computation. This, together with the remarkable 5 loop knowledge of the $\beta_{\overline{\text{MS}}}$ function [83, 106, 105], implies the coupling's uncertainty at the weak scale to be dominated by the ones of the Λ_{RGI}-parameter, so that it has become customary for lattice practitioners to talk in terms of this nonperturbatively defined, renormalization group invariant quantity.

6.3.1. Methodology

To compute the $\Lambda_{\text{RGI}}^{\overline{\text{MS}}}$-parameter, we take the ratio of eq. (2.32) with eq. (2.33), obtaining

$$\frac{\Lambda_{\text{RGI}}^{\overline{\text{MS}}}}{M_{\text{RGI}}} = \frac{\mu}{\overline{m}_{\overline{\text{MS}}}(\mu)} \frac{\left(b_0 \overline{g}^2_{\overline{\text{MS}}}(\mu)\right)^{-b_1/(2b_0^2)}}{\left(2b_0 \overline{g}^2_{\overline{\text{MS}}}(\mu)\right)^{-d_0/(2b_0)}} \times \exp\left\{ -\frac{1}{2b_0 \overline{g}^2_{\overline{\text{MS}}}(\mu)} - \int_0^{\overline{g}_{\overline{\text{MS}}}(\mu)} \mathrm{d}x \left[\frac{1-\tau_{\overline{\text{MS}}}(x)}{\beta_{\overline{\text{MS}}}(x)} + \frac{1}{b_0 x^3} - \frac{b_1}{b_0^2 x} + \frac{d_0}{b_0 x} \right] \right\}, \quad (6.18)$$

where $\beta_{\overline{\text{MS}}}$ and $\tau_{\overline{\text{MS}}}$ are known[II] perturbatively to 5 loops [37, 83] (note, however, if $\beta_{\overline{\text{MS}}}$ to L loops is used, τ to $L-1$ loops is of the same order in the integrand). With the previously introduced rewriting

[II] Note how β here is not defined through α, but rather through the coupling g of the Lagrangian. Latin b_i letters indicate the expansion coefficients in terms of g and greek β_i letters those in terms of α, i.e.

$$\beta(\alpha) = \frac{\mathrm{d}\alpha}{\mathrm{d}\ln m_*^2} = \frac{1}{4\pi}\frac{\mathrm{d}g^2}{\mathrm{d}\ln m_*^2} = \frac{g}{4\pi}\frac{\mathrm{d}g}{\mathrm{d}\ln m_*} = \frac{g}{4\pi}\beta(g) = \frac{1}{4\pi}\left\{-b_0 g^4 - b_1 g^6 - b_2 g^8 + \mathscr{O}\left(g^{10}\right)\right\} \quad (6.19)$$

$$= \frac{1}{4\pi}\left\{-b_0(4\pi\alpha)^2 - b_1(4\pi\alpha)^3 - b_2(4\pi\alpha)^4 + \mathscr{O}\left(g^{10}\right)\right\} = -\beta_0\alpha^2 - \beta_1\alpha^3 - \beta_2\alpha^4 + \mathscr{O}\left(\alpha^5\right), \quad (6.20)$$

so that we obtain $\beta_i = (4\pi)^{i+1} b_i$, for $i \geq 0$, i.e. $\vec{\beta} = [11/4\pi, 102/(4\pi)^2, 2857/(2(4\pi)^3), \ldots]$. We mostly use g in this section and will explicitly write α if it is intended.

of $\mu_s = s\overline{m}_{\overline{\text{MS}}}(\mu_s)$ and in appropriate t_0 units we get

$$\sqrt{8t_0}\Lambda_{\text{RGI}}^{\overline{\text{MS}}} = z\cdot s\cdot \frac{\left(b_0\overline{g}^2_{\overline{\text{MS}}}(\mu_s)\right)^{-b_1/(2b_0^2)}}{\left(2b_0\overline{g}^2_{\overline{\text{MS}}}(\mu_s)\right)^{-d_0/(2b_0)}} \times \exp\left\{-\frac{1}{2b_0\overline{g}^2_{\overline{\text{MS}}}(\mu_s)} - \int_0^{\overline{g}_{\overline{\text{MS}}}(\mu_s)} \mathrm{d}x \left[\frac{1-\tau_{\overline{\text{MS}}}(x)}{\beta_{\overline{\text{MS}}}(x)} + \frac{1}{b_0x^3} - \frac{b_1}{b_0^2x} + \frac{d_0}{b_0x}\right]\right\}. \quad (6.21)$$

The integral is computed numerically as follows: the whole integrand is expanded in a polynomial up to x^5, starting from the asymptotic expression for $\tau_{\overline{\text{MS}}}(x)$ in the numerator, then the one for $\beta_{\overline{\text{MS}}}(x)$ in the denominator, which is further expanded as a geometric series. Thus, one obtains a trivially integrable polynomial, since the divergences are *exactly* canceled by the explicit terms (which, we remind, only depend on universal coefficients). Expanding all of the integrand is a choice that avoids singular integrand terms, whereas keeping $\beta_{\overline{\text{MS}}}(x)$ and $\tau_{\overline{\text{MS}}}(x)$ expanded to all known orders in the ratio and *numerically integrating* may lead to numerical cancellation of the singular terms, which however poses no a-priori problem. We thus straightforwardly evaluate

$$\sqrt{8t_0}\Lambda_{\text{RGI}}^{\overline{\text{MS}}} = z\cdot s\cdot \frac{\left(b_0\overline{g}^2_{\overline{\text{MS}}}(\mu_s)\right)^{-b_1/(2b_0^2)}}{\left(2b_0\overline{g}^2_{\overline{\text{MS}}}(\mu_s)\right)^{-d_0/(2b_0)}} \times \exp\left\{-\frac{1}{2b_0\overline{g}^2_{\overline{\text{MS}}}(\mu_s)} - \frac{p_1}{2}\overline{g}^2_{\overline{\text{MS}}}(\mu_s) - \frac{p_2}{4}\overline{g}^4_{\overline{\text{MS}}}(\mu_s) - \frac{p_3}{6}\overline{g}^6_{\overline{\text{MS}}}(\mu_s)\right\}, \quad (6.22)$$

where the p_i are trivially obtained when expanding β and anomalous dimension and thus depend on higher order, non-universal coefficients of b_i and d_j, with $i \geq 2$ and $j \geq 1$.

Altogether, for each of the 2 observables under scrutiny we obtain values of the $\sqrt{8t_0}\Lambda_{\text{RGI}}^{\overline{\text{MS}}}$ for varying z, s. We now want to check what the truncation error is in this observable, for which we remind its definition eq. (2.32) to be

$$\Lambda_{\text{RGI}} = \mu(b_0\overline{g}^2)^{-b_1/(2b_0^2)}\exp\left\{-\frac{1}{2b_0\overline{g}^2} - \int_0^{\overline{g}}\mathrm{d}x\left[\frac{1}{\beta(x)} + \frac{1}{b_0x^3} - \frac{b_1}{b_0^2x}\right]\right\}. \quad (6.23)$$

From this equation we can see the sensitivity of Λ_{RGI} on the coupling is given by its leading divergent contribution for $\overline{g}\to 0$. The truncation uncertainty $\Delta_T(\alpha_{\overline{\text{MS}}}) = \mathscr{O}\left(\alpha^4_{\overline{\text{MS}}}\right)$ of eq. (6.13) in $\mathscr{R}_n$ implies, at leading order, and together with[III]

[III] To obtain eq. (6.26) one can simply take the differential RGE

$$\mathrm{d}\log\mu = \frac{\mathrm{d}\overline{g}}{\beta(\overline{g})} \xrightarrow{\int} \log\frac{\Lambda^\epsilon}{\mu} = -\int_\varepsilon^{\overline{g}}\frac{\mathrm{d}x}{\beta(x)} \xrightarrow{\mathrm{d}/\mathrm{d}\overline{g}^2} \frac{\mathrm{d}}{\mathrm{d}\overline{g}^2}\frac{\Lambda^\epsilon}{\mu} = \exp\left\{-\int_\varepsilon^{\overline{g}}\frac{\mathrm{d}x}{\beta(x)}\right\}\cdot\frac{(-1)}{2\overline{g}\beta(\overline{g})}, \quad (6.24)$$

where we trivially used Leibniz's integral rule, i.e.

$$\frac{\mathrm{d}}{\mathrm{d}c}\int_{a(c)}^{b(c)}\mathrm{d}t\, f(t,c) = \frac{\mathrm{d}b}{\mathrm{d}c}f(b,c) - \frac{\mathrm{d}a}{\mathrm{d}c}f(a,c) + \int_{a(c)}^{b(c)}\frac{\partial f(t,c)}{\partial c}\mathrm{d}t. \quad (6.25)$$

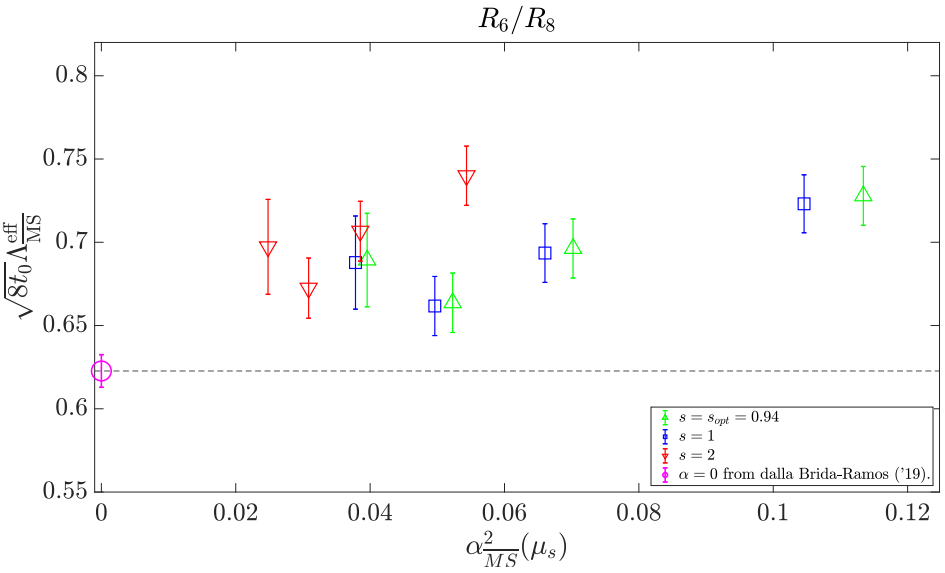

Figure 6.5: *Values for $\Lambda_{\overline{\text{MS}}}$ as a function of $\alpha^2_{\overline{\text{MS}}}$, both as extracted from moment R_6/R_8, for several values of s.*

$$\frac{\mathrm{d}}{\mathrm{d}\alpha^2_{\overline{\text{MS}}}}\left(\frac{\Lambda}{\mu}\right) \sim \frac{1}{\alpha^2_{\overline{\text{MS}}}} + \dots , \tag{6.26}$$

an asymptotic scaling of Λ_{RGI} as

$$\Delta_T(\Lambda) = \frac{\mathrm{d}}{\mathrm{d}\alpha_{\overline{\text{MS}}}}\left(\frac{\Lambda}{\mu}\right)\Delta_T\left(\alpha_{\overline{\text{MS}}}\right) = \frac{k}{\alpha^2_{\overline{\text{MS}}}}\alpha^4_{\overline{\text{MS}}}\left(1+\mathscr{O}\left(\alpha_{\overline{\text{MS}}}\right)\right) \implies \Lambda^{\text{eff}}_{\overline{\text{MS}}} = \Lambda_{\overline{\text{MS}}} + \mathscr{O}\left(\alpha^2_{\overline{\text{MS}}}\right), \tag{6.27}$$

for some unknown constant k and where we label the extracted Λ_{RGI}-parameter with "eff", indicating "effective". Note that k is the prefactor of the $\alpha^2_{\overline{\text{MS}}}$ term only, beyond which many more contributions may be present – depending on the energy scale – up and foremost those of higher order in $\alpha_{\overline{\text{MS}}}$, but also power corrections (sometimes referred to as non-perturbative corrections, although a clear and rigorous separation of perturbative and non-perturbative is not achievable).

6.3.2. Results

We thus plot the extracted Λ_{RGI} vs. $\alpha^2_{\overline{\text{MS}}}(\mu_s)$, where both have been obtained from the moments' ratios under scrutiny, in figs. 6.5 and 6.6. We do so for three different choices of s and we also plot the result by [47], valid for $\alpha = 0$.

First, we start by noticing the truncated part to be quite large at a considerably high energy scale. The data does point towards values of $\Lambda_{\overline{\text{MS}}}$ known from other studies, but with a far-from-flat behavior. As expected, higher moments have a larger deviation w.r.t. the asymptotic $\alpha \to 0$ value, but they can rely on more precise lattice results – this is nothing more than the statement of the window problem we are dealing with.

Then, we note some variation with s is present, yet it is not large enough to account for the scaling

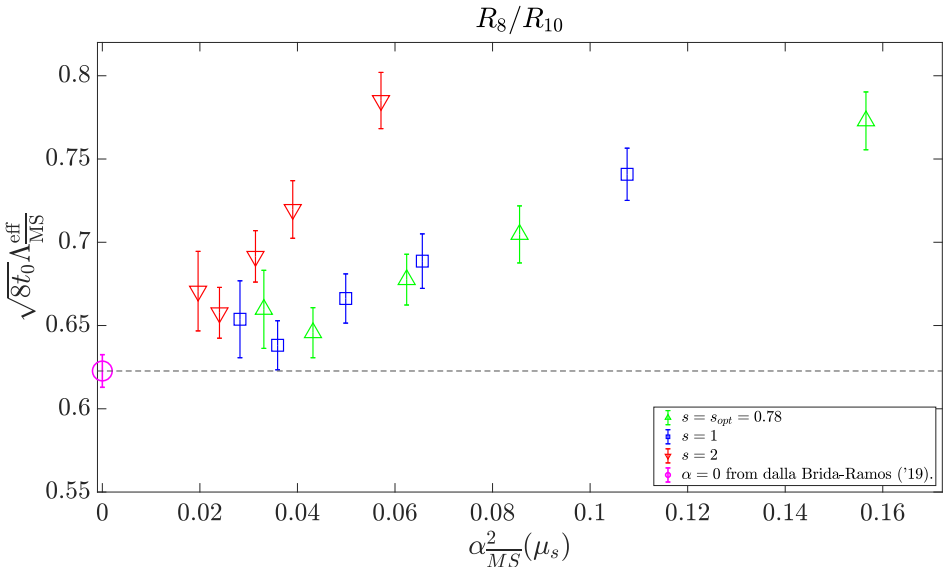

Figure 6.6: *Values for $\Lambda_{\overline{\text{MS}}}$ as a function of $\alpha^2_{\overline{\text{MS}}}$, both as extracted from moment R_8/R_{10}, for several values of s.*

violations. Looking closely at $\Lambda^{\text{eff}}_{\overline{\text{MS}}}$ for equal values of z (or heavy quark mass), e.g. taking the rightmost point of each color, one can notice varying s changes $\Lambda^{\text{eff}}_{\overline{\text{MS}}}$ a little bit, but really does not account for the large distance $\Lambda^{\text{eff}}_{\overline{\text{MS}}} - \Lambda_{\overline{\text{MS}}}$. Since a difference between $s = 1$ and s_{opt} is almost absent, for what follows we decide to use the results at $s = 1$.

We try to fit linearly in α^2 and to extrapolate to $\alpha \to 0$. We do so keeping track of all correlations that are present between our different data points. We fit like

$$f(\alpha^2) = d_0 + d_1\alpha^2\,, \tag{6.28}$$

and also try to fit the quadratic term only, setting the constant term to the result by [47], as can be seen in fig. 6.7. Already by naked eye one may think a fit cubic in $\alpha_{\overline{\text{MS}}}$ to be problematic, nonetheless we try it obtaining close to indistinguishable extrapolated values, so that we only report the former. The constrained quadratic fit agrees very well with the unconstrained one, giving reassurance about the α^2-scaling Ansatz as well as supporting evidence of overall consistency. We also plot a dashed, purple vertical line at the energy scale of twice the charm quark mass as a reference.

Considering the fits in figs. 6.7a and 6.7b, with functional form

$$\sqrt{8t_0}\Lambda^{\text{eff}}_{\overline{\text{MS}}}(\alpha) = \sqrt{8t_0}\Lambda_{\overline{\text{MS}}} + d_1\alpha^2\,, \tag{6.29}$$

we report the results

$$[\sqrt{8t_0}\Lambda_{\overline{\text{MS}}}, d_1] = \begin{cases} [0.6332(246), 0.85(23)]\,, & R_6/R_8\,, \quad \text{range } \alpha^2 \in [0.0378, 0.105] \\ [0.6003(165), 1.31(17)]\,, & R_8/R_{10}\,, \quad \text{range } \alpha^2 \in [0.0282, 0.108] \end{cases}\,. \tag{6.30}$$

The values of d_1 reflect the expectation of a smaller effect of the truncation error for lower moments,

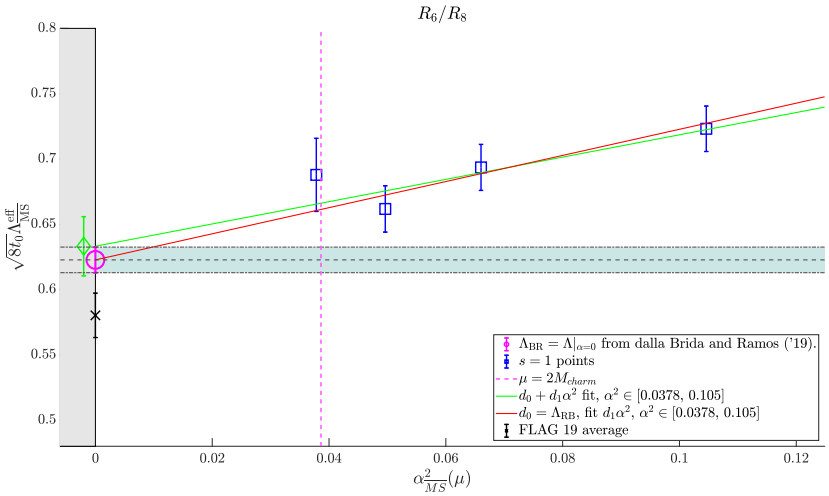

(a) *Fit for $\Lambda_{\overline{\rm MS}}$ as a function of $\alpha^2_{\overline{\rm MS}}$, compared with a fit constrained to pass through $\Lambda_{\rm BR}$ of [47], extracted from R_6/R_8.*

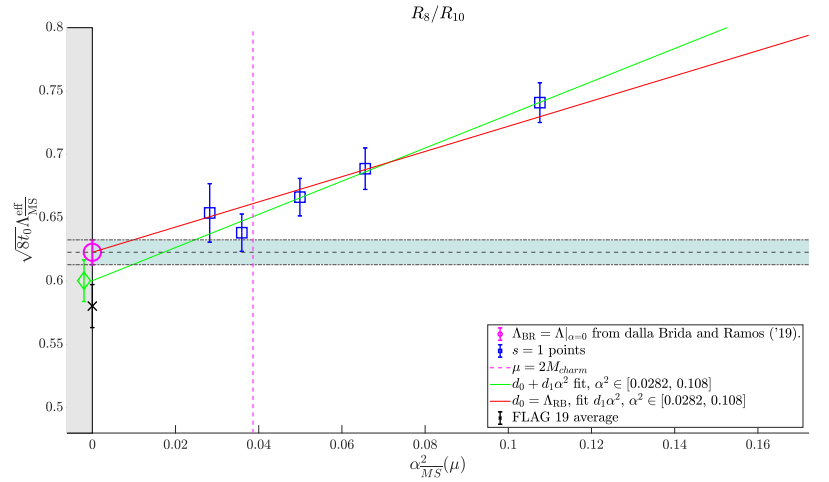

(b) *Fit for $\Lambda_{\overline{\rm MS}}$ as a function of $\alpha^2_{\overline{\rm MS}}$, compared with a fit constrained to pass through $\Lambda_{\rm BR}$ of [47], extracted from R_8/R_{10}.*

Figure 6.7: *Main result of this thesis, namely violations to the asymptotic scaling with $\alpha_{\overline{\rm MS}}$ in the $\Lambda_{\overline{\rm MS}}$ parameter for the two main observables studied, built with appropriate ratios of moments. Plotted against $\alpha^2_{\overline{\rm MS}}$, see eq. (6.27). Also reported, the older FLAG19 [5, 92, 96, 27, 72, 35] average of the quenched Λ-parameter, which does not contain the very precise result in [47], with which there is some tension.*

although not being able to include the result at highest energy ($z = 13.5, M/M_c \simeq 3.5$) results in a larger uncertainty in d_1. However, it is important to stress once more that the above fit *does not include* (and it is hard to believe it could do so with an acceptable sensitivity) the aforementioned higher order terms in α and power corrections, introduced in eq. (1.17) and eq. (1.16) and which are present. Once this caveat about extrapolations and functional form is understood, we still see the fit parameters as an important result, since as an interpolation they can be used to estimate truncation error at a given value of α. A full account of the results in figs. 6.5 and 6.6 in a table analogue to the one for α (table 6.3) can be found in table 6.4.

	z	s_{opt}	$s = 1$	$s = 1.5$	$s = 2$
R_6/R_8	13.5	0.7471(40)	0.7458(38)	0.7450(30)	0.7548(26)
	9	0.6893(29)	0.6878(27)	0.6868(21)	0.6973(18)
	6	0.6637(25)	0.6617(24)	0.6603(17)	0.6724(15)
	4.5	0.6963(32)	0.6935(30)	0.6914(21)	0.7067(17)
	3	0.7279(49)	0.7231(45)	0.7191(29)	0.7400(23)
R_8/R_{10}	13.5	0.6597(21)	0.6538(18)	0.6575(14)	0.6707(12)
	9	0.6457(18)	0.6381(15)	0.6425(11)	0.6576(10)
	6	0.6776(25)	0.6662(20)	0.6719(15)	0.6915(12)
	4.5	0.7047(37)	0.6887(28)	0.6957(20)	0.7197(17)
	3	0.7729(63)	0.7408(41)	0.7510(27)	0.7851(22)

Table 6.4: *Values of $\Lambda^{eff}_{\overline{\text{MS}}}$ extracted from R_6/R_8 (upper half) and R_8/R_{10} (lower half) for varying heavy quark masses z and scale parameter s (for s_{opt} see eq. (6.15)). Also reported the result from R_6/R_8 at $z = 13.5$, for completeness, although in that case we were not able to reliably extrapolate to the continuum.*

Finally, we report our full error budget for $\Lambda_{\overline{\text{MS}}}$ computed from the two observables in fig. 6.8. As expected the smallest lattice spacing is key to the overall precision and estimating all possible effects tied to it is of utmost importance to obtain better results. Note that t_0 for `sft7` is distinguished as far as it had to be computed separately, while t_0 at lower β is included in the ensembles themselves. However, we also point out that a larger area in the pie chart does not necessarily mean the corresponding error source to be large, on the contrary: a very precise result on, say, `sft7` will have a large weight in continuum extrapolations and will thus dominate the error budget.

As a final remark, let us mention this error budget should by no means overshadow the key message that is being stated, namely that *the truncation of the perturbative series is a large and hard-to-estimate systematic effect. In our quenched computation with a really small lattice spacing of $a \simeq 0.01$ fm, unreachable otherwise, the largest error one needs to be aware of when trying to extract QCD parameters with moments of heavy quark correlators appears to be the truncation*. This point is especially important to keep in mind when thinking about the future usage of this method with dynamical quark flavors: *simply decreasing further the lattice spacing (by the reasonable amount to be expected within the close future) will not suffice to improve the precision of the results while having truly all systematic errors under control.*

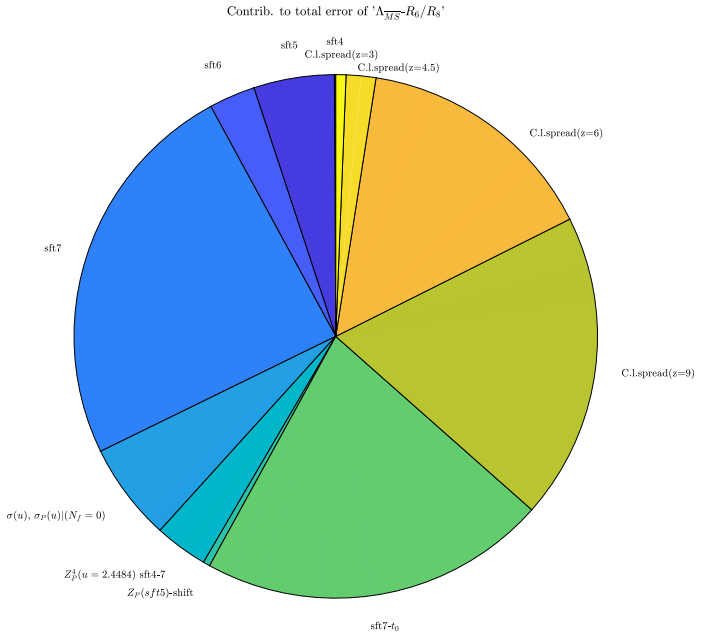

(a) *Case R_6/R_8, given the observable to be dominated by shorter distances the extra systematic error we assigned to the continuum limit has a bigger role here.*

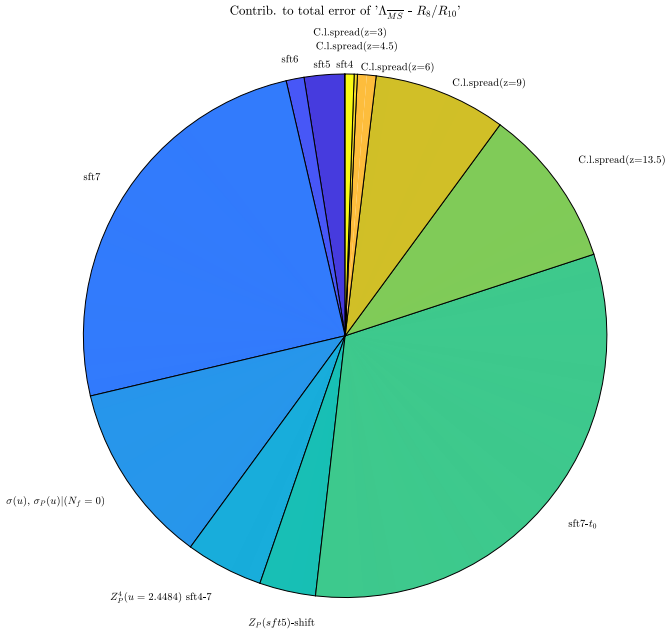

(b) *For R_8/R_{10} there is clear dominance of the statistical error of the smallest lattice spacing together with the precise evaluation therein of t_0/a^2.*

Figure 6.8: *Error budget of the extracted $\Lambda_{\overline{\text{MS}}}$ parameter with linear fit in $\alpha^2_{\overline{\text{MS}}}$ (truncation error excluded, of course). The area is proportional to the partial squared error of each source. "C.l.spread" indicates the extra error obtained when taking the spread of continuum extrapolations, see eq. (6.5), $Z_P(sft5)-$shift is due to the discrepancy between eq. (5.17) and eq. (5.18), see also green and red point in fig. 5.3, and σ is the running error.*

6.3.3. Comparison to $N_f = 3$ Computations

We here want to remind the reader the discussion around eq. (4.7), where it was explained how the fully quenched model can arguably give a not only qualitative, but also quantitative insight into the truncation errors of $N_f = 3, 4$ studies. Here it becomes interesting to carry out a short comparison with some studies present in the literature.

The only computation that permits a direct comparison with our results, since to the best of our knowledge *only therein moments have been computed for a range of energies*, is [137], with its update [138], done with $N_f = 3$ HISQ- staggered quarks [61]. Direct comparison here really means commenting their methodology as compared to ours, where it should be noted due to their dynamical flavors they are restricted to a lower a^{-1} value which then leads them to parameterize cutoff effects in complicated ways, leaving more space for uncontrolled continuum extrapolations. Results for $\Lambda_{\overline{\text{MS}}}$ are extracted from R_4 without addressing the issue of $\log a$ [77, 43] corrections to scaling discussed in Subsection 6.1.1. Moreover, whether topological freezing did play a role in their computations remains unclear.

In any case, the information at multiple energies is then not used for computing Λ_{RGI} through an extrapolation, but rather the truncation error is estimated by supposing the first unknown coefficient 5 times larger than the last known one [137] and adding this error source in quadrature to the others. The quoted final result (blue band of fig. 6.9) is then a weighted average of values obtained at different s and different heavy quark mass, the error bar chosen in order to contain all central values.

In fig. 6.9 we also plot the value by the ALPHA Collaboration [31] in red and a subset of the points of [138], those at $s = 1$ (or $\mu/m_h = 1$ in the notation of the paper). The two values, all in all, agree quite well. It is clear, however, that if the points were to be computed more precisely and the error bars to decrease, the overall situation could easily change. In any case, an average of results at different s and heavy quark mass is theoretically not well motivated.

For completeness, we only quote results and strategies used by other collaborations utilizing moments: [3, 36] introduce Bayesian priors in the analysis, while [126] (as well as [23, 24], which do not produce lattice results themselves, but rather do an analysis of the ones present in literature) mostly rely on varying the scale s.

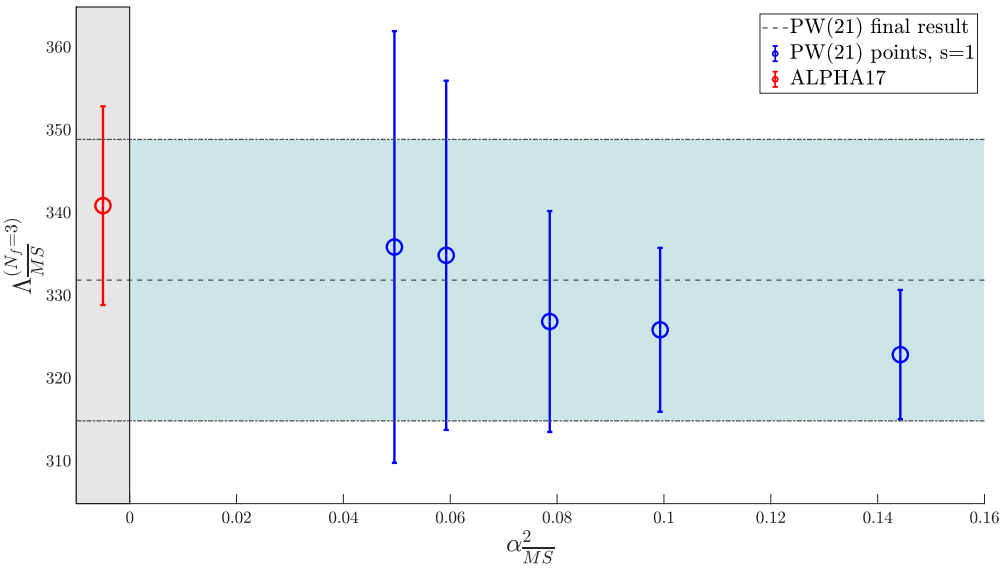

Figure 6.9: *$N_f = 3$ results at $s = 1$ by [138] (in blue) at different values of α, compared to the $\alpha \to 0$ result (in red) by the ALPHA Collaboration [31]. For more information, see text.*

7 | Conclusions

In this work, we have thoroughly studied the behavior of the perturbative, weak coupling expansion of moments of heavy quark correlators within QCD. In order to reliably extrapolate lattice observables to the continuum, $N_f = 0$ dynamical quark flavors (the so-called quenched theory) were employed and lattice spacings down to $a \simeq 0.01\,\text{fm}$ were simulated, a size not attainable for this kind of observable in fully dynamical QCD. With eq. (4.7) we argued why this is a good indicator of what happens in real QCD, namely because the largest effect of the coupling's running is due to purely gluonic effects.

From appropriate ratios of moments with $n = 6, 8, 10$, defined in eq. (3.64), we computed the strong coupling by inversion of their perturbative expansion known to 4 loops in perturbation theory [121]. This was done for a range of scales from slightly below the mass of the charm all the way to above 3 times the charm mass, thus obtaining the running of the quenched coupling $\alpha_{\overline{\text{MS}}}(\mu)$ over a factor 4 in energy μ.

Our goal was to study the unavoidably present $\mathcal{O}(\alpha_{\overline{\text{MS}}}^4)$ truncation uncertainty and its effect in the determination of the coupling through moments. Since most of the error in $\alpha_{\overline{\text{MS}}}(M_Z)$ comes from $\Lambda_{\overline{\text{MS}}}$, we looked at its leftover dependence on $\alpha_{\overline{\text{MS}}}$ due to unknown higher terms, the *leading* one being $\mathcal{O}(\alpha_{\overline{\text{MS}}}^2)$. One should not erroneously think of the main result of the present work being d_1 in eq. (6.29), as though it represented the unknown higher order coefficient. As already stressed, in our computation of d_1 higher order terms and power corrections are neglected. We rather see the distance of our points $(\alpha_{\overline{\text{MS}}}, \Lambda_{\overline{\text{MS}}}^{\text{eff}})$ in figs. 6.5 to 6.7 to the known $\Lambda_{\overline{\text{MS}}}$ values, or ignoring previous knowledge, simply the non-trivial slope of our points as $\alpha_{\overline{\text{MS}}}$ varies, as the main findings.

Moments of heavy quark correlators seem to be an observable where higher order coefficients of the perturbative expansion are important at the heavy flavor energy scale and we urge some caution when using this method and trying to extract the coupling from this observable. These aspects are reflected in the large cutoff effects we observe, showing a hard-to-tackle window problem for a concurrent use of perturbative and lattice results. Estimates of the truncation error could be better estimated by variation of the mass scale and subsequent extrapolations, rather than with coefficient guesswork or by varying the perturbative scale (what we called the scale factor s).

Unfortunately, this study does not really help with the $\Lambda_{\overline{\text{MS}}}^{(0)}$ discrepancy discussed in FLAG 21 [6]. This is especially disappointing at a time where renewed interest in precision results for it are mounting due to ALPHA's decoupling project [50, 48, 49], which requires $\Lambda_{\overline{\text{MS}}}^{(0)}$ as an important ingredient.

As a byproduct of this project, a study of logarithmic contributions in the small t region of integrated lattice observables – precisely speaking, of two point functions $G(t)$ with kernel $K(t)$, such that $G(t)K(t) \sim t$ for small t – has been initiated [77, 43], with possible applications to high precision lattice computations of the muon $g-2$ and to smoothed spectral functions.

In general, as a closing remark, one should not forget the asymptotic nature of perturbative expansions, which entails both its applicability domain and the estimation of truncated pieces. Guessing the size of coefficients should not be customary in nowadays realm of precision physics. Whether at a given energy one is in the asymptotic regime or not should be verified by varying the *physical* scale – not to be confused with the perturbative concept of a renormalization scale – *rather than be assumed*. In fig. 6.7 we have been able to vary the scale μ and thus $\alpha_{\overline{\rm MS}}(\mu)$ in a significant range. In this way, we have verified the size of the truncation directly, finding it to be considerable and larger than claimed in other studies.

We remind the reader once more that strictly speaking this statement holds for $N_f = 0$. On the other hand, for $N_f > 0$ the natural assumption is a quantitative, but not qualitative change. Whether in that case the situation is improved and, if so, by how much, needs to be shown along the lines of our $N_f = 0$ investigation.

APPENDIX A

SYMANZIK IMPROVEMENT

In this appendix we concisely explain some topics related to Symanzik improvement [155, 156] for completeness. Whenever we consider an explicit form of some lattice correlator $G(t,a) = \langle O_1(x)O_2(0)\rangle$, it is important to realize it has to reproduce its continuum counterpart for $a \to 0$. However, at $a > 0$, a whole variety of choices in the discretization, of both action and operators O_i appearing in G, are possible. In statistical field theory language, one can add "irrelevant" (in the sense of higher dimensional), local operators which change the continuum approach of lattice correlators as $a \to 0$, with the goal of speeding this limit up and thus gaining in precision (or in simulation time).

In Subsection 6.1.1 we mentioned the effective field theory (EFT) point of view can be taken to study cutoff effects present in a given correlator for some action choice. One may imagine the energy cutoff a^{-1} as a scale for some new, unknown physics of which continuum QCD is a low energy EFT. In this framework one may then describe the physics at a scale $E \ll a^{-1}$ (i.e. towards the continuum limit) through EFT methods, for instance by adding to the Lagrangian operators of mass dimension 5 with the correct lattice symmetries and with an extra a factor in front of them. Turning this around, one may imagine to add appropriately tuned counter-terms to the action in order to *avoid* the presence of cutoff effects at a given order in a, where the needed coefficients can be computed in lattice perturbation theory or through non-perturbative methods, being functions of the bare coupling g_0.

Below we briefly sketch some ideas and results in the case of Wilson fermions and then move on to twisted mass and its much celebrated automatic $\mathcal{O}(a)$-improvement, which we rely a lot on in this work.

A.1. THE CLOVER TERM

Let us remind here the explicit form of the Wilson fermion action eq. (3.18)

$$\mathcal{S}_F = a^4 \sum_x \overline{\Psi}(x) \left\{ \sum_{\nu=0}^{3} \left(\gamma_\nu \frac{\nabla_\nu + \nabla_\nu^*}{2} - \frac{a}{2} \nabla_\nu^* \nabla_\nu \right) + \mathbb{M} \right\} \Psi(x)\,, \tag{A.1}$$

from which we start. To understand why in the improved action eq. (3.45) (apart from the twisted mass term, to be discussed later) only one term is present, namely the *clover* or Sheikholeslami-Wohlert

term, the strategy (which we only illustrate and state results of) entails:

1. Enumerating a basis of continuum, higher dimensional operators $\{\mathscr{B}_i\}$ with the correct lattice symmetries.
2. Reducing this basis through field equations.
3. Carrying out a further reduction by reabsorbing some operators in already present parts through a redefinition of couplings.
4. Finally, one needs to choose a specific discretization of these operators, which will in turn introduce lattice effects, but which only affect higher orders in a.

After some computations, for 1 one arrives at

$$\mathscr{B}_1(x) = i\,\overline{\psi}(x)\sigma_{\mu\nu}F_{\mu\nu}(x)\psi(x)\,, \quad \sigma_{\mu\nu} = \frac{i}{2}\left[\gamma_\mu,\gamma_\nu\right]\,, \tag{A.2}$$

$$\mathscr{B}_2(x) = \overline{\psi}(x)D_\mu D_\mu\psi(x) + \overline{\psi}(x)\overleftarrow{D}_\mu\overleftarrow{D}_\mu\psi(x)\,, \tag{A.3}$$

$$\mathscr{B}_3(x) = m\,\overline{\psi}(x)\,\mathrm{tr}\{F_{\mu\nu}(x)F_{\mu\nu}\}(x)\,, \tag{A.4}$$

$$\mathscr{B}_4(x) = m\left\{\overline{\psi}(x)\gamma_\mu D_\mu\psi(x) - \overline{\psi}(x)\overleftarrow{D}_\mu\gamma_\mu\psi(x)\right\}\,, \tag{A.5}$$

$$\mathscr{B}_5(x) = m^2\,\overline{\psi}(x)\psi(x)\,, \tag{A.6}$$

which can further be reduced. Employing the following equations of motions (i.e. point 2), valid at tree-level in perturbation theory (but which can be generalized), one obtains

$$\mathscr{B}_1 - \mathscr{B}_2 + 2\mathscr{B}_5 = 0\,, \quad \mathscr{B}_4 + 2\mathscr{B}_5 = 0\,, \tag{A.7}$$

which leaves us with $\mathscr{B}_i$, $i = 1,3,5$. In Section 3 of [104], to which we refer to, it is shown in detail how $\mathscr{B}_3$ and $\mathscr{B}_5$ can be reabsorbed appropriately, respectively, in the pure gauge and in the fermion mass terms (point 3). We are now only left with the Pauli term eq. (A.2), which is the clover term once an appropriate lattice (point 4) choice $\hat{F}_{\mu\nu}$ of the field strength tensor is given. We follow the notation in [104], i.e.

$$\hat{F}_{\mu\nu}(x) = \frac{1}{8a^2}\left\{Q_{\mu\nu}(x) - Q_{\nu\mu}(x)\right\}\,, \tag{A.8}$$

$$\begin{aligned} Q_{\mu\nu}(x) = {} & U(x,\mu)U(x+a\hat{\mu},\nu)U^{-1}(x+a\hat{\nu},\mu)U^{-1}(x,\nu) \\ & + U(x,\nu)U^{-1}(x-a\hat{\mu}+a\hat{\nu},\mu)U^{-1}(x-a\hat{\mu},\nu)U(x-a\hat{\mu},\mu) \\ & + U^{-1}(x-a\hat{\mu},\mu)U^{-1}(x-a\hat{\mu}-a\hat{\nu},\nu)U(x-a\hat{\mu}-a\hat{\nu},\mu)U(x-a\hat{\nu},\nu) \\ & + U^{-1}(x-a\hat{\nu},\nu)U(x-a\hat{\nu},\mu)U(x+a\hat{\mu}-a\hat{\nu},\nu)U^{-1}(x,\mu)\,. \end{aligned} \tag{A.9}$$

A.2. AUTOMATIC $\mathscr{O}(a)$ IMPROVEMENT

In this appendix we briefly discuss a key feature of maximal twist, namely the presence of a finite transformation $\mathscr{P}_{\mu_{\mathrm{tm}}} \subset SU(2)_A$ which has the property $\mathscr{P}^2_{\mu_{\mathrm{tm}}} = \mathbb{1}$, so that an associated parity exists.

Operators can have a well defined $\mathscr{P}_{\mu_{\rm tm}}$ - parity and interestingly $\mathscr{P}_{\mu_{\rm tm}}$ - even (odd) fields are free from $\mathcal{O}(a^{2k+1})$ effects ($\mathcal{O}(a^{2k})$ effects), meaning even fields are *automatically* $\mathcal{O}(a)$*-improved* [62] whereas odd fields are a pure cutoff effect, i.e. their continuum limit vanishes.

We will not derive this property here, for which we refer the interested reader to the original literature or to two excellent reviews [62, 150, 149]. Rather, we will show here what the $\mathscr{P}_{\mu_{\rm tm}}$ symmetry of correlators used in the present work is. We studied 2-point functions of quark bilinears with fixed flavor assignment, i.e.

$$\mathcal{O}^{PP} = P^{\pm}(x)P^{\mp}(y)\,, \quad \text{and} \quad \mathcal{O}^{AP} = \partial_\mu A_\mu^{\pm}(x)P^{\mp}(y)\,, \tag{A.10}$$

where $P^{\pm}(x) = P^1(x) \pm iP^2(x)$ and $P^c(x) = \overline{\chi}(x)\gamma_5\frac{\tau^c}{2}\chi(x)$, with τ^c referring to the Pauli matrices. Applying $\mathscr{P}_{\mu_{\rm tm}}$ on twisted field doublets $\chi^T = (h, h')$ amounts to

$$\mathscr{P}_{\mu_{\rm tm}} : \begin{cases} \chi & \longrightarrow i\gamma_5\tau_1\chi \\ \overline{\chi} & \longrightarrow \overline{\chi}i\gamma_5\tau_1 \end{cases}. \tag{A.11}$$

If an operator $\mathcal{O}$ is even w.r.t. the $\mathscr{P}_{\mu_{\rm tm}} = i\gamma_5\tau_1$ parity it can be shown that $\delta\mathcal{O} = 0$, i.e. the field is automatically "$\mathcal{O}(a)$-improved" in the sense that its expectation value on the lattice will have discretization effects starting from $\mathcal{O}(a^2)$.

The expectation value of $\mathcal{O}^{PP}$, used to compute moments, will turn out being automatically $\mathcal{O}(a)$-improved, whereas $\mathcal{O}^{AP}$ present in m_{PCAC} and used to monitor the maximal twist condition, will be shown to be a pure $\mathcal{O}(a)$-effect.

Simplifying notation by dropping momentarily spacetime dependence we have for the pseudoscalar

$$P^{\pm} = \overline{\chi}\gamma_5\frac{\tau_1 \pm i\tau_2}{2}\chi \longrightarrow \overline{\chi}i\gamma_5\tau_1\frac{\tau_1 \pm i\tau_2}{2}\gamma_5 i\gamma_5\tau_1\chi = \frac{-1}{2}\overline{\chi}\gamma_5(\tau_1 \pm i\tau_1\tau_2\tau_1)\chi\,, \tag{A.12}$$

and using trivial properties of the Pauli matrices one can obtain

$$\mathscr{P}_{\mu_{\rm tm}}\left[P^{\pm}\right] = -P^{\mp}\,, \tag{A.13}$$

which for the PS-PS operator yields

$$\mathscr{P}_{\mu_{\rm tm}}\left[P^{\pm}(x)P^{\mp}(y)\right] = P^{\mp}(x)P^{\pm}(y) \equiv P^{\pm}(x)P^{\mp}(y)[h \leftrightarrow h'] \equiv P^{\pm}(x)P^{\mp}(y)[\mu_{\rm tm} \to -\mu_{\rm tm}]\,, \tag{A.14}$$

where the dependence on $\mu_{\rm tm}$ is everywhere quadratic and we thus re-obtain the 2-point function we started with.

For the axial vector current's "four-divergence" we similarly obtain

$$\mathscr{P}_{\mu_{\rm tm}}\left[A_\mu^{\pm}\right] = A_\mu^{\pm} \pm (A_\mu^{-} - A_\mu^{+}) = A_\mu^{\mp}\,, \tag{A.15}$$

which for the A-PS operator $\mathcal{O}^{AP}$ means

$$\mathscr{P}_{\mu_{\rm tm}}\left[\partial_\mu A_\mu^{\pm}(x)P^{\mp}(y)\right] = -\partial_\mu A_\mu^{\mp}(x)P^{\pm}(y) \equiv -\partial_\mu A_\mu^{\pm}(x)P^{\mp}(y)[\mu_{\rm tm}\to-\mu_{\rm tm}]\,, \tag{A.16}$$

thus showing the PCAC mass, build of the above operators, to be an $\mathcal{O}(a)$ effect.

This, of course, should not lead to believe automatic $\mathcal{O}(a)$-improvement might be spoiled, since

$$\underbrace{\left\langle \partial_\mu A_\mu^a(x)\,\mathcal{O}_{\rm even}(y)\right\rangle}_{\mathcal{O}(a^2)} = \underbrace{m_{PCAC}}_{\mathcal{O}(a)}\underbrace{\left\langle P^a(x)\,\mathcal{O}_{\rm even}(y)\right\rangle}_{\mathcal{O}(a)}, \tag{A.17}$$

which clearly shows m_{PCAC}'s leading scaling to be linear, as we showed in figs. 5.6 to 5.8, D.8 and D.9 and discussed in Subsection 5.5.2.

APPENDIX B

CORRELATION OF Z_P WITH $M_{\mathrm{RGI}}/\overline{m}$

One last points needs a closer look, related to the multiple definitions of Z_P employed throughout the study, and written in eqs. (5.11) to (5.14). We now show that dropping the correlation between $M_{\mathrm{RGI}}/\overline{m}_{SF}(\mu_{\mathrm{ref}})$ and Z_P in eq. (5.26) is a good enough approximation and is thus justified. Too see this, start by

$$\Delta^2\mathscr{R}_n = \left(\frac{\partial\mathscr{R}_n}{\partial\ln z}\right)^2 \sum_{i,j=1}^{3} \left\langle \left.\frac{\partial\ln z}{\partial\ln b_i}\right|_{\mathrm{th}} \Delta\ln b_i \left.\frac{\partial\ln z}{\partial\ln b_j}\right|_{\mathrm{th}} \Delta\ln b_j \right\rangle . \tag{B.1}$$

where $i=1,2,3$ corresponds to $M_{\mathrm{RGI}}/\overline{m}_{SF}$, $\sqrt{t_0}/a$, Z_P^{SF}. Taking the logarithm of z's definition, eq. (5.7), we have up to higher orders in a

$$\log(z) = \log\left(\frac{\sqrt{8t_0}}{a}\right) + \log\left(\frac{M_{\mathrm{RGI}}}{\overline{m}_{SF}(\mu)}\right) - \log\left(Z_P^{SF}(a\mu,\beta)\right) + \log\left(a\mu_{\mathrm{tm}}\right), \tag{B.2}$$

from which it is clear all derivative terms are equal in modulo for all sources of error. So we really want to know whether

$$2\Big\langle \Delta(\log Z_P)\Delta(\log M_{\mathrm{RGI}}/\overline{m}_{SF})\Big\rangle \overset{?}{\ll} \Big\langle \Delta(\log Z_P)\Big\rangle^2 + \Big\langle \Delta\log(M_{\mathrm{RGI}}/\overline{m}_{SF})\Big\rangle^2 . \tag{B.3}$$

From the property[I] of the covariance $|\sigma_{1,2}| \leq \sqrt{\sigma_{1,1}\sigma_{2,2}}$ we can try to find an upper limit to the l.h.s. of eq. (B.3). This inequality is a measure of correlations, its saturation being a signal of strong correlation. Labeling $\log Z_P$ with "1" and $\log(M_{\mathrm{RGI}}/\overline{m}_{SF})$ with "2", we study whether

$$2\sqrt{\sigma_{1,1}\,\sigma_{2,2}} \overset{?}{\ll} \sigma_{1,1} + \sigma_{2,2}\,, \tag{B.4}$$

holds. Remembering $\sqrt{\sigma_{2,2}} \simeq 0.008$ (since we consider logarithms, σ is equal to the relative error) and reporting $\sqrt{\sigma_{1,1}}$ in table B.1 we obtain the results in table B.2. Thus, eq. (B.4) *does not hold*. Still, if the correlation (l.h.s. of eq. (B.3)) is negative, the error would be smaller than what we claim by at most $\sim 25\%$, which we find as acceptable. On the other hand, if it is positive, looking at the last row of table B.2, we would be underestimating the error squared by at most $\sim 40\%$ and the error by

[I] Since we indicate by $\Delta x_i = x_i - \bar{x}_i$, we have $\sigma_{i,j} = \langle (x_i-\bar{x}_i)(x_j-\bar{x}_j)\rangle$.

β	6.1628	6.2885	6.4956	6.7859	7.1146	7.3600	7.700
$\sqrt{\sigma_{1,1}}\,[10^{-3}]$	3.3	4.0	3.3	2.8	1.7	1.8	3.2

Table B.1: *Error on* $\log Z_P^{SF}$*, to be confronted with error on* $M_{RGI}/\overline{m}_{SF}$*.*

β	6.1628	6.2885	6.4956	6.7859	7.1146	7.3600	7.700
$2\sqrt{\sigma_{1,1}\,\sigma_{2,2}}\,[10^{-5}]$	5.2	6.4	5.3	4.4	2.6	2.9	5.1
$\sigma_{1,1}+\sigma_{2,2}\,[10^{-5}]$	7.4	8.0	7.4	7.1	6.6	6.7	7.4
max effect of correlation, in %	41	45	41	38	28	30	41

Table B.2: *Numerical values for the r.h.s. of eq.* (B.3)*, an upper limit for the l.h.s., namely* $|\sigma_{1,2}|$*, and the correlation's share of the total error related to* Z_P *and* $M_{RGI}/\overline{m}$*. For ensembles* $\beta > 6.5$ *only an improbable and unexpectedly strong correlation would impact the error in a significant way.*

$\sim 20\%$ for $\beta > 6.3$, which we also find to be a reasonable approximation, given the overall size of all error sources.

A larger error on Z_P could invalidate the dropping of correlations, but do note *only the error on measured* Z_P values of [35] in eqs. (5.11) to (5.14) is considered in this discussion. Any $s_P(u)$ appearing in $Z_{P,i}$ definitions, which make Z_P's error larger than what we have written in this section for low β, is automatically cross-correlated to $M_{\mathrm{RGI}}/\overline{m}$.

APPENDIX C

TREE LEVEL OF MOMENTS

In this appendix we work out in detail the somewhat lengthy computations regarding the moments' tree-level. All is computed in the time-momentum representation, particularly useful when dealing with lattice computations, and keeping T infinite. In Section C.1 we start with the $L=\infty$, continuum case, then move to continuum moments for $L<\infty$ in order to quantify tree-level finite volume effects (Section C.2).

Afterwards, we move to the finite lattice spacing theory, detailing first (for completeness) in Section C.3 how to obtain the propagator, finally developing in Section C.4 all the steps necessary to obtain the finite a moments at tree-level. We do so first in infinite spatial volume and, to conclude, give the $a>0$ and $L<\infty$ tree-level expression.

C.1. CONTINUUM CALCULATION

Starting from the definition

$$\mathscr{M}_n = \int_{-\infty}^{\infty} \mathrm{d}t\, t^n \int \mathrm{d}^3\vec{x}\, \langle 0|\, \mathscr{T}\left\{J^\dagger(x)J(0)\right\}|0\rangle \tag{C.1}$$

where the current is $J(x)=im_h\overline{h}(x)\gamma_5 h'(x)$, and defining the free quark propagator $S_f^{a,b}(x)$ in time-momentum space explicitly through

$$S_f^{a,b}(x)=\langle \psi_f^a(x)\,\overline{\psi}_f^b(0)\rangle = \int \frac{\mathrm{d}^4p}{(2\pi)^4} e^{ip\cdot x}\widetilde{S}_f^{a,b}(p) = \int \frac{\mathrm{d}^3\vec{p}}{(2\pi)^3}\, e^{i\vec{p}\cdot\vec{x}}\, S_f^{a,b}(t;\vec{p})\,, \tag{C.2}$$

where f identifies the flavor degrees of freedom, while a,b superscripts indicate the color ones. They will be suppressed while discussing continuum computations, and repeated indices will indicate summation with Euclidean metric. *Considering only the tree level* from now on, we want to calculate

$$S(t,\vec{p}) = \int_{-\infty}^{\infty} \frac{\mathrm{d}p_0}{2\pi} \mathrm{e}^{ip_0 t}\, \frac{m_h - i\gamma_\mu p_\mu}{p^2+m_h^2}\,, \tag{C.3}$$

which can be readily evaluated through standard techniques, obtaining

$$S(t;\vec{p}) = \theta(t)\,\frac{e^{-Et}}{2E}\,(m_h+\gamma_0 E - i\vec{p}\cdot\vec{\gamma}) + \theta(-t)\,\frac{e^{+Et}}{2E}\,(m_h-\gamma_0 E - i\vec{p}\cdot\vec{\gamma})\,, \tag{C.4}$$

from which can be seen $\gamma_5 S(-x)\gamma_5 = S^\dagger(x)$.

By representing in Fourier space the spatial part of both $S_(x)$ and $S^\dagger_{h'}(x)$,we have

$$\mathscr{M}_n = m^2\int_{-\infty}^{\infty}\mathrm{d}t\,t^n\int\mathrm{d}^3\vec{x}\,\frac{\mathrm{d}^3\vec{p}}{(2\pi)^3}\frac{\mathrm{d}^3\vec{q}}{(2\pi)^3}e^{i\vec{x}\cdot(\vec{p}-\vec{q})}\,\mathrm{tr}\left\{S(t;\vec{p})\,S^\dagger(t;\vec{q})\right\}. \tag{C.5}$$

Using the integral over space and the exponential we obtain a Dirac-delta $\delta^3(\vec{p}-\vec{q})$, so that we can integrate over $\vec{q}$ and then use the explicit form of (C.4) in order to obtain

$$\begin{aligned}\mathscr{M}_n &= m_h^2\int_{-\infty}^{\infty}\mathrm{d}t\,t^n\int\frac{\mathrm{d}^3\vec{p}}{(2\pi)^3}\,\mathrm{tr}\left\{\theta(t)\frac{e^{-2Et}}{(2E)^2}\left[(m_h+\gamma_0E)^2+\vec{p}^{\,2}\right]\right.\\ &\qquad\left.+\theta(-t)\frac{e^{+2Et}}{(2E)^2}\left[(m_h-\gamma_0E)^2+\vec{p}^{\,2}\right]\right\}\\ &= m_h^2\int_{-\infty}^{\infty}\mathrm{d}t\,t^n\int\frac{\mathrm{d}^3\vec{p}}{(2\pi)^3}\,\mathrm{tr}\left\{\theta(t)\frac{e^{-2Et}}{(2E)^2}\left[m_h^2+E^2+\vec{p}^{\,2}\right]\right.\\ &\qquad\left.+\theta(-t)\frac{e^{+2Et}}{(2E)^2}\left[m_h^2+E^2+\vec{p}^{\,2}\right]\right\},\end{aligned} \tag{C.6}$$

where in the last line we have automatically dropped terms linear in γ due to the trace. This finally leads to

$$\begin{aligned}\mathscr{M}_n &= \frac{m_h^2}{2}\int_{-\infty}^{\infty}\mathrm{d}t\,t^n\int\frac{\mathrm{d}^3\vec{p}}{(2\pi)^3}N_c\,\mathrm{tr}\,\mathbb{1}_4\left(\theta(t)e^{-2Et}+\theta(-t)e^{+2Et}\right)\\ &= 12m_h^2\int_0^{\infty}\mathrm{d}t\,t^n\int\frac{\mathrm{d}^3\vec{p}}{(2\pi)^3}e^{-2Et},\end{aligned} \tag{C.7}$$

as long as n is even. This happens due to the fact that the negative and positive time pieces give exactly the same contribution, as can be seen by mapping $t\to -t$ in the integral over $(-\infty,0)$. Setting $\alpha = 2\sqrt{m_h^2+\vec{p}^{\,2}}$ we obtain

$$\begin{aligned}\mathscr{M}_n &= 12m_h^2\frac{4\pi}{8\pi^3}\int_0^{\infty}p^2\mathrm{d}p\int_0^{\infty}\mathrm{d}t\,t^ne^{-2\alpha t} = \frac{6m_h^2}{\pi^2}\int_0^{\infty}p^2\alpha^{-n-1}\mathrm{d}p\int_0^{\infty}\mathrm{d}(\alpha t)\,(\alpha t)^ne^{-\alpha t}\\ &= 3\frac{m_h^2}{2^n\pi^2}\int_0^{\infty}\frac{p^2}{(p^2+m_h^2)^{(n+1)/2}}\Gamma(n+1)\,\mathrm{d}p\\ &= 3\frac{n!}{2^n}\frac{m_h^2}{\pi^2}\int_0^{\infty}\frac{(p/m_h)^2}{((p/m_h)^2+1)^{(n+1)/2}}m_h^{2+1-n-1}\,\mathrm{d}\left(\frac{p}{m_h}\right)\end{aligned} \tag{C.8}$$

where we change to the variable $u = (p/m_h)^2$ which yields $\mathrm{d}u = 2(p/m_h)\mathrm{d}(p/m_h)$, obtaining

$$\mathscr{M}_n = 3\frac{n!}{2^n}\frac{m_h^{4-n}}{2\pi^2}\int_0^\infty \frac{u^{1/2}}{(1+u)^{(n+1)/2}}\mathrm{d}u\,. \tag{C.9}$$

Remembering the following integral representation of Euler's beta-function

$$\beta(x,y) = \int_0^\infty \mathrm{d}t\, t^{x-1}(1+t)^{-x-y}, \quad \mathrm{Re}(x,y) > 0\,, \tag{C.10}$$

and the basic property relating this special function to Euler's gamma-function

$$\beta(x,y) = \frac{\Gamma(x)\Gamma(y)}{\Gamma(x+y)}\,, \tag{C.11}$$

we obtain

$$\mathscr{M}_n = 3\frac{n!}{2^n}\frac{m_h^{4-n}}{2\pi^2}\frac{\Gamma\left(\frac{3}{2}\right)\Gamma\left(\frac{n-2}{2}\right)}{\Gamma\left(\frac{n+1}{2}\right)}\,. \tag{C.12}$$

C.2. FINITE VOLUME EFFECTS

Taking (C.5) at finite volume, one has

$$\int \mathrm{d}^3\vec{x}\,\frac{\mathrm{d}^3\vec{p}}{(2\pi)^3}\frac{\mathrm{d}^3\vec{q}}{(2\pi)^3}e^{i\vec{x}\cdot(\vec{p}-\vec{q})} \longrightarrow \int_{L^3,\mathrm{pbc}}\mathrm{d}^3\vec{x}\,\frac{1}{L^3}\sum_{\vec{p}}\frac{1}{L^3}\sum_{\vec{q}}e^{i\vec{x}\cdot(\vec{p}-\vec{q})}\,, \tag{C.13}$$

where the periodic boundary conditions (pbc) in space imply moments are discretized (but still countably infinite) like $\vec{p} = \vec{m}2\pi/L$, and likewise for $\vec{q}$. Since

$$\int_{L^3,\mathrm{pbc}}\mathrm{d}^3\vec{x}\,e^{i\vec{x}\cdot(\vec{p}-\vec{q})} = L^3\delta(\vec{p}-\vec{q})\,, \tag{C.14}$$

we obtain an expression analogous to (C.7)

$$\mathscr{M}_n(L) = 12\,m_h^2\int_0^\infty \mathrm{d}t\, t^n\frac{1}{L^3}\sum_{\vec{p}}e^{-2Et}\,, \tag{C.15}$$

where the integral in t is unaffected by the finite volume. We write

$$\Delta\mathscr{M}_n^L = 12m_h^2\frac{\Gamma(n+1)}{2^{n+1}}\left(\frac{1}{L^3}\sum_{\vec{p}} - \int\frac{\mathrm{d}^3\vec{p}}{(2\pi)^3}\right)E(\vec{p})^{-n-1}\,, \quad E(\vec{p}) = \sqrt{\vec{p}^2+m_h^2}\,, \tag{C.16}$$

where $\Delta\mathscr{M}_n^L = \mathscr{M}_n(L) - \mathscr{M}_n(\infty)$. Here one can apply Poisson's summation formula[I] to the sum to recast it as

$$\Delta\mathscr{M}_n^L = 12m_h^2 \frac{\Gamma(n+1)}{2^{n+1}} \sum_{\vec{l}\in\mathbb{N}^3\setminus\vec{0}} \int \frac{\mathrm{d}^3\vec{p}}{(2\pi)^3} \frac{\mathrm{e}^{iL\vec{p}\cdot\vec{l}}}{E(\vec{p})^{n+1}}\,. \tag{C.18}$$

To evaluate the integral, let us use a Scwhinger parametrization

$$\frac{1}{C^\alpha} = \frac{1}{\Gamma(\alpha)} \int_0^\infty \mathrm{d}u\, u^{\alpha-1}\mathrm{e}^{-Cu}\,, \quad C = 1+\vec{p}^{\,2}/m_h^2\,,\ \alpha = (n+1)/2\,, \tag{C.19}$$

so that

$$\Delta\mathscr{M}_n^L = 12m_h^2 \frac{\Gamma(n+1)}{(2m_h)^{n+1}} \sum_{\vec{l}\in\mathbb{N}^3\setminus\vec{0}} \frac{1}{\Gamma(\alpha)} \int_0^\infty \mathrm{d}u\, u^{\alpha-1}\mathrm{e}^{-u} \int \frac{\mathrm{d}^3\vec{p}}{(2\pi)^3} \mathrm{e}^{iL\vec{p}\cdot\vec{l}}\, \mathrm{e}^{-u\vec{p}^{\,2}/m_h^2}\,. \tag{C.20}$$

We can complete the square in the momentum integral to transform it into a Gaussian integral via

$$-u\frac{\vec{p}^{\,2}}{m_h^2} + iL\vec{p}\cdot\vec{l} = -\left(\frac{\sqrt{u}}{m_h}\vec{p} - i\frac{Lm_h\vec{l}}{2\sqrt{u}}\right)^2 - \frac{L^2m_h^2\vec{l}^{\,2}}{4u}\,, \tag{C.21}$$

which gives

$$\Delta\mathscr{M}_n^L = 12m_h^2 \frac{\Gamma(n+1)}{(2m_h)^{n+1}} \sum_{\vec{l}\in\mathbb{N}^3\setminus\vec{0}} \frac{1}{\Gamma(\alpha)} \int_0^\infty \mathrm{d}u\, u^{\alpha-1}\mathrm{e}^{-u}\mathrm{e}^{-\vec{l}^{\,2}m_h^2L^2/4u}u^{-3/2}m_h^3 \int \frac{\mathrm{d}^3\vec{p}}{(2\pi)^3}\mathrm{e}^{\vec{p}^{\,2}} \tag{C.22}$$

$$= \frac{3m_h^{4-n}\Gamma(n+1)}{2^{n+2}\,\pi^{3/2}\Gamma(\frac{n+1}{2})} \sum_{\vec{l}\in\mathbb{N}^3\setminus\vec{0}} \int_0^\infty \mathrm{d}u\, u^{(n-4)/2}\mathrm{e}^{-u-z^2/4u}\,, \quad z = m_hL|\vec{l}\,|\,. \tag{C.23}$$

The integral is a modified Bessel function of second kind, defined as

$$K_\nu(z) = \frac{1}{2}\left(\frac{1}{2}z\right)^\nu \int_0^\infty \mathrm{d}u \exp\left(-u - \frac{z^2}{4u}\right) u^{-\nu-1}\,, \tag{C.24}$$

which for large z has an asymptotic expansion

$$K_\nu(z) \sim \left(\frac{\pi}{2z}\right)^{1/2} \mathrm{e}^{-z} \sum_{k=0}^\infty \frac{a_k(\nu)}{z^k}\,, \quad a_k(\nu) = \frac{(1/2-\nu)_k\,(1/2+\nu)_k}{(-2)^k k!}\,, \tag{C.25}$$

[I] Which with our Fourier transform conventions (see also footnote VI in Subsection 4.4.2) we can define as

$$\sum_{n\in\mathbb{Z}} f(nL) = \frac{1}{L}\sum_{k\in\mathbb{Z}} \tilde{f}\left(2\pi\frac{k}{L}\right)\,, \quad \tilde{f}(p) = \int_{-\infty}^\infty \mathrm{d}x f(x)\,\mathrm{e}^{ipx}\,, \tag{C.17}$$

of which the three-dimensional case is a straightforward generalization.

with $a_0(\nu) = 1$, which is the relevant part for the leading large z behavior[II] . Thus, with $\nu = 1 - n/2$ we are lead to

$$\Delta\mathscr{M}_n^L = \frac{3m_h^{4-n}\Gamma(n+1)}{2^{n+2}\pi^{3/2}\Gamma(\frac{n+1}{2})} \sum_{\vec{l}\in\mathbb{N}^3\setminus\vec{0}} 2K_{1-n/2}(m_hL|\vec{l}|)\left(\frac{2}{m_hL|\vec{l}|}\right)^{1-n/2} \tag{C.27}$$

$$\overset{m_hL\to\infty}{\sim} \frac{3m_h^{4-n}\Gamma(n+1)}{2^{n+2}\pi^{3/2}\Gamma(\frac{n+1}{2})} \sum_{\vec{l}\in\mathbb{N}^3\setminus\vec{0}} \sqrt{\pi}\left(\frac{2}{m_hL|\vec{l}|}\right)^{\frac{3-n}{2}} \mathrm{e}^{-m_hL|\vec{l}|}\left(1+\mathscr{O}\left(\frac{1}{m_hL|\vec{l}|}\right)\right) \tag{C.28}$$

$$\overset{m_hL\to\infty}{\sim} \frac{3m_h^{4-n}\Gamma(n+1)}{2^{n+2}\pi^{3/2}\Gamma(\frac{n+1}{2})}\sqrt{\pi}\left(\frac{2}{m_hL}\right)^{\frac{3-n}{2}} \mathrm{e}^{-m_hL}\left(1+\mathscr{O}\left(\frac{1}{m_hL}\right)\right), \tag{C.29}$$

from which we can easily parameterize the relative size of finite volume effects, given by

$$\frac{\Delta\mathscr{M}_n^L}{\mathscr{M}_n(\infty)} \overset{m_hL\to\infty}{\sim} \frac{\pi}{2}\Gamma(3/2)\,\Gamma\left(\frac{n-2}{2}\right)\left(\frac{2}{m_hL}\right)^{\frac{3-n}{2}} \mathrm{e}^{-m_hL}\left(1+\mathscr{O}\left(\frac{1}{m_hL}\right)\right). \tag{C.30}$$

Numerical results for eq. (C.30) can be found in table C.2, where used y-values can be found in table C.1.

m_*/m_c	$L/a = 24$	32	36	48	64	96	128	192
3.5	42.39	44.61	41.41	41.26	37.38	36.94	36.37	35.93
2.3	29.77	31.33	29.09	28.98	26.26	25.94	25.54	25.24
1.6	21.10	22.20	20.61	20.54	18.61	18.38	18.10	17.89
1.2	16.64	17.52	16.26	16.20	14.68	14.50	14.28	14.11
0.8	12.09	12.72	11.81	11.77	10.66	10.54	10.37	10.25

Table C.1: *Values for $y = Lm_*$ used, for different masses m_* and number of lattice points L/a. For readability we give here an approximate value of m_*/m_c rather than the exact z.*

y	6	8	10	11	12	13	14	15
$n = 4$	0.0060	0.00093	1.4e-04	5.5e-05	2.1e-05	8.0e-06	3.1e-06	1.2e-06
$n = 6$	0.018	0.0037	0.0016	3.0e-04	1.3e-04	5.2e-05	2.1e-05	8.7e-06
$n = 8$	0.11	0.030	0.0071	0.0033	1.5e-03	6.8e-04	3.0e-04	1.3e-04
$n = 10$	0.97	0.36	0.11	0.054	0.027	0.013	0.0063	3.0e-03

Table C.2: *Relative TL-FV effects eq. (C.30), normalized by $L = \infty$ value, as function of $y = Lm_*$. From table C.1 we see for $m_*/m_c \geq 1.2$ we have $y > 14$, i.e. tree-level finite volume effects are* at most, *for $n = 10$ only, around half a percent. Note that for the conclusions in Chapter 6 and Chapter 7 the relevant values are the medium and high masses so that in our quenched study FV effects can safely be neglected.*

[II] The notation $(a)_n$ refers to the Pochhammer symbol defined as

$$(a)_n = \frac{\Gamma(a+n)}{\Gamma(a)}. \tag{C.26}$$

C.3. THE LATTICE PROPAGATOR

The Wilson twisted mass action with a doublet of mass degenerate quarks is given by

$$\mathscr{S}_F = a^4 \sum_x \overline{\chi}(x) \left\{ \sum_{\nu=0}^{3} \left(\gamma_\nu \frac{\nabla_\nu + \nabla_\nu^*}{2} - \frac{a}{2} \nabla_\nu^* \nabla_\nu + c_{sw} a \sum_{\mu=0}^{3} \frac{i}{4} \sigma_{\mu\nu} \hat{F}_{\mu\nu} \right) \mathbb{1}_f + m \mathbb{1}_f + i \mu_{tm} \gamma_5 \tau_3 \right\} \chi(x) , \tag{C.31}$$

so that for a single flavor $f_\pm = h, h'$ one has

$$\mathscr{S}_F^\pm = a^4 \sum_x \overline{f}_\pm(x) \left\{ \sum_{\nu=0}^{3} \left(\gamma_\nu \frac{\nabla_\nu + \nabla_\nu^*}{2} - \frac{a}{2} \nabla_\nu^* \nabla_\nu + c_{sw} a \sum_{\mu=0}^{3} \frac{i}{4} \sigma_{\mu\nu} \hat{F}_{\mu\nu} \right) + m \pm i \mu_{tm} \gamma_5 \right\} f_\pm(x) . \tag{C.32}$$

At tree level $\nabla_\nu \to \partial_\nu$ and $\hat{F}_{\mu,\nu} \equiv 0$, giving a free action

$$\begin{aligned} \mathscr{S}_F^\pm =& a^4 \sum_{x,y} \overline{f_\pm}(x) D_{\mu_{\rm tm}} f_\pm(y) = a^4 \sum_x \overline{f_\pm}(x) \left(m \pm \mu_{\rm tm} i \gamma_5 \right) f_\pm(x) \\ & - \frac{a^4}{2a} \sum_{x,\mu} \overline{f_\pm}(x) \left[f_\pm(x + a\hat{\mu}) - 2 f_\pm(x) + f_\pm(x - a\hat{\mu}) + \gamma_\mu \left(f_\pm(x + a\hat{\mu}) - f_\pm(x - a\hat{\mu}) \right) \right] , \end{aligned} \tag{C.33}$$

leading us to

$$\begin{aligned} D_{\mu_{\rm tm}} &= \left(m \pm \mu_{\rm tm} i \gamma_5 + \frac{4}{a} \right) \delta_{x,y} - \frac{1}{2a} \sum_\mu \left\{ (\delta_{y,x+a\hat{\mu}} + \delta_{y,x-a\hat{\mu}}) + \gamma_\mu (\delta_{x+a\hat{\mu},y} - \delta_{x-a\hat{\mu},y}) \right\} \\ &= \left(m \pm \mu_{tm} i \gamma_5 + \frac{4}{a} \right) \delta_{x,y} - \frac{1}{2a} \sum_\mu \left\{ \delta_{y,x+a\hat{\mu}} (1 - \gamma_\mu) + \delta_{y,x-a\hat{\mu}} (1 + \gamma_\mu) \right\} . \end{aligned} \tag{C.34}$$

Using the following momentum-space representation (and considering one Brillouin zone) of the Kronecker delta

$$\delta_{x,y} = a^4 \int_{-\pi/a}^{\pi/a} \frac{\mathrm{d}^4 p}{(2\pi)^4} \mathrm{e}^{ip\cdot(x-y)} , \tag{C.35}$$

we can manipulate the above expression in order to identify the Fourier transform of the Dirac operator, namely from

$$\begin{aligned} D_{\mu_{\rm tm}} = a^4 \int_{-\pi/a}^{\pi/a} \frac{\mathrm{d}^4 p}{(2\pi)^4} \Bigg\{ & \mathrm{e}^{ip\cdot(x-y)} \left(\frac{4}{a} \pm i \gamma_5 \mu_{\rm tm} + m \right) \\ & - \frac{1}{2a} \sum_\mu \left[(1 - \gamma_\mu) \mathrm{e}^{ip\cdot(x+a\hat{\mu}-y)} + (1 + \gamma_\mu) \mathrm{e}^{ip\cdot(x-a\hat{\mu}-y)} \right] \Bigg\} \end{aligned} \tag{C.36}$$

we further rewrite

$$\begin{aligned} D_{\mu_{\rm tm}} &= a^4 \int_{-\pi/a}^{\pi/a} \frac{\mathrm{d}^4 p}{(2\pi)^4} \mathrm{e}^{ip\cdot(x-y)} \left\{ \frac{4}{a} \pm i\gamma_5 \mu_{\rm tm} + m - \frac{1}{2a} \sum_\mu \left[\mathrm{e}^{ip_\mu a}(1-\gamma_\mu) + \mathrm{e}^{-ip_\mu a}(1+\gamma_\mu) \right] \right\} \\ &= a^4 \int_{-\pi/a}^{\pi/a} \frac{\mathrm{d}^4 p}{(2\pi)^4} \mathrm{e}^{ip\cdot(x-y)} \left\{ \frac{4}{a} \pm i\gamma_5 \mu_{\rm tm} + m - \frac{1}{a} \sum_\mu \left[\cos\big(ap_\mu\big) - i\gamma_\mu \sin\big(ap_\mu\big) \right] \right\} \\ &= a^4 \int_{-\pi/a}^{\pi/a} \frac{\mathrm{d}^4 p}{(2\pi)^4} \mathrm{e}^{ip\cdot(x-y)} \widetilde{S}^{-1}(p)\,. \end{aligned} \tag{C.37}$$

Thus the inverse propagator is

$$\begin{aligned} \widetilde{S}_\pm^{-1}(p,a,m,\mu_{\rm tm}) &= m \pm i\gamma_5\mu_{\rm tm} + a^{-1} \sum_{\mu=0}^{3} \left[(1-\cos\big(ap_\mu\big)) + i\gamma_\mu \sin\big(ap_\mu\big) \right] \\ &= m \pm i\gamma_5\mu_{\rm tm} + a^{-1} \sum_{\mu=0}^{3} \left[2\sin^2(ap_\mu/2) + i\gamma_\mu \sin\big(ap_\mu\big) \right] , \end{aligned} \tag{C.38}$$

leading us to define (note we use a somewhat non-standard notation here)

$$\tilde{p}_\mu \stackrel{\text{def.}}{=} a^{-1} \sin\left(ap_\mu\right), \tag{C.39}$$

$$\hat{p}_\mu \stackrel{\text{def.}}{=} \frac{2}{a} \sin\left(\frac{ap_\mu}{2}\right). \tag{C.40}$$

With these definitions, we can easily invert the propagator by multiplying the formal inverse by its complex conjugate in the numerator and denominator. The latter thus results in the sum of real part squared and imaginary part squared, i.e.

$$\begin{aligned} \widetilde{S}_\pm(p,a,m,\mu_{\rm tm}) &= \left[m + \frac{a}{2} \sum_{\mu=0}^{3} \hat{p}_\mu^2 + i\,\gamma_\mu \tilde{p}_\mu \pm \gamma_5 \mu_{\rm tm} \right]^{-1} \times \\ &\times \frac{\left(m + \frac{a}{2}\sum_{\mu=0}^{3} \hat{p}_\mu^2 \right) - i\left(\gamma_\mu \tilde{p}_\mu \pm \gamma_5 \mu_{\rm tm} \right)}{\left(m + \frac{a}{2}\sum_{\mu=0}^{3} \hat{p}_\mu^2 \right) - i\left(\gamma_\mu \tilde{p}_\mu \pm \gamma_5 \mu_{\rm tm} \right)} = \frac{M(p) - i\tilde{\not{p}} \mp i\mu_{\rm tm}\gamma_5}{M^2(p) + \mu_{\rm tm}^2 + \tilde{p}^2}\,, \end{aligned} \tag{C.41}$$

where in the last line we have introduced the very compact notations $M(p) = m + \frac{a}{2}\sum_{\mu=0}^{3} \hat{p}_\mu^2$ and $\tilde{\not{p}} = a^{-1}\sum_{\mu=0}^{3} \gamma_\mu \sin\left(ap_\mu\right)$, and where there spinor-space structure in the denominator is trivial as far as the terms that turn up are proportional to one of the following

$$\gamma_\mu^2 = \mathbb{1}\,, \quad \gamma_5^2 = \mathbb{1}\,, \quad \gamma_\mu\gamma_\nu + \gamma_\nu\gamma_\mu \equiv 0 \text{ if } \mu \neq \nu\,, \quad \gamma_5\gamma_\mu + \gamma_\mu\gamma_5 \equiv 0\,. \tag{C.42}$$

The time-momentum propagator[III] will now be

$$S_{\pm}(t,\vec{p}\,) = \int_{-\pi/a}^{\pi/a} \frac{\mathrm{d}p_0}{2\pi} \mathrm{e}^{ip_0 t} \frac{M(p) - i\tilde{\not{p}} \mp i\mu_{\mathrm{tm}}\gamma_5}{M^2(p) + \mu_{\mathrm{tm}}^2 + \tilde{p}^2}$$
$$= \int_{-\pi/a}^{\pi/a} \frac{\mathrm{d}\phi}{2\pi} \frac{\mathrm{e}^{i\phi n}\left[am + (1-\cos\phi) + \frac{a^2}{2}\vec{\tilde{p}}^{\,2} - i\gamma_0\sin\phi - ia\vec{\gamma}\cdot\vec{\tilde{p}} \mp ia\mu_{\mathrm{tm}}\gamma_5\right]}{(a\mu_{\mathrm{tm}})^2 + \sin^2\phi + a^2\vec{\tilde{p}}^{\,2} + (am + \frac{a^2}{2}\vec{\tilde{p}}^{\,2})^2 + (1-\cos\phi)^2 + 2(1-\cos\phi)(am + \frac{a^2}{2}\vec{\tilde{p}}^{\,2})}\,. \tag{C.43}$$

Let us define $A = A(\vec{p}\,)$, which only depends on spatial components of the momentum

$$A \overset{\text{def.}}{=} 1 + am + \frac{a^2}{2}\vec{\tilde{p}}^{\,2}\,, \tag{C.44}$$

change variable to $u = e^{i\phi} \to \frac{\mathrm{d}\phi}{2\pi} = \frac{1}{2\pi i}\frac{\mathrm{d}u}{u}$, and consider the case $t > 0$

$$\theta(t)\, S_{\pm}(t,\vec{p}\,) = \oint_{|u|=1} \frac{1}{2\pi i}\frac{\mathrm{d}u}{u} u^n \frac{A - (u+u^{-1})/2 - \gamma_0(u-u^{-1})/2 - ia\vec{\gamma}\cdot\vec{\tilde{p}} \mp ia\mu_{\mathrm{tm}}\gamma_5}{1 + A^2 + a^2\vec{\tilde{p}}^{\,2} + (a\mu_{\mathrm{tm}})^2 - A(u+u^{-1})}\,. \tag{C.45}$$

Looking at the denominator, it is apparent that if $u = u_+$ is a zero, then $u = u_- = u_+^{-1}$ is one too. Thus, we parametrize the zeros as $u_{\pm} = \mathrm{e}^{\pm\omega(\vec{p}\,)}$, of which only $u_- = \mathrm{e}^{-\omega}$ will be inside the unit-radius circle. This yields $den. = -A(u - \mathrm{e}^{-\omega})(u - \mathrm{e}^{\omega}) \to -A(\mathrm{e}^{-\omega} - \mathrm{e}^{\omega})$ and $u \to \mathrm{e}^{-\omega}$ in the numerator, giving

$$\theta(t)\, S_{\pm}(t,\vec{p}\,) = \mathrm{e}^{-\omega n} \frac{A - \cosh(\omega) + \gamma_0\sinh(\omega) - ia\vec{\gamma}\cdot\vec{\tilde{p}} \mp ia\mu_{\mathrm{tm}}\gamma_5}{2A\sinh(\omega)} \tag{C.46}$$

yielding the full propagator, in terms of $aE(\vec{p}\,) = \omega(\vec{p}\,)$

$$S_{\pm}(t,\vec{p}\,) = \theta(t)\,\mathrm{e}^{-Et}\frac{A - \cosh(aE) + \gamma_0\sinh(aE) - ia\vec{\gamma}\cdot\vec{\tilde{p}} \mp ia\mu_{\mathrm{tm}}\gamma_5}{2A\sinh(aE)}$$
$$+ \theta(-t)\,\mathrm{e}^{Et}\frac{A - \cosh(aE) - \gamma_0\sinh(aE) - ia\vec{\gamma}\cdot\vec{\tilde{p}} \mp ia\mu_{\mathrm{tm}}\gamma_5}{2A\sinh(aE)}\,, \qquad A = 1 + am + \frac{a^2}{2}\vec{\tilde{p}}^{\,2}\,, \tag{C.47}$$

where, finally, $aE(\vec{p}\,)$ is implicitly given by the following equation[IV]

$$2\cosh(aE(\vec{p}\,)) = A + \frac{1 + a^2\vec{\tilde{p}}^{\,2} + (a\mu_{\mathrm{tm}})^2}{A}\,. \tag{C.48}$$

Note it is immediate to obtain the formula for full twist by simply setting the bare Wilson quark mass $m = 0$ and, likewise, to obtain the standard Wilson quark propagator without a twisted mass by simply setting $\mu_{\mathrm{tm}} = 0$.

[III] With some notational abbreviations such as $\vec{\tilde{p}}^{\,2} = a^{-2}\sum_{i=1}^{3}\sin^2(ap_i)$ and where we now drop the lattice spacing and mass dependence.

[IV] This is a direct consequence of the zeros of the denominator in (C.45), and since the poles in p_0 (in this case, inside the unit circle) of the propagator determine the energy of the one particle state, we immediately see that for ω satisfying the denominator being zero we have (C.48).

C.4. MOMENTS AT FINITE LATTICE SPACING

The formula for the TL of moments on an infinite lattice becomes then, with $M^2 = \mu_{\rm tm}^2 + m^2$ and where for this section only we indicate with $x_0 = t/a$ (with $[t] = 1$)

$$\mathscr{M}_n = M^2 \sum_{x_0=-\infty}^{\infty} a\,(x_0\,a)^n \sum_{\vec{x}=-\infty}^{\infty} a^3\ \mathrm{tr}\left\{S_h(x)\gamma_5 S_{h'}(-x)\gamma_5\right\}, \tag{C.49}$$

where it is immediate to see that $S_h(x) \leftrightarrow S_+(x)$ and $S_{h'}(x) \leftrightarrow S_-(x)$. Thus, noticing the twisted mass term to change sign when taking the hermitean conjugate, we see that $\gamma_5 S_-(-x)\gamma_5 = S_+^\dagger(x)$ (where we remind $\pm$ indicates the sign of $\mu_{\rm tm}$), giving a formula analogous to (C.5)

$$\begin{aligned}\mathscr{M}_n &= M^2 \sum_{x_0=-\infty}^{\infty} a\,(x_0 a)^n \sum_{\vec{x}=-\infty}^{\infty} a^3 \int_{-\pi/a}^{\pi/a} \frac{\mathrm{d}^3\vec{p}}{(2\pi)^3}\frac{\mathrm{d}^3\vec{q}}{(2\pi)^3} e^{i\vec{x}\cdot(\vec{p}-\vec{q})}\,\mathrm{tr}\left\{S_+(x_0;\vec{p})\,S_+^\dagger(x_0;\vec{q})\right\} \\ &= M^2 a^{n+4-3} \sum_{x_0=-\infty}^{\infty} x_0^n \int_{-\pi/a}^{\pi/a} \frac{\mathrm{d}^3\vec{p}}{(2\pi)^3}\,\mathrm{tr}\left\{S_+(x_0;\vec{p})\,S_+^\dagger(x_0;\vec{p})\right\},\end{aligned} \tag{C.50}$$

where as for the continuum case we have obtained a $\delta^3(p-q)$ from the sum (series) over space[V] . . The trace for positive time will give, just like in the case above (using the cyclic property of the trace and the anticommutation relations of 2 γ-matrices),

$$\mathrm{tr} \to N_c \frac{\mathrm{e}^{-2aEx_0}}{4A^2\sinh^2(aE)}\,\mathrm{tr}[\mathbb{1}]\left\{(A-\cosh(aE))^2 + \sinh^2(aE) + a^2\vec{\tilde{p}}^{\,2} + (a\mu_{\rm tm})^2\right\}. \tag{C.53}$$

Looking at the positive and negative time components of the time-momentum propagator, it is immediate to notice the trace yields the same result with $x_0 \to -x_0$, thus we can immediately write for even n

$$\mathscr{M}_n = 6M^2 a^{n+1} \int_{-\pi/a}^{\pi/a} \frac{\mathrm{d}^3\vec{p}}{(2\pi)^3} \frac{(A-\cosh(aE))^2 + \sinh^2(aE) + a^2\vec{\tilde{p}}^{\,2} + (a\mu_{\rm tm})^2}{A^2\sinh^2(aE)} \sum_{x_0=0}^{\infty} x_0^n \mathrm{e}^{-2aEx_0}, \tag{C.54}$$

[V] One of the definitions of the δ function can be inferred from

$$f(q) = \lim_{n\to\infty}\int_I \mathrm{d}p\, f(p) \sum_{x=-n}^{n} \frac{\mathrm{e}^{ix(p-q)}}{2\pi}, \quad \text{i.e. one writes the formal representation} \tag{C.51}$$

$$\delta(p-q) = \frac{1}{2\pi}\sum_{x=-\infty}^{\infty} \mathrm{e}^{ix(p-q)}, \tag{C.52}$$

where this δ is adimensional, whereas the spacial momentum integral was not, thus leading to the extra a^{-3} factor.

where it is straightforward to sum[VI] the x_0 part via ($E_{\rm den}(2aE)$ standing for "E denominator")

$$\begin{aligned} E_{\rm den}(2aE) &\stackrel{\rm def.}{=} \sum_{x_0=0}^{\infty}\left[(-1)^n\frac{{\rm d}^n}{d(2aE)^n}{\rm e}^{-2aEx_0}\right] \\ &= (-1)^n\frac{{\rm d}^n}{d(2aE)^n}\sum_{x_0=0}^{\infty}\left({\rm e}^{-2aE}\right)^{x_0} = (-1)^n\frac{{\rm d}^n}{d(2aE)^n}\frac{1}{1-{\rm e}^{-2aE}}\,, \end{aligned} \tag{C.56}$$

which can effortlessly be obtained for typical cases $n=4,6,8,10$.For the maximal twist case, all put together, we hae

$$\mathscr{M}_n = 6\mu^2 a^{n+1}\int_{-\pi/a}^{\pi/a}\frac{{\rm d}^3\vec{p}}{(2\pi)^3}\frac{(A-\cosh(aE))^2+\sinh^2(aE)+a^2\vec{\tilde{p}}^{\,2}+(a\mu_{\rm tm})^2}{A^2\sinh^2(aE)}E_{\rm den}(2aE) \tag{C.57}$$

$$= 6(a\mu)^2 a^{n-4}\int_{-\pi}^{\pi}\frac{{\rm d}^3(a\vec{p})}{(2\pi)^3}\frac{(A-\cosh(aE))^2+\sinh^2(aE)+a^2\vec{\tilde{p}}^{\,2}+(a\mu_{\rm tm})^2}{A^2\sinh^2(aE)}E_{\rm den}(2aE)\,, \tag{C.58}$$

where now $A(\vec{p}) = 1+a^2\vec{\hat{p}}^{\,2}/2$. For completeness, we give the deviation w.r.t. the continuum the dispersion relation (C.48), obtained by expanding in powers of a

$$2\left\{1+(aE)^2/2!+(aE)^4/4!+\ldots\right\} = \tag{C.59}$$

$$1+2\left\{\sum_i\left[(ap_i/2)^2-(ap_i/2)^4/3+\ldots\right]\right\}+\left\{1+a^2\mu_{\rm tm}^2+\sum_l[(ap_l)^2-(ap_l)^4/3+\ldots]\right\}\times \tag{C.60}$$

$$\left\{1-2\sum_i\left[(ap_i/2)^2-(ap_i/2)^4/3+\ldots\right]+4\left[\sum_i(ap_i/2)^2\right]^2+\ldots\right\} \tag{C.61}$$

$$\longrightarrow (aE)^2+\frac{(aE)^4}{12} = \frac{(a\vec{p})^2}{2}-\frac{\sum_i(ap_i)^4}{24}+(a\mu_{\rm tm})^2+(a\vec{p})^2 \tag{C.62}$$

$$-\frac{\sum_l(ap_l)^4}{3}-\frac{(a\vec{p})^2}{2}+\frac{\sum_i(ap_i)^4}{24}+\frac{(a\vec{p})^4}{4}-\frac{a^4(\mu_{\rm tm}^2+\vec{p}^{\,2})\vec{p}^{\,2}}{2} \tag{C.63}$$

$$\longrightarrow (aE)^2 = -\frac{(aE)^4}{12}+(a\mu_{\rm tm})^2+(a\vec{p})^2+a^4\left\{-\frac{1}{3}\sum_l p_l^4-\frac{1}{4}\vec{p}^{\,4}-\frac{1}{2}\mu_{\rm tm}^2\vec{p}^{\,2}\right\} \tag{C.64}$$

$$\longrightarrow E^2 = \mu_{\rm tm}^2+\vec{p}^{\,2}+\frac{a^2}{3}\left\{-\frac{\mu_{\rm tm}^4}{4}-\vec{p}^{\,4}-2\mu_{\rm tm}^2\vec{p}^{\,2}-\sum_l p_l^4\right\}+\mathscr{O}(a^4)\,, \tag{C.65}$$

where in the last line we have substituted $E^4\to(\mu_{\rm tm}^2+\vec{p}^{\,2})^2$, as far as any other corrections to the energy are of higher order in a in that term. Also note that the only Lorentz symmetry-breaking term is

[VI] Note the integral is significantly different from the series, as far as we would have

$$(2E)^{-n-1}\int_0^{\infty}{\rm d}(2Ex_0)\,(2Ex_0)^n{\rm e}^{-2Ex_0} = \frac{\Gamma(n+1)}{(2E)^{n+1}}\,. \tag{C.55}$$

Of course, as mentioned in the main text, this is recovered from the discrete sum in the continuum limit. The discreteness of the timeslices (which encodes cutoff effects in some sense) changes qualitatively the behavior of this term much like the discreteness of energy levels in Planck's black-body treatment UV-completes the Rayleigh-Jeans theory (only that there the UV completion is known and physical).

$\sum_l p_l^4$, which is the only dimension 4 operator that can appear at this order[VII]. This however contains the bare mass $\mu_{\rm tm}$, which has to substituted with $E(\vec{p}=\vec{0})\equiv\bar{\mu}_{tm}$, the renormalized mass, after which we obtain

$$E^2=\bar{\mu}_{tm}^2+\vec{p}^{\,2}-\frac{a^2}{3}\left\{\vec{p}^{\,4}+2\bar{\mu}_{tm}^2\vec{p}^{\,2}+\sum_l p_l^4\right\}+\mathscr{O}(a^4)\,. \tag{C.67}$$

Finite Volume Effects in the Discretized Theory

In the case of a finite spatial extent L but infinite time extent T, the tree-level lattice moment (C.68) becomes simply

$$\mathscr{M}_n=6a^2\mu_{\rm tm}^2a^{n-4}\left(\frac{a}{L}\right)^3\sum_{\vec{p}=0}^{(N-1)2\pi/L}\frac{(A-\cosh(aE))^2+\sinh^2(aE)+a^2\vec{\tilde{p}}^{\,2}+(a\mu_{\rm tm})^2}{A^2\sinh^2(aE)}\times \tag{C.68}$$

$$\sum_{x_0=0}^{\infty}x_0^n\mathrm{e}^{-2aEx_0}\,,\quad N=L/a\,,\quad A(\vec{p})=1+a^2\vec{\tilde{p}}^{\,2}/2\,, \tag{C.69}$$

which can similarly be evaluated numerically. The similarity of the above with the infinite volume case follows from the fact that the time-slice propagator is defined as an integral over p_0, which is still a continuous integration variable. The sum over time-slices defining the moment also does not change, so the only possible difference lies in the Fourier representations used in (C.50). As a matter of fact, with periodic boundary conditions, thanks to n-th partial sum of the geometric series, the expression of the Krönecker δ perfectly resembles that of the Dirac-δ, i.e. in one dimension

$$\delta_{p,q}=\frac{a}{L}\sum_{x=0}^{L/a-1}\mathrm{e}^{ix(p-q)}=\begin{cases}\frac{1-\mathrm{e}^{i(p-q)L/a}}{1-\mathrm{e}^{i(p-q)}}=\frac{a}{L}\frac{1-1}{1-\mathrm{e}^{i(p-q)}}\equiv 0 & p\neq q\\ \frac{a}{L}\sum_{x=0}^{L/a-1}\mathrm{e}^0=\frac{a}{L}\frac{L}{a}=1 & p=q\end{cases}. \tag{C.70}$$

[VII] Note that (C.65) can also be written as

$$E^2=\mu_{\rm tm}^2+\vec{p}^{\,2}-\frac{a^2}{3}\left\{\frac{\mu_{\rm tm}^4}{4}+2\mu_{\rm tm}^2\vec{p}^{\,2}+2(p_1^2p_2^2+p_1^2p_3^2+p_2^2p_3^2)+2\sum_l p_l^4\right\}+\mathscr{O}(a^4)\,. \tag{C.66}$$

APPENDIX D

SUPPLEMENTARY PLOTS

In this appendix we collect supplementary plots.

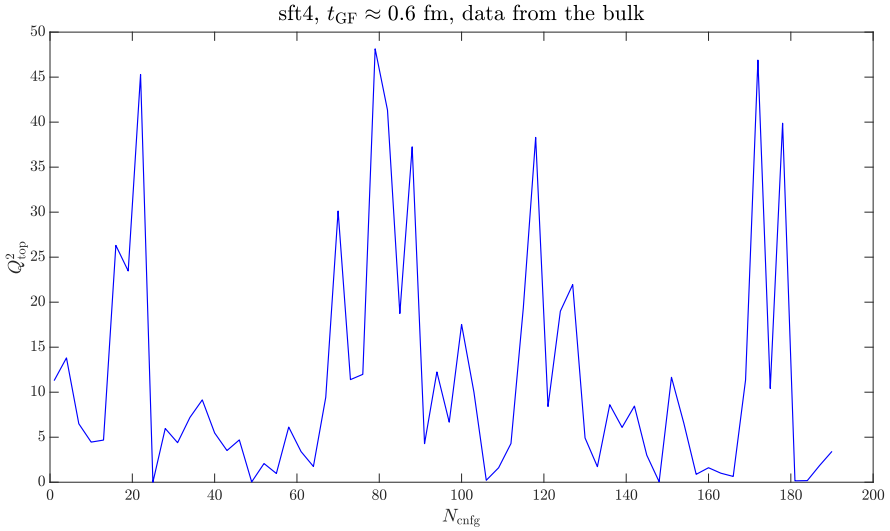

Figure D.1: *Variation of topological charge squared $Q^2(t_{GF})$ for the ensemble sft4.*

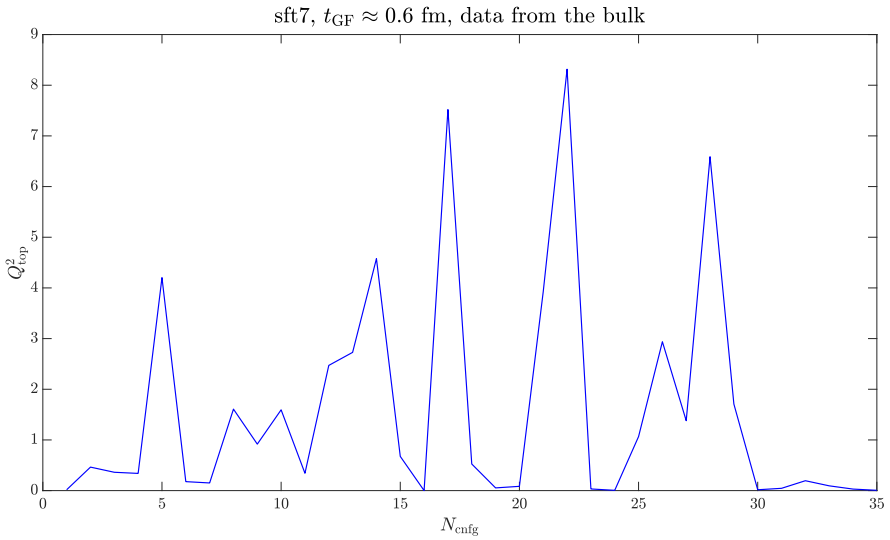

Figure D.2: *Variation of topological charge squared $Q^2(t_{GF})$ for the ensemble sft7.*

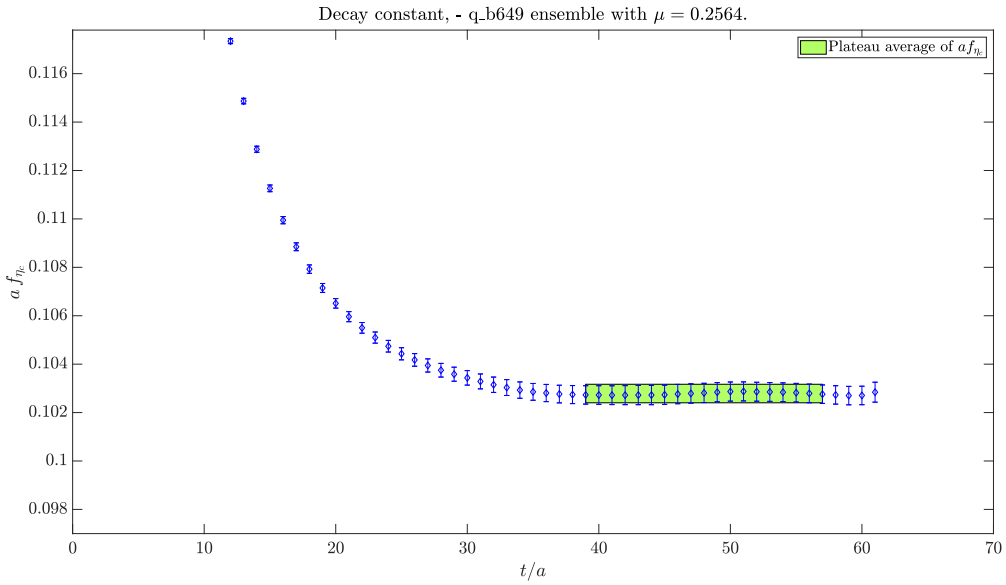

Figure D.3: *Decay constant in lattice units and its plateau for a coarse ensemble and medium mass. There is no issue whatsoever in selecting a plateau in this case.*

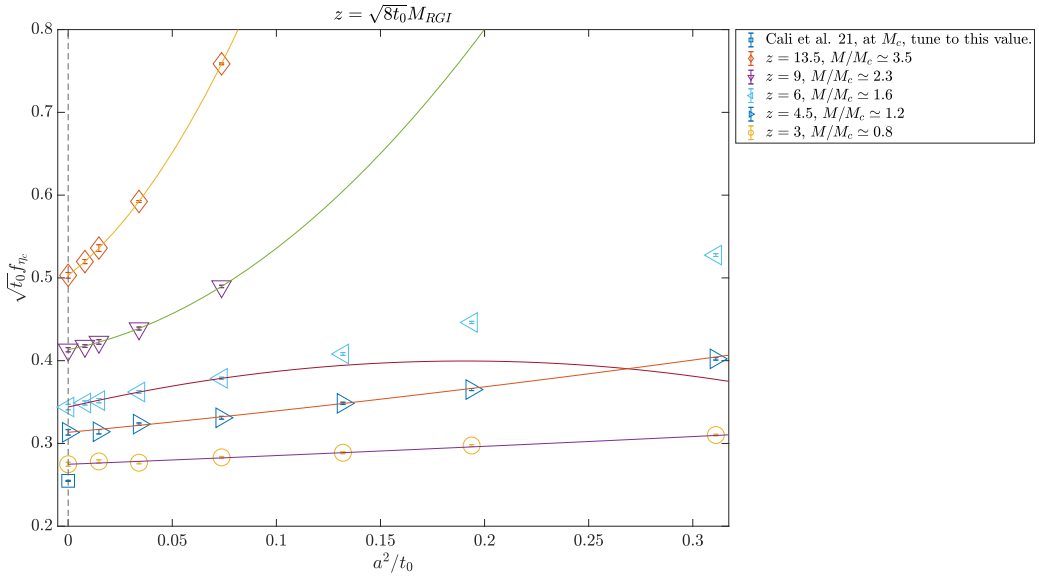

Figure D.4: *Continuum limits of f_{η_h} for all z values show a smooth behavior and validate our tuning was carried out well. Fit parameters given in table 5.8. Note, of the point by Calì et al. [33] at $a = 0$ only the magnitude matters, since their M_c differs from ours. Whatever value they were to choose, the behavior of (m_{PS}, f_{η_c}) in fig. 5.11 would still be universal.*

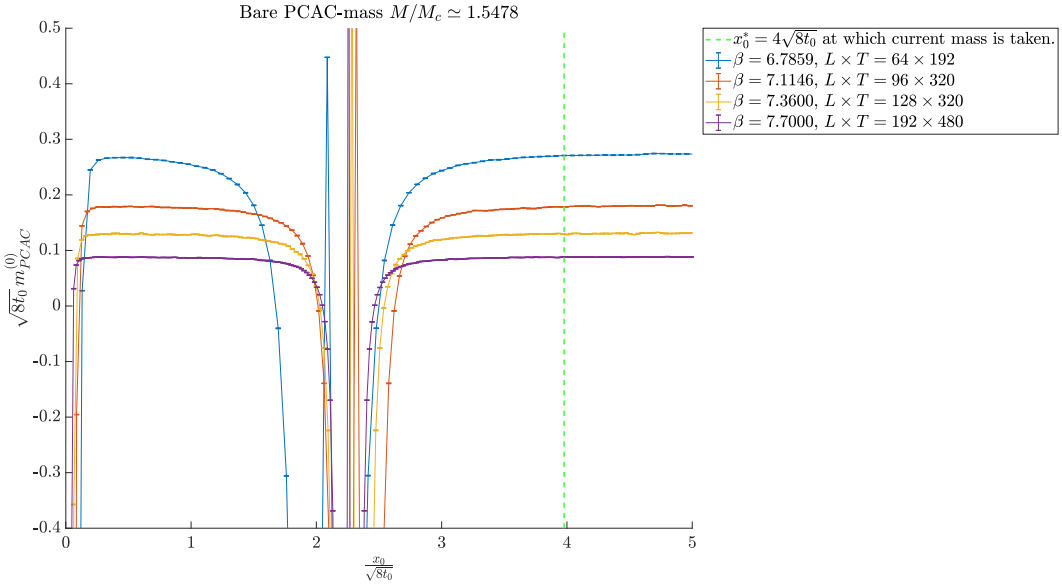

Figure D.5: *Bare PCAC mass as a function of Euclidean time (in physical units), for several β values, all at fixed physical mass $M/M_c \simeq 1.55$. Close to $x_0/\sqrt{8t_0} = 0$ the effect of the boundary can be seen, whereas the results we use are in the depth of the bulk, on the opposite side of the source time-slice.*

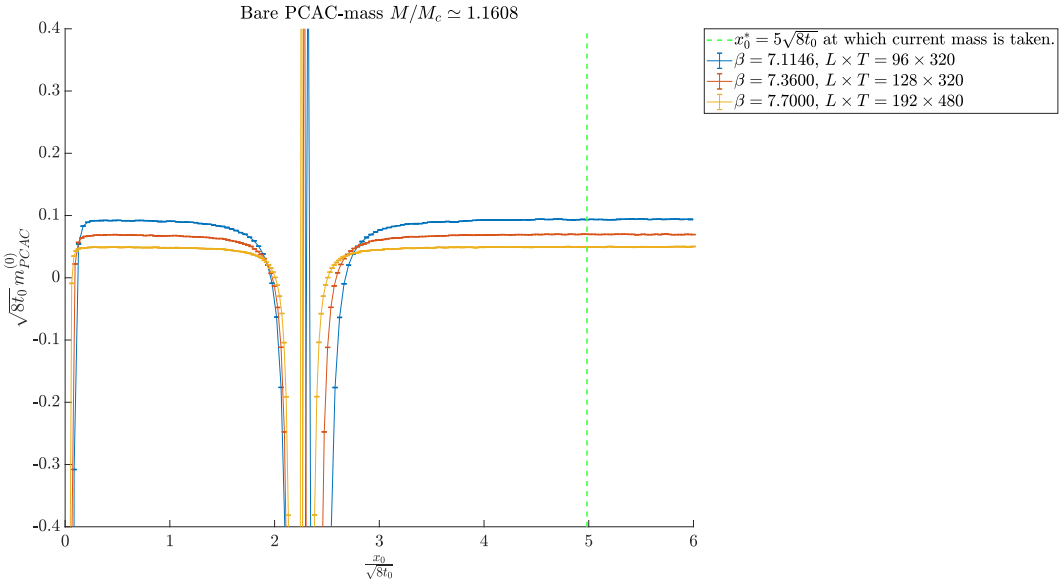

Figure D.6: *Bare PCAC mass as a function of Euclidean time (in physical units), for several β values, all at fixed physical mass $M/M_c \simeq 1.16$. Close to $x_0/\sqrt{8t_0} = 0$ the effect of the boundary can be seen, whereas the results we use are in the depth of the bulk, on the opposite side of the source time-slice.*

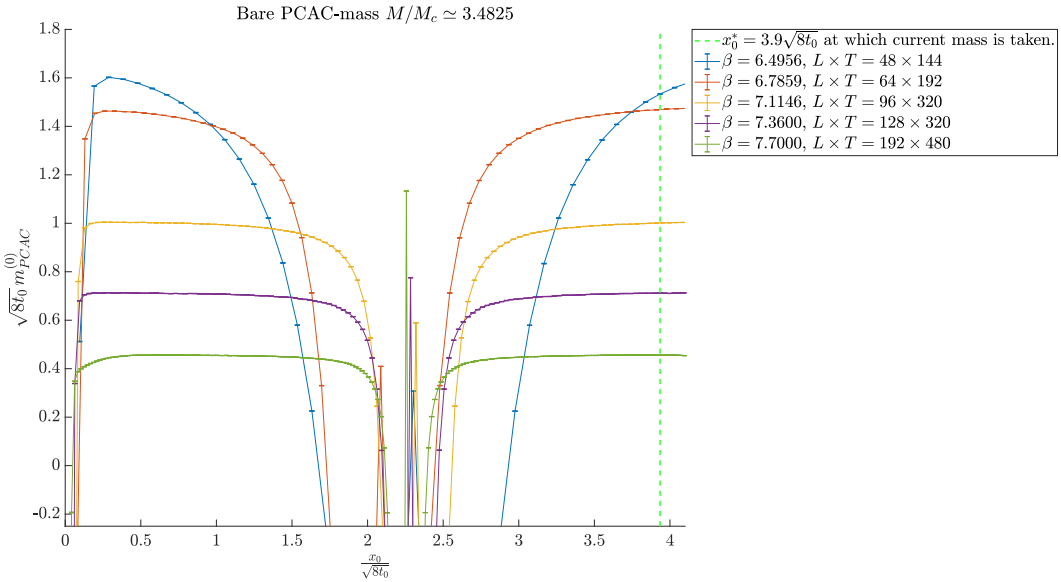

Figure D.7: *Bare PCAC mass as a function of Euclidean time (in physical units), for several β values, all at fixed physical mass $M/M_c \simeq 3.48$. Close to $x_0/\sqrt{8t_0} = 0$ the effect of the boundary can be seen, whereas the results we use are in the depth of the bulk, on the opposite side of the source time-slice.*

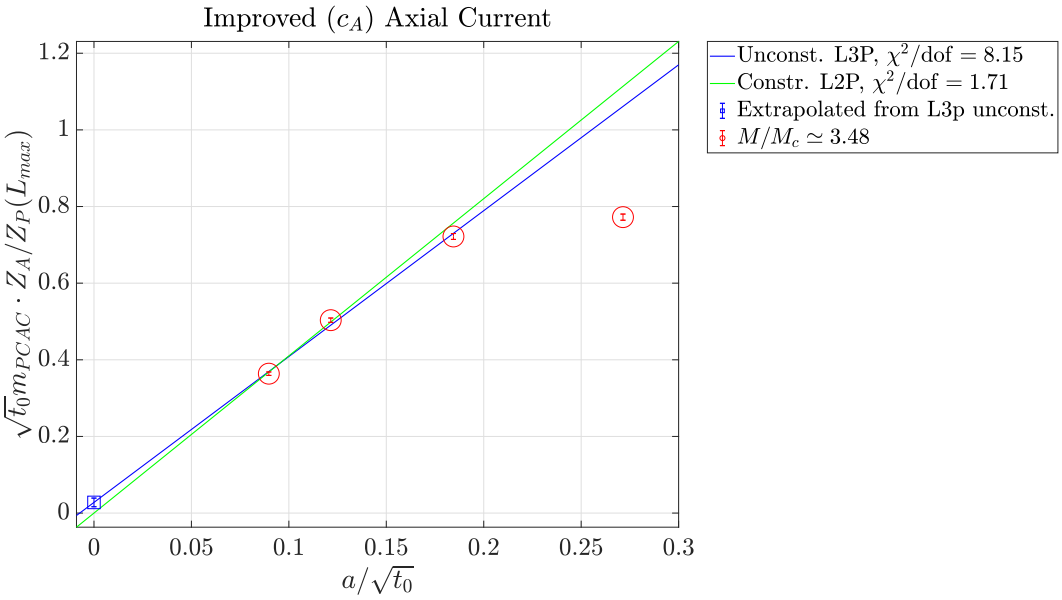

Figure D.8: *Improved PCAC-mass as a function of $a/\sqrt{t_0}$. "Constr." means the fit has been constrained to go through zero, whereas LNP as usually inidicates Linear N-Point fit. Discretization effects scale very linearly for small enough a.*

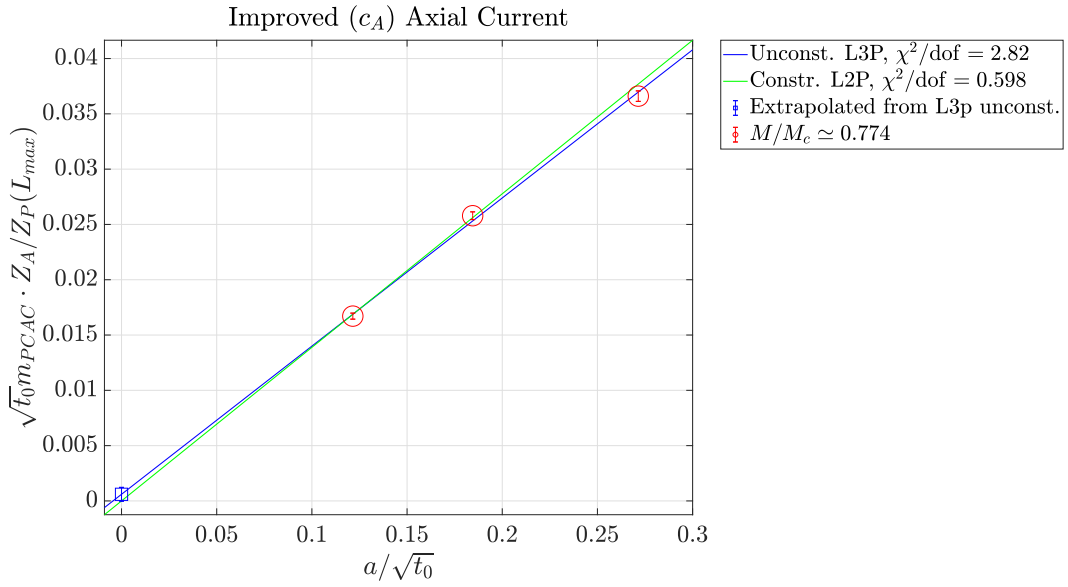

Figure D.9: *Improved PCAC-mass as a function of $a/\sqrt{t_0}$. "Constr." means the fit has been constrained to go through zero, whereas LNP as usually inidicates Linear N-Point fit. Discretization effects scale very linearly.*

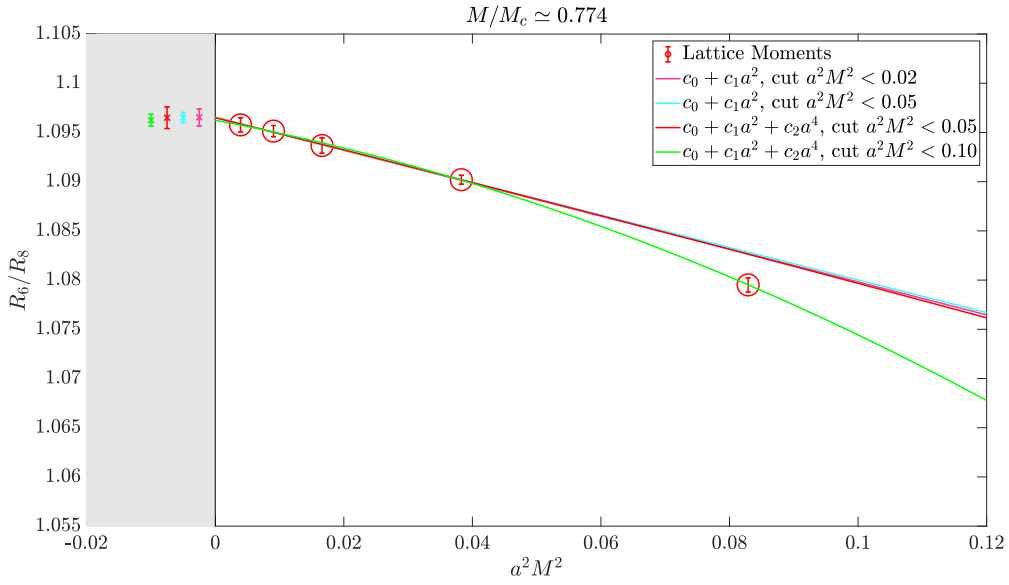

Figure D.10: *Continuum limit of R_6/R_8 for mass $M/M_c \simeq 0.77$. Several fit Ansätze are shown. In the gray band on the left hand side the value and error of the extrapolation for each Ansatz can be seen.*

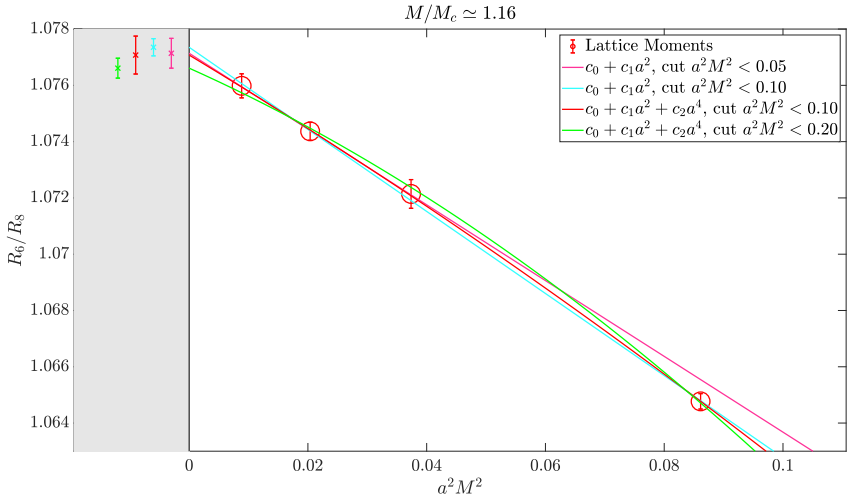

Figure D.11: *Continuum limit of R_6/R_8 for mass $M/M_c \simeq 1.16$. Several fit Ansätze are shown. In the gray band on the left hand side the value and error of the extrapolation for each Ansatz can be seen.*

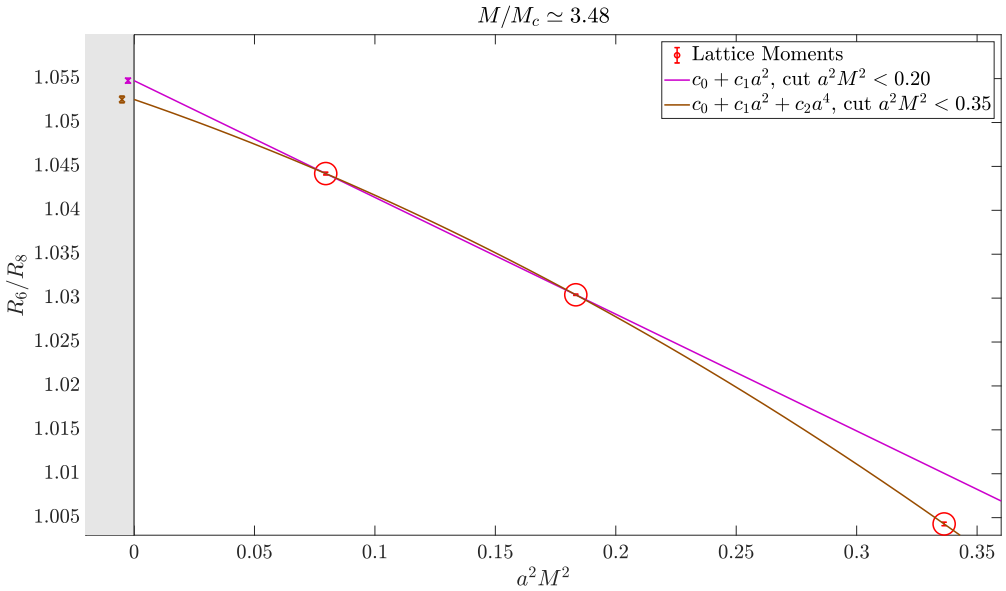

Figure D.12: *Continuum limit of R_6/R_8 for mass $M/M_c \simeq 3.48$. Several fit Ansätze are shown. In the gray band on the left hand side the value and error of the extrapolation for each Ansatz can be seen.*

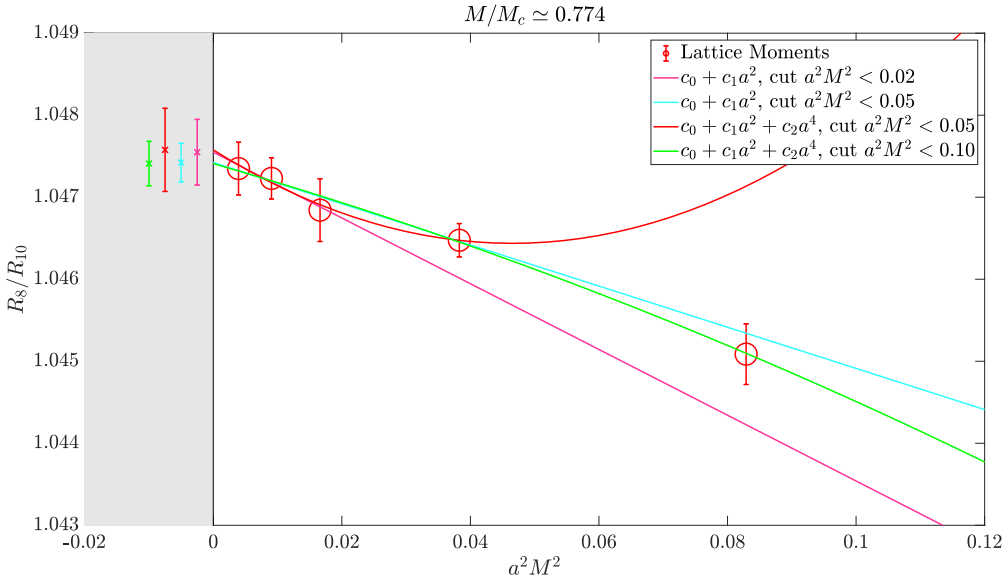

Figure D.13: *Continuum limit of R_8/R_{10} for mass $M/M_c \simeq 0.77$. Several fit Ansätze are shown. In the gray band on the left hand side the value and error of the extrapolation for each Ansatz can be seen.*

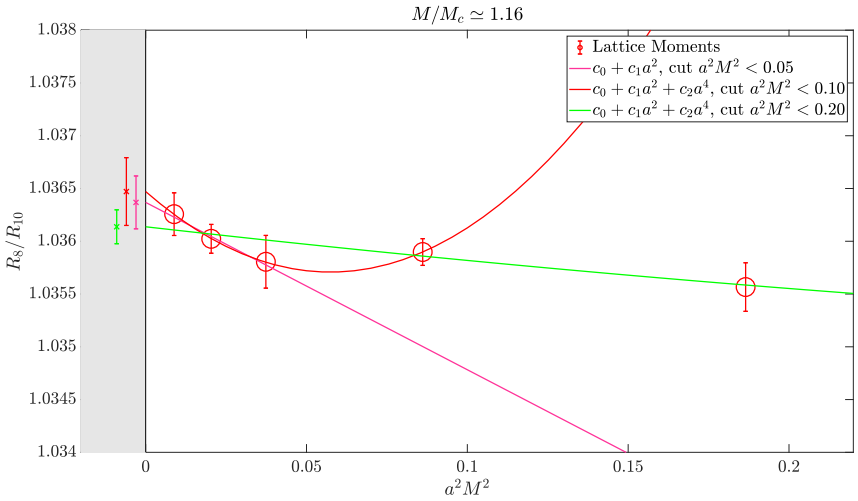

Figure D.14: *Continuum limit of R_8/R_{10} for mass $M/M_c \simeq 1.16$. Several fit Ansätze are shown. In the gray band on the left hand side the value and error of the extrapolation for each Ansatz can be seen.*

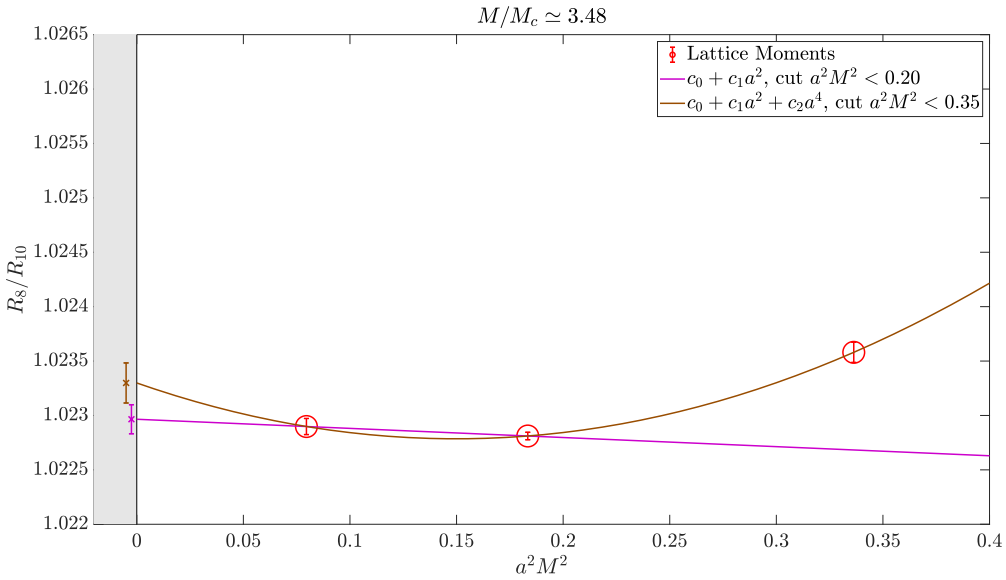

Figure D.15: *Continuum limit of R_8/R_{10} for mass $M/M_c \simeq 3.48$. Several fit Ansätze are shown. In the gray band on the left hand side the value and error of the extrapolation for each Ansatz can be seen.*

BIBLIOGRAPHY

[1] A. Blondel et al., eds. *Theory for the FCC-ee: Report on the 11th FCC-ee Workshop Theory and Experiments*. Vol. 3/2020. CERN Yellow Reports: Monographs. Geneva: CERN, May 2019. DOI: 10.23731/CYRM-2020-003. arXiv: 1905.05078 [hep-ph].

[2] Stephen L. Adler. "Overrelaxation Algorithms for Lattice Field Theories". In: *Phys. Rev. D* 37 (1988), p. 458. DOI: 10.1103/PhysRevD.37.458.

[3] I. Allison et al. "High-Precision Charm-Quark Mass from Current-Current Correlators in Lattice and Continuum QCD". In: *Phys. Rev. D* 78 (2008), p. 054513. DOI: 10.1103/PhysRevD.78.054513. arXiv: 0805.2999 [hep-lat].

[4] Charalampos Anastasiou et al. "High precision determination of the gluon fusion Higgs boson cross-section at the LHC". In: *JHEP* 05 (2016), p. 058. DOI: 10.1007/JHEP05(2016)058. arXiv: 1602.00695 [hep-ph].

[5] S. Aoki et al. "FLAG Review 2019: Flavour Lattice Averaging Group (FLAG)". In: *Eur. Phys. J. C* 80.2 (2020), p. 113. DOI: 10.1140/epjc/s10052-019-7354-7. arXiv: 1902.08191 [hep-lat].

[6] Y. Aoki et al. "FLAG Review 2021". In: (Nov. 2021). arXiv: 2111.09849 [hep-lat].

[7] Thomas Appelquist and J. Carazzone. "Infrared Singularities and Massive Fields". In: *Phys. Rev. D* 11 (1975), p. 2856. DOI: 10.1103/PhysRevD.11.2856.

[8] Andreas Athenodorou et al. "How perturbative are heavy sea quarks?" In: *Nucl. Phys. B* 943 (2019), p. 114612. DOI: 10.1016/j.nuclphysb.2019.114612. arXiv: 1809.03383 [hep-lat].

[9] Michael Francis Atiyah and Isadore Manuel Singer. "The index of elliptic operators on compact manifolds". In: *Bulletin of the American Mathematical Society* 69 (1963), pp. 422–433.

[10] Owe Axelsson. "Conjugate gradient type methods for unsymmetric and inconsistent systems of linear equations". In: *Linear Algebra and its Applications* 29 (1980). Special Volume Dedicated to Alson S. Householder, pp. 1–16. ISSN: 0024-3795. DOI: https://doi.org/10.1016/0024-3795(80)90226-8. URL: https://www.sciencedirect.com/science/article/pii/0024379580902268.

[11] P. A. Baikov, K. G. Chetyrkin, and J. H. Kühn. "Five-Loop Running of the QCD coupling constant". In: *Phys. Rev. Lett.* 118.8 (2017), p. 082002. DOI: 10.1103/PhysRevLett.118.082002. arXiv: 1606.08659 [hep-ph].

[12] P. A. Baikov, K. G. Chetyrkin, and Johann H. Kuhn. "Scalar correlator at O(alpha(s)**4), Higgs decay into b-quarks and bounds on the light quark masses". In: *Phys. Rev. Lett.* 96 (2006), p. 012003. DOI: 10.1103/PhysRevLett.96.012003. arXiv: hep-ph/0511063.

[13] D. Becirevic et al. "Exploring twisted mass lattice QCD with the Clover term". In: *Phys. Rev. D* 74 (2006), p. 034501. DOI: 10.1103/PhysRevD.74.034501. arXiv: hep-lat/0605006.

[14] A. A. Belavin et al. "Pseudoparticle Solutions of the Yang-Mills Equations". In: *Phys. Lett. B* 59 (1975). Ed. by J. C. Taylor, pp. 85–87. DOI: 10.1016/0370-2693(75)90163-X.

[15] C.M. Bender, S. Orszag, and S.A. Orszag. *Advanced Mathematical Methods for Scientists and Engineers I: Asymptotic Methods and Perturbation Theory*. Advanced Mathematical Methods for Scientists and Engineers. Springer, 1999. ISBN: 9780387989310. URL: https://books.google.de/books?id=-yQXwhE6iWMC.

[16] Miguel A. Benitez-Rathgeb et al. "Reconciling the contour-improved and fixed-order approaches for τ hadronic spectral moments. Part I. Renormalon-free gluon condensate scheme". In: *JHEP* 07 (2022), p. 016. DOI: 10.1007/JHEP07(2022)016. arXiv: 2202.10957 [hep-ph].

[17] Miguel A. Benitez-Rathgeb et al. "Reconciling the contour-improved and fixed-order approaches for τ hadronic spectral moments. Part II. Renormalon norm and application in α_s determinations". In: *JHEP* 09 (2022), p. 223. DOI: 10.1007/JHEP09(2022)223. arXiv: 2207.01116 [hep-ph].

[18] David Bernecker and Harvey B. Meyer. "Vector Correlators in Lattice QCD: Methods and applications". In: *Eur. Phys. J. A* 47 (2011), p. 148. DOI: 10.1140/epja/i2011-11148-6. arXiv: 1107.4388 [hep-lat].

[19] Werner Bernreuther and Werner Wetzel. "Decoupling of Heavy Quarks in the Minimal Subtraction Scheme". In: *Nucl. Phys. B* 197 (1982). [Erratum: Nucl.Phys.B 513, 758–758 (1998)], pp. 228–236. DOI: 10.1016/0550-3213(82)90288-7.

[20] A. Blondel et al. "Standard model theory for the FCC-ee Tera-Z stage". In: *Mini Workshop on Precision EW and QCD Calculations for the FCC Studies : Methods and Techniques*. Vol. 3/2019. CERN Yellow Reports: Monographs. Geneva: CERN, Sept. 2018. DOI: 10.23731/CYRM-2019-003. arXiv: 1809.01830 [hep-ph].

[21] Marco Bochicchio et al. "Chiral Symmetry on the Lattice with Wilson Fermions". In: *Nucl. Phys. B* 262 (1985), p. 331. DOI: 10.1016/0550-3213(85)90290-1.

[22] N. Bohr, R. Peierls, and G. Placzek. "Nuclear Reactions in the Continuous Energy Region". In: *Nature* 144 (3639 1939), pp. 200–201. DOI: 10.1038/144200a0. URL: https://doi.org/10.1038/144200a0.

[23] Diogo Boito and Vicent Mateu. "Precise α_s determination from charmonium sum rules". In: *Phys. Lett. B* 806 (2020), p. 135482. DOI: 10.1016/j.physletb.2020.135482. arXiv: 1912.06237 [hep-ph].

[24] Diogo Boito and Vicent Mateu. "Precise determination of α_s from relativistic quarkonium sum rules". In: *JHEP* 03 (2020), p. 094. DOI: 10.1007/JHEP03(2020)094. arXiv: 2001.11041 [hep-ph].

[25] Sz. Borsanyi et al. "Leading hadronic contribution to the muon magnetic moment from lattice QCD". In: *Nature* 593.7857 (2021), pp. 51–55. DOI: 10.1038/s41586-021-03418-1. arXiv: 2002.12347 [hep-lat].

[26] Szabolcs Borsanyi et al. "High-precision scale setting in lattice QCD". In: *JHEP* 09 (2012), p. 010. DOI: 10.1007/JHEP09(2012)010. arXiv: 1203.4469 [hep-lat].

[27] Nora Brambilla et al. "Precision determination of $r_0\Lambda^-_{MS}$ from the QCD static energy". In: *Phys. Rev. Lett.* 105 (2010). [Erratum: Phys.Rev.Lett. 108, 269903 (2012)], p. 212001. DOI: 10.1103/PhysRevLett.105.212001. arXiv: 1006.2066 [hep-ph].

[28] Frank R. Brown and Thomas J. Woch. "Overrelaxed Heat Bath and Metropolis Algorithms for Accelerating Pure Gauge Monte Carlo Calculations". In: *Phys. Rev. Lett.* 58 (1987), p. 2394. DOI: 10.1103/PhysRevLett.58.2394.

[29] Mattia Bruno, Tomasz Korzec, and Stefan Schaefer. "Setting the scale for the CLS $2+1$ flavor ensembles". In: *Phys. Rev. D* 95.7 (2017), p. 074504. DOI: 10.1103/PhysRevD.95.074504. arXiv: 1608.08900 [hep-lat].

[30] Mattia Bruno and Rainer Sommer. "On fits to correlated and auto-correlated data". In: *Comput. Phys. Commun.* 285 (2023), p. 108643. DOI: 10.1016/j.cpc.2022.108643. arXiv: 2209.14188 [hep-lat].

[31] Mattia Bruno et al. "QCD Coupling from a Nonperturbative Determination of the Three-Flavor Λ Parameter". In: *Phys. Rev. Lett.* 119.10 (2017), p. 102001. DOI: 10.1103/PhysRevLett.119.102001. arXiv: 1706.03821 [hep-lat].

[32] N. Cabibbo and E. Marinari. "A New Method for Updating SU(N) Matrices in Computer Simulations of Gauge Theories". In: *Phys. Lett. B* 119 (1982), pp. 387–390. DOI: 10.1016/0370-2693(82)90696-7.

[33] Salvatore Cali et al. "Charm sea effects on charmonium decay constants and heavy meson masses". In: *Eur. Phys. J. C* 81.8 (2021), p. 733. DOI: 10.1140/epjc/s10052-021-09520-y. arXiv: 2105.12278 [hep-lat].

[34] Curtis G. Callan. "Broken Scale Invariance in Scalar Field Theory". In: *Phys. Rev. D* 2 (8 1970), pp. 1541–1547. DOI: 10.1103/PhysRevD.2.1541. URL: https://link.aps.org/doi/10.1103/PhysRevD.2.1541.

[35] Stefano Capitani et al. “Non-perturbative quark mass renormalization in quenched lattice QCD”. In: *Nucl. Phys.* B544 (1999). [Erratum: Nucl. Phys.B582,762(2000)], pp. 669–698. DOI: 10.1016/S0550-3213(00)00163-2,10.1016/S0550-3213(98)00857-8. arXiv: hep-lat/9810063 [hep-lat].

[36] Bipasha Chakraborty et al. “High-precision quark masses and QCD coupling from $n_f = 4$ lattice QCD”. In: *Phys. Rev.* D91.5 (2015), p. 054508. DOI: 10.1103/PhysRevD.91.054508. arXiv: 1408.4169 [hep-lat].

[37] K. G. Chetyrkin. “Quark mass anomalous dimension to O (alpha-s**4)”. In: *Phys. Lett. B* 404 (1997), pp. 161–165. DOI: 10.1016/S0370-2693(97)00535-2. arXiv: hep-ph/9703278.

[38] K. G. Chetyrkin, Johann H. Kuhn, and M. Steinhauser. “Heavy quark current correlators to O (alpha-s**2)”. In: *Nucl. Phys. B* 505 (1997), pp. 40–64. DOI: 10.1016/S0550-3213(97)00481-1. arXiv: hep-ph/9705254.

[39] K. G. Chetyrkin, Johann H. Kuhn, and M. Steinhauser. “Heavy quark vacuum polarization to three loops”. In: *Phys. Lett. B* 371 (1996), pp. 93–98. DOI: 10.1016/0370-2693(95)01593-0. arXiv: hep-ph/9511430.

[40] K. G. Chetyrkin, Johann H. Kuhn, and M. Steinhauser. “Three loop polarization function and O (alpha-s**2) corrections to the production of heavy quarks”. In: *Nucl. Phys. B* 482 (1996), pp. 213–240. DOI: 10.1016/S0550-3213(96)00534-2. arXiv: hep-ph/9606230.

[41] K. G. Chetyrkin, Johann H. Kuhn, and Christian Sturm. “QCD decoupling at four loops”. In: *Nucl. Phys. B* 744 (2006), pp. 121–135. DOI: 10.1016/j.nuclphysb.2006.03.020. arXiv: hep-ph/0512060.

[42] K. G. Chetyrkin and M. F. Zoller. “Leading QCD-induced four-loop contributions to the β-function of the Higgs self-coupling in the SM and vacuum stability”. In: *JHEP* 06 (2016), p. 175. DOI: 10.1007/JHEP06(2016)175. arXiv: 1604.00853 [hep-ph].

[43] Leonardo Chimirri, Nikolai Husung, and Rainer Sommer. “Log-enhanced discretization errors in integrated correlation functions”. In: *39th International Symposium on Lattice Field Theory*. Nov. 2022. arXiv: 2211.15750 [hep-lat].

[44] Sidney R. Coleman and Erick J. Weinberg. “Radiative Corrections as the Origin of Spontaneous Symmetry Breaking”. In: *Phys. Rev. D* 7 (1973), pp. 1888–1910. DOI: 10.1103/PhysRevD.7.1888.

[45] Amanda M. Cooper-Sarkar et al. “Simultaneous extraction of α_s and m_t from LHC $t\bar{t}$ differential distributions”. In: (Oct. 2020). arXiv: 2010.04171 [hep-ph].

[46] Michael Creutz. “Overrelaxation and Monte Carlo Simulation”. In: *Phys. Rev. D* 36 (1987), p. 515. DOI: 10.1103/PhysRevD.36.515.

[47] Mattia Dalla Brida and Alberto Ramos. “The gradient flow coupling at high-energy and the scale of SU(3) Yang–Mills theory”. In: *Eur. Phys. J. C* 79.8 (2019), p. 720. DOI: 10.1140/epjc/s10052-019-7228-z. arXiv: 1905.05147 [hep-lat].

[48] Mattia Dalla Brida et al. “Determination of $\alpha_s(m_Z)$ by the non-perturbative decoupling method”. In: *Eur. Phys. J. C* 82.12 (2022), p. 1092. DOI: 10.1140/epjc/s10052-022-10998-3. arXiv: 2209.14204 [hep-lat].

[49] Mattia Dalla Brida et al. “Heavy Quarks in a Can and the QCD Coupling”. In: *PoS* LATTICE2022 (2023), p. 286. DOI: 10.22323/1.430.0286.

[50] Mattia Dalla Brida et al. “Non-perturbative renormalization by decoupling”. In: *Phys. Lett. B* 807 (2020), p. 135571. DOI: 10.1016/j.physletb.2020.135571. arXiv: 1912.06001 [hep-lat].

[51] Roger Dashen and David J. Gross. “Relationship between lattice and continuum definitions of the gauge-theory coupling”. In: *Phys. Rev. D* 23 (10 1981), pp. 2340–2348. DOI: 10.1103/PhysRevD.23.2340. URL: https://link.aps.org/doi/10.1103/PhysRevD.23.2340.

[52] Luigi Del Debbio, Haralambos Panagopoulos, and Ettore Vicari. “θ dependence of SU(N) gauge theories”. In: *Journal of High Energy Physics* 2002.08 (2002), pp. 044–044. DOI: 10.1088/1126-6708/2002/08/044. URL: https://doi.org/10.1088/1126-6708/2002/08/044.

[53] Luigi Del Debbio and Alberto Ramos. “Lattice determinations of the strong coupling”. In: (Jan. 2021). DOI: 10.1016/j.physrep.2021.03.005. arXiv: 2101.04762 [hep-lat].

[54] P. Dimopoulos, H. Simma, and A. Vladikas. “Quenched B(K)-parameter from Osterwalder-Seiler tmQCD quarks and mass-splitting discretization effects”. In: *JHEP* 07 (2009), p. 007. DOI: 10.1088/1126-6708/2009/07/007. arXiv: 0902.1074 [hep-lat].

[55] Michael Donnellan et al. “Determination of the Static Potential with Dynamical Fermions”. In: *Nucl. Phys. B* 849 (2011), pp. 45–63. DOI: 10.1016/j.nuclphysb.2011.03.013. arXiv: 1012.3037 [hep-lat].

[56] Simon Duane et al. “Hybrid Monte Carlo”. In: *Physics Letters B* 195.2 (1987), pp. 216–222. ISSN: 0370-2693. DOI: https://doi.org/10.1016/0370-2693(87)91197-X. URL: https://www.sciencedirect.com/science/article/pii/037026938791197X.

[57] S. Durr et al. “Ab-Initio Determination of Light Hadron Masses”. In: *Science* 322 (2008), pp. 1224–1227. DOI: 10.1126/science.1163233. arXiv: 0906.3599 [hep-lat].

[58] Stanley Eisenstat, Howard Elman, and Martin Schultz. “Variational Iterative Methods for Nonsymmetric Systems of Linear Equations”. In: *SIAM Journal on Numerical Analysis* 20 (Apr. 1983), pp. 345–357. DOI: 10.1137/0720023.

[59] R. P. Feynman. “Space-Time Approach to Non-Relativistic Quantum Mechanics”. In: *Rev. Mod. Phys.* 20 (2 1948), pp. 367–387. DOI: 10.1103/RevModPhys.20.367. URL: https://link.aps.org/doi/10.1103/RevModPhys.20.367.

[60] D. de Florian et al. “Handbook of LHC Higgs Cross Sections: 4. Deciphering the Nature of the Higgs Sector”. In: 2/2017 (Oct. 2016). DOI: 10.23731/CYRM-2017-002. arXiv: 1610.07922 [hep-ph].

[61] E. Follana et al. “Highly improved staggered quarks on the lattice with applications to charm physics”. In: *Phys. Rev. D* 75 (5 2007), p. 054502. DOI: 10.1103/PhysRevD.75.054502. URL: https://link.aps.org/doi/10.1103/PhysRevD.75.054502.

[62] R. Frezzotti and G. C. Rossi. “Chirally improving Wilson fermions. 1. O(a) improvement”. In: *JHEP* 08 (2004), p. 007. DOI: 10.1088/1126-6708/2004/08/007. arXiv: hep-lat/0306014.

[63] R. Frezzotti et al. “Reducing cutoff effects in maximally twisted lattice QCD close to the chiral limit”. In: *JHEP* 04 (2006), p. 038. DOI: 10.1088/1126-6708/2006/04/038. arXiv: hep-lat/0503034.

[64] Roberto Frezzotti et al. “Lattice QCD with a chirally twisted mass term”. In: *JHEP* 08 (2001), p. 058. DOI: 10.1088/1126-6708/2001/08/058. arXiv: hep-lat/0101001.

[65] D. Friedan. “A proof of the Nielsen-Ninomiya theorem”. English (US). In: *Communications In Mathematical Physics* 85.4 (Dec. 1982), pp. 481–490. ISSN: 0010-3616. DOI: https://doi.org/10.1007/BF01403500.

[66] Stefano Frixione and Bryan R. Webber. “Matching NLO QCD computations and parton shower simulations”. In: *JHEP* 06 (2002), p. 029. DOI: 10.1088/1126-6708/2002/06/029. arXiv: hep-ph/0204244.

[67] Christof Gattringer and Christian B. Lang. *Quantum chromodynamics on the lattice*. Vol. 788. Berlin: Springer, 2010. ISBN: 978-3-642-01849-7, 978-3-642-01850-3. DOI: 10.1007/978-3-642-01850-3.

[68] Murray Gell-Mann and F. E. Low. “Quantum electrodynamics at small distances”. In: *Phys. Rev.* 95 (1954), pp. 1300–1312. DOI: 10.1103/PhysRev.95.1300.

[69] Murray Gell-Mann, R. J. Oakes, and B. Renner. “Behavior of Current Divergences under $SU_3 \times SU_3$”. In: *Phys. Rev.* 175 (5 1968), pp. 2195–2199. DOI: 10.1103/PhysRev.175.2195. URL: https://link.aps.org/doi/10.1103/PhysRev.175.2195.

[70] Howard Georgi. *Lie algebras in particle physics*. 2nd ed. Vol. 54. Reading, MA: Perseus Books, 1999.

[71] Paul H. Ginsparg and Kenneth G. Wilson. “A remnant of chiral symmetry on the lattice”. In: *Phys. Rev. D* 25 (10 1982), pp. 2649–2657. DOI: 10.1103/PhysRevD.25.2649. URL: https://link.aps.org/doi/10.1103/PhysRevD.25.2649.

[72] M. Gockeler et al. “A Determination of the Lambda parameter from full lattice QCD”. In: *Phys. Rev. D* 73 (2006), p. 014513. DOI: 10.1103/PhysRevD.73.014513. arXiv: hep-ph/0502212.

[73] David J. Gross and R. Jackiw. “Effect of Anomalies on Quasi-Renormalizable Theories”. In: *Phys. Rev. D* 6 (2 1972), pp. 477–493. DOI: 10.1103/PhysRevD.6.477. URL: https://link.aps.org/doi/10.1103/PhysRevD.6.477.

[74] David J. Gross and Frank Wilczek. “Ultraviolet Behavior of Non-Abelian Gauge Theories”. In: *Phys. Rev. Lett.* 30 (26 1973), pp. 1343–1346. DOI: 10.1103/PhysRevLett.30.1343. URL: https://link.aps.org/doi/10.1103/PhysRevLett.30.1343.

[75] Marco Guagnelli et al. “Nonperturbative results for the coefficients b(m) and b(a) - b(P) in O(a) improved lattice QCD”. In: *Nucl. Phys. B* 595 (2001), pp. 44–62. DOI: 10.1016/S0550-3213(00)00675-1. arXiv: hep-lat/0009021.

[76] Rajan Gupta. “Introduction to lattice QCD: Course”. In: *Les Houches Summer School in Theoretical Physics, Session 68: Probing the Standard Model of Particle Interactions*. July 1997, pp. 83–219. arXiv: hep-lat/9807028.

[77] Tim Harris et al. “Vacuum correlators at short distances from lattice QCD”. In: *PoS* LATTICE2021 (2021), p. 572. DOI: 10.22323/1.396.0572. arXiv: 2111.07948 [hep-lat].

[78] Anna Hasenfratz and Peter Hasenfratz. “The connection between the Λ parameters of lattice and continuum QCD”. In: *Physics Letters B* 93 (1980), pp. 165–169.

[79] Peter Hasenfratz, Victor Laliena, and Ferenc Niedermayer. “The Index theorem in QCD with a finite cutoff”. In: *Phys. Lett. B* 427 (1998), pp. 125–131. DOI: 10.1016/S0370-2693(98)00315-3. arXiv: hep-lat/9801021.

[80] W. K. Hastings. “Monte Carlo sampling methods using Markov chains and their applications”. In: *Biometrika* 57.1 (Apr. 1970), pp. 97–109. ISSN: 0006-3444. DOI: 10.1093/biomet/57.1.97. eprint: https://academic.oup.com/biomet/article-pdf/57/1/97/23940249/57-1-97.pdf. URL: https://doi.org/10.1093/biomet/57.1.97.

[81] Sven Heinemeyer, Stanislaw Jadach, and Jürgen Reuter. “Theory requirements for SM Higgs and EW precision physics at the FCC-ee”. In: *Eur. Phys. J. Plus* 136.9 (2021), p. 911. DOI: 10.1140/epjp/s13360-021-01875-1. arXiv: 2106.11802 [hep-ph].

[82] Jochen Heitger, Martin Kurth, and Rainer Sommer. “Nonperturbative renormalization of the static axial current in quenched QCD”. In: *Nucl. Phys.* B669 (2003), pp. 173–206. DOI: 10.1016/S0550-3213(03)00552-2. arXiv: hep-lat/0302019 [hep-lat].

[83] F. Herzog et al. “The five-loop beta function of Yang-Mills theory with fermions”. In: *JHEP* 02 (2017), p. 090. DOI: 10.1007/JHEP02(2017)090. arXiv: 1701.01404 [hep-ph].

[84] Magnus R. Hestenes and Eduard Stiefel. “Methods of conjugate gradients for solving linear systems”. In: *Journal of research of the National Bureau of Standards* 49 (1952), pp. 409–435.

[85] Peter W. Higgs. “Broken Symmetries and the Masses of Gauge Bosons”. In: *Phys. Rev. Lett.* 13 (16 1964), pp. 508–509. DOI: 10.1103/PhysRevLett.13.508. URL: https://link.aps.org/doi/10.1103/PhysRevLett.13.508.

[86] André H. Hoang. “What is the Top Quark Mass?” In: *Ann. Rev. Nucl. Part. Sci.* 70 (2020), pp. 225–255. DOI: 10.1146/annurev-nucl-101918-023530. arXiv: 2004.12915 [hep-ph].

[87] Christian Hoelbling. "Lattice QCD: concepts, techniques and some results". In: *Acta Phys. Polon. B* 45.12 (2014). Ed. by Michal Praszalowicz, p. 2143. DOI: 10.5506/APhysPolB.45.2143. arXiv: 1410.3403 [hep-lat].

[88] Gerard 't Hooft and M. J. G. Veltman. "Regularization and Renormalization of Gauge Fields". In: *Nucl. Phys. B* 44 (1972), pp. 189–213. DOI: 10.1016/0550-3213(72)90279-9.

[89] Nikolai Husung. "Logarithmic corrections to O(a) and O(a^2) effects in lattice QCD with Wilson or Ginsparg–Wilson quarks". In: *Eur. Phys. J. C* 83.2 (2023), p. 142. DOI: 10.1140/epjc/s10052-023-11258-8. arXiv: 2206.03536 [hep-lat].

[90] Nikolai Husung, Peter Marquard, and Rainer Sommer. "Asymptotic behavior of cutoff effects in Yang–Mills theory and in Wilson's lattice QCD". In: *Eur. Phys. J. C* 80.3 (2020), p. 200. DOI: 10.1140/epjc/s10052-020-7685-4. arXiv: 1912.08498 [hep-lat].

[91] Nikolai Husung et al. "SU(3) Yang Mills theory at small distances and fine lattices". In: *EPJ Web Conf.* 175 (2018). Ed. by M. Della Morte et al., p. 14024. DOI: 10.1051/epjconf/201817514024. arXiv: 1711.01860 [hep-lat].

[92] Ken-Ichi Ishikawa et al. "Non-perturbative determination of the Λ-parameter in the pure SU(3) gauge theory from the twisted gradient flow coupling". In: *JHEP* 12 (2017), p. 067. DOI: 10.1007/JHEP12(2017)067. arXiv: 1702.06289 [hep-lat].

[93] Karl Jansen, Marcus Petschlies, and Carsten Urbach. "Charm Current-Current Correlators in Twisted Mass Lattice QCD". In: *PoS* LATTICE2011 (2011). Ed. by Pavlos Vranas, p. 234. DOI: 10.22323/1.139.0234. arXiv: 1111.5252 [hep-lat].

[94] Andreas Jüttner. "Precision lattice computations in the heavy quark sector". PhD thesis. Humboldt U., Berlin, 2004. arXiv: hep-lat/0503040 [hep-lat].

[95] David B. Kaplan. "A method for simulating chiral fermions on the lattice". In: *Physics Letters B* 288.3 (1992), pp. 342–347. ISSN: 0370-2693. DOI: https://doi.org/10.1016/0370-2693(92)91112-M. URL: https://www.sciencedirect.com/science/article/pii/037026939291112M.

[96] Masakiyo Kitazawa et al. "Equation of State for SU(3) Gauge Theory via the Energy-Momentum Tensor under Gradient Flow". In: *Phys. Rev. D* 94.11 (2016), p. 114512. DOI: 10.1103/PhysRevD.94.114512. arXiv: 1610.07810 [hep-lat].

[97] Y. Kiyo et al. "Reconstruction of heavy quark current correlators at O(alpha(s)**3)". In: *Nucl. Phys. B* 823 (2009), pp. 269–287. DOI: 10.1016/j.nuclphysb.2009.08.010. arXiv: 0907.2120 [hep-ph].

[98] John Kogut and Leonard Susskind. "Hamiltonian formulation of Wilson's lattice gauge theories". In: *Phys. Rev. D* 11 (2 1975), pp. 395–408. DOI: 10.1103/PhysRevD.11.395. URL: https://link.aps.org/doi/10.1103/PhysRevD.11.395.

[99] L.D. Landau, A.A. Abrikosov, and I. M. Khalatnikov. “An asymptotic expression for the Green function of a photon in quantum electrodynamics”. In: *Dokl. Akad. Nauk. SSSR* 95 (1954), p. 1177.

[100] L.D. Landau, A.A. Abrikosov, and I. M. Khalatnikov. “Asymptotic expression of the Green’s function of the electron in quantum electrodynamics”. In: *Dokl. Akad. Nauk. SSSR* 95 (1954), p. 773.

[101] L.D. Landau, A.A. Abrikosov, and I. M. Khalatnikov. “On the removal of infinities in quantum electrodynamics”. In: *Dokl. Akad. Nauk. SSSR* 95 (1954), p. 497.

[102] M. Luscher. “Construction of a Selfadjoint, Strictly Positive Transfer Matrix for Euclidean Lattice Gauge Theories”. In: *Commun. Math. Phys.* 54 (1977), p. 283. DOI: 10.1007/BF01614090.

[103] Martin Luscher. “Lattice QCD and the Schwarz alternating procedure”. In: *JHEP* 05 (2003), p. 052. DOI: 10.1088/1126-6708/2003/05/052. arXiv: hep-lat/0304007.

[104] Martin Luscher et al. “Chiral symmetry and O(a) improvement in lattice QCD”. In: *Nucl. Phys. B* 478 (1996), pp. 365–400. DOI: 10.1016/0550-3213(96)00378-1. arXiv: hep-lat/9605038.

[105] Thomas Luthe et al. “The five-loop Beta function for a general gauge group and anomalous dimensions beyond Feynman gauge”. In: *JHEP* 10 (2017), p. 166. DOI: 10.1007/JHEP10(2017)166. arXiv: 1709.07718 [hep-ph].

[106] Thomas Luthe et al. “Towards the five-loop Beta function for a general gauge group”. In: *JHEP* 07 (2016), p. 127. DOI: 10.1007/JHEP07(2016)127. arXiv: 1606.08662 [hep-ph].

[107] M. Lüscher and P. Weisz. “Computation of the action for on-shell improved lattice gauge theories at weak coupling”. In: *Physics Letters B* 158.3 (1985), pp. 250–254. ISSN: 0370-2693. DOI: https://doi.org/10.1016/0370-2693(85)90966-9. URL: https://www.sciencedirect.com/science/article/pii/0370269385909669.

[108] Martin Lüscher. “Advanced lattice QCD”. In: *Les Houches Summer School in Theoretical Physics, Session 68: Probing the Standard Model of Particle Interactions*. Feb. 1998, pp. 229–280. arXiv: hep-lat/9802029.

[109] Martin Lüscher. “Computational Strategies in Lattice QCD”. In: *Les Houches Summer School: Session 93: Modern perspectives in lattice QCD: Quantum field theory and high performance computing*. Feb. 2010, pp. 331–399. arXiv: 1002.4232 [hep-lat].

[110] Martin Lüscher. “Exact chiral symmetry on the lattice and the Ginsparg-Wilson relation”. In: *Physics Letters B* 428.3 (1998), pp. 342–345. ISSN: 0370-2693. DOI: https://doi.org/10.1016/S0370-2693(98)00423-7. URL: https://www.sciencedirect.com/science/article/pii/S0370269398004237.

[111] Martin Lüscher. "Properties and uses of the Wilson flow in lattice QCD". In: *JHEP* 08 (2010). [Erratum: JHEP03,092(2014)], p. 071. DOI: 10.1007/JHEP08(2010)071, 10.1007/JHEP03(2014)092. arXiv: 1006.4518 [hep-lat].

[112] Martin Lüscher. "Solution of the Dirac equation in lattice QCD using a domain decomposition method". In: *Comput. Phys. Commun.* 156 (2004), pp. 209–220. DOI: 10.1016/S0010-4655(03)00486-7. arXiv: hep-lat/0310048.

[113] Martin Lüscher and Stefan Schaefer. "Lattice QCD without topology barriers". In: *JHEP* 07 (2011), p. 036. DOI: 10.1007/JHEP07(2011)036. arXiv: 1105.4749 [hep-lat].

[114] Martin Lüscher and Peter Weisz. "Perturbative analysis of the gradient flow in non-abelian gauge theories". In: *JHEP* 02 (2011), p. 051. DOI: 10.1007/JHEP02(2011)051. arXiv: 1101.0963 [hep-th].

[115] Martin Lüscher et al. "Computation of the running coupling in the SU(2) Yang-Mills theory". In: *Nucl. Phys. B* 389 (1993), pp. 247–264. DOI: 10.1016/0550-3213(93)90292-W. arXiv: hep-lat/9207010.

[116] Martin Lüscher et al. "Nonperturbative determination of the axial current normalization constant in O(a) improved lattice QCD". In: *Nucl. Phys. B* 491 (1997), pp. 344–364. DOI: 10.1016/S0550-3213(97)00087-4. arXiv: hep-lat/9611015.

[117] Martin Lüscher et al. "Nonperturbative O(a) improvement of lattice QCD". In: *Nucl. Phys. B* 491 (1997), pp. 323–343. DOI: 10.1016/S0550-3213(97)00080-1. arXiv: hep-lat/9609035.

[118] Neal Madras and Alan D. Sokal. "The pivot algorithm: A highly efficient Monte Carlo method for the self-avoiding walk". In: *Journal of Statistical Physics* 50 (1988), pp. 109–186. DOI: 10.1007/BF01022990. URL: https://doi.org/10.1007/BF01022990.

[119] L. Maiani and M. Testa. "Final state interactions from Euclidean correlation functions". In: *Phys. Lett. B* 245 (1990), pp. 585–590. DOI: 10.1016/0370-2693(90)90695-3.

[120] A. Maier, P. Maierhofer, and P. Marquard. "The Second physical moment of the heavy quark vector correlator at O(alpha**3(s))". In: *Phys. Lett. B* 669 (2008), pp. 88–91. DOI: 10.1016/j.physletb.2008.09.041. arXiv: 0806.3405 [hep-ph].

[121] A. Maier et al. "Low energy moments of heavy quark current correlators at four loops". In: *Nucl. Phys.* B824 (2010), pp. 1–18. DOI: 10.1016/j.nuclphysb.2009.08.011. arXiv: 0907.2117 [hep-ph].

[122] G. Martinelli and Christopher T. Sachrajda. "On the difficulty of computing higher twist corrections". In: *Nucl. Phys. B* 478 (1996), pp. 660–686. DOI: 10.1016/0550-3213(96)00415-4. arXiv: hep-ph/9605336.

[123] C. McNeile et al. "High-Precision c and b Masses, and QCD Coupling from Current-Current Correlators in Lattice and Continuum QCD". In: *Phys. Rev. D* 82 (2010), p. 034512. DOI: 10.1103/PhysRevD.82.034512. arXiv: 1004.4285 [hep-lat].

[124] Nicholas Metropolis et al. “Equation of State Calculations by Fast Computing Machines”. In: *The Journal of Chemical Physics* 21.6 (1953), pp. 1087–1092. DOI: 10.1063/1.1699114. eprint: https://doi.org/10.1063/1.1699114. URL: https://doi.org/10.1063/1.1699114.

[125] Colin J. Morningstar and Mike J. Peardon. “The Glueball spectrum from an anisotropic lattice study”. In: *Phys. Rev. D* 60 (1999), p. 034509. DOI: 10.1103/PhysRevD.60.034509. arXiv: hep-lat/9901004.

[126] Katsumasa Nakayama, Brendan Fahy, and Shoji Hashimoto. “Short-distance charmonium correlator on the lattice with Möbius domain-wall fermion and a determination of charm quark mass”. In: *Phys. Rev.* D94.5 (2016), p. 054507. DOI: 10.1103/PhysRevD.94.054507. arXiv: 1606.01002 [hep-lat].

[127] Herbert Neuberger. “Exactly massless quarks on the lattice”. In: *Physics Letters B* 417.1 (1998), pp. 141–144. ISSN: 0370-2693. DOI: https://doi.org/10.1016/S0370-2693(97)01368-3. URL: https://www.sciencedirect.com/science/article/pii/S0370269397013683.

[128] Herbert Neuberger. “More about exactly massless quarks on the lattice”. In: *Physics Letters B* 427.3 (1998), pp. 353–355. ISSN: 0370-2693. DOI: https://doi.org/10.1016/S0370-2693(98)00355-4. URL: https://www.sciencedirect.com/science/article/pii/S0370269398003554.

[129] H.B. Nielsen and M. Ninomiya. “Absence of neutrinos on a lattice: (I). Proof by homotopy theory”. In: *Nuclear Physics B* 185.1 (1981), pp. 20–40. ISSN: 0550-3213. DOI: https://doi.org/10.1016/0550-3213(81)90361-8. URL: https://www.sciencedirect.com/science/article/pii/0550321381903618.

[130] H.B. Nielsen and M. Ninomiya. “Absence of neutrinos on a lattice: (II). Intuitive topological proof”. In: *Nuclear Physics B* 193.1 (1981), pp. 173–194. ISSN: 0550-3213. DOI: https://doi.org/10.1016/0550-3213(81)90524-1. URL: https://www.sciencedirect.com/science/article/pii/0550321381905241.

[131] K. Osterwalder. “Euclidean green’s functions and wightman distributions”. In: *International School of Mathematical Physics, Ettore Majorana: 1st course: Constructive Quantum Field Theory*. 1973, pp. 71–93.

[132] K. Osterwalder and E. Seiler. “Gauge Field Theories on the Lattice”. In: *Annals Phys.* 110 (1978), p. 440. DOI: 10.1016/0003-4916(78)90039-8.

[133] Konrad Osterwalder and Robert Schrader. “AXIOMS FOR EUCLIDEAN GREEN’S FUNCTIONS”. In: *Commun. Math. Phys.* 31 (1973), pp. 83–112. DOI: 10.1007/BF01645738.

[134] Konrad Osterwalder and Robert Schrader. “Axioms for Euclidean Green’s Functions. 2.” In: *Commun. Math. Phys.* 42 (1975), p. 281. DOI: 10.1007/BF01608978.

[135] Agostino Patella. "QED Corrections to Hadronic Observables". In: *PoS* LATTICE2016 (2017), p. 020. DOI: 10.22323/1.256.0020. arXiv: 1702.03857 [hep-lat].

[136] Michael E. Peskin and Daniel V. Schroeder. *An Introduction to quantum field theory*. Reading, USA: Addison-Wesley, 1995. ISBN: 9780201503975, 0201503972. URL: http://www.slac.stanford.edu/~mpeskin/QFT.html.

[137] P. Petreczky and J. H. Weber. "Strong coupling constant and heavy quark masses in (2+1)-flavor QCD". In: *Phys. Rev. D* 100.3 (2019), p. 034519. DOI: 10.1103/PhysRevD.100.034519. arXiv: 1901.06424 [hep-lat].

[138] Peter Petreczky and Johannes Heinrich Weber. "Strong coupling constant from moments of quarkonium correlators revisited". In: *Eur. Phys. J. C* 82.1 (2022), p. 64. DOI: 10.1140/epjc/s10052-022-09998-0. arXiv: 2012.06193 [hep-lat].

[139] Antonio Pich and Antonio Rodríguez-Sánchez. "Determination of the QCD coupling from ALEPH τ decay data". In: *Phys. Rev. D* 94.3 (2016), p. 034027. DOI: 10.1103/PhysRevD.94.034027. arXiv: 1605.06830 [hep-ph].

[140] H. David Politzer. "Reliable Perturbative Results for Strong Interactions?" In: *Phys. Rev. Lett.* 30 (26 1973), pp. 1346–1349. DOI: 10.1103/PhysRevLett.30.1346. URL: https://link.aps.org/doi/10.1103/PhysRevLett.30.1346.

[141] Johann Rafelski and Jean Letessier. "Testing limits of statistical hadronization". In: *Nuclear Physics A* 715 (2003). Quark Matter 2002, pp. 98c–107c. ISSN: 0375-9474. DOI: https://doi.org/10.1016/S0375-9474(02)01418-5. URL: https://www.sciencedirect.com/science/article/pii/S0375947402014185.

[142] R. Rajaraman. *SOLITONS AND INSTANTONS. AN INTRODUCTION TO SOLITONS AND INSTANTONS IN QUANTUM FIELD THEORY*. 1982.

[143] Juri Rolf and Stefan Sint. "A Precise determination of the charm quark's mass in quenched QCD". In: *JHEP* 12 (2002), p. 007. DOI: 10.1088/1126-6708/2002/12/007. arXiv: hep-ph/0209255.

[144] Stefan Schaefer. "Algorithms for lattice QCD: progress and challenges". In: *AIP Conf. Proc.* 1343 (2011). Ed. by F. J. Llanes-Estrada and J. R. Peláez, pp. 93–98. DOI: 10.1063/1.3574948. arXiv: 1011.5641 [hep-ph].

[145] Stefan Schaefer, Rainer Sommer, and Francesco Virotta. "Critical slowing down and error analysis in lattice QCD simulations". In: *Nucl. Phys.* B845 (2011), pp. 93–119. DOI: 10.1016/j.nuclphysb.2010.11.020. arXiv: 1009.5228 [hep-lat].

[146] Y. Schroder and M. Steinhauser. "Four-loop decoupling relations for the strong coupling". In: *JHEP* 01 (2006), p. 051. DOI: 10.1088/1126-6708/2006/01/051. arXiv: hep-ph/0512058.

[147] B. Sheikholeslami and R. Wohlert. “Improved Continuum Limit Lattice Action for QCD with Wilson Fermions”. In: *Nucl. Phys. B* 259 (1985), p. 572. DOI: 10.1016/0550-3213(85)90002-1.

[148] Jonathan R Shewchuk. *An Introduction to the Conjugate Gradient Method Without the Agonizing Pain*. Tech. rep. USA, 1994.

[149] Andrea Shindler. “Twisted mass lattice QCD”. In: *Phys. Rept.* 461 (2008), pp. 37–110. DOI: 10.1016/j.physrep.2008.03.001. arXiv: 0707.4093 [hep-lat].

[150] Stefan Sint. “Lattice QCD with a chiral twist”. In: *Workshop on Perspectives in Lattice QCD Nara, Japan, October 31-November 11, 2005*. 2007. DOI: 10.1142/9789812790927_0004. arXiv: hep-lat/0702008 [hep-lat].

[151] Rainer Sommer. “Non-perturbative QCD: Renormalization, O(a)-improvement and matching to Heavy Quark Effective Theory”. In: *Workshop on Perspectives in Lattice QCD*. Nov. 2006. arXiv: hep-lat/0611020.

[152] Rainer Sommer. “Scale setting in lattice QCD”. In: *PoS* LATTICE2013 (2014), p. 015. DOI: 10.22323/1.187.0015. arXiv: 1401.3270 [hep-lat].

[153] Christian Sturm. “Moments of Heavy Quark Current Correlators at Four-Loop Order in Perturbative QCD”. In: *JHEP* 09 (2008), p. 075. DOI: 10.1088/1126-6708/2008/09/075. arXiv: 0805.3358 [hep-ph].

[154] K. Symanzik. “Small distance behavior in field theory and power counting”. In: *Commun. Math. Phys.* 18 (1970), pp. 227–246. DOI: 10.1007/BF01649434.

[155] Kurt Symanzik. “Continuum limit and improved action in lattice theories:(I). Principles and $\varphi 4$ theory”. In: *Nuclear Physics B* 226.1 (1983), pp. 187–204.

[156] Kurt Symanzik. “Continuum limit and improved action in lattice theories:(II). O (N) non-linear sigma model in perturbation theory”. In: *Nuclear Physics B* 226.1 (1983), pp. 205–227.

[157] J. A. M. Vermaseren, S. A. Larin, and T. van Ritbergen. “The four loop quark mass anomalous dimension and the invariant quark mass”. In: *Phys. Lett. B* 405 (1997), pp. 327–333. DOI: 10.1016/S0370-2693(97)00660-6. arXiv: hep-ph/9703284.

[158] Steven Weinberg. “A Model of Leptons”. In: *Phys. Rev. Lett.* 19 (21 1967), pp. 1264–1266. DOI: 10.1103/PhysRevLett.19.1264. URL: https://link.aps.org/doi/10.1103/PhysRevLett.19.1264.

[159] Steven Weinberg. “Effective Gauge Theories”. In: *Phys. Lett. B* 91 (1980), pp. 51–55. DOI: 10.1016/0370-2693(80)90660-7.

[160] G. C. Wick. “The Evaluation of the Collision Matrix”. In: *Phys. Rev.* 80 (2 1950), pp. 268–272. DOI: 10.1103/PhysRev.80.268. URL: https://link.aps.org/doi/10.1103/PhysRev.80.268.

[161] Wikipedia. *Elementary Particle Interactions*. Accessed 08/11/2022. 2007. URL: https://en.wikipedia.org/wiki/File:Interactions.png.

[162] Kenneth G. Wilson. "Confinement of quarks". In: *Phys. Rev. D* 10 (8 1974), pp. 2445–2459. DOI: 10.1103/PhysRevD.10.2445. URL: https://link.aps.org/doi/10.1103/PhysRevD.10.2445.

[163] Kenneth G. Wilson. "Quarks and Strings on a Lattice". In: *New Phenomena in Subnuclear Physics: Part A*. Ed. by Antonino Zichichi. Boston, MA: Springer US, 1977, pp. 69–142. ISBN: 978-1-4613-4208-3. DOI: 10.1007/978-1-4613-4208-3_6. URL: https://doi.org/10.1007/978-1-4613-4208-3_6.

[164] Ulli Wolff. "Monte Carlo errors with less errors". In: *Comput. Phys. Commun.* 156 (2004). [Erratum: Comput. Phys. Commun.176,383(2007)], pp. 143–153. DOI: 10.1016/S0010-4655(03)00467-3, 10.1016/j.cpc.2006.12.001. arXiv: hep-lat/0306017 [hep-lat].

[165] R. L. Workman and Others. "Review of Particle Physics". In: *PTEP* 2022 (2022), p. 083C01. DOI: 10.1093/ptep/ptac097.

[166] C. N. Yang and R. L. Mills. "Conservation of Isotopic Spin and Isotopic Gauge Invariance". In: *Phys. Rev.* 96 (1 1954), pp. 191–195. DOI: 10.1103/PhysRev.96.191. URL: https://link.aps.org/doi/10.1103/PhysRev.96.191.

[167] Yi-Bo Yang et al. "Charm and strange quark masses and f_{D_s} from overlap fermions". In: *Phys. Rev. D* 92.3 (2015), p. 034517. DOI: 10.1103/PhysRevD.92.034517. arXiv: 1410.3343 [hep-lat].

LIST OF FIGURES

LIST OF TABLES

ERKLÄRUNG

Ich erkläre, dass ich die Dissertation selbständig und nur unter Verwendung der von mir gemäß § 7 Abs. 3 der Promotionsordnung der Mathematisch-Naturwissenschaftlichen Fakultät, veröffentlicht im Amtlichen Mitteilungsblatt der Humboldt-Universität zu Berlin Nr. 42/2018 am 11.07.2018, angegebenen Hilfsmittel angefertigt habe.

Berlin, November 10, 2023

Leonardo Chimirri